CREATING A 3D STEM CELL MICROENVIRONMENT TO PRODUCE HUMAN DEVELOPING CARDIAC TISSUES FOR SCALE-UP AND DISEASE MODELING

by

Petra Kerscher

A Dissertation
Submitted To The Graduate Faculty
of Auburn University
In Partial Fulfillment of the Requirements
For The Degree of Doctor of Philosophy

Auburn, Alabama
August 6, 2016

Keywords: PEG-fibrinogen, GelMA, hydrogel, biomaterial, cardiac tissue

Approved by

Elizabeth A. Lipke, Chair, Mary and John H. Sanders Associate Professor of Chemical Engineering
Virginia A. Davis, Alumni Professor of Chemical Engineering
Allan E. David, John W. Brown Assistant Professor of Chemical Engineering
Seung-Woo Jung, Assistant Professor of Cardiology, Clinical Sciences
Kevin D. Costa, Associate Professor of Medicine (Cardiology), Cardiovascular Research Center, Icahn School of Medicine at Mount Sinai

Abstract

In the field of tissue engineering, the use of human induced pluripotent stem cells (hiPSCs) has proven extremely valuable based on their ability to differentiate into almost any cell type within the human body, but keep their inherent biological origin. Until now, human physiology, disease modeling and regeneration, as well as organ development are not well understood due to the lack of available human-based tissues for experimentation and cell therapy. These challenges are used as the ultimate goal in cardiac tissue engineering, and are sought to be overcome by using hiPSCs to create authentic 3D developing heart tissue *in vitro*. HiPSCs can be differentiated into contracting cardiomyocytes, following natural pathways of human heart development.

Here we created a highly-reproducible, single-cell handling step procedure to encapsulate hiPSCs in PEG-fibrinogen hydrogels to generate functional and maturing 3D developing human engineered cardiac tissues (3D-dhECTs) in the geometry of immobilized microislands. This single-cell handling procedure not only reduced processing steps, but also allowed cells to form important cell-cell and cell-material interactions. The feasibility of differentiating hiPSCs within PEG-fibrinogen to create 3D-dhECT microislands was compared to an already published, highly efficient cardiac differentiation procedure which produced 2D cardiac monolayers. After validation of our novel 3D model, 3D-dhECTs were exposed to the known teratogen thalidomide, which

microislands were used to detect differences in tissue growth, frequency of contraction, total cell number and percent CMs, as well as CM size, sarcomere distance, and mitochondria distribution between control and thalidomide-treated CMs. Next, 3D cardiac microspheres were produced by applying our single-cell handling approach. Microspheres were created by encapsulating hiPSCs within PEG-fibrinogen and formed by a water-in-oil emulsion technique in a custom microfluidic device. Once encapsulated, hiPSCs grew and differentiated into contracting cardiac microspheres with CMs responding to drug treatment and outside electrical pacing. Finally, we wanted to evaluate the suitability of other biomaterials to create a favorable microenvironment for hiPSC encapsulation and cardiac differentiation. Gelatin methacryloyl (GelMA) was used due to its successful implementation in other tissue engineering and bioprinting applications. GelMA was synthesized and characterized using NMR; acellular GelMA hydrogels successfully degraded in the presence of collagenase. Once hiPSCs were encapsulated, cells grew and degraded the hydrogel over time. HiPSCs differentiated into CMs to produce GelMA developing human engineered cardiac tissues (GEhECTs), with frequency and velocity of contraction increasing over time. GEhECT CMs developed defined and aligned sarcomeres; CMs also responded to outside pacing and drug treatment.

Acknowledgments

I would like to thank Dr. Elizabeth Lipke for her continuous guidance and mentorship on this work. I would like to thank past and current members of the Lipke Lab, Dr. David Dunn, Dr. Aaron Seeto, Alex Hodge, and Shantanu Pradhan for their help and advice in various aspects of my project. Thank you to the undergraduate students, Jennifer Kaczmarek, Sara Head, and Blakely Bussie, who have assisted me in the experiments and data analysis of this work. My special appreciation goes to Dr. Kevin Costa and Dr. Irene Turnbull at Icahn School of Medicine at Mount Sinai, New York, for providing consistent, valuable scientific input on my project and welcoming me in the Costa Lab for one week to learn create 3D tissues using their PDMS mold. I also would like to thank Dr. Joonyul Kim for his help in RT-qPCR, Dr. Christopher Easley for allowing me to run RT-qPCR in his lab and his help in image analysis. Thank you to Dr. McDevitt and the Ethier lab at Georgia Tech who allowed and helped me use their Microsquisher for mechanical testing and Dr. Vishnu Suppiramaniam for providing MEA equipment. I would like to thank Dr. Virginia Davis, Dr. Allan David, Dr. Seungwoo Jung, Dr. Kevin Costa, and Dr. Raj Amin for their willingness to serve on my committee and their support on my doctoral work. Finally, I would like to thank my parents, Marianne and Josef Kerscher, as well as my brother Stefan for their continuous support and for believing in me.

Table of Contents

List of Tables

List of Figures

List of Supplementary Movies

List of Abbreviations

αSA	Alpha sarcomeric actinin
αMHC (MYH6)	Alpha myosin heavy chain
βMHC (MYH7)	Beta myosin heavy chain
AHA	American heart association
AP	Action potential
BMP	Bone morphogenic protein
BSA	Bovine serum albumin
CHD	Congenital heart defect
CM	Cardiomyocyte
cTnT	Cardiac troponin T
Cx43	Connexin 43
DMSO	Dimethyl sulfoxide
EB	Embryoid body
EC	Endothelial cell
ECM	Extracellular matrix
FBS	Fetal bovine serum
FDA	Food and Drug Administration
FFT	Fast Fourier Transform
H&E	Hematoxylin and eosin

hESC	Human embryonic stem cells
hiPSC	Human induced pluripotent stem cells
hPSC	Human pluripotent stem cells
mESC	Mouse embryonic stem cells
MLC2	Myosin light chain 2
NIH	National Institute of Health
NMR	Nuclear magnetic resonance
PBS	Phosphate buffered saline
PDMS	Polydimethylsiloxane
PEG	Poly(ethylene glycol)
PEG-DA	Poly(ethylene glycol) diacrylate
RNA	Ribonucleic acid
RT-qPCR	Reverse transcription quantitative polymerase chain reaction
SC-CM	Stem cell-derived cardiomyocyte
TCPS	Tissue culture polystyrene
TEM	Transmission electron microscopy

1. INTRODUCTION

Cardiac disease is the number one cause of death worldwide, accounting for approximately 40% of the accumulated mortality rate, with an estimated 25 million people suffering from heart failure each year (Bui, Horwich and Fonarow 2011). CMs are highly specialized cells and have limited ability to regenerate after a myocardial infarct. Following myocardial injury, available treatment options include pharmacological therapies (e.g. angiotensin-converting enzyme (ACE) inhibitors or β-blockers) to decrease work load (Dobner et al. 2009), interventional therapies (e.g. implantation of pacemaker) to inhibit arrhythmias (Hawkins et al. 2006), and total heart transplants, which are rare and only a small fraction of patients receive the required organ on time. Currently, researchers have the ability to generate autologous human CMs *in vitro* which could restore cardiac function within a short turnover time after the infarct and without immune rejection. Cellular function, transplantation, and integration into the native heart are obstacles that need to be understood and tested in the future (Nelson et al. 2011) to make cell therapy a possible treatment option.

1.1 Stem cells sources for CM production

The ultimate goal of regenerative medicine is to repair damaged or degenerated tissue. Stem cells, with their ability to self-renew in a pluripotent state and differentiate into any somatic cell type within the human body, are strong candidates for these regenerative applications. Several stem cell sources have been investigated for their potential applications; some of which include: fetal stem cells (from terminated fetuses), perinatal stem cells (from amniotic fluid, placenta, umbilical cord) (de Lazaro, Yilmazer and

Kostarelos 2014, Phinney and Prockop 2007), and embryonic stem cells. Although great knowledge has been collected from hESCs since 1998 (Thomson et al. 1998), ethical controversy has shadowed the stem cell collection from destroyed human embryos. In 2006, Dr. Shinya Yamanaka and coworkers revolutionized the field of regenerative medicine with their concept to reprogram fibroblasts via nuclear transfer mediated reprogramming (viral gene transfer of pluripotency transcription factors), from mouse (Takahashi and Yamanaka 2006) and human (Takahashi et al. 2007) cells, producing so called induced pluripotent stem cells. Until now, fibroblasts (skin cells) have been used excessively due to their availability and ease to harvest (Lowry et al. 2008). In addition to overcoming ethical issues, hiPSCs have several other advantages over hESCs, which include: production of autologous cell types for personalized treatment options (Ebben et al. 2011) and maintenance of genetic inheritance for personalized medicine and disease modeling (Yazawa and Dolmetsch 2013, Matsa, Burridge and Wu 2014) while still having their ability to efficiently differentiate into all somatic cell types of the human body, including functional CMs (Zhang et al. 2009), which is of upmost importance for this work (**Fig. 1.1**) (Burridge et al. 2012).

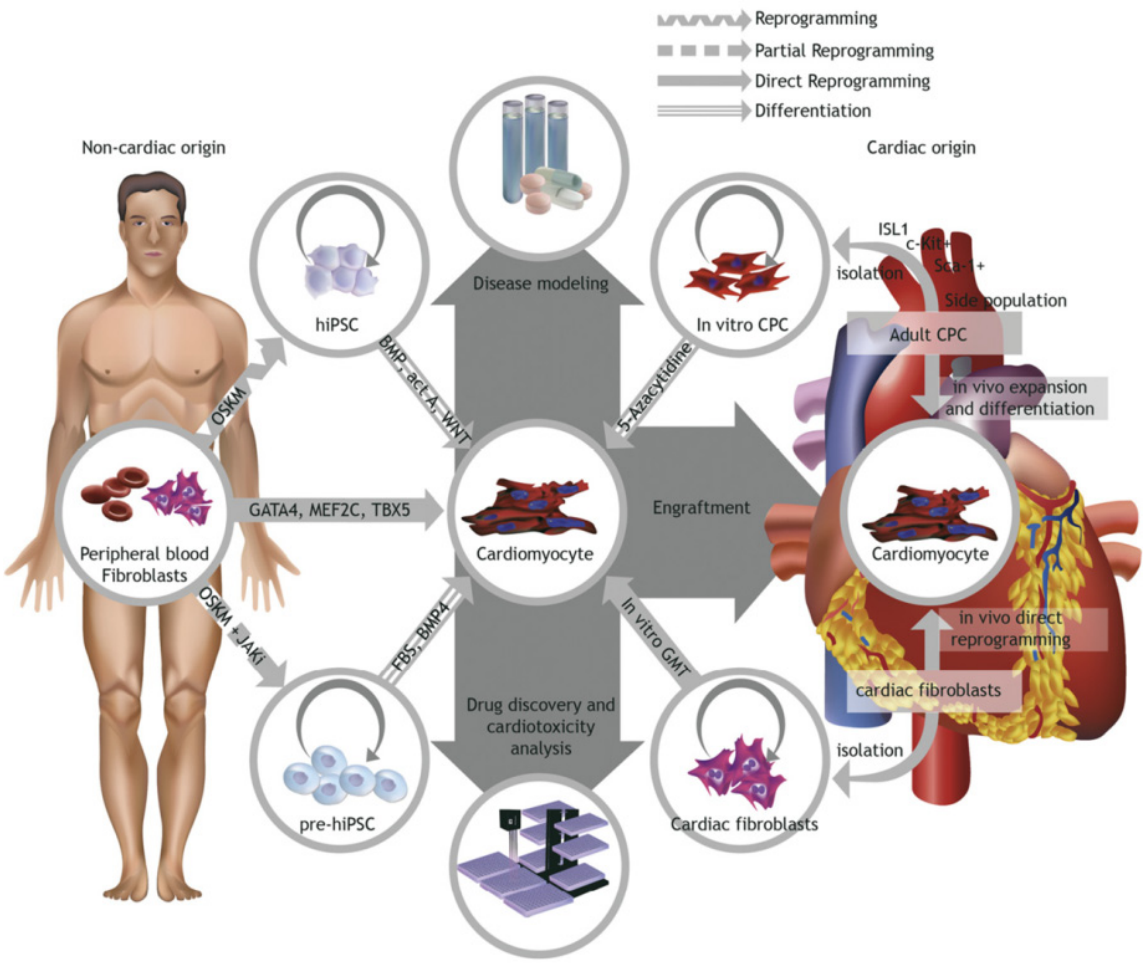

Fig. 1.1. Production of hiPSCs through reprogramming provides human CMs for regenerative medicine applications. Somatic cells from adult patients can be used to obtain hiPSCs (reprogramming) which can be differentiated into cells of all three germ layers (ectoderm, endoderm, and mesoderm). Differentiation of hiPSCs into CMs (mesoderm) can be used for disease modeling, drug discovery, and myocardial repair. Courtesy: Burridge et al., *Cell Stem Cell*. 2012;10:16-28.

1.2 Cardiac differentiation of hPSCs

Worldwide, heart disease is the number one cause of death, mainly caused by heart attacks or myocardial infarcts resulting in cell death of over 1 billion CMs (Murry, Reinecke and Pabon 2006) in the left ventricle alone. With their limited ability to regenerate, CM production for myocardial repair is one of the leading research areas in the field of regenerative medicine. Three differentiation methods have been shown to successfully produce stem cell-derived cardiomyocytes (SC-CMs): EB formation in suspension culture with the addition of serum-based media (Zwi et al. 2009, Gherghiceanu et al. 2011), EB formation via forced aggregation using serum-based or fully defined media (Burridge et al. 2011, Elliott et al. 2011), and 2D monolayer production with fully defined media supplemented with small molecules (Hazeltine et al. 2012, Zhang et al. 2012, Lian et al. 2012). Production of 2D cardiac monolayers using temporal addition of small molecules has shown that >98% pure CMs can be produced, making it a popular differentiation approach for tissue engineering while providing a good CM differentiation platform for more in-depth experimentation and future applications.

1.3 Current and future implementations of SC-CMs

Heart repair of the damaged human myocardium is the ultimate goal of cardiac regenerative engineering and therefore focuses on the implementation of SC-CMs towards *in vivo* translation. However, before cell therapy for myocardial diseases becomes a reality, there is still a lot to be learned. For now, researchers focus on the

translation of SC-CMs for drug-testing applications and disease modeling, as well as pre-clinical *in vivo* testing.

In vitro drug-testing models still rely on primary cells (Lu et al. 2008), which have several limitations and disadvantages due to their animal origin, including expense of large numbers of animals, time-consuming isolation procedures, animal variability, species-variations, and limited culture lifespan *in vitro*. The use of human SC-CMs can overcome these obstacles and in addition provide the potential for personalized medicine and disease modeling.

Several studies have focused on testing SC-CMs and their responses to well-known and widely studied active pharmaceutical ingredients. Two major questions arise when developing new drug-testing platforms for more accurate drug-screening using SC-CMs. First, how can we produce large-scale experimental platforms that better mimic cell-cell and cell-material interactions similar to the native heart; second, can we use patient-derived hiPSCs for disease modeling? The production of heart tissues as reliable drug-testing platform has been studied by producing engineered heart tissues (EHTs) where isolated neonatal rat cardiac cells or SC-CMs were combined with a fibrin-based matrix (Schaaf et al. 2011, Hansen et al. 2010) and were tested for their changes in calcium handling, electrophysiological properties, and force of contraction in response to certain pharmaceuticals. Their automated drug-testing assembly method has been shown to provide a sensitive tool for detecting drug-induced changes. Although multiple reviews mention the use of 3D cardiac models for drug-testing and screening applications (Wang et al. 2014b), only a few selected groups have shown proof-of-concept.

In addition to the use of SC-CMs for drug-testing, first attempts have been made to produce patient-derived hiPSCs from healthy patients and patients with inherent arrhythmogenic heart disorders, such as long QT syndrome, familial hypertrophic cardiomyopathy, dilated cardiomyopathy, and mitochondrial cardiomyopathy (Liang et al. 2013, Wang et al. 2014a, Han et al. 2014). Recent studies have shown that a library of patient-derived hiPSCs can be produced and further applied for CM differentiation while exhibiting disease-related electrophysiological differences. Current and future challenges involve the production of patient-specific heart tissues instead of only 2D sheets. A suitable 3D microenvironment during cell culture can provide a favorable 3D architecture, develop tight cell-cell junctions, and enhance CM function and maturation, all of which is not achieved in 2D cardiac differentiation.

The translation from *in vitro* to *in vivo* of SC-CMs for myocardial repair are currently studied in animal subjects (Ong et al. 2015, Plotkin et al. 2014). Initially, when CM differentiation protocols were inefficient, significant differences in CM purity slowed down *in vivo* related research (Kehat et al. 2001, Snir et al. 2003); the goal of cell therapy was far from reach. Now, cardiac differentiation protocols using small molecules and their ability for upscale CM production, as well as pro-survival factors to reduced cell death post-implantation imply hope (Laflamme et al. 2007). While successful graft integration with the host tissue has proven successful (Kehat et al. 2004, Li et al. 1999, Kutschka et al. 2006), a new set of questions and challenges have evolved, which include: *in vivo* electrophysiological and electromechanical integration and behavior, as well as the need for larger, reproducible implantable tissues (Tambara et al. 2003, Pouzet et al. 2001) using human SC-CMs. Strategies to overcome these potential issues will

include bioengineered matrixes for improved cell survival, CM alignment and mechanical and electrical integration with the host tissue post-implantation (Wendel et al. 2015, Pecha, Eschenhagen and Reichenspurner 2016).

2. INVESTIGATING HUMAN HEART DEVELOPMENT

2.1 Role of ECM in Cardiac Development

The ECM plays an important role throughout development of the heart. The physiology of heart development is highly complex and involves a variety of different components which interact both with each other and with their surroundings (**Fig. 2.1**) (McCulley and Black 2012). Mechanical and structural cues are important in guiding embryogenesis and are highly influenced by the cell's ECM. Furthermore, ECM is known to be essential for cell survival, proliferation, morphology, differentiation, as well as for mechanical properties and structural support of cardiac tissues (Daley, Peters and Larsen 2008). Therefore, interactions between cardiac cells, ECM, and proteoglycans play a vital role in heart development. Additionally, understanding the role of different transcription factors and transforming growth factors, including activation of their genetic and biochemical partners and the resulting responses, is essential to understanding normal and abnormal heart development.

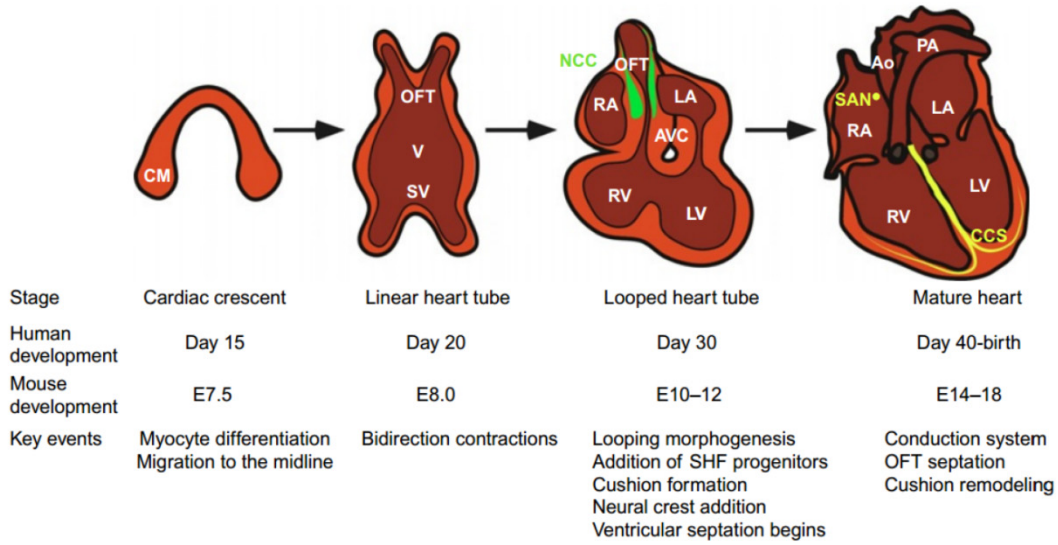

Fig. 2.1. Key events during the development of the heart. Courtesy: McCulley DJ and Black BL, *Current Topics in Developmental Biology*. 2012;100:253-77.

The developing heart tube is arranged as an EC layer surrounded by myocardial cells, with an acellular matrix composed of proteoglycans, collagens, and glycoproteins (Bursac et al. 2007). This matrix serves to maintain tube structure and proper regulation of flow during embryologic heart development. Overall, these different ECM components play essential roles during heart development; they provide and enable cell signaling (mechanical, electrical, and chemical), structural support, myocyte connections, contractile alignment, force transmittance, tensile strength, and gene expression changes (Bowers, Banerjee and Baudino 2010, Brown 2005).

Collagen is a primary component of the heart's ECM, playing an important role in regulating the stiffness and compliance of the heart (Norton et al. 1997). Multiple types of collagen are present in the heart, with collagen type I and type III being the most abundant. Both collagen type I and type III influence developmental changes during embryogenesis (Liu et al. 1997). Expression of the different collagen types is tightly

regulated both in terms of location and in terms of time, thereby regulating the regional stiffness and valve structure and function required for proper heart tissue development (Peacock et al. 2008). Collagen crosslinking by the structural protein hydroxypyridinium (HP) increases during development and throughout life and, thereby, also plays a role in determining the local mechanical microenvironment experienced by developing heart cells (Gosselin et al. 1998). Alteration in expression of collagen type I and type III can lead to serious congenital heart defects (CHDs) (Liu et al. 1997, Glesby and Pyeritz 1989) (**Table 2.1**). Therefore, studying different biomimetic materials that can support stem cell encapsulation, survival, and cardiac differentiation is desired to understand how collagen in influencing the developing human heart.

Versican, a chondroitin sulfate proteoglycan, is very important for normal heart development (Qu et al. 2008, Kruithof, Krawitz and Gaussin 2007, Kern et al. 2007, Kern et al. 2006, Henderson and Copp 1998, Yamamura et al. 1997) (**Table 2.1**). Throughout embryogenesis different cell types express versican at different concentrations; for instance, it has been shown that versican concentrations increase during the course of cardiac differentiation (Chan et al. 2010). This proteoglycan requires the β-catenin/T-cell factor complex present at its active site for it to be active (Rahmani, Carthy and McManus 2012). Disrupting the versican gene is fatal to the mouse embryo starting at the midpoint of development. Finally, recent studies regarding the NDRG4 gene, a gene that regulates versican expression, have shown that down regulation of NDRG4 reduces CM proliferation, which may ultimately result in cardiac hypoplasia (Qu et al. 2008). Taken together, understanding the role of essential ECM proteins during development is critical for engineering healthy heart tissue. Additionally, modification of ECM protein

expression may offer a venue for creation of engineered cardiac tissue with certain disease phenotypes.

Table 2.1. A list of genes and ECM proteins which contribute to the formation of congenital defects.

Gene/ECM Material	Associated cardiac structures	Associated congenital heart defects	Ref.
Nkx2.5	• Cardiac progenitor differentiation, proliferation, specification • Heart chamber development	• First degree AV block • Idiopathic AV block • Atrial septal defect • Tetralogy of Fallot	(Benson et al. 1999, Schott et al. 1998)
Gata4	• Cardiovascular lineage • Atrium and ventricle division • AV node gap junctions	• Atrial fibrillation • Cardiac septal defect	(Rojas et al. 2008, Garg et al. 2003, Posch et al. 2010, Munshi et al. 2009)
Collagen type I, III	• Fibrillogenesis • AV heart valve remodeling	• Ehlers-Danlos syndrome • Osteogenesis Imperfecta	(Liu et al. 1997, Peacock et al. 2008, Glesby and Pyeritz 1989)
Versican	• Cardiomyocyte proliferation • Cardiac cushion formation • AV development • Ventricular septation • Outflow tract development	• Ventricular septal defect • AV canal defect • Atrial septal defect • Double outlet right ventricle defect	(Qu et al. 2008, Kruithof et al. 2007, Kern et al. 2007, Kern et al. 2006, Henderson and Copp 1998, Yamamura et al. 1997)

In summary, ECM components, including collagen and versican play critical roles both in cardiac development and in adult heart disease. Biomimetic material design for cardiac tissue engineering applications can be informed by these physiological changes in ECM protein expression.

2.2 Role of Transcription Factors in Cardiac Development

As research advances, the importance of transcription factors during heart development are increasingly better recognized and understood. Transcription factors important for directing proper cardiac development include Nkx2.5, Gata4, and T-box; mutations or changes in expression levels of these genes have been implicated in the formation of CHDs.

Nkx2.5, an important transcription factor in embryogenesis overall, is a NK-2 homeobox gene that is important for cardiogenesis (Benson et al. 1999). Mutations in Nkx2.5 during heart development can result in a range of heart defects, including atrioventricular (AV) block (Schott et al. 1998), atrial septal defect (ASD) (Schott et al. 1998), tetralogy of Fallot (TOF), as well as many others (Schott et al. 1998, Benson et al. 1999) (**Table 2.1**). This list of CHDs shows that Nkx2.5 is essential in AV node formation and conduction as well as atrial, ventricular, and conotruncal septation (Benson et al. 1999).

T-box genes are transcription factors with a DNA-binding domain which have also an important part in heart development. T-box genes Tbx1 - Tbx5, Tbx18, and Tbx20, are involved in proper valve and heart chamber formation, and cardiac lineage (Plageman and Yutzey 2005). T-box plays an important part in heart development, with expression initiated even before valve development happens, to ensure proper morphological development and cardiac conduction system (due to the interaction with Nkx2.5) of the developing embryo (Suzuki et al. 2004, Liberatore et al. 2002, Lien et al. 1999, Lien et al. 2002). The concentration of T-box genes within the heart is closely dependent on growth factors, primarily Nkx2.5, which have the ability to induce them

(Hatcher and Basson 2001). Tbx5 is the most studied T-box gene due to its important role in guiding embryogenesis and forming a functional myocardium by interacting with other transcription factors which are also essential for normal heart development (**Table 2.1**). The lack of Tbx5 results in insufficient atria development and heart tube formation which can cause atrial septal and ventricular defects (ASD and VSD) as well as AV block. Expression levels must be tightly controlled, however; Tbx5 overexpression prevents ventricular maturation (Liberatore, Searcy-Schrick and Yutzey 2000). Insufficient expression of Tbx5 within the human heart was first detected in Holt-Oram syndrome patients (Li et al. 1997) (Holt-Oram syndrome is a limb abnormality due to upper limb formation and conduction system abnormalities). Given the connection between T-box genes and developmental abnormalities, implementation of growth factors which impact the expression of T-box genes is an important consideration in the development of biomimetic materials for cardiac regeneration.

In addition to their individual roles, interactions of multiple transcription factors are also critical to proper heart development. Cardiac septal defects (CSDs) are common defects in the congenital heart. During abnormal development caused by Gata4 mutations, the cardiac atrium and ventricle are not dividing in a proper manner to form left and right chambers of the heart. As a consequence, oxygenated and deoxygenated blood cannot be separated which causes a life threatening dysfunction for the infant and can only be resolved by open heart surgery. Recently, the origin of CSDs started to be understood by researchers focusing on mutations in the transcription factor genes Gata4, Nkx2.5, and Tbx5 (Garg et al. 2003). This defect is present in mice at E15.5 where insufficient development of the ventricular myocardium is a consequence of the lack of

interactions between these transcription factor genes. Gata4 not only interacts with Tbx5 and Nkx2.5, but also with many other transcription factors essential for normal heart development, which makes Gata4 a very important component throughout embryogenesis (Rojas et al. 2008, Posch et al. 2010) (**Table 2.1**). Furthermore, insufficient formation of these interactions will result in the lack of gap junction proteins in the AV node. These gap junctions are important to have contractile delay between atrial and ventricular chambers (Munshi et al. 2009).

Many different ECM proteins and transcription factors play vital roles in heart embryogenesis; however, changes in expression and interactions among proteins and transcription factors has made the monitoring of each factor, as well as identification of each factor's importance, a challenging endeavor. Temporal differences in expression vary by species as do the relative expression levels. Studies investigating the role of these proteins and signaling molecules have been performed predominantly in small animals, such as mice or zebrafish; furthermore, the ability to examine the molecular signaling activity of these effectors in the context of human development is non-trivial. Biomimetic materials offer an important tool in investigating the role of these molecules in human development and in cardiac regeneration.

Differentiation of hPSCs into CMs mirrors, at least to some extent, the process of human heart development. Therefore, ECM proteins and growth factors reported above are critical for normal heart development and can influence stem cell differentiation. Additional ECM proteins, growth factors, and signaling pathways play important roles in human heart development as well, even if not directly implicated in causing abnormalities, and are therefore also essential to deriving CMs from hPSCs. To mimic

embryonic heart development throughout stem cell differentiation, specific cues are given to the cells through temporal manipulation of the culture environment and media composition. Across all the major cardiac differentiation protocols, including spontaneous EB formation (Zwi et al. 2009, Yang et al. 2008, Laflamme et al. 2007), forced aggregation (Burridge et al. 2011, Elliott et al. 2011), and direct monolayer differentiation (Zhang et al. 2012, Lian et al. 2012, Hazeltine et al. 2012, Lian et al. 2013), promoting and silencing specific signaling pathways (e.g. promoting Wnt/β-Catenin signaling pathways during early development/differentiation) (Naito et al. 2006, Ueno et al. 2007) via supplementation with growth factors is essential. These facts raise high potential of using hPSCs as tools to mimic human heart development.

Using materials, in combination with hPSCs, which can mimic the heart's natural microenvironment during development, will positively influence cell fate and maturation. Modulating delivery and expression of transcription factors using biomimetic materials can be used not only to study human heart development, but also to produce mature human CMs *in vitro* for heart regeneration.

3. BIOMATERIALS FOR CARDIAC TISSUE ENGINEERING

The dynamic, developing heart grows primarily due to CM proliferation during the embryonic and fetal stage of development (Li et al. 1996), which changes significantly after birth (Mollova et al. 2013). Although the heart continues to grow, post-fetal growth is primarily caused by hypertrophy (CM enlargement) (Laflamme and Murry 2011) in response to increased mechanical load (Russell, Motlagh and Ashley 2000, Frey and Olson 2003). Size and shape of CMs is important due to the influence of its capacity to

propagate electrical impulses and contractile force (Spach et al. 2004). Adult CMs have a length-to-width ratio of 7 to 9.5 (Gerdes et al. 1992) with a rod-shaped structure (Louch, Sheehan and Wolska 2011, Zhang et al. 2009); these features, in addition to others, can be used to distinguish between immature and mature CMs *in vitro*. Finally, the adult myocardium is composed of aligned, elongated CMs, which provides extreme challenges when using 2D culture systems (sheet differentiation); cells don't self-align in 2D culture and therefore produce myocyte disarray.

After birth, the heart's stiffness significantly increases and plays an important role in normal heart development and CM function (Jacot, Martin and Hunt 2010, Prakash et al. 1999). Numerous 2D studies, including the culture of hPSCs, neonatal rat CMs, and SC-CMs on material substrates that mimic physiological stiffness of the heart (~10-50 kPa), showed significant changes in stem cell pluripotency (Musah et al. 2012, Sun et al. 2012), differentiation (Engler et al. 2007, Engler et al. 2006), CM maturation and sarcomere alignment (Hazeltine et al. 2014, Hazeltine et al. 2012), and more uniform and stronger mechanical contractile force. On the contrary, stiffer substrate materials worsen CM function (Hazeltine et al. 2012). It has been shown that, during EB formation for SC-CM differentiation, EB size plays an essential role for successful cardiac differentiation due to the experienced force upon cells. Studies of encapsulated EBs in elastin-like hydrogels ranging between 0.45-2.4 kPa was shown successful; these EB-hydrogels were also electrically paced (Chung et al. 2012b). Contracting CMs cultured in medium (4 kPa) and stiff (up to 100 kPa) polyacrylamide hydrogels showed significant changes in contractile function and time of culture (up to 2 months) (Hazeltine et al. 2012).

Biomaterials are designed to mimic features of the native tissue microenvironment, provide 3D architecture, and enable tight cell-cell junctions to generate a better model platform of the human heart (**Fig. 3.1**). Additionally, biomaterials should support cell survival and proliferation while facilitating the production of reproducible and large-scale tissues for myocardial repair and providing specific environmental cues similar to native ECM proteins and stiffness found in the heart. Currently, several key aspects should be considered when using and designing new biomaterials: Will the biomaterial promote cell survival, adhesion, proliferation, and migration? Will the biomaterial degrade to allow cells to form a fully integrated tissue, and if so, will these degradation products cause toxic side-effects? And, will the biomaterial cause an inflammatory response to the host tissue? While many different biomaterials are currently investigated, some researchers attempt to form scaffold-free 3D tissues, using isolated rat or chick embryonic CMs (Shimizu et al. 2002b, Shimizu et al. 2002a) as well as hESC-CMs (Stevens et al. 2009), to overcome potential *in vivo* complications.

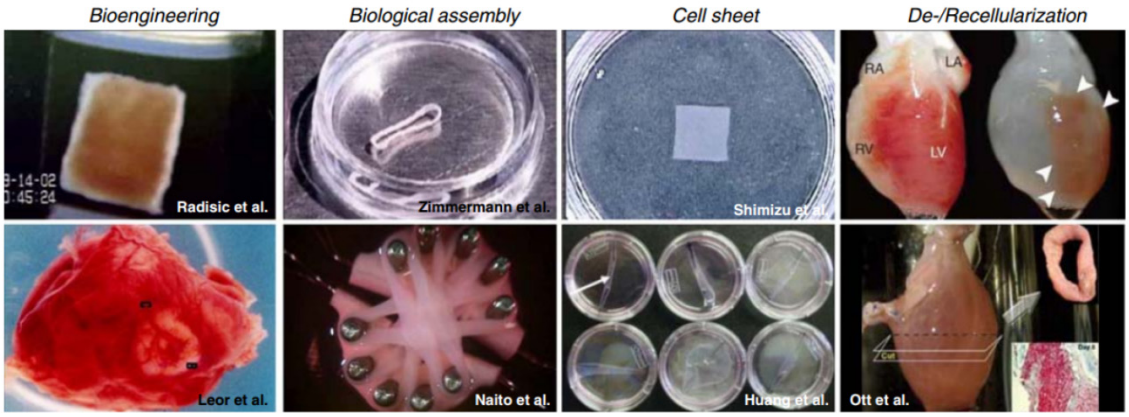

Fig. 3.1. Biomimetic approaches for in vitro cardiac tissue formation. Courtesy: Zimmermann WH and Cesnjevar R, *Pediatric Cardiology*. 2009;30:716-23.

Biomaterials, also called "biomimetic materials" are specifically designed and chosen to mimic the microenvironment of the tissue of interest. Materials for tissue engineering applications can be divided into three categories: natural, synthetic, and hybrid. Several examples include, but are not limited to:

Natural biomaterials: collagen, elastin, gelatin, hyaluronic acid, matrigel, laminin, fibrin(ogen)

Synthetic biomaterials: PEG, poly(lactic) acid, poly(vinyl) alcohol

Hybrid biomaterials: PEGylated proteins (e.g. PEG-fibrinogen)

Several key aspects are important to consider when creating a physiologically relevant model of the human heart: functional, synchronously contracting CMs, 3D tissue architecture, and cell alignment and maturation. Anisotropic tissue properties aids synchronous contraction of CMs by cell elongation and unidirectional calcium drift throughout samples. Several approaches using biomaterials have enhanced CM alignment

and elongation by topographical changes of the substrate surface, e.g. surface patterning (Chen et al. 2014, Kim et al. 2010) and microcontact-printing (McDevitt et al. 2002, Bray, Sheehy and Parker 2008), cyclic mechanical stretch (Mihic et al. 2014), electrical pacing, or a combination of more than one (Mansour et al. 2004) (**Fig. 3.2**).

While biomaterials can be used as a substrate for 2D cell culture, improve cell alignment and CM function, a 3D architecture is essential to enhance cell-cell and cell-material interactions *in vitro*, therefore allowing for more accurate drug-testing and myocardial repair applications.

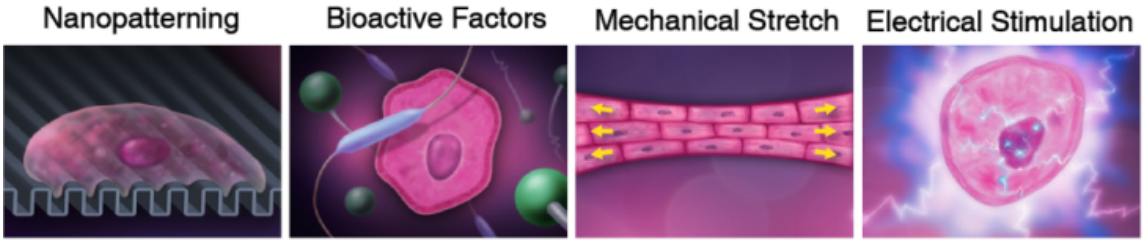

Fig. 3.2. Biomaterials enhance cell function by providing advanced microenviromental cues. Courtesy: Dunn et al., *Wiley Interdisciplinary Reviews Nanomedicine And Nanobiotechnology*. 2014;6:15-39.

Natural biomaterials present an interesting option for tissue engineering applications. Natural biomaterials have several advantages and disadvantages (**Table 3.1**), which should be considered based on the tissue of interest and future applications. Overall, biomaterials are rarely used alone, but in combination with others (mostly natural-natural or natural-synthetic) during 3D *in vitro* cell culture.

Table 3.1. Advantages and disadvantages of natural biomaterials.

Advantage	Disadvantage
No "foreign material" immune response	Poor mechanical properties
Provide "natural environment" *in vitro*	Variations in physical properties
	Animal-based origin
	Protein sterilization

Table 3.2. Advantages and disadvantages of synthetic biomaterials.

Advantage	Disadvantage
Easy to process and manufacture, highly tunable	Non-degradable materials inhibit tissue ingrowth and nutrient supply
Readily available	
Biocompatible and biodegradable	
Tunable and reproducible mechanical and physical properties	

Matrigel/Collagen Biomaterials

Matrigel, a basement membrane protein mixture secreted by mouse sarcoma cells (Hughes, Postovit and Lajoie 2010), has a very low shear modulus of about <35 Pa (Georges and Janmey 2005) and is commonly used as substrate to culture and expand hPSCs as well as differentiate them into 2D cardiac sheets (monolayer differentiation) (Lian et al. 2013, Zhang et al. 2012) but is not used as biomaterial for 3D tissue

production. Collagen, the most abundant protein in the human body, on the other hand, has been shown incapable to be used alone without conjunction of a secondary biomaterial (Gonen-Wadmany, Gepstein and Seliktar 2004), structural support (Serpooshan et al. 2013), or decellularized ECM (Duan et al. 2011). Collagen-based biomaterials used in cardiac tissue engineering are often in combination with Matrigel. Collagen/Matrigel biomaterials have been shown to enhance CM survival post-transplantation where implanted tissues lead to improved left ventricular function (Kutschka et al. 2006). Additionally, collagen/Matrigel biomaterials are used successfully to assemble engineered cardiac tissues (Turnbull et al. 2014, Zimmermann et al. 2002) or so called "biowires" (Nunes et al. 2013) providing an enhanced microenvironment for improved tissue function and maturation. Some key characteristics of this assembling technique are the extended polymerization time (~2 h) and the compaction of cell-laden tissues over time (**Fig. 3.3**).

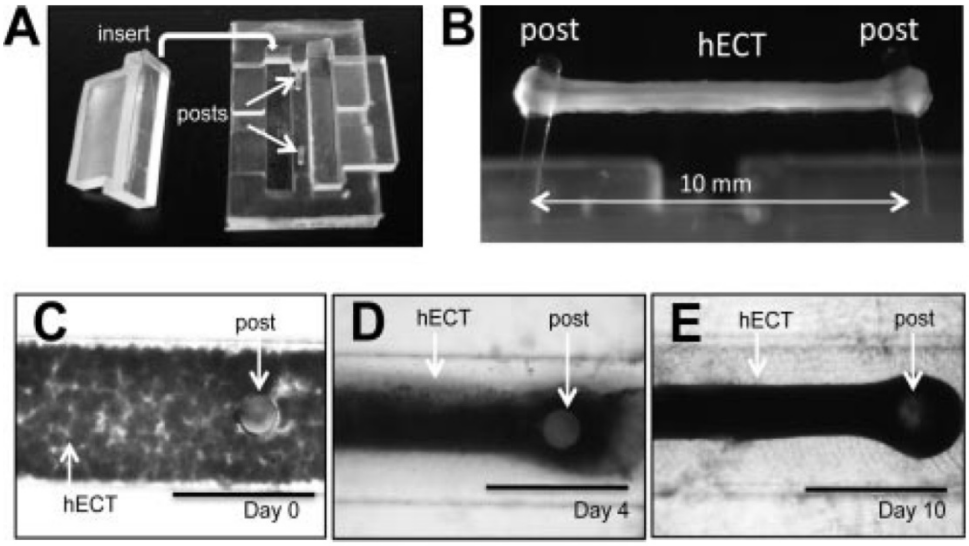

Fig. 3.3. Creation of human engineered cardiac tissues using a collagen/matrigel biomaterial. PDMS mold with removable inserts and integrated, deflecting posts (A). Side-view of an engineered heart tissue during contraction (visible post-deflection, B). Seeded SC-CM/collagen/matrigel cocktail can be evenly seeded into the desired mold where it compacts to form a dense, uniformly contracting cardiac tissue over time (C-E). Courtesy: Turnbull et al., *FASEB*. 2014;28:644-54.

Hyaluronan

Hyaluronan (HA), a glycoaminoclycan protein essential during embryonic development as well as CM performance (Chopra et al. 2012, Young and Engler 2011), is a widely used biomaterial in cardiac tissue engineering due to its ease for chemical modification (Shu et al. 2002, Burdick et al. 2005) that can be applied to mimic different stages of cardiac development. Once crosslinked, HA hydrogels can have stronger mechanical properties (elastic modulus ~10 kPa) than other natural biomaterials, like collagen. HA-based hydrogels have been used successfully for hESC (pre-aggregated cell masses)

growth in their pluripotent state (Gerecht et al. 2007) and to mimic mechanical cues during heart development (Young and Engler 2011).

Gelatin methacryloyl (GelMA) hydrogels

Gelatin, a water-soluble protein obtained from collagen (acid or alkaline hydrolysis), can be substituted with methacryloyl groups to form GelMA (**Fig. 3.4 A, B**) (Nichol et al. 2010). GelMA can be photocrosslinked with the addition of a photoinitiator to form 3D hydrogels. Gelatin is inexpensive and can be obtained in its denatured form from a large number of sources, still keeping important cell binding motifs (Galis and Khatri 2002, Van den Steen et al. 2002). GelMA can be prepared with varying methacryloyl substitution degrees (20%-80%) which directly influenced hydrogel stiffness and swelling properties (Nichol et al. 2010), important for 3D differentiation. Additionally, low gelatin methacryloyl substitution shows low elastic moduli (**Fig. 3.4 C**), which might be desired for cardiac differentiation in 3D GelMA hydrogels. It has been shown that 3T3 fibroblast cells (Nichol et al. 2010, Aubin et al. 2010) can be encapsulated into GelMA where cells remained viable, elongated and migrated within the hydrogel (Nichol et al. 2010). Finally, cells can degrade the hydrogel over time, where time of degradation depends on the methacryloyl substitution, cell type, and cell seeding density. Additionally, gelatin based substrates have been shown to improve CM maturation and enabled long-term culture (Lundy et al. 2013).

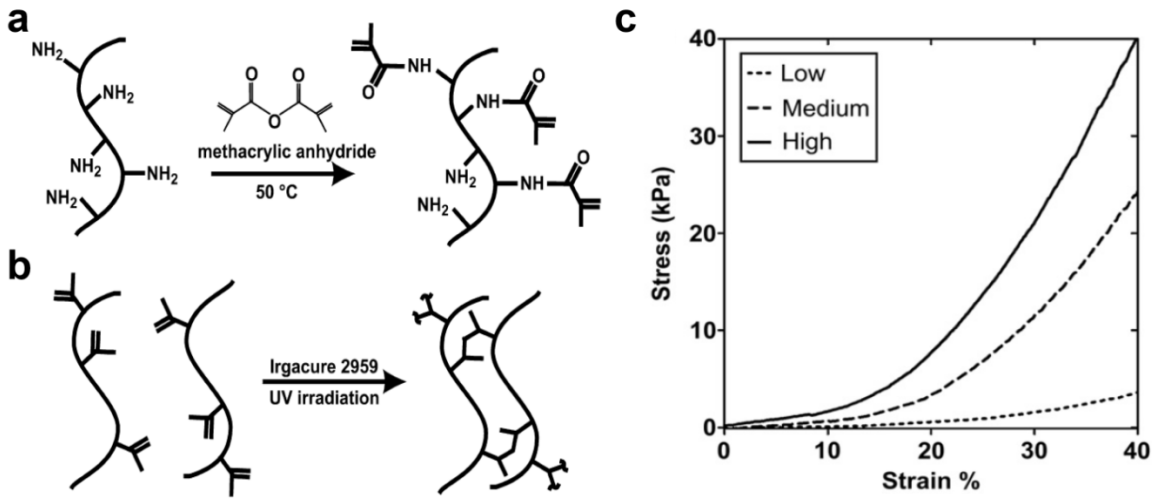

Fig. 3.4. Synthesis of gelatin methacryloyl and its mechanical properties. (A) Gelatin macromeres in affiliation with amine groups are reacted with methacrylic anhydride. (B) GelMA can form a hydrogel construct by the addition of a photoinitiator and light exposure. (C) Representative stress-strain curves of various degrees of methacrylated gelatin. Adopted from Nichol et al., *Biomaterials*. 2010;31:5536-44.

Fibrin and Fibrinogen-based hydrogels

Fibrin has successfully been used in cardiac tissue engineering, e.g. creating cardiac tissue patches (Tao et al. 2014), 3D cardiac tissues (Schaaf et al. 2011, Hansen et al. 2010, Schaaf et al. 2014) in combination with a bioreactor designs (Morgan and Black 2014). The natural biomaterial is also used in affiliation with the synthetic biomaterial PEG.

PEG conjugated proteins have normally different biological characteristics than their unconjugated counterparts due to variations after coupling, which adds challenges when using PEGylated hydrogels. However, fibrinogen-based hydrogels have been shown successful in wound healing and other surgical procedures, where PEG is

covalently coupled to fibrinogen (**Fig. 3.5**), which allows for cell attachment and controlled biodegradation of the material. The fibrinogen monomer has three potential integrin binding sites and other non-integrin binging sites that enhance cell adhesion when encapsulated. Based on the desired speed of degradation, PEG and fibrinogen contents can be varied to achieve fast (25:1), intermediate (100:1), or slow (150:1) biodegradation. Degree of biodegradation might also play an essential role when integrated into the host species for successful tissue integration on site (depending on the healing characteristics of the tissue) (Peled et al. 2007). Liquid PEG-fibrinogen precursor solution has the ability to form a gel-like hydrogel using non-toxic photoinitiators (Mironi-Harpaz et al. 2012) which accelerate the crosslinking process. It has been shown that PEGylation of various proteins can influence their biological activity and biophysical characteristics leading to undesired effects, like cell death, when combined and crosslinked with cells. Fibrin is one of the most abundant and widely used ECM proteins in the field of tissue regeneration. The precursor to fibrin is called fibrinogen, fibrin is part of the coagulation cascade, where fibrinogen is cleaved from thrombin after injury to form fibrin (fibrin is the most abundant component of blood clots). It has been shown that fibrinogen cleavage products during coagulation are bioactive. Fibrin gels have limited control over mechanical properties, unregulated biodegradation, and a tendency to become highly compacted by cellular remodeling. PEG-fibrinogen hydrogels have been proven successful in producing cell-laden tissues using smooth muscle cells (Almany and Seliktar 2005), NRVMs (**Fig. 3.6**) (Shapira-Schweitzer and Seliktar 2007), hESC-CMs (Shapira-Schweitzer et al. 2009), and others. Currently, PEG-fibrinogen is in clinical

trials in Europe, making it a desirable hybrid biomaterial for tissue engineering applications.

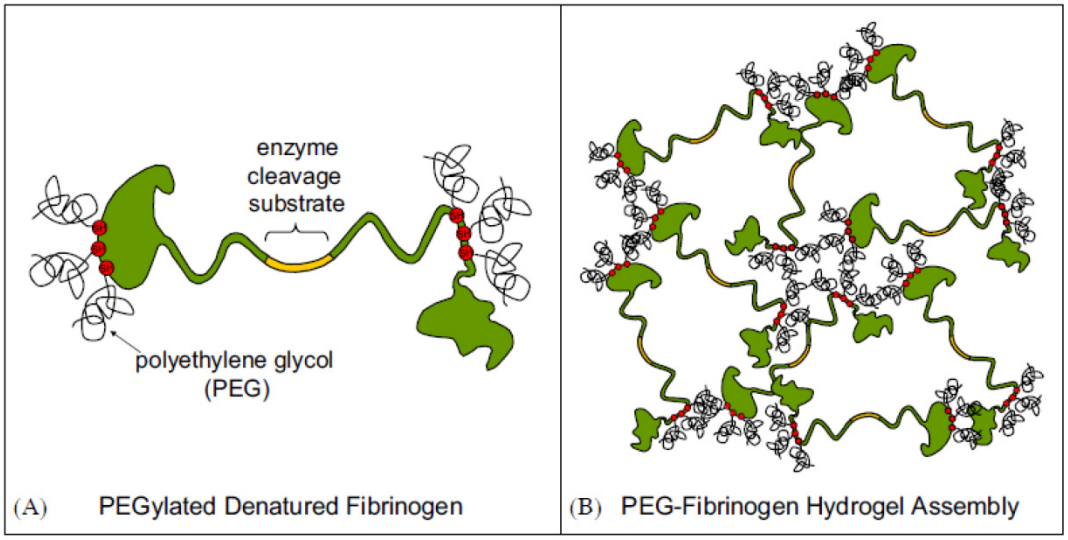

Fig. 3.5. PEG-fibrinogen hydrogel assembly. PEG is covalently conjugated to fibrinogen by unpaired thiols; PEG-fibrinogen also contains natural enzyme cleavage sites and can assemble to form a hydrogel by photoinitiation of unreacted PEG-DA. Courtesy: Almany L and Seliktar D., *Biomaterials*. 2005;26:2467-77.

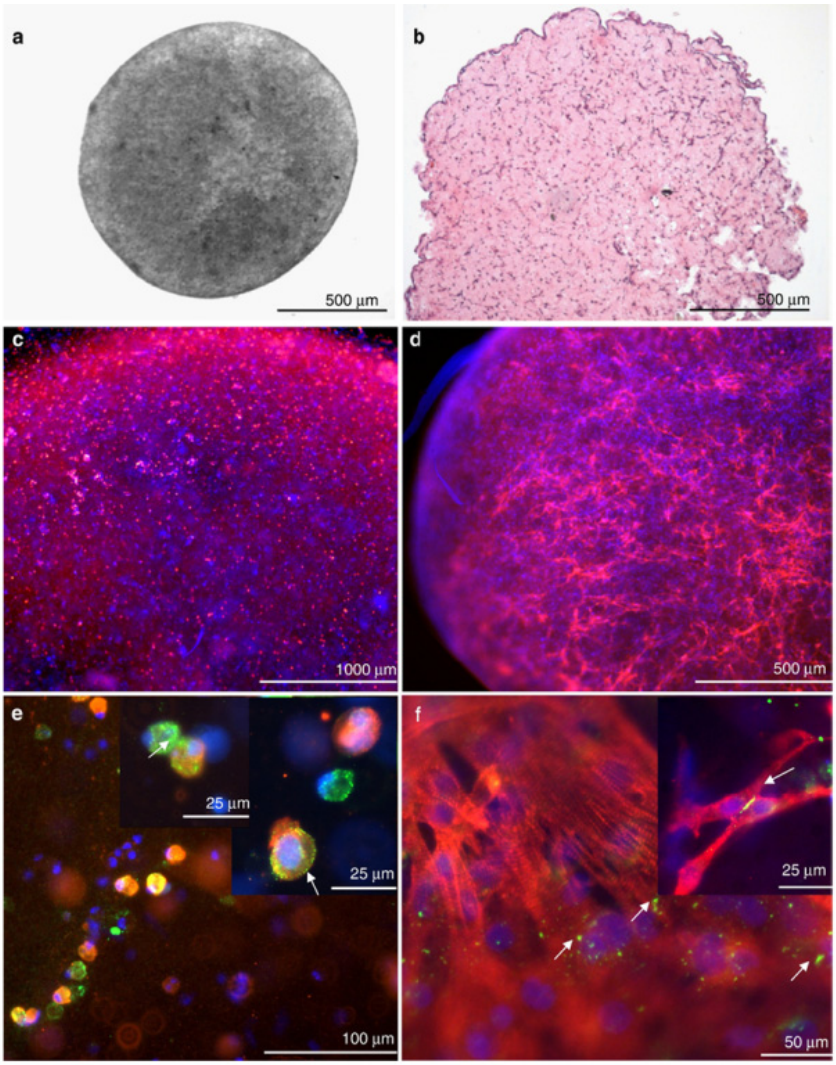

Fig. 3.6. PEG-fibrinogen hydrogels support NRVM culture. Tissue morphology of encapsulated NRVMs in PEG-fibrinogen (a), H&E staining of cardiac tissue 7 days post-encapsulation (b), fluorescently labeled tissue construct with the cardiac marker αSA on day 1 (c) and day 7 (d) show tissue formation over time. Additionally, Cx43 expression was visible on day 1 (e) and day 7 (f) of culture. Courtesy: Shapira-Schweitzer et al., *Journal of Molecular And Cellular Cardiology*. 2009;46:213-24.

4. SUMMARY OF CHAPTERS

4.1 Chapter 5

Human engineered heart tissues have potential to revolutionize cardiac development research, drug testing, and treatment of heart disease; however, implementation is limited by the need to use pre-differentiated cardiomyocytes (CMs). By providing a 3D poly(ethylene glycol)-fibrinogen hydrogel microenvironment, direct differentiate of human pluripotent stem cells (hPSCs) into contracting heart tissues was achieved with high reproducibility. This straight-forward, ontomimetic approach, imitating the process of development, requires only a single cell-handling step, provides reproducible results for a range of tested geometries and size scales, and overcomes inherent limitations in cell maintenance and maturation, while achieving high yields of CMs with developmentally appropriate temporal changes in gene expression. This study demonstrated that hPSCs encapsulated within this biomimetic 3D hydrogel microenvironment develop into functional cardiac tissues composed of self-aligned CMs with evidence of ultrastructural maturation, mimicking heart development, and enabling investigation of disease mechanisms and screening of compounds on developing human heart tissue.

4.2 Chapter 6

Drug-induced changes of the developing human heart are unpredictable and difficult to understand due to the lack of available *in vitro* platforms of human based CMs. In this study we hypothesize that contributing factors leading to the formation of congenital heart defects can be identified by analyzing changes during hiPSC differentiation in

response to cardiac mutagens, including the known teratogen thalidomide. Thalidomide caused congenital birth defects in more than 10,000 newborns and is known to act in a species-dependent manner, making it an interesting model-drug to study with the help of our *in vitro* 3D developing human engineered cardiac tissue (3D-dhECT) model. The production of 3D-dhECTs is used as a model system of the developing heart to determine thalidomide-induced changes in a human-based *in vitro* model. In this chapter we showed that our 3D-dhECT platform is robust and can be used to identify thalidomide-induced changes during stem cell differentiation. Thalidomide and control treatments were administered to 3D-dhECTs starting on day 1 of differentiation. Early during differentiation, changes in tissue formation and tissue growth were detected between thalidomide-treated and control tissues. All control and thalidomide-treated 3D-dhECTs started to spontaneously contract, although initial areas of contraction were visualized one or two days later in thalidomide-treated 3D-dhECTs than age-matched controls and the frequency of contraction was consistently slower than control 3D-dhECTs. Differences in tissue architecture, cell number per tissue, as well as sarcomere and mitochondria development were also detected in 3D-dhECTs, which had not yet been reported. We demonstrated that our 3D-dhECT approach can efficiently detect early and late stage thalidomide-induced changes, making it a suitable developmental drug-testing platform to screen future pharmaceuticals.

4.3 Chapter 7

The use of human CMs for regenerative medicine applications is limited by their immature nature, as well as low viability and poor integration once injected into the host

myocardium. We developed a reproducible, high-throughput microsphere production approach using hiPSC encapsulation in PEG-fibrinogen hydrogels. Our single-cell handling approach allows us to manufacture hiPSC-laden microspheres in a custom-built microfluidic device, followed by direct differentiation of encapsulated hiPSCs to form cardiac microspheres with high efficiency. HiPSC grew within and beyond the PEG-fibrinogen hydrogel boundaries, producing soft (<40 Pa) tissues that started spontaneous contraction on day 8 of differentiation, even after applied shear stress. Cardiac differentiation was efficient (>70%), with microsphere CMs responding to the β-adrenergic agonist isoproterenol, antagonist propranolol, and receptor blocker sotalol. CMs also responded to outside pacing frequencies up to 6.0 Hz, which was higher than what we previously detected with 3D-dhECTs. Over time, cells remodeled their provided PEG-fibrinogen hydrogel and produced their own ECM proteins, while forming cell-cell junctions and aligned myofibril structures. This study demonstrated the successful production of hiPSC-laden microspheres using a scalable tissue fabrication approach that resulted in high CM yield and cells surviving applied shear, making it a favorable platform for myocardial regeneration cell production.

4.4 Chapter 8

Direct stem cell encapsulation and cardiac differentiation within supporting biomaterial scaffolds are critical for reproducible and scalable production of the functional human tissues needed in regenerative medicine and drug-testing applications. Producing cardiac tissues directly from pluripotent stem cells rather than assembling tissues using pre-differentiated cells can eliminate multiple cell-handling steps that otherwise limit the

potential for process automation and production scale-up. This objective focused on the translation of the previous tissue production process using poly(ethylene glycol)-fibrinogen hydrogels towards other widely used biomaterials. The naturally modified, photocrosslinkable, widely used, and printable gelatin methacryloyl (GelMA) biomaterial was chosen for this study. The presented studies demonstrate that low density GelMA hydrogels can be formed rapidly using visible light (<1 min) and successfully employed to encapsulate human pluripotent stem cells (hPSCs) while maintaining high cell viability. GelMA supported tissue growth and dynamic remodeling and facilitated high efficiency cardiac differentiation (>70%) to produce spontaneously contracting GelMA human engineered cardiac tissues (GEhECTs). GEhECTs showed first spontaneous contractions on day 8 of differentiation, with synchronicity, frequency, and velocity of contraction increasing over time. GEhECT cardiomyocytes displayed well-defined and aligned sarcomeres spaced at 1.85 ± 0.1 μm and responded appropriately to drug treatments, including the β-adrenergic agonist isoproterenol and antagonist propranolol, as well as to outside pacing up to 3.0 Hz. Overall results demonstrate that GelMA is a suitable biomaterial for the production of developing cardiac tissues and has the potential to be employed in scale-up production and bioprinting of GEhECTs.

5. ENCAPSULATION AND DIFFERENTIATION OF HIPSCS IN 3D PEG-FIBRINOGEN HYDROGEL SCAFFOLDS

5.1 Introduction and Motivation

Limited access to samples of human cardiac tissue severely impedes cardiology research, drug testing, and clinical cardiac regeneration efforts. Predicting cardiac toxicity and the triggering of arrhythmias represents a major hurdle for pharmaceutical compound development, resulting in 20-30% of drugs receiving a black box warning or being withdrawn from the market (Lasser et al. 2002, Frank et al. 2014) and having devastating economic and societal consequences. Human pluripotent stem cells (hPSCs) provide the potential to produce large quantities of physiologically relevant, species-specific and even patient-specific cardiomyocytes (CMs) *in vitro* through directed differentiation. Engineered human heart tissues created from such cells can address the challenge of widespread cardiac tissue access, thereby providing the ability to study normal and abnormal human heart development, as well as revolutionizing high-throughput drug screening, modeling of human cardiac diseases, and the field of regenerative medicine. However, these tissues must develop structural and functional properties representative of the native human myocardium (Yang, Pabon and Murry 2014). In addition, their fabrication needs to be straightforward, automatable, scalable, and highly reproducible (Bertassoni et al. 2014). Achieving these goals has proven difficult.

Originally, hPSC differentiation protocols used cell aggregation to create 3D embryoid bodies (EBs) (Zwi et al. 2009, Kattman et al. 2011), which facilitated hPSC differentiation into spontaneously beating stem cell-derived cardiomyocytes (SC-CMs). To overcome the issues of inefficient CM production and irregular reproducibility using

this EB cardiac differentiation protocol, researchers have recently focused on modulating the chemical environment of differentiating SC monolayers. Through the temporal introduction of soluble factors, this approach strives to replicate the cues directing native heart development (Lev, Kehat and Gepstein 2005, Kattman et al. 2011). These highly efficient 2D differentiation protocols have revolutionized CM production from hPSCs (Lian et al. 2013, Burridge et al. 2014); however, this monolayer-based approach does not replicate the fundamental 3D nature of myocardial development.

Tissue engineering offers a 3D solution to the 2D cell culture problem. The established paradigm for creation of engineered heart tissues requires a source of CMs, either isolated from rodent hearts or pre-differentiated from PSCs. Following dissociation, the CMs are combined with a biomaterial scaffold and re-assembled into cardiac tissues (Nunes et al. 2013, Turnbull et al. 2014, Zhang et al. 2013, Schaaf et al. 2011, Tulloch et al. 2011). Although this approach has been successful in creating human cardiac tissue, the required pre-differentiation and subsequent dissociation of spontaneously contracting SC-CMs precludes direct production of mature cardiac tissues from hPSCs. This hinders the investigation on the importance of a cellular microenvironment during early human cardiac development. The multiple cell-handling steps involved create processing and fabrication challenges, and limit the ability for tissue biomanufacturing. They also disrupt important cell-cell junctions, and cause a high degree of cell loss. Establishing a simple workflow that reduces the number of cell-handling steps and provides a 3D microenvironment throughout differentiation would transform the fabrication of human cardiac tissues, which will be critical for their

successful utilization in developmental biology research, high-throughput pharmaceutical screening, and generation of mature SC-CMs for basic science and clinical applications.

Natural biomaterials (*e.g.*, fibrin, gelatin, Type-I collagen) have been frequently used to support classic engineered cardiac tissue formation (Schaaf et al. 2011, Nunes et al. 2013, Mihic et al. 2014) but present limitations due to their inherent batch-to-batch variability, lack of immediate structural support, and the degradation of contractility during long-term cardiac tissue maintenance *in vitro*. In comparison, synthetic materials are completely defined and rapidly crosslinkable with tunable properties, but typically lack biological components inherent to natural scaffolds. Hybrid biomaterials, having both natural and synthetic components, provide unique advantages for tissue engineering applications. Particularly relevant to forming cardiac tissues, hybrid biomaterials have tunable mechanical properties combined with natural sites to support cell survival, adhesion, proliferation, and differentiation, as well as degradation and remodeling of the scaffolds (Shapira-Schweitzer and Seliktar 2007, Mironi-Harpaz et al. 2012). Therefore, hybrid biomaterials, such as poly(ethylene glycol)-fibrinogen (PEG-fibrinogen), enable properties of both components to be exploited in guiding hPSC differentiation and the process of human engineered cardiac tissue formation (**Table 5.1**).

Here we asked whether it is possible to directly create a 3D tissue construct emulating key stages of cardiac embryologic development, growth, and maturation in an ontogeny-mimicking (*i.e.*, ontomimetic) model of human heart muscle. We found that human induced pluripotent stem cells (hiPSCs) can successfully be differentiated into contracting CMs while encapsulated within PEG-fibrinogen hydrogels, thereby directly forming functional 3D developing human engineered cardiac tissues (3D-dhECTs) with a

single cell-handling step during the cell-encapsulation process. For the first time, we have successfully encapsulated and differentiated hiPSCs within a controlled biomimetic hydrogel microenvironment, achieving developmentally-appropriate temporal changes in gene expression, high CM yield, and calcium handling properties similar to age-matched CMs produced using high-efficiency 2D monolayer differentiation. Furthermore, CMs within our 3D-dhECTs became progressively anisotropic without external electromechanical stimuli and developed ultrastructural features characteristic of mature CMs. These results demonstrate that providing a 3D architecture during and after hiPSC differentiation without disturbing cell-cell junctions and providing continuous 3D cell-cell and cell-material interactions is advantageous for creating an ontomimetic model of native human myocardium.

Table 5.1. 3D encapsulation and maintenance of stem cells and stem cell-derived cardiomyocytes.

Author	Type of Hydrogel/ 3-D matrix material	Encapsulated / suspended cells	End stage cells	CM differentiation after encapsulation	CM differentiation protocol	Characterization of CM differentiation	Longest time reported for encapsulated cells
(Bearzi et al. 2014)	PEG-fibrinogen	miPSC	Mouse iPSC-derived CM	Yes	(Rizzi et al. 2012)	Immunofluorescence: αSA and Cx43 PCR: Mhy6 and cTnnI	14 days
(Shapira-Schweitzer et al. 2009)	PEG-fibrinogen	hESC-CM (Kehat et al. 2001)(hESC H9.2 line)	Human embryonic stem cell-derived CM	No	N/A	Immunofluorescence: αSA and CX43 TEM Functional: contractile displacement amplitude, drug treatment.	14 days
(Liu, Collins and Suggs 2006)	PEG-fibrinogen	R1 murine ESC	R1 murine embryonic stem cells EBs	No	(Liu and Roy 2005)	PCR: brachyury	12 days
(Geuss et al. 2015)	PEGylated fibrin hydrogels	Mouse HL-1 CMs (Claycomb et al. 1998)	Mouse HL-1 CMs	No	N/A	Immunofluorescence: αSA and Cx43 Functional: contractile activity (loss of activity)	14 days
(Ruan et al. 2015)	Type I collagen plus basement membrane proteins (Tulloch et al. 2011)	HESC (H7 line) and hiPSCs (IMR90 and IBJ line)	Tripotential cardiovascular progenitor (CVP) population (CMs, endothelial cells and smooth muscle-like cells)	Yes	(Yang et al. 2008) (Kattman et al. 2011) (Paige et al. 2012)	Immunohistochemistry: Nkx 2.5 and cTnT Flow cytometry, Western: cTnT PCR: αMHC, βMHC and Nkx2.5. Functional: calcium transients and contractility	14 days
(Ban et al. 2014)	PA-RGDS	mESC (J1)-CM (EBs)	Mouse embryonic stem cell (J1) derived CM	No	N/A	Live/dead stain. Flow cytometry for cardiac markers	14 days
(Zhao et al. 2014)	Microcapsules with an alginate hydrogel core or sodium carboxymethyl cellulose for microcapsules with a liquid core.	Murine ESCs	Murine ES-derived CM (beating aggregates)	Yes	DMEM+BMP-4, bFGF for 3 days, followed by DMEM w/ 20% FBS	PCR: brachyury, Nkx2.5, and cTnT Functional: counting beating focci	14 days
(Bauwens et al. 2005)	Agarose hydrogel microcapsules (Ryan, Nguyen and Sullivan 1995) inoculated into spinner flasks	mESCs	Mouse ES-derived CM	Yes	(Zandstra et al. 2003)	PCR: MLC2v and αMHC. Immunoflorescence: α-actin (MF20 and EA 53)	14 days
Current	PEG-fibrinogen	hiPSC (IMR90-1 line from WiCell)	Human iPSC-derived CMs	Yes	(Lian et al. 2013)	Flow cytometry, PCR, Immunofluorescence, TEM Functional: Calcium transient, drug treatment, MEA	4 months
Current	PEG-fibrinogen	hiPSC (19-9-11 line from WiCell)	Human iPSC-derived CMs	Yes	(Lian et al. 2013)	Flow cytometry: cTnT Functional: video analysis	>1 month

Abbreviations:
CM: cardiomyocytes
cTNT: cardiac troponin T
iPSC: induced pluripotent stem cells
PA-RGDS: Arg- peptide amphiphile (PA) Gly-Asp-Ser (RGDS)
PEG: poly(ethylene glycol)

5.2 Materials and Methods

5.2.1 HiPSC expansion and culture

IMR-90 Clone 1 and 19-9-11 human induced pluripotent stem cells (hiPSCs) were purchased from WiCell and maintained at 37ºC, 5% CO_2, and 85% relative humidity. HiPSCs were cultured as colonies on hESC qualified Matrigel (BD Biosciences) using mTeSR-1 medium (Stem Cell Technologies). HiPSCs were passaged using Versene (Life Technologies) and 5 μM ROCK inhibitor (Y-27632, R&D Systems) was added to the mTeSR-1 medium for 24 h post-seeding.

5.2.2 Glass acrylation and PDMS mold preparation

All chemicals were purchased from Sigma-Aldrich unless specified otherwise. In order to accurately track tissue development over time, microisland tissues were fabricated and immobilized on acrylated glass coverslips. Circular glass coverslips (21 mm, No. 1, Fisher Scientific) were cleaned using 30% hydrogen peroxide (H_2O_2) and 70% sulfuric acid (H_2SO_4), followed by thorough ethanol rinsing and air-drying prior to glass acrylation. Cleaned glass coverslips were incubated overnight using diluted acetic acid (9%), 3-(Trimethoxysilyl) propyl methacrylate, and 200-proof ethanol at 25°C. After incubation, the acrylated glass coverslips were rinsed in ethanol followed by air-drying.

Polydimethylsiloxane (PDMS) molds were prepared by combining SLYGARD 184 silicone elastomer curing agent and SLYGARD 184 elastomer base (Dow Corning Corporation). PDMS precursor solution was transferred onto a glass slide fixed with 200 μm thick spacers on all edges. A second slide was placed on top and the entire assembly was bound together by binder clips. The assembly was transferred into an oven at 70ºC

for 2 h for curing of the PDMS. The cured PDMS was peeled off the assembly and three cylindrical holes with diameters of 6 mm were punched into the PDMS mold using a cork borer. The PDMS mold and acrylated glass coverslips were soaked in 70% ethanol for 24 h followed by complete air-drying under UV-light for at least 24 h to ensure complete sterilization. Before use in cell encapsulation, the PDMS mold with three cylindrical holes for tissue production was placed on the circular, acrylated glass coverslips and pressed down firmly to prevent leakage.

5.2.3 PEG-fibrinogen synthesis and precursor preparation

PEG-fibrinogen was prepared as previously described (Dikovsky, Bianco-Peled and Seliktar 2006). First, poly(ethylene glycol)-diacrylate (PEG-DA) was prepared by reacting linear PEG-OH (10 kDa) with acryloyl chloride and triethylamine. The product was precipitated in ice-cold diethyl ether, followed by vacuum drying for 48 h. The degree of acrylation was quantified by proton ^{1}H NMR.

For PEG-fibrinogen synthesis, tris(2-carboxyethyl) phosphine hydrochloride (TCEP-HCl) was combined with 7 mg/ml fibrinogen in PBS with 8 M urea (1.5:1 TCEP to fibrinogen molar ratio). Next, for PEGylation of fibrinogen, PEG-DA was reacted with fibrinogen (4:1 molar ratio) for 3 h, precipitated in acetone and dissolved in PBS with 8 M urea. The reacted PEG-fibrinogen was dialyzed against PBS at 4ºC for 48 h followed by lyophilization. To characterize the PEGylated product, fibrinogen content was measured using Pierce BCA assay (Thermo Scientific).

Lyophilized PEG-fibrinogen powder was re-dissolved in PBS to obtain a final fibrinogen concentration of 10 mg/ml. PEG-fibrinogen precursor solution was prepared

by combining PEG-fibrinogen with 1.5% triethanolamine (TEOA), 3.96 µl/ml N-vinyl pyrrolidone (NVP), and 10 mM eosin Y (Fisher Scientific) photoinitiator (in PBS) (Franco, Price and West 2011).

5.2.4 HiPSC dissociation and microisland formation

HiPSCs were dissociated using Versene (cluster hiPSC encapsulation for IMR90-1 and 19-9-11 hiPSC lines) or Accutase (single IMR90-1 hiPSC encapsulation, Innovative Cell Technologies) to form 3D developing human engineered cardiac tissue (3D-dhECT) microislands (day -3). Cluster or single hiPSCs were resuspended in mTeSR-1 medium and centrifuged for 5 min at 200 g. The supernatant was aspirated using a glass Pasteur pipette and complete aspiration was insured through inversion of the tube without disturbing the cell pellet. Cluster or single hiPSCs were resuspended uniformly at a density of $55 \pm 8.5 \times 10^6$ hiPSCs/ml of PEG-fibrinogen precursor solution using a wide orifice pipette tip. 10 µl of this mixture was added to each of the three cylindrical holes in the PDMS mold on acrylated glass coverslips and crosslinked using visible light (intensity of 48 mW/cm^2 at a distance 3 cm away) for 1 min. The PDMS mold surrounding the three crosslinked hydrogels (3D-dhECT microislands) was then carefully detached and the acrylated glass coverslip with covalently coupled microislands was transferred to a 12-well plate (three tissues per well) and cultured in 2 ml mTeSR-1 medium supplemented with 5 µM ROCK inhibitor for 24 h (day -3). On the two days following encapsulation (day -2, day -1), 3D-dhECT microislands were cultured in mTeSR-1 medium with daily medium exchange. On the third day post-encapsulation (day 0), cardiac differentiation was initiated. All encapsulations resulted into successfully contracting cardiac tissues.

5.2.5 2D monolayer differentiation of hiPSCs

For 2D monolayer differentiation of hiPSCs (IMR90-1 hiPSC line), the composition of the media and timeline of differentiation was based on a previously published method (Lian et al. 2013); 2D differentiating monolayers were used as controls. Briefly, hiPSCs were dissociated using Accutase, resuspended in mTeSR-1 medium, counted, and centrifuged. HiPSCs were seeded at 1×10^6 hiPSCs/well in a Matrigel coated 6-well plate with 4 ml mTeSR-1 medium + 5 μM ROCK inhibitor for 24 h (day -4). From day -3 until day 0, mTeSR-1 medium was replaced daily. On day 0 of differentiation, medium was changed to 4 ml RPMI/B27 without insulin (Life Technologies) + 12 μM CHIR99021 (Selleckchem) for 24 h. Medium was changed to 4 ml RPMI/B27 without insulin for an additional 48 h. On day 3, 2 ml RPMI/B27 without insulin and 5 μM IWP2 (Tocris) were combined with 2 ml old RPMI/B27 without insulin ("combined medium") and cells were cultured until day 5, when medium was changed back to RPMI/B27 without insulin. On day 7 and every three days thereafter, medium was replaced with RPMI/B27 (Life Technologies).

5.2.6 3D cardiac differentiation of cluster and single hiPSCs in PEG-fibrinogen hydrogels

Cluster and single encapsulated hiPSCs underwent differentiation following the same protocol used for the 2D monolayer differentiation of hiPSCs. On day 0 of differentiation, medium was changed from mTeSR-1 to 2 ml RPMI/B27 without insulin + 12 μM CHIR99021 per well. After 24 h (day 1), medium was changed to 2 ml RPMI/B27 without insulin. On day 3 of differentiation, medium was replaced with 1 ml

fresh RPMI/B27 without insulin, 5 μM IWP2, and 1 ml old RPMI/B27 without insulin and cultured for an additional 48 h. On day 5, medium was switched back to 2 ml RPMI/B27 without insulin and followed by 2 ml RPMI/B27 medium on day 7, medium being replaced thereafter every three days.

5.2.7 HiPSC viability and immunofluorescence

HiPSC viability on day -2 (24 h post-encapsulation) was assessed using a LIVE/DEAD® viability kit (Molecular Probes) following manufacturer's instructions. Confocal Z-stacks (step size = 5 μm) were taken through the entire tissue thickness at several randomly selected locations within each 3D-dhECT microisland (n = 3) using a Nikon A1R laser-scanning confocal microscope and NIS Elements software (Nikon). To assess 3D-dhECT protein expression of proliferation markers proliferating cell nuclear antigen (PCNA) and Ki67, cardiac markers cardiac troponin T (cTnT) and sarcomeric α-actinin (αSA), and gap junction protein connexin 43 (Cx43), tissue samples were prepared for immunofluorescence. To assess the area and circularity of single CMs, dissociated 3D-dhECT cells were immunostained using αSA and Caveolin 3 (T-tubules). First, samples were fixed using methanol for PCNA, 4% paraformaldehyde (Electron Microscopy Sciences) for Ki67, cTnT, αSA, and Caveolin 3, or 50/50 ice-cold acetone/ethanol for Cx43. Fixed tissues and dissociated cells were permeabilized with PBS-T (PBS with 1% bovine serum albumin (BSA) and 0.2% Triton X-100) and blocked (3% fetal bovine serum (FBS, Atlanta Biologicals) in PBS). Samples were consecutively incubated in primary and secondary antibody (**Table 5.2**). All primary and secondary antibodies were applied for at least 24 hours at 4ºC. Cell nuclei were stained with 4',6-diamidino-2-

phenylindole (DAPI, Molecular Probes). All fluorescently labeled samples were visualized using a Nikon A1si confocal microscope. For subsequent characterization studies and comparisons to 2D monolayers, cluster encapsulated 3D-dhECTs were used.

5.2.8 Tissue area growth

Throughout the initial stages of hiPSC encapsulation, images of entire tissues from both hiPSC lines were acquired daily at low magnification using a phase contrast microscope (Ti Eclipse, Nikon) equipped with an Andor Luca S camera. Tissue edges were identified and the lateral surface area of 3D-dhECTs was analyzed in ImageJ with standard analysis plugins (n = 3-4 tissues per hiPSC line). Tissue growth was based on normalized day 0 tissue surface area.

5.2.9 Flow cytometry

On day 20, 2D monolayers were washed with PBS and incubated in 0.25% trypsin (EDTA, Mediatech) at 37ºC for 5 min. Age-matched 3D-dhECTs from both hiPSC lines were washed with PBS followed by 2 h incubation at 37ºC on a rotator (Boekel Orbitron Rotator, Model 260250, Boekel Scientific) with collagenase Type 2 (1 mg/ml, Worthington) in 120 mM NaCl, 5.4 mM KCl, 5 mM $MgSO_4$, 5 mM Na-pyruvate, 20 mM glucose, 20 mM taurine, and 10 mM HEPES (pH 6.9) supplemented with 30 µM $CaCl_2$, followed by incubation in 0.25% trypsin (EDTA) at 37ºC for 5 min. All cells (in 2D monolayers and 3D-dhECTs) were then singularized by pipetting (using a 1000 µl pipette), transferred to a centrifuge tube with RPMI20 medium (RPMI 1640 medium with 20% FBS) and centrifuged for 5 min at 200 g. The supernatant was removed and the cell

pellet was resuspended in 4% paraformaldehyde and incubated for 20 min at 25°C. Cells were centrifuged for 5 min at 200 g, supernatant was aspirated and the cell pellet was resuspended in 90% cold methanol and incubated at 4ºC for 15 min. The fixed cells were blocked with 5% BSA in PBS for 5 min and centrifuged for 5 min at 200 g. After washing two more times with 5% BSA in PBS, cells were incubated in 100 µl primary antibody (**Table 5.2**) diluted in 0.5% BSA and 0.1% Triton X-100 in PBS. To analyze CMs, proliferating cells, and fibroblasts, the primary antibody combinations cTnT/Ki67 and cTnT/P4HB were chosen. After incubation at 4ºC overnight, cells were washed with 0.5% BSA and 0.1% Triton X-100 in PBS, which was repeated twice. Cells were further incubated in 100 µl secondary antibody (**Table 5.2**) diluted in 0.5% BSA and 0.1% Triton X-100 in PBS for 30 min at room temperature, protected from light. Finally, cells were washed with 0.5% BSA and 0.1% Triton X-100 in PBS three times and resuspended for analysis in 500 µl 5% BSA in PBS. Samples were run on a BD Accuri C6 (BD Biosciences) and were analyzed using FlowJo V10.

5.2.10 Reverse transcription quantitative PCR

Total RNA was extracted from hiPSCs, 2D monolayers, and 3D-dhECTs on days 0, 10, 20, and 30 of differentiation ($n = 3$ independent differentiations) using Nucleospin RNA kit (Macherey-Nagel). Reverse transcription quantitative PCR (RT-qPCR) was performed using SuperScript III Platinum One-Step RT-qPCR kit (Invitrogen) in conjunction with Taqman probes (Integrated DNA Technologies). Equal amounts of RNA (50 ng/19 µl) were used for each measurement. The RT-qPCR protocol consisted of 1 cycle at 50 ºC (15 min), 1 cycle of 95ºC (3 min), 45 cycles of 95ºC (15 s)

and 55ºC (30 s). Gene expression levels were normalized to the housekeeping gene *GAPDH* using the 2-ΔC_t method. Duplex RT-qPCR was used for *Oct4*, *MYL2v*, and *Cx43* genes; *αMHC*, *βMHC*, and *GAPDH* were quantified separately (**Table 5.3**).

5.2.11 Frequency of contraction

Video recordings of spontaneously contracting 3D-dhECTs were acquired on a phase contrast microscope (Ti Eclipse, Nikon) using a high speed camera (Andor Luca S) to determine frequency of contraction. The number of contractions per minute at early (day 8-11), intermediate (day 20-25), late (day 30-33, $n = 3$ independent differentiation batches), and long-term (days 50, 60, and 90, $n = 2$ tissues) time points were analyzed using NIS Elements and ImageJ software. Contractility differences between single and cluster encapsulated hiPSCs were determined by video analysis of the relative changes in transmitted light intensity of spontaneously contracting cardiac tissues on day 14 of differentiation.

5.2.12 Sarcomere alignment and spacing in 3D cardiac tissues

Throughout the differentiation process, sarcomere alignment of days 20, 30, and 124 αSA-stained cardiac tissues was analyzed using ImageJ software version 1.48q (NIH) in affiliation with the fast Fourier transform (FFT) analysis tool. Images were imported into ImageJ, and sarcomere pattern formation over time was assessed by increasing periodicity, alignment, and pattern convergence in the FFT output spectra. Sarcomere alignment and spacing was also determined by manually drawn linear paths along visible sarcomeres. In addition to sarcomere alignment, day 124 αSA-stained CMs were used to

quantify sarcomere spacing; for this, manually drawn linear paths along well-defined sarcomeres (n = 200 CMs) were used to collect an intensity profile for each chosen CM where distances between peaks were analyzed using Microscoft Excel. Sarcomeres chosen for alignment and spacing were selected based on continuity of sarcomeres in a single field of view.

5.2.13 3D-dhECT CM size, circularity, length-to-width ratio and Caveolin 3 immunofluorescence staining

For size and circularity measurements, day 52-60 tissues were dissociated into single cells (see tissue dissociation section in Flow Cytometry) and re-plated onto fibronectin coated PDMS coverslips. After three days, cells were immunofluorescently stained and imaged. Cells were analyzed for their cell area and circularity using ImageJ software with standard analysis plugins (n = 32 CMs). These samples were also used for αSA/Caveolin 3 staining. Four month old 3D-dhECTs were enzymatically dissociated and seeded onto fibronectin-coated well plates. 24 hrs after dissociation, phase contract images were taken of three separately dissociated tissues. Length and width of 60 cells were measured using ImageJ and the ratio was calculated. Cell clusters of two or more cells were excluded for this analysis.

5.2.14 Calcium handling

To immobilize cells for proper calcium transient acquisition, glass coverslips (21 mm, No. 1, Fisher Scientific) were coated with PDMS using a WS-400-6NPP spin coater (Laurell Technologies Corporation). Briefly, SLYGARD 184 silicone elastomer curing

agent was mixed with SLYGARD 184 elastomer base (Dow Corning Corporation) at a ratio of 1:10, applied on the glass coverslips and evenly spin-coated to obtain PDMS coated coverslips. These were cured at 60ºC for several hours, sterilized using 70% ethanol, and then dried under sterile conditions for at least 24 h. In order for successful single CM attachment, 25µg/ml fibronectin in ice-cold ultrapure water was applied on PDMS coated coverslips and incubated for at least one hour at room temperature.

Day 14 2D monolayers and 3D-dhECTs were dissociated using 0.25% trypsin (EDTA) at 37ºC for 5 and 8 min, respectively. Cells were singularized by pipetting, added to RPMI20 medium (Lian et al. 2012), and centrifuged for 5 min at 200 g. Singularized cells were resuspended in RPMI20 + 5 µM ROCK inhibitor and transferred onto fibronectin-coated PDMS-glass coverslips. Cells were incubated for 48 h to ensure uniform cell attachment. Medium was then switched to RPMI/B27 and cells maintained for 3 to 5 days. CM calcium transient recordings were obtained using an IonOptix Myocyte Calcium and Contractility Recording System. Samples were incubated in 5 µM Fura-2AM dye (Molecular Probes) in 37ºC warm Tyrode's solution (1.8 mM $CaCl_2$, 5 mM glucose, 5 mM HEPES, 1 mM $MgCl_2$, 5.4 mM KCl, 135 mM NaCl, and 0.33 mM NaH_2PO_4, pH 7.4) for 30 min. CMs were paced at frequencies from 0.5 - 2.0 Hz (0.5 Hz increments) and stimulated at 30 V; maximum capture rate was defined as the highest pacing frequency for which there was a 1:1 correspondence between exogenous pacing and cell response. Calcium transients were recorded 100 frames per second and calcium transient duration at 50% and 80% time to baseline was measured. In addition to responses to outside electrical stimuli, spontaneously contracting 3D-dhECT CM

response to 0.5 μM isoproterenol (Molecular Devices) was examined. Representative calcium transient traces were processed by temporal averaging of five time steps.

5.2.15 Multielectrode array (MEA)

Day 20 3D-dhECTs were dissociated for 2 hrs in collagenase solution (as previously described for flow cytometry), resuspended in RPMI20 medium supplemented with 5 μM ROCK inhibitor, and cultured on a S2 type MEA200/30-Ti-gr (Multichannel Systems) for at least 24 hrs. Spontaneously contracting CMs were perfused with Tyrode's solution at 37 ºC using a MEA system with Multichannel Systems 1060-Inv-BC amplifier. When stabilized, baseline field potential recordings were acquired at a sampling frequency of 10 kHz. CMs were exogenously paced at 0.5, 1, 2, and 3 Hz. To assess drug response, 1 μM isoproterenol was added with a subsequent addition of 1 μM propranolol (Molecular Devices). Drugs were washed out to recover the baseline field potential profile.

5.2.16 Transmission electron microscopy (TEM)

Day 24 and day 124 3D-dhECTs were fixed in 3% glutaraldehyde (Electron Microscopy Science) at 4ºC before shipping to the pathology core at Icahn School of Medicine at Mount Sinai, NY. Tissue samples were sectioned (50 - 60 nm) and stained with Uranyl Acetate Solution and Reynold's Lead Citrate Solution. Processed tissue slices were examined using a transmission electron microscope (H-7650, Hitachi High Technologies).

5.2.17 Quantification of sarcomere structure

The prevalence of H-zones and I-bands were measured to quantify the sarcomere structural features. The numerical ratio of H-zones to sarcomeres, and the ratio of I-bands to Z-lines were analyzed from TEM images from day 124 3D-dhECTs using ImageJ software version 1.49v (NIH) with the Plot Profile analysis tool. Each image was imported into ImageJ and a linear region of interest was manually drawn across the length of a selected sarcomere; a 25-pixel line width was used to improve signal to noise, with the live plot option allowing real-time evaluation of the gray scale intensity pattern. The variation in gray scale values was used to identify Z-lines (pronounced decrease in the gray scale value), I-bands (pronounced increase in the gray scale value bordering the Z-lines) and H-zones (increase in gray value in the central region between each pair of Z-lines). A total of 101 sarcomeres and 142 z-lines were measured from 3 TEM images at 2-2.5K magnification.

5.2.18 Statistics

Results were analyzed from a minimum of three replicates for each experiment using Minitab 16. All values presented are mean ± SD. Data were compared using one-way analysis of variance (ANOVA) followed by Tukey's test, $P < 0.05$ was considered statistically significant.

Tables 5.2. Primary and secondary antibodies for immunofluorescence (IF) and flow cytometry (FC)

Antibody	Specification	Dilution
Sarcomeric alpha actinin	Mouse IgG1/Sigma-Aldrich/A7811	1:200 (IF)
Connexin 43	Rabbit IgG/Sigma-Aldrich/C6219	1:200 (IF)
Proliferating cell nuclear antigen	Mouse IgG2a/Millipore/MAB1691	1:200 (IF)
Caveolin 3	Rabbit IgG/Abcam/ab2912	1:200 (IF)
Cardiac troponin T	Mouse IgG1/Thermo Scientific/MA512960	1:200 (IF), 1:20 (FC)
Ki67	Rabbit IgG/Abcam/ab92742	1:200 (IF), 1:100 (FC)
P4HB	Rabbit IgG/Abcam/ab137110	1:100 (FC)
Caveolin 3	Rabbit IgG/Abcam/ab2912	1:200 (IF)
Mouse isotype control	Mouse IgG1/Thermo Scientific/MA110406	1:100 (FC)
Rabbit isotype control	Rabbit IgG/Thermo Scientific/PA523090	1:50 (FC)
Secondary antibody	Alexa 488 Goat anti-Rabbit IgG/A-11008	1:200 (IF), 1:1000 (FC)
Secondary antibody	Alexa 568 Goat anti-Mouse IgG/A-11004	1:200 (IF)
Secondary antibody	Alexa 647 Goat anti-Mouse IgG/A-20990	1:1000 (FC)

Table 5.3. **Primer and Taqman probe sequences for RT-qPCR**

Name	Product	Sequence	Citation
GAPDH	GAPDH	F: CCCCTTCATTGACCTCAACTACA	(Lian et al. 2012)
		R: TTGCTGATGATCTTGAGGCTGT	
		P: /5Cy5/AAATCCCATCACCATCTTCCAGGAGC/3IAbRQSp/	
POU5F1	Oct4	F: CCTGGGGGTTCTATTTGGGA	(Zwi-Dantsis et al. 2013)
		R: CCACCCACTTCTGCAGCAA	
		P: /56-FAM/CAAACGACC /ZEN/ATCTGCCGCTTTGAG /3IABkFZ/	
MYL2	MYL2v	F: GGGCGGAGTGTGGAATTCTT	(Lian et al. 2013)
		R: CCCGGCTCTCTTCTTTGCTT	
		P: /56-FAM/AGTGCTGGG /ZEN/TCCTTTCCACCAT /3IABkFQ/	
MYH6	αMHC	F: ACCAACCTGTCCAAGTTCCG	(Lian et al. 2013)
		R: TTGCTTGGCACCAATGTCAC	
		P: /56-FAM/AGCATGAGC /ZEN/TGGATGAGGCAGAG /3IABkFQ/	
MYH7	βMHC	F: CACAGCCATGGGAGATTCGG	(Lian et al. 2013)
		R: CAGGCACGAAGACATCCTTCT	
		P: /56-FAM/CCTACCTGC /ZEN/GCAAGTCAGAGAAGG /3IABkFQ/	
GJA1	Cx43	F: TGAGCAGTCTGCCTTTCGTT	(Lian et al. 2013)
		R: CCAGAAGCGCACATGAGAGA	
		P: /56-FAM/ACACTCAGC/ZEN/AACCTGGTTGTGAAA/3IABkFQ/	

F: forward primer, R: reverse primer, P: Taqman probe

5.3 Results

5.3.1 PEG-fibrinogen hydrogels support stem cell survival and proliferation

HiPSCs are frequently cultured and passaged in multi-cellular clusters, which has been reported to enhance cell viability and maintenance of pluripotency when compared to single cell dissociation (Beers et al. 2012). On the other hand, the inherent variability in cluster size might present a challenge for creating highly reproducible 3D-dhECTs from hiPSCs. In this work we established the ability to create 3D tissues using both cluster and single dissociated hiPSCs. In both cases, a cell suspension of $(55 \pm 8.5) \times 10^4$ hiPSCs per tissue was combined with aqueous PEG-fibrinogen precursor solution and photocrosslinked using visible light to create 200 μm thick 3D "microisland" tissues (**Fig. 5.1**). Both cluster and single hiPSCs were uniformly distributed throughout the 3D-dhECT microislands (**Fig. 5.2 A, F**); tissues formed using single hiPSCs appeared more homogeneous compared to cluster encapsulated hiPSCs (**Fig. 5.3 A**). HiPSC viability 24 h post-encapsulation (day -2, **Fig. 5.2 B, G**) was comparable to standard hiPSC passage and culture (Nie et al. 2014).

Encapsulated cluster and single dissociated hiPSCs grew and proliferated within the PEG-fibrinogen hydrogels both prior to (day -2 to day 0, **Fig. 5.3 A**) and following initiation of differentiation (day 0), which resulted in an expanded microisland lateral surface area of 20.1 ± 8.0% (IMR90-1 hiPSC line) and 25.5 ± 8.0% (19-9-11 hiPSC line) percent area increase by day 5 of differentiation (**Fig. 5.3 B**). Cell proliferation on day 10 was observed by immunostaining for proliferating cell nuclear antigen (PCNA, **Supplementary Movie 5.1**), with the high numbers of proliferating cells located on the tissue edges (**Fig. 5.3 C**). During early stages of cardiac differentiation, cluster

dissociated hiPSCs continued to grow as aggregates. Cells occupied the entire hydrogel volume quickly (**Fig. 5.2 C-E**) and tissues exhibited more growth at the edges than in the center. Tissue thickness increased from ~200 μm to 300 μm between days 3 and 5, with a dense tissue ring forming around the perimeter of the microisland (**Fig. 5.3 D**). In comparison, encapsulated single hiPSCs first formed small colonies and then subsequently formed interconnected tissue structures (**Fig. 5.2 H-J**).

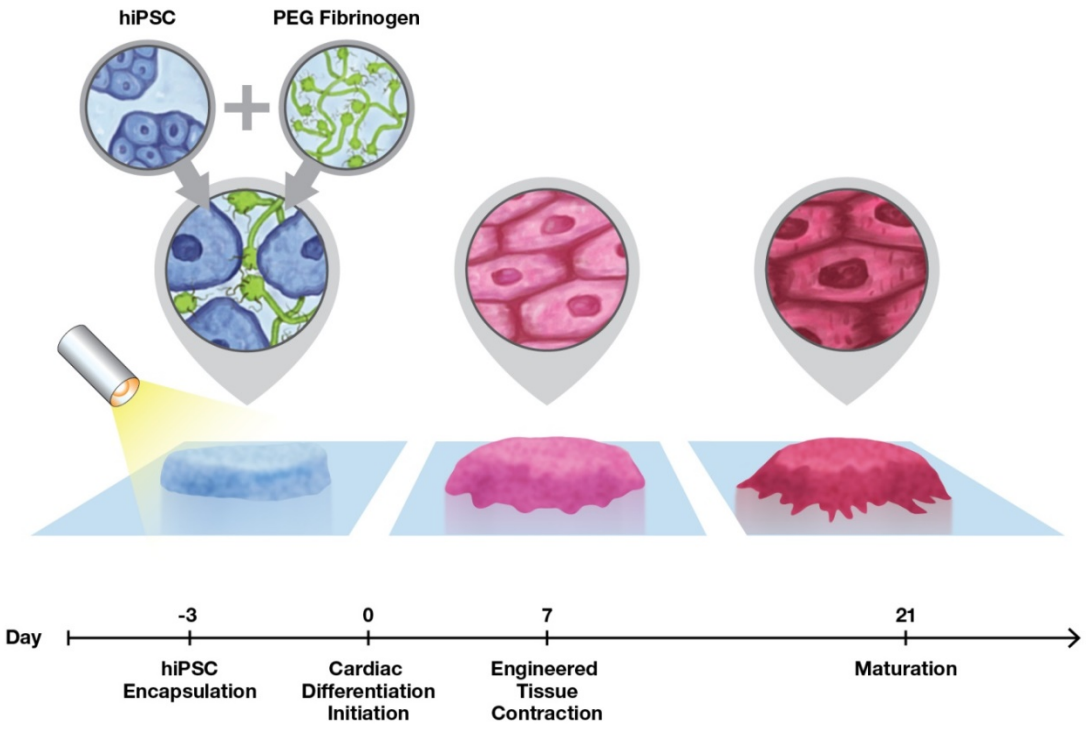

Fig. 5.1. Schematic of hiPSC encapsulation to produce 3D cardiac microislands. HiPSCs are combined with liquid PEG-fibrinogen precursor, added into a PDMS mold (not shown) on acrylated glass, and photocrosslinked under visible light to form microislands. All encapsulated hiPSCs are maintained in their pluripotent state for three days, followed by induction of cardiac differentiation to produce uniform contracting, cardiac tissues. Illustration by Brennen Reece.

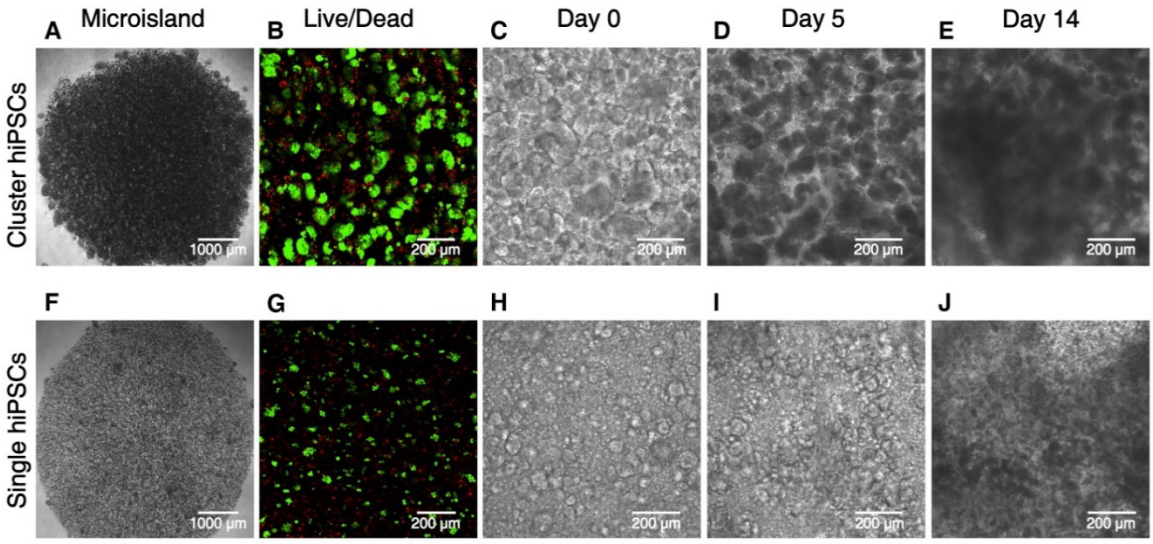

Fig. 5.2. Cluster and single encapsulated hiPSCs remained viable and proliferated in PEG fibrinogen hydrogel to form 3D cardiac tissues over time. Encapsulated (A) cluster and (F) single hiPSCs formed "microisland" tissues (images taken on day 0 of differentiation). (B, G) HiPSCs remained viable (green) 24 h post-encapsulation (n = 3 tissues) and (C-E, H-J) proliferated during early stages of cardiac differentiation. E, J represent **Supplementary Movies 5.3 and 5.4**.

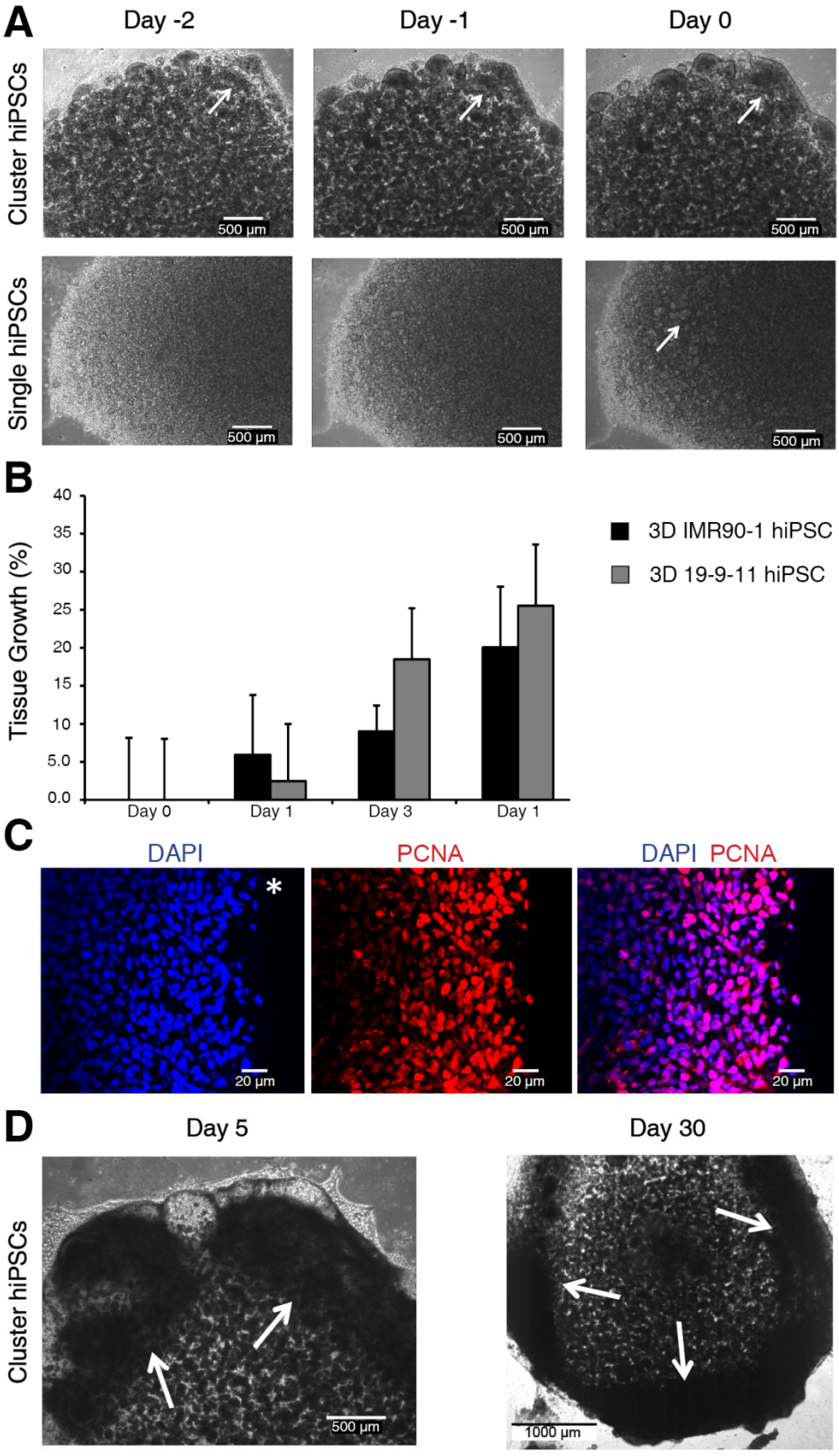
A
Day -2
Day -1
Day 0
Cluster hiPSCs
Single hiPSCs
500 µm
B
Tissue Growth (%)
40
35
30
25
20
15
10
5.0
0.0
Day 0
Day 1
Day 3
Day 1
3D IMR90-1 hiPSC
3D 19-9-11 hiPSC
C
DAPI
PCNA
DAPI PCNA
*
20 µm
D
Day 5
Day 30
Cluster hiPSCs
500 µm
1000 µm

Fig. 5.3. Cluster and single encapsulated hiPSCs grew and proliferated in PEG-fibrinogen hydrogels. (A) Higher numbers of cluster hiPSCs proliferated on tissue edges, while encapsulated single hiPSCs grew independent of tissue location. (B) Initially, cells grew and occupied void spaces within the pre-existing tissue footprint, followed by a tissue growth beyond the original microisland boundaries which resulted in a lateral surface area increase of 20.1 ± 8.0 % for IMR90-1 hiPSC encapsulations and 25.5 ± 8.0 % for 19-9-11 hiPSC encapsulation between days 0 and5 of differentiation (n = 3-4 tissues). (C) Z-stack slice of day 10 PCNA-stained cluster encapsulated tissue edge indicated a high number of proliferating cells on the edge of the tissue. Cell nuclei were counterstained with DAPI. Star is on side of tissue edge. (D) High magnification phase contrast images of cluster encapsulated hiPSCs on day 5 and day 30 revealed differences in tissue density, leading to a dense tissue ring around the microisland perimeter. White arrows indicate locations with higher cell density.

5.3.2 Encapsulated hiPSCs form uniformly contracting, functional cardiac tissues

This direct encapsulation and cardiac differentiation process resulted in uniformly contracting cardiac tissues with a high degree of repeatability, while requiring only one cell-handling step. All 3D-dhECTs were observed to spontaneously contract, with contraction initiating consistently on day 6 for the cluster 19-9-11 hiPSC line encapsulations (n = 3 independent differentiations, **Supplementary Movie 5.2**), day 7 for all cluster IMR90-1 hiPSC line encapsulations (n > 40 independent differentiations), and between days 9-11 for all single encapsulated hiPSCs (n = 3 independent

differentiations), which compares to day 8-9 for control 2D monolayers ($n > 20$ independent differentiations). The number of spontaneously contracting areas and synchronicity of contraction increased over time for both cluster and single cell 3D-dhECTs, consistently resulting in essentially uniform contracting tissues by day 14 (**Supplementary Movies 5.3 and 5.4**). Frequency of spontaneous contraction for cluster 3D-dhECTs was slowest during early differentiation (0.60 ± 0.21 Hz, days 8-11) and increased throughout the differentiation process to 1.37 ± 0.04 Hz by days 30-33 ($n = 3$ separate differentiations, **Fig. 5.4**). During long-term culture, the spontaneous contraction rate reached its highest frequency (2.2 ± 0.1 Hz) on day 50 ($n = 2$ tissues) and then began to decrease, stabilizing at 1.35 ± 0.05 Hz at day 90 (**Fig. 5.4**). Frequency of contraction for single cell 3D-dhECTs tended to be slower than for cluster 3D-dhECTs (0.48 ± 0.50 Hz, $n = 2$ vs. 0.60 ± 0.21 Hz) during early stages of differentiation, and contractility did not appear to be as strong as that of age-matched cluster 3D-dhECTs (**Fig. 5.5**). Cluster hiPSC encapsulation was chosen for all subsequent experiments due to the higher batch-to-batch consistency of cluster 3D-dhECTs, particularly with respect to the time point for initiation of contraction, as compared to single cell 3D-dhECTs.

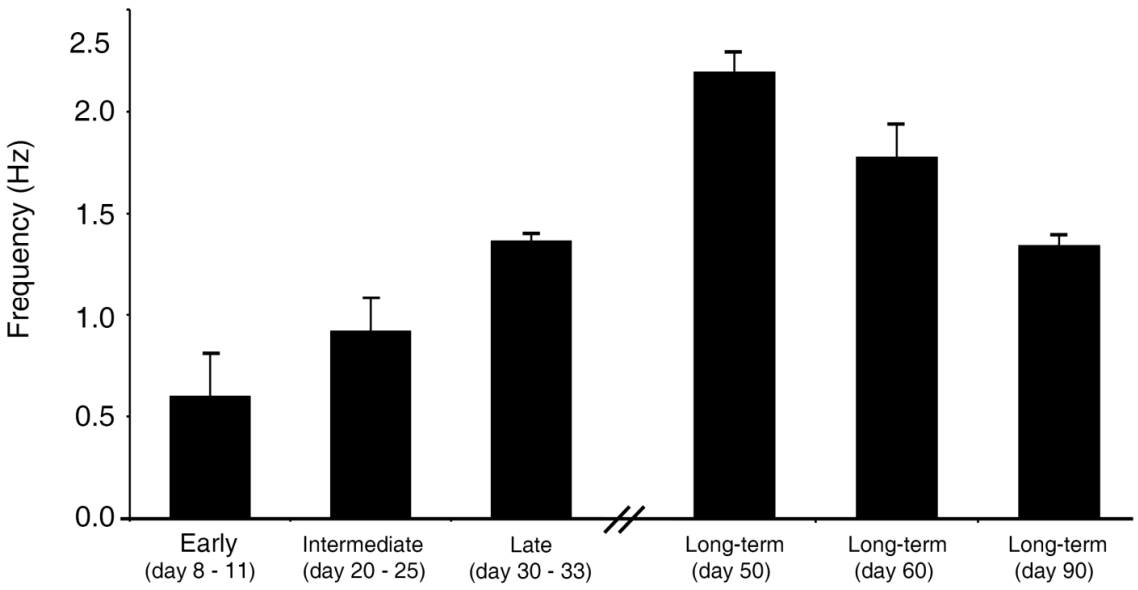

Fig. 5.4. Contraction properties of 3D-dhECTs. Frequency of spontaneous contraction increased in cluster encapsulation cardiac tissues over time, ranging from 0.60 ± 0.21 Hz (Early) to 0.92 ± 0.16 Hz (Intermediate) to 1.37±0.04 Hz (Late). n = 3 independent differentiation batches. Mean ± s.d. During long-term culture, frequency of contraction increased to 2.2 ± 0.1 Hz (day 50) followed by a subsequent decrease to 1.78 ± 0.16 Hz (day 60) and 1.35 ± 0.05 Hz (day 90). n = 2 3D-dhECTs. Mean ± s.d.

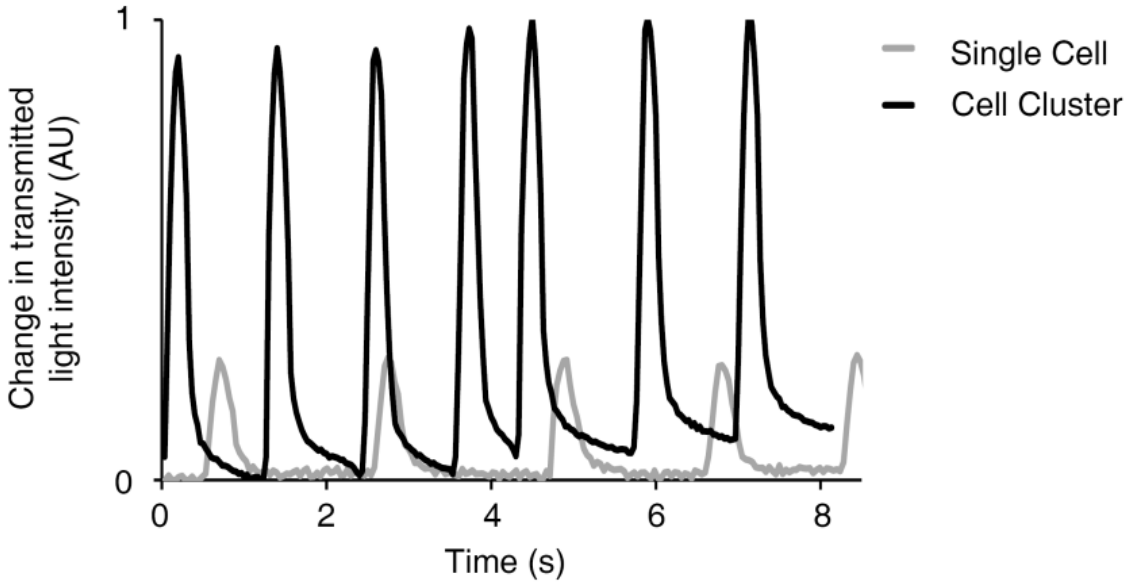

Fig. 5.5. 3D-dhECTs formed with cluster hiPSCs resulted in stronger contracting tissues than single hiPSCs. Microislands formed using cluster encapsulated hiPSCs displayed higher contractility (vs. single hiPSC microislands) based on video analysis of spontaneously contracting cardiac tissues on day 14 of differentiation (see corresponding **Supplementary Movies 5.3 and 5.4**). Y-axis represents the change in transmitted light intensity obtained from bright field microscopy as an index of contractility. Valleys correspond to the relaxed state, and peaks indicate contraction. AU (arbitrary units).

5.3.3 3D-dhECTs demonstrate differentiation efficiency and cardiac gene expression similar to 2D monolayers

Cardiac differentiation within the 3D-dhECTs resulted in high CM yield and temporal changes in gene expression that were analogous to those in age-matched 2D monolayers. To determine the efficiency of cardiac differentiation within 3D-dhECTs, the percentage of cells expressing cardiac troponin T (cTnT, cardiac specific marker) was evaluated by

flow cytometry and immunofluorescence on day 20. The 3D-dhECTs were composed of 72.5 ± 3.2% (IMR90-1 hiPSCs) and 75.65 ± 1.8% (19-9-11 hiPSCs) cTnT positive cells, of which 8.4 ± 0.7% also expressed the proliferation marker Ki67 (IMR90-1 hiPSCs, **Fig. 5.6 A**); cardiac differentiation was similar to age-matched 2D monolayers which had 74.3 ± 4.4% cTnT positive cells, 26.6 ± 0.5% of which also expressed Ki67 (IMR90-1, **Fig. 5.6 B**). Immunofluorescence of 3D-dhECTs also confirmed the expression of cTnT and Ki67 (**Fig. 5.6 C**). Of the remaining 3D-dhECT cells, 5.24 ± 2.72% were fibroblasts (P4HB positive, **Fig. 5.7**) and 2.96 ± 1.98% expressed Ki67 (**Fig. 5.6 A**).

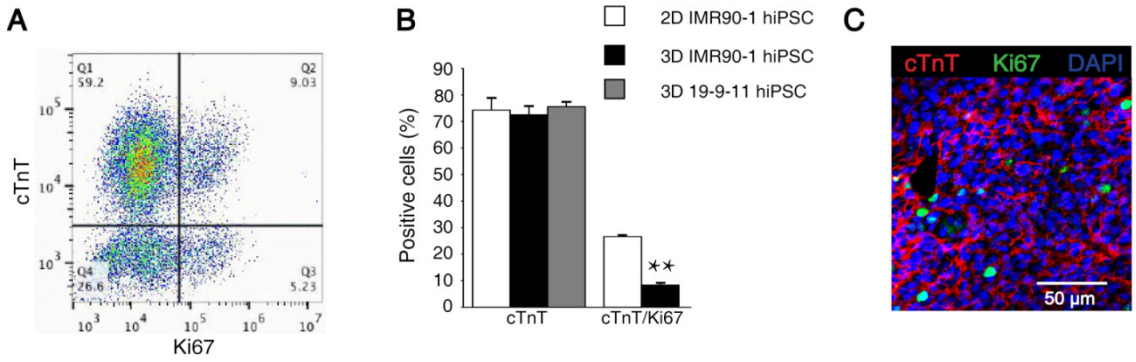

Fig. 5.6. 3D-dhECTs enabled efficient cardiac differentiation. (A) Representative flow cytometry results from day 20 3D-dhECTs. (B) 3D-dhECTs and aged-matched 2D monolayers (control) showed comparable differentiation efficiency on day 20 of differentiation. n = 3-5 biological replicates per group. Mean ± s.d. ANOVA $P < 0.05$, ** vs. 2D (C) Cardiac marker cTnT and proliferation marker Ki67 were also observed using immunofluorescence staining of day 20 cardiac tissues.

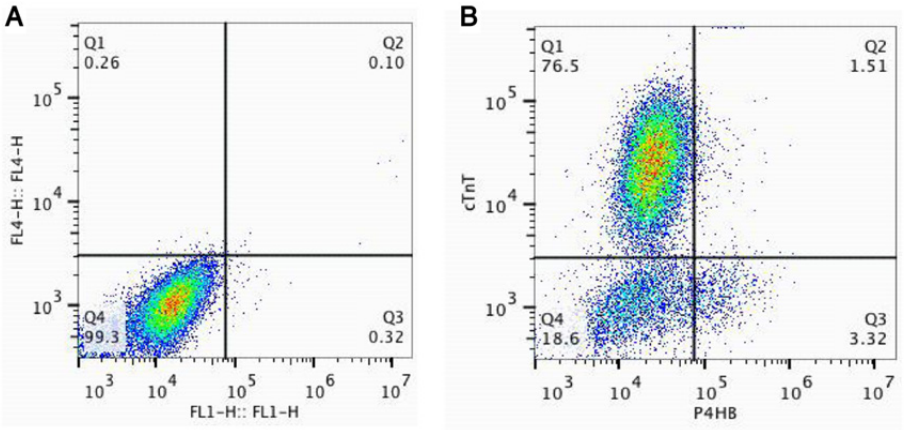

Fig. 5.7. Isotype control and supplementary flow cytometry results. (A) Isotype control and (B) cTnT (cardiac marker) and P4HB (fibroblast marker) stained 3D-dhECT cells resulted in 72.5 ± 3.2% CMs (n = 5 tissues) and 5.24 ± 2.72 % fibroblast positive cells (n = 3 tissues).

Temporal changes in pluripotency and cardiac gene expression in 3D-dhECTs paralleled that of age-matched control 2D monolayers. Three days post-encapsulation (day 0), expression of the pluripotency gene *Oct4* continued to be similar to hiPSCs (day -3) in both culture systems, as assessed by RT-qPCR. By day 10 of differentiation, *Oct4* expression had decreased significantly compared to hiPSCs and remained low (**Fig. 5.8 A**). The decrease in pluripotency was paired with a simultaneous upregulation in cardiac and functional gene expression. *MLC2v*, an early cardiac marker, increased in both 2D monolayers and 3D-dhECTs from day 10 to day 30 of differentiation (**Fig. 5.8 B**). Cardiac development was also tracked through assessment of *αMHC* and *βMHC* expression, where *βMHC* is the predominant isoform in the healthy adult human ventricle (Lowes et al. 1997). 2D monolayers and 3D-dhECTs expressed *αMHC* from day 10

through day 30. Expression of *αMHC* in 3D-dhECTs did not change significantly between days 10-30 whereas *βMHC* expression increased by day 30 (**Fig. 5.8 C, D**). This increase in *βMHC* gene expression by day 30 of differentiation suggests that cardiac maturation occurs over time within the 3D-dhECTs, similar to 2D differentiation. Expression of the *Cx43* gene, which encodes for a gap junction protein important for cardiac function, increased significantly from day 20 to day 30 in 3D-dhECTs and control 2D monolayers and could contribute to maturation of cell-cell junctions between adjacent CMs (**Fig. 5.8 E**).

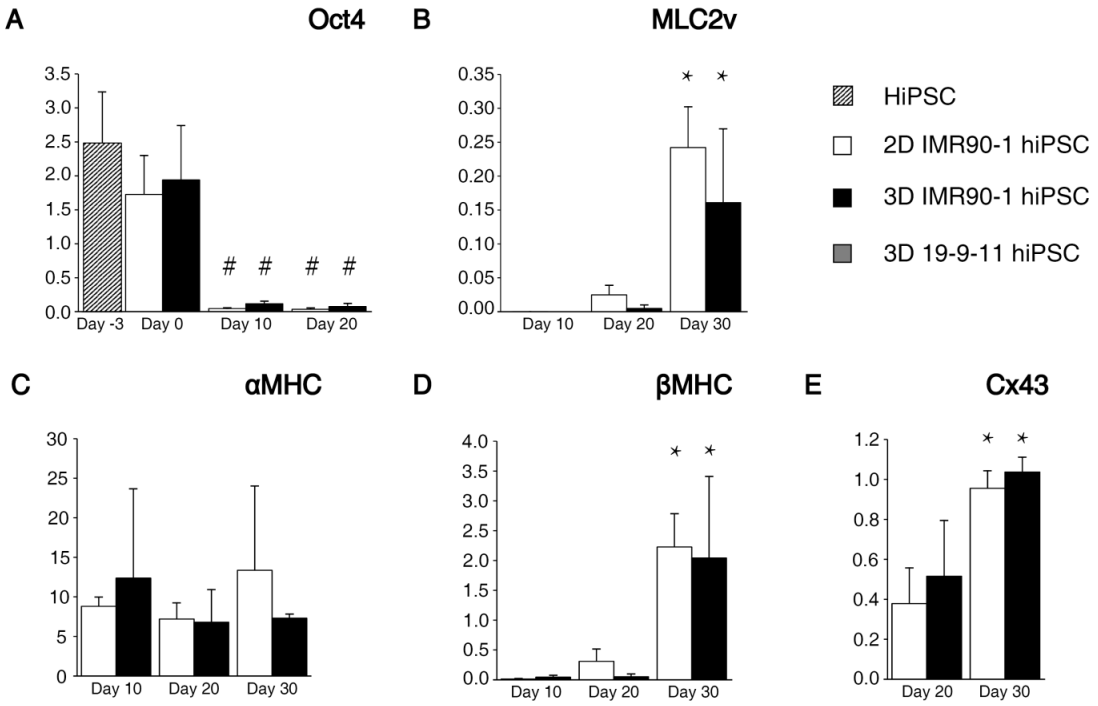

Fig. 5.8. 3D-dhECTs express cardiac genes similar to control 2D monolayers. (A) Pluripotency gene *Oct4* decreased following initiation of differentiation, while cardiac genes (F) *MLC2v*, (C) *αMHC*, (D) *βMHC*, as well as (E) the functional gene *Cx43* showed trends towards CM maturation over time. All mRNA levels were normalized to the housekeeping gene *GAPDH*. $n = 3$ biological replicates per group. Mean ± s.d. ANOVA $P < 0.05$, # vs hiPSCs and day 0; * vs. earlier time point. Y-axis represents gene expression relative to the housekeeping gene GAPDH.

5.3.4 3D-dhECT CMs exhibit similar calcium handling to CMs from 2D cardiac monolayers

In addition to 3D-dhECTs demonstrating high CM yields and appropriate cardiac gene expression profiles similar to age-matched 2D monolayers, CMs from both systems had similar contractile function and calcium handling properties, which are critical features of

differentiating CMs (Itzhaki et al. 2011). To study these properties, CMs were enzymatically dissociated from 3D-dhECTs and 2D monolayers at day 14. Isolated CMs continued to contract spontaneously and also responded to exogenous pacing, exhibiting a maximum 1:1 capture rate of 1.5 Hz for both 3D- and 2D-differentiated CMs Calcium transient durations for 3D-dhECT CMs were similar to those of control 2D monolayer CMs (**Fig. 5.9 A-C**). Calcium transient duration decreased in response to increased pacing frequency for both groups of CMs, mimicking the frequency-dependent physiological response of healthy myocardium (Lou et al. 2011). CMs also responded appropriately to treatment with isoproterenol (0.5 μM for 3 min), a β-adrenergic agonist; the frequency of spontaneous contraction increased by 1.2-fold and calcium transient duration shortened significantly (**Fig. 5.10 A, B**). The frequency of 3D-dhECT spontaneous contraction slowed significantly after the addition of the β-adrenergic antagonist propranolol. First, 1 μM isoproterenol was administered to whole tissues, which caused a significant increase in contraction frequency. As previously observed from isolated cells (Planat-Benard et al. 2004, Matsuura et al. 2004), the addition of propranolol reversed this initial increase in beats per minute, demonstrating that our 3D-dhECTs respond to beta agonists and antagonists (**Fig. 5.10 C**). These responses to exogenous pacing and β-adrenergic agonist and antagonist were further verified using MEA analysis (**Fig. 5.11**). Dissociated day 20 3D-dhECTs responded to outside pacing frequencies up to 3.0 Hz (**Fig. 5.11 A**) and spontaneously contracting CMs increased in response to isoproterenol and was reversed after the addition of propranolol (**Fig. 5.11 B**).

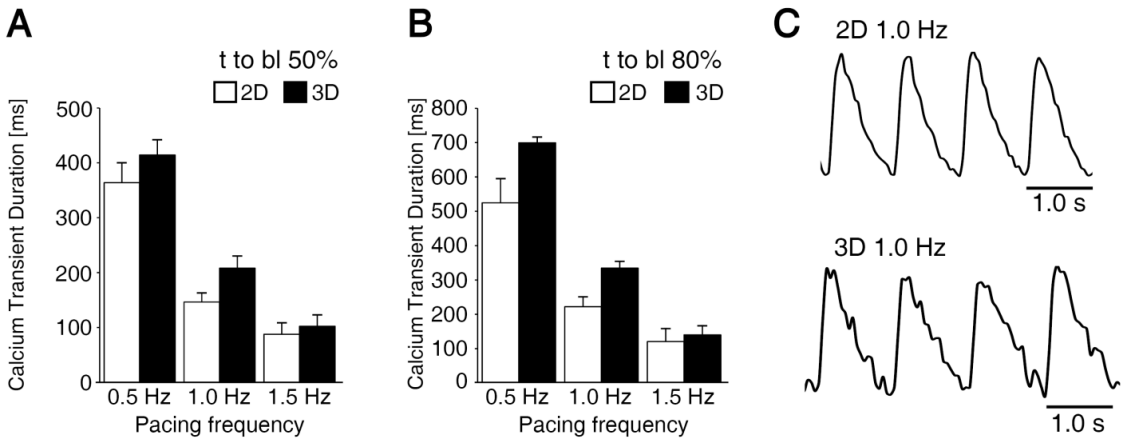

Fig. 5.9. 3D-dhECT CMs responded to exogenous pacing. During exogenous pacing, time to baseline (t to bl) (A) 50% and (B) 80% were similar for 2D and 3D cultured CMs (day 14). (C) Representative calcium transient traces of 2D and 3D cultured cells at 1 Hz pacing frequency.

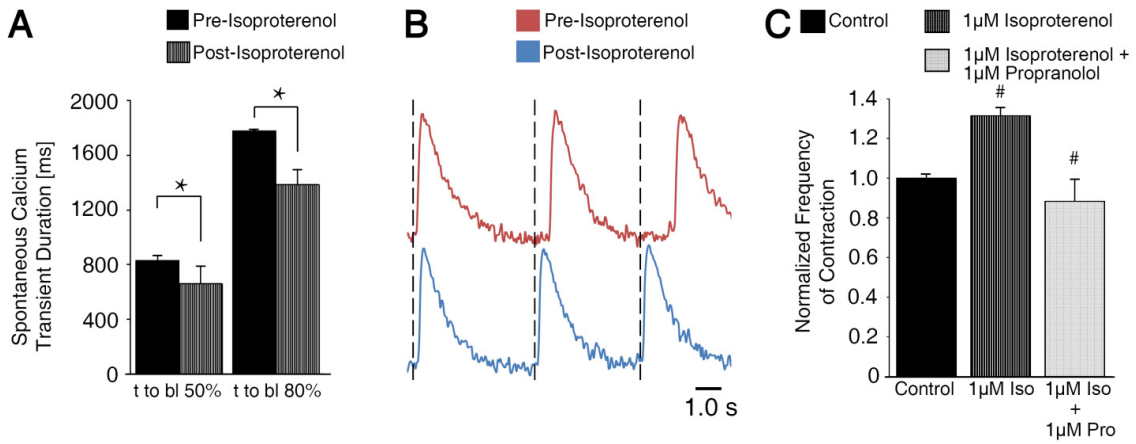

Fig. 5.10. Beta adrenergic agonist and antagonist drug treatment influenced calcium transient duration and frequency of contraction. (A) Addition of 0.5 μM isoproterenol shortened spontaneously contracting 3D-dhECT CM calcium transient *t to bl 50%* and *80%*, suggesting that the chronotopic response to β-adrenergic signaling is operational. (B) In these early stage 3D-dhECT CMs, isoproterenol increased the rate of spontaneous contraction. n = 3. Mean ± s.d. ANOVA $P < 0.05$, * vs. Pre-Isoproterenol. (C) Rate of 3D-dhECT spontaneous contraction increased after the addition of isoproterenol (1 μM) and decreased after subsequent addition of the β-adrenergic antagonist propranolol (1 μM). # vs. earlier condition.

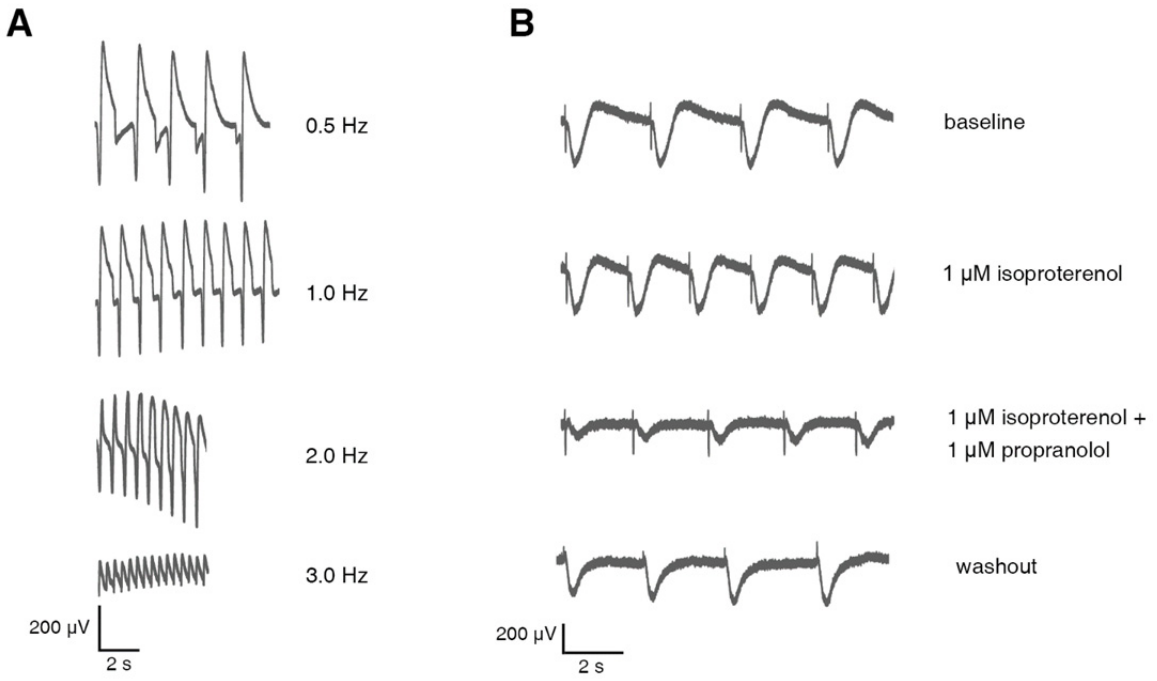

Fig. 5.11. MEA recordings of 3D-dhECTs responding to exogenous pacing and beta-adrenergic agonist and antagonist drug treatment. (A) Day 20 3D-dhECTs responded to exogenous pacing up to 3 Hz (at 37ºC). (B) Representative traces of 3D-dhECT spontaneous activity showing changes in field potential duration of baseline, following 1 µM isoproterenol addition, subsequent 1 µM propranolol addition, and after washout.

5.3.5 3D-dhECT CMs develop mature structural features over time

3D-dhECTs were able to be maintained long-term, with CMs developing aligned and more defined sarcomeres over time and establishing mature ultrastructural features. Cells within the 3D-dhECTs self-aligned, particularly on tissue edges, by day 30 of differentiation; immunofluorescence staining for the cardiac marker sarcomeric α-actinin (αSA) on days 10, 20, and 30 revealed progressive sarcomere development with better defined and aligned sarcomeres by day 30 of differentiation (**Fig. 5.12 A**). This result was unexpected; extrinsic stimuli, such as mechanical stretching (Zimmermann et al. 2002,

Fink et al. 2000, Nunes et al. 2013, Tiburcy et al. 2011) or electrical pacing (Nunes et al. 2013, Radisic et al. 2004a, Hirt et al. 2014), have often been used to enhance the ability of CMs to mature, align, and uniformly contract within engineered cardiac tissues assembled using pre-differentiated SC-CMs. However, the temporal upregulation of cardiac gene expression and increased organization of cardiac proteins suggested CM maturation within 3D-dhECTs was progressing spontaneously, which led us to further investigate CM organization and ultrastructural development during long-term tissue culture. Based on 2D fast Fourier Transform (FFT) analysis of immunofluorescence images from day 20, 30, and 124 3D-dhECTs, sarcomeres became more defined over time (**Fig. 5.13 A-C**). Some discrete sarcomere structure was observed during early stages of differentiation (day 20); by day 124 3D-dhECT CMs had aligned, organized, well-defined sarcomeres with an average relaxed length of 1.8 ± 0.1 μm (**Fig. 5.13 D**, n = 200 cells), similar to mature human CM sarcomere structure (Bird et al. 2003, Zhang et al. 2013). Following extended *in vitro* culture (day 52-60), tissue dissociation into single CMs revealed a wide range of cell sizes (400-5,800 μm^2, mean = 2,163 μm^2) and circularities (0.10-0.86, mean = 0.43) (**Fig. 5.12 B, C**). When maintained long-term, 3D-dhECTs CMs showed features of mature CMs (**Fig. 5.14 A**) and 3D-dhECTs continued to have higher cell density on the tissue edges with CMs growing outward from the tissue onto the supporting substrate (**Fig. 5.14 B, C**). Cellular organization within the long-term cultured 3D-dhECTs (day 124) exhibited large cell nuclei (**Fig. 5.12 D**) and developed characteristics of mature electromechanically anisotropic cardiac tissues, including aligned CMs with the gap junction protein connexin 43 (Cx43) located on the transverse ends (**Fig. 5.12 E**) of adjoining cells. When dissociated, 3D-dhECT CMs exhibited an

elongated, anisotropic morphology with a length-to-width ratio of 6.2±2.2 (n = 60 CMs), similar to morphologies expected in mature CMs (Gerdes et al. 1992, Yang et al. 2014, Hirt et al. 2014).

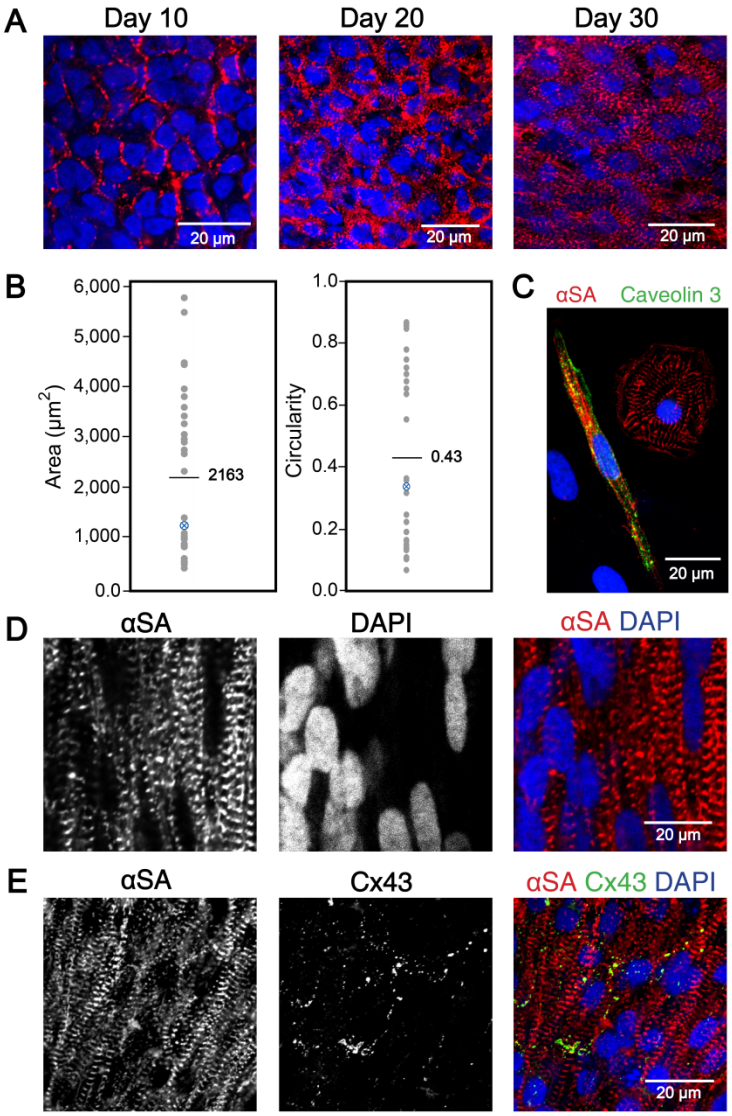

Fig. 5.12. Ontogenetic tissue development generating well-defined and aligned sarcomeres over time. (A) Sarcomere definition and alignment became more pronounced with culture time. Immunofluorescence staining with cardiac marker αSA on days 10, 20, and 30 of differentiation showed increased sarcomere definition and

alignment in 3D-dhECT CMs. (B) Day 52-60 dissociated 3D-dhECT CM area and circularity ranged from 400-5,800 μm^2 (mean = 2,163 μm^2) and 0.10 – 0.86 (mean = 0.43), respectively (n = 32). Blue highlighted data points indicate medians. (C) Representative day 52 dissociated CMs stained with αSA (red) and Caveolin 3 (green) for T-tubule development. Long-term cultured 3D-dhECT (day 124) CMs (D) developed highly aligned sarcomeres and contained large and elongated cell nuclei. (E) Additionally, these CMs expressed Cx43 on their transverse ends between adjoining cells.

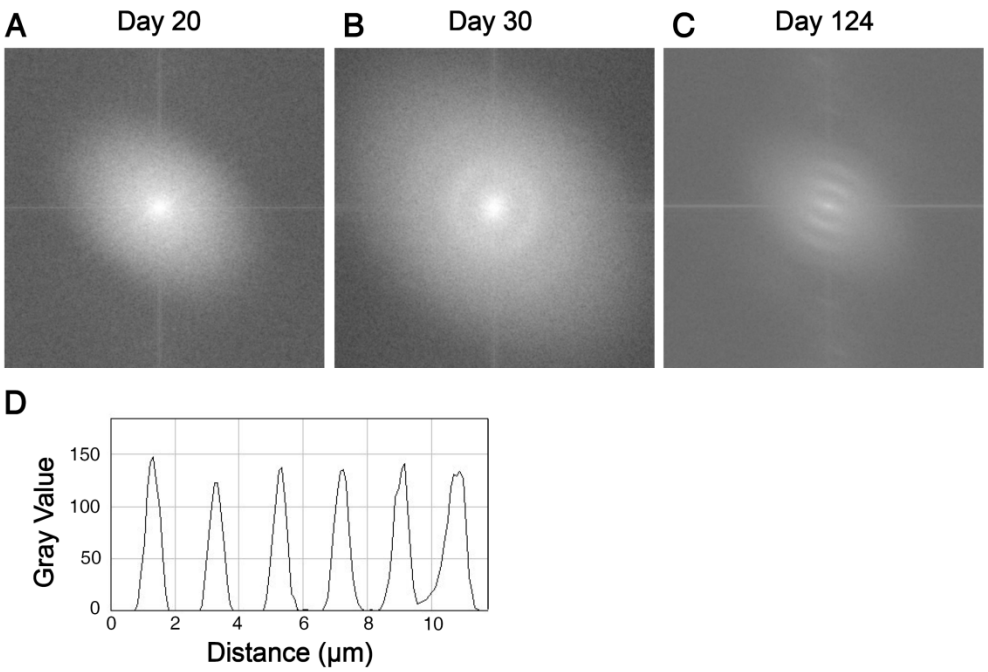

Fig. 5.13. Development of discrete sarcomere structure during ontomimetic cardiac differentiation. (A-C) 2D FFT analysis of selected αSA-stained 3D-dhECTs provided evidence to an increase in sarcomere alignment and definition over time, represented by the transition from no visible rings (day 20) to visible, full rings (day 30) to more defined, aligned (direction of sarcomeres) rings (day 124). (D) Sarcomere distance of day 124 3D-dhECT CMs was quantified by generated intensity plots (increased gray scale represents existing sarcomere).

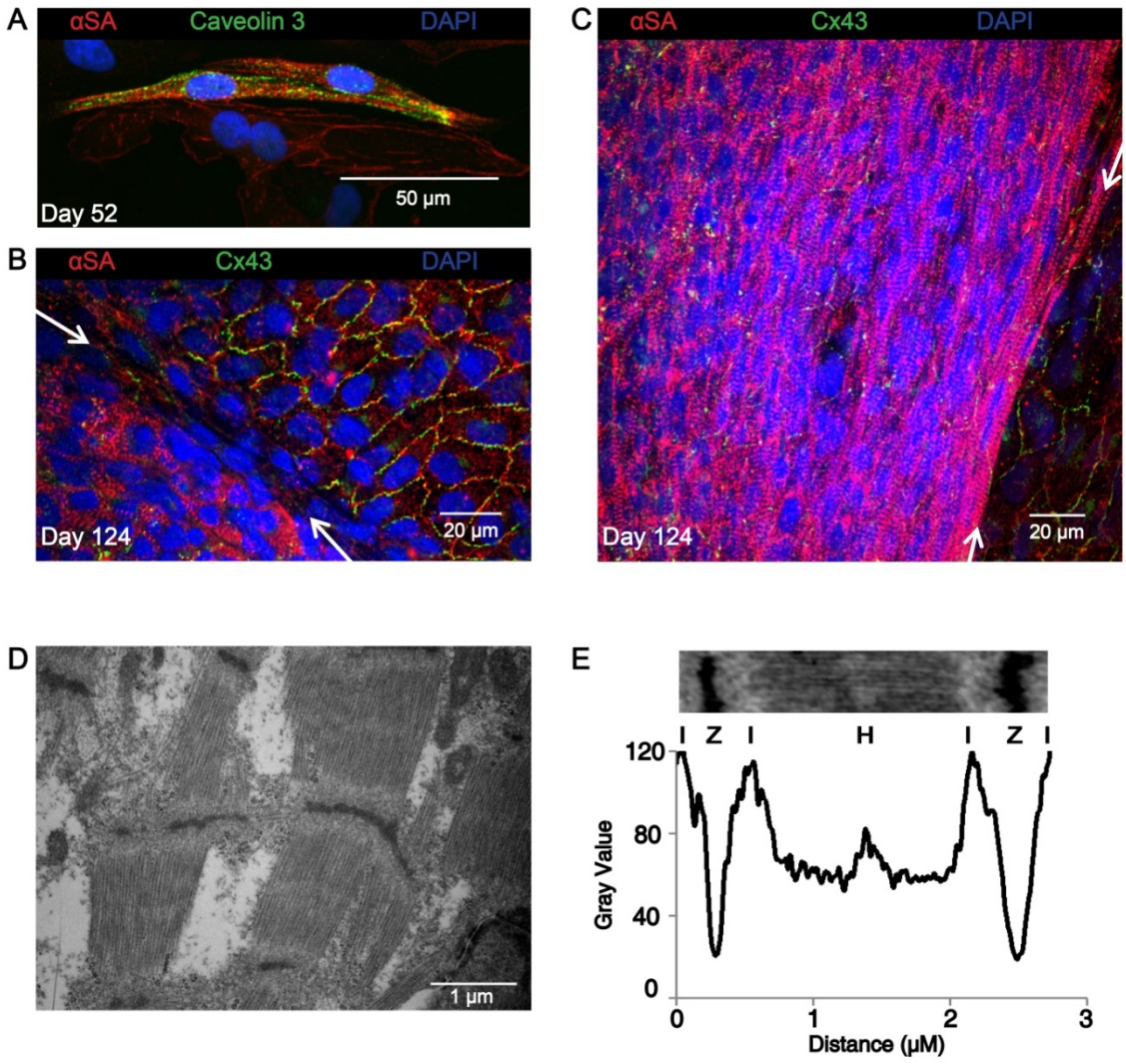

Fig. 5.14. CMs within the dense 3D-dhECTs continue to develop during extended in vitro culture. (A) Day 52 dissociated 3D-dhECT CMs exhibited an elongated morphology and stained positive for Caveolin 3, providing a first indication of T-tubule development. (B, C) In long-term cultured cardiac tissues, an area of increased cell density was observed on tissue edges as well as tissue outgrowth onto the acrylated glass; this tissue outgrowth contained CMs that exhibited a less mature phenotype with less defined sarcomeres and Cx43 distributed in a punctate pattern along the borders of the cells. Images are focused to visualize the bottom 2D tissue outgrowth (B) and overall

tissue structure (C). Arrows indicates tissue edge. (D) Example subregion of TEM image (day 124) and (E) plot of grayscale intensity profile for identification and counting of Z-lines (Z), neighboring I-bands (I), and H-zone (H).

To further investigate 3D-dhECT CM maturation, cardiac ultrastructural features were visualized using TEM. Day 24 cardiac tissues showed the presence of Z-lines and mitochondria (**Fig. 5.15 A**), reflecting early developmental stages of functional CMs. 3D-dhECTs maintained long-term (day 124) were composed of CMs with ultrastructural features approximating those of mature CMs. TEM images revealed numerous mitochondria, and myofibrils with well-defined sarcomeric Z-lines, I-bands, and H-zones, with a H-zone to sarcomere ratio of 0.257 and an I-band to Z-line ratio of 0.669 (**Fig. 5.14 D**). Other features of 3D-dhECT CMs included intercalated discs on the transverse edges of CMs with adjacent gap junctions (**Fig. 5.15 B**), caveolae in the plasma membrane, and presence of basement membrane. Most notably, 3D-dhECT CMs exhibited transverse tubules (T-tubules) which were structurally aligned with Z-lines (**Fig. 5.15 C**); up until now, T-tubules have only been observed in primary CMs isolated from postnatal and adult mammalian hearts (Ziman et al. 2010), but have not been reported in any other *in vitro* human SC-CM study (Knollmann 2013, Robertson, Tran and George 2013, Priori et al. 2013).

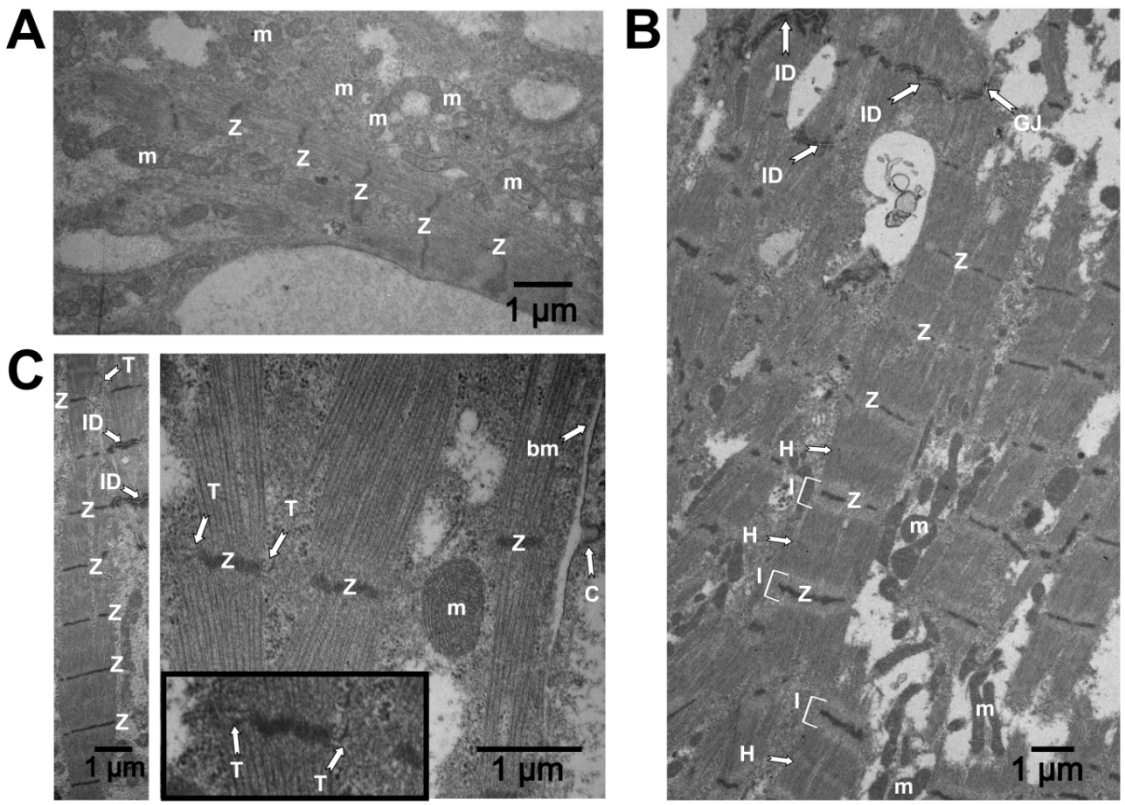

Fig. 5.15. Ontomimetic environment resulted in 3D-dhECT CMs exhibiting mature ultrastructural features. (A) Day 24 3D-dhECT CMs developed first characteristics of a muscle cell including mitochondria (m) and Z-lines (Z). (B) Ultrastructural images of 124 day old 3D-dhECT CMs showed sarcomere structures, including Z-lines (Z), I-bands (I), H-zones (H), intercalated discs (ID), gap junctions (GJ), and mitochondria (m). (C) Additionally, CMs contained caveolae (C) adjacent to basement membrane (bm), mitochondria with well-defined cristae, and T-tubules (T) adjacent to Z-lines, a key component of functional mature CMs. Insert: magnified view processed to highlight T-tubules.

5.3.6 Multiple geometries support cardiac tissue formation through direct hydrogel encapsulation

This straightforward 3D-dhECT formation process was extended to fabricate cardiac tissues across multiple size scales and geometries, demonstrating our ability to create tissues exploitable for a wide range of possible applications (**Fig. 5.16**). Furthermore, immobilization of the 3D-dhECTs through covalent attachment to the glass coverslips was found not to be necessary for cardiac tissue formation; 3D-dhECTs in suspension culture also formed contracting tissues that were consistently maintained for multiple months. In addition to the immobilized microislands (**Fig. 5.16 A**) described above, tested geometries included macrotissues (**Fig. 5.16 B**) and microspheres (**Fig. 5.16 C**). Macrotissues (**Fig. 5.16 B**) of varying lengths, thicknesses of 800-900 μm and widths greater than 2 mm were formed and cultured in suspension. Analogous to the microislands, contracting areas were first observed in the macrotissues on day 7 of differentiation, resulting in robust, uniform contraction early in the differentiation process (day 12) and appearing strong over the entire culture period (**Supplementary Movie 5.5**). Similarly, suspension culture of 3D-dhECT microspheres of diameter 280 ± 70 μm ($n = 25$, **Fig. 5.16 C**) resulted in uniformly contracting spheres that again could be maintained over extended time periods (**Supplementary Movie 5.6**). Finally, all cardiac tissue geometries were successfully dissociated into individual CMs (**Fig. 5.16 D**), enabling subsequent single-cell experiments or collection and re-suspension as might be required for delivery as a cell therapy.

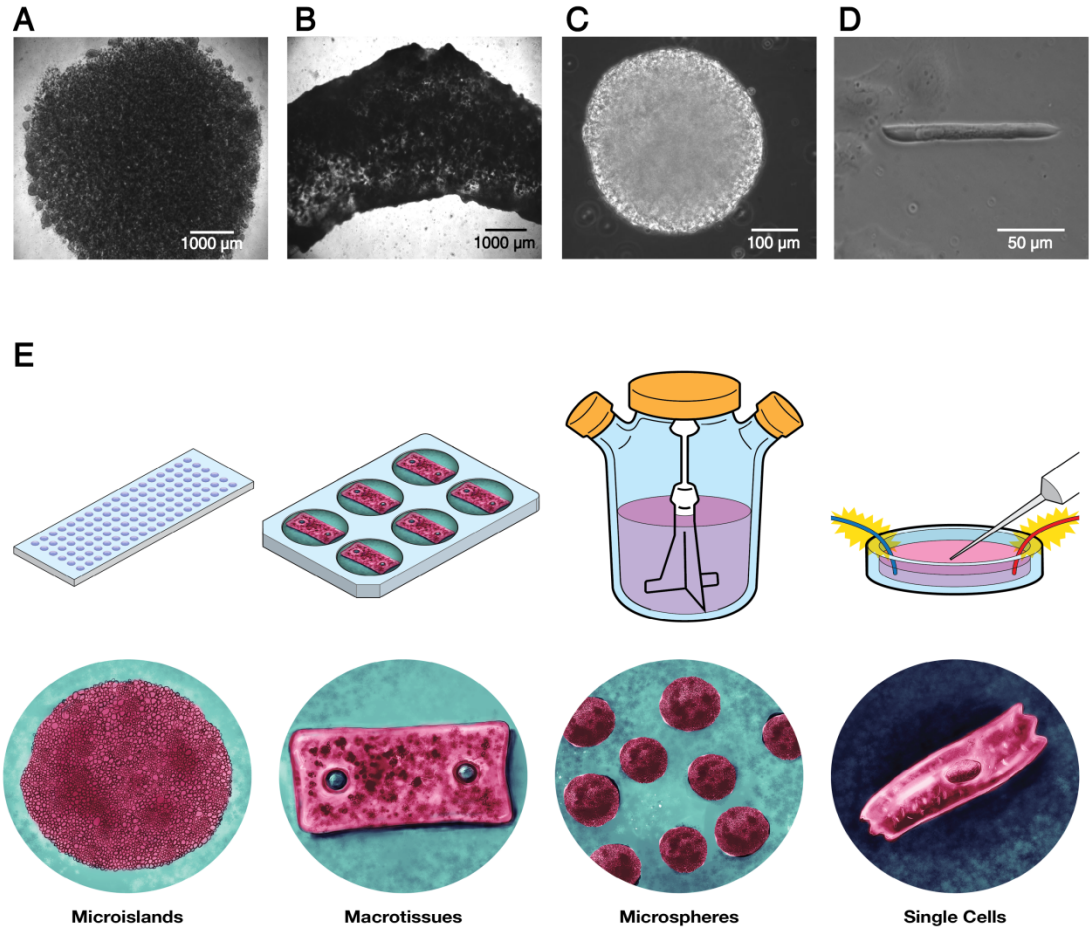

Fig. 5.16. Using this single cell-handling approach, different tissue sizes and geometries of 3D-dhECTs can be formed. Uniformly contracting tissues, in addition to (A) immobilized microislands, included: (B) macrotissues and (C) microspheres, all of which were able to be used to obtain (D) 3D-dhECT-dissociated single CMs. (E) Tissue sizes and geometries can be varied based on desired future applications, e.g., microislands for high-throughput drug-screening, macrotissues for large-scale mechanical testing and cardiac patches, injectable cardiac tissue spheroids, or single CMs post-tissue digestion for automated patch clamping.

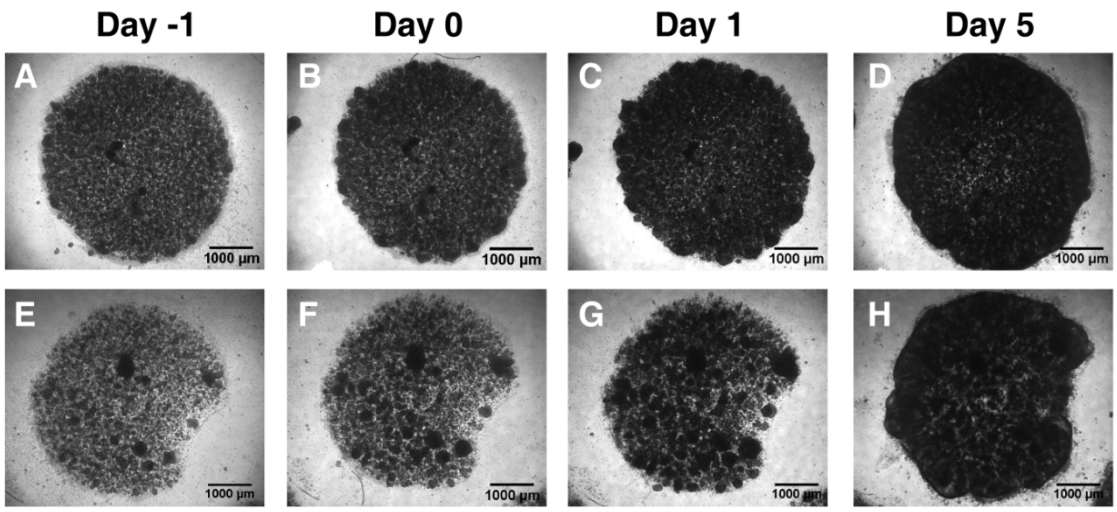

Fig. 5.17. Initial cell-seeding density can be varied to produce contracting 3D-dhECTs. (A-D) Original cell-seeding density (60 million/ml) and (E-H) 50% of original cell-seeding density (30 million/ml) was compared during early stages of tissue formation. Increase in cell number (darkening effect) over time was observed for both cell-seeding densities.

5.4 Discussion

Differentiation of encapsulated hiPSCs to directly produce cardiac tissues *in vitro* opens a wide range of possibilities in the field of cardiac tissue engineering. In this work we established that hiPSCs can be readily and efficiently encapsulated within PEG-fibrinogen hydrogels and directly differentiated to produce uniformly contracting 3D-dhECTs. Gene expression, CM yield, and calcium handling were similar to hiPSC differentiation using the current gold-standard, high efficiency 2D monolayer differentiation. Moreover, using 3D-dhECTs to produce cardiac tissues has distinct advantages over 2D monolayer differentiation (Lundy et al. 2013): it enables long-term

CM culture and maturation without having to disrupt pre-differentiated SC-CMs, and it does not require the re-formation of functionally critical cell-cell junctions, which is notoriously problematic for CMs, particularly as they mature. The minimal cell-handling requirements and applicability of this cardiac tissue production technique to a wide range of tissue sizes and geometries facilitates high-throughput and cost-effective formation of human cardiac tissue for an array of future applications. PEG-fibrinogen can be rapidly photocrosslinked using a non-toxic photoinitiator and visible light, creating a controlled 3D microenvironment for encapsulated cells with potential for automation of the tissue production process using bioprinting of structurally organized microislands and other printed 3D tissue geometries (Murphy and Atala 2014, Stanton, Samitier and Sanchez 2015) or microfluidics for microsphere production (Workman et al. 2007, Chung et al. 2012a). Previous studies have optimized the initial mechanical properties of the PEG-fibrinogen hydrogels for neonatal CM encapsulation[16], pre-differentiated SC-CMs encapsulation (Shapira-Schweitzer and Seliktar 2007, Shapira-Schweitzer et al. 2009), or SC-CMs seeded onto PEG-fibrinogen hydrogels (Bearzi et al. 2014) (**Table 5.1**). However, encapsulation and maintenance of hiPSCs within PEG-fibrinogen, and their direct differentiation in the presence of PEG-fibrinogen, had not previously been investigated. The encapsulation procedure established in this study allows for hiPSC survival with maintenance of pluripotency for at least three days within this optimized PEG-fibrinogen hydrogel formulation. Maintenance of encapsulated hiPSC pluripotency during extended culture periods has not been investigated; however, other biomaterials have previously been used for large-scale hPSC culture and expansion (Lei and Schaffer 2013, Amit et al. 2011, Zweigerdt et al. 2011).

Even when varying the initial hiPSC seeding density, cell proliferation and contracting cardiac tissue formation was attainable in PEG-fibrinogen hydrogels (**Fig. 5.17**). In contrast, the successful production of 2D cardiac monolayers can only be achieved within a narrow range of initial cell-seeding densities (Lian et al. 2013). We believe the biomimetic microenvironment provided by the hydrogel plays a central role in successful hiPSC 3D culture, proliferation, and cardiac differentiation, while initial cell-seeding density may influence the uniformity of contraction within the cardiac tissue over time. Both microenvironment and seeding density directly influence the rate of degradation and temporal remodeling of PEG-fibrinogen hydrogels, thereby allowing cells to secrete ECM proteins and form a continuous tissue.

During initial stages of SC differentiation, we have seen a steady increase in frequency of spontaneous contraction over time (day 8-50), which could be due to the temporal development of cell-cell junctions and calcium handling capabilities of maturing SC-CMs. 3D-dhECT contraction frequency decreased from its maximum of 2.2 ± 0.1 Hz on day 50 to 1.35 ± 0.05 Hz on day 90. A reduction in the rate of spontaneous contraction is anticipated when modeling the developing human heart; human heart rate *in vivo* slows down significantly during maturation (~3.0 Hz during fetal stage to 1.0-1.5 Hz in adults) (Arduini 1995). Based on published results using the small molecule protocol employed in this study (Lian et al. 2013), our 3D-dhECTs are likely composed of a distribution of ventricular, atrial, and nodal CM subtypes, which is appropriate for mimicking heart development. To enrich for ventricular myocytes, recently published small molecule differentiation protocols (Burridge et al. 2014, Weng et al. 2014) could potentially be adapted for use with our 3D-dhECT system.

CM proliferation and hyperplasia is a phenomenon seen during fetal heart growth and early post-natal development (Li et al. 1996), after which it diminishes over time (Laflamme and Murry 2011, Mollova et al. 2013). On day 20 of cardiac differentiation, both 2D monolayers and 3D-dhECTs were composed of a similar percentage of CMs. However, the percentage of proliferating CMs in 2D was higher than that in the 3D-dhECTs. This difference in CM proliferation was also seen previously between engineered "biowires" and embryoid bodies (Nunes et al. 2013). Alternatively, considering the low rates of CM proliferation during *in vivo* development (Mollova et al. 2013, Bensley et al. 2010) and that cell proliferation rates generally differ in 2D versus 3D culture (Mann and West 2002), the observed lower CM proliferation might be a consequence of a more physiologic microenvironment in the 3D-dhECTs.

Having a platform that replicates key features of ontogenic CM maturation will enable new opportunities for investigating this critical process, and thereby could provide important insights about how developing human heart tissue remodels after birth. Furthermore, achieving CM maturation within an *in vitro* 3D environment will provide more physiologically relevant tools for toxicology screening and disease modeling using patient-specific hiPSCs (Liang et al. 2013, Doyle et al. 2015, Yazawa et al. 2011) to engineer mature cardiac tissues (Yang et al. 2014) that current differentiation systems cannot provide. In addition, there is a high demand for cardiac tissues that can be used in patients for myocardial repair (Chong et al. 2014); to avoid induction of deadly arrhythmias, clinical applications require CMs that can achieve appropriate mechanical and electrical integration with native tissues. Balancing the needs for both CM plasticity and suitable maturation to achieve this goal is an area of intense research (Dunn, Hodge

and Lipke 2014); we have demonstrated that 3D-dhECTs can be used to produce CMs from early time points in stem cell differentiation through ultrastructural maturation, providing the flexibility to meet future specifications for optimizing cardiac cell therapy.

T-tubule formation and other mature ultrastructural features that are important in excitation-contraction coupling (Lieu et al. 2009, Wei et al. 2010) have been detected in our long-term cultured 3D-dhECT CMs; day 52-60 dissociated CMs showed Caveolin 3 positive staining, indicating the development of T-tubule formation. Neonatal rat ventricular myocytes incorporated into engineered heart tissues have previously shown to support formation of T-tubules (Shapira-Schweitzer et al. 2009). However, T-tubule formation in SC-CMs has not been previously reported (Lundy et al. 2013, Lieu et al. 2009, Baharvand et al. 2005, Nunes et al. 2013, Priori et al. 2013). Initiation of differentiation and long-term culture within an *in vitro* 3D environment may better support CM maturation, which is important for establishment of more physiologically relevant tools for toxicology screening and disease modeling of adult human myocardium (Yang et al. 2014).

Although immobilized microislands are advantageous for high-throughput applications, this tissue size and geometry also have some drawbacks. At the tested diameter of 6 mm, cell growth and proliferation resulted in non-uniform tissue thickness and the generation of CMs with a range of levels of maturity. Since these regional differences in cell growth were observed prior to the onset of contraction, space limitations at the microisland center could potentially be a contributing factor; in comparison, hiPSCs on tissue edges grew both upwards and radially outwards from the original hydrogel boundaries. In a previous study, a similar tissue morphology (scaffold-

free tissue patch) showed higher levels of cardiac maturation and CM purity on tissue edges compared to tissue centers (Stevens et al. 2009). Additional testing will be required to determine whether observed regional differences in microisland 3D-dhECTs are also observed at smaller diameters or when using alternative fabrication techniques, such as microprinting, versus molds.

Our study reveals the first 3D ontomimetic model of human heart development, enabling hiPSC growth and cardiac differentiation in a controlled 3D microenvironment. 3D-dhECTs have been used to produce CMs from early time points in SC differentiation through ultrastructural maturation, providing the flexibility to meet future specifications for optimizing cardiac cell therapy. Translatable to a variety of tissue sizes and geometries, this robust approach will ease and improve the cardiac tissue formation process, thereby impacting the ability to produce human heart tissue for a range of applications from investigating the role of 3D microenvironmental cues in human heart development to advancing clinical treatments for heart disease.

6. DEVELOPING HUMAN CARDIAC TISSUE CAN DETECT DRUG-INDUCED CONGENITAL HEART DEFECTS

6.1 Introduction

Congenital heart defects (CHDs) are the most common kind of birth defect worldwide (Pediatric Cardiac Genomics et al. 2013), with approximately 1.35 million infants born with a CHD each year (van der Linde et al. 2011). Moreover, CHDs cause the majority of infant deaths (Dean, Udelsman and Breuer 2012). However, the underlying causes are only partially understood, particularly in the absence of drug-induced mutations during organ development. Although great progress has been shown, many cardiac defects, like ventricular septal defects (VSDs), must currently be repaired by open heart surgery (Limperopoulos et al. 1999), or in severe cases, by pediatric heart transplantation. These procedures, even when successful, can cause developmental delays, long-term cardiac complications, and shorter life expectancy. Developmental toxicity studies have primarily focused on small animal models, which do not recapitulate human heart development and might result in false information on the effect of potential, new pharmaceuticals on the developing organ. Although attempts to incorporate stem cell technology into pharmaceutical testing have been made (Caspi et al. 2009), current state-of-the-art drug-screening platforms for developmental toxicology identification still employ a wide range of animal subjects, which are not only expensive and time-consuming, but also raise concern due to interspecies variability which can result in false-positive and false-negative results.

Thalidomide ((±)2-(2,6-Dioxo-3-piperidinyl)-1H-isoindole-1,3(2H)-dione) (Kumar et al. 2012), a sedative drug launched in 1957 (Smithells and Newman 1992), caused birth

defects in more than 10,000 children and is a key example of the limitations of animal testing. Approximately 6% of affected infants showed CHDs including VSDs and ASDs, 30-40% diseased after birth due to severe defects (Smithells and Newman 1992), and an unknown number of miscarriages were the aftermath of thalidomide (Ito, Ando and Handa 2011). Although thalidomide caused several different kinds of birth defects, the drug is mainly affiliated with limb deformation (Therapontos et al. 2009). Thalidomide was considered a "wonder drug" due to its non-lethal effects when overdosing (Smithells and Newman 1992) and was publicized immediately after small animal experimentations. Studies now show that thalidomide's interactions during organogenesis are species-dependent, which brought about severe obstacles to effectively screen future candidate drugs. Although thalidomide changed the field of drug testing procedures and regulations, thalidomide's power to cure and impair sever illnesses, such as multiple myeloma and leprosy, led to its FDA approval in 1998 (Jenkins et al. 2007). Due to its significance and known effects, thalidomide was chosen as a model drug for demonstrating the applicability of the *in vitro* 3D developing human engineered cardiac tissue model to detect adverse pharmaceutical effects during human heart development.

Stem cell-based *in vitro* models with the ability to mimic human developmental processes can be used to better understand heart development but also enhance drug discovery and toxicology. This is a powerful option to significantly change the field of pediatric cardiology and revolutionize developmental toxicity screening by improving patient safety and eliminate errors resulting from interspecies variations during pharmaceutical testing (Adler et al. 2008). Specification and differentiation of cardiac cells from human induced pluripotent stem cells (hiPSCs) *in vitro* follow pathways

analogous to those involved during development of the heart *in vivo* (van den Heuvel et al. 2014). Stem cell biologists have drawn upon developmental biology to establish high-efficiency protocols for differentiation of hiPSCs into cardiomyocytes (CMs) which now can be employed to mimic development and to study and better predict cardiac toxicity of pharmaceuticals. Small molecule-based differentiation using Wnt/β-catenin signaling has proven efficient; in recent studies it has been shown that β-catenin is essential for mesoderm formation and cardiogenesis (Lian et al. 2012)**.**

Here we study thalidomide-induced developmental changes during the cardiac differentiation process of hiPSCs to produce 3D developing human engineered cardiac tissues (3D-dhECTs). By providing a 3D microenvironment throughout the timeline of stem cell differentiation, thalidomide-induced developmental changes and abnormalities were identified in 3D-dhECTs. Although thalidomide is a widely studied pharmaceutical, less is known about its interactions with differentiating hiPSCs.

We applied our previously developed single-cell handling approach to create hiPSC-laden hydrogels that develop into ontomimetic 3D-dhECTs over time (Kerscher et al. 2015b) and tested whether it can be used to identify thalidomide-induced changes which have not been previously detected in any other *in vitro* drug-testing models. During initial studies we verified that 70 μM thalidomide did not change short term hiPSC viability, proliferation, and mitochondria distribution when compared to control groups. Thalidomide-treatment groups were administered to 3D-dhECTs starting from day 1 of cardiac differentiation and showed effects after initial dosage administration. Tissue growth in thalidomide-treated 3D-dhECTs was less on days 3 and 5 when compared to control 3D-dhECTs. In our 3D-dhECT model we detected changes in tissue architecture

and total cell number per tissue early after onset of spontaneous contraction. Contraction frequencies of thalidomide-treated 3D-dhECTs were significantly slower and the formation of a dense tissue was less apparent than in control tissues. When dissociated, thalidomide-treated CMs contained localized and clustered mitochondria while control CMs developed more evenly spread out mitochondria throughout the cytoplasm. Overall, findings show that our 3D-dhECT model of the developing heart is a robust 3D developmental tissue platform to detect human-specific drug-induced changes during development. We showed that thalidomide negatively influenced cardiac tissue formation, contractile function, mitochondria development, and calcium transient duration.

6.2 Materials and Methods

6.2.1 HiPSC culture and maintenance

Human induced pluripotent stem cells (hiPSCs, IMR-90 Clone 1, WiCell) were cultured on hESC qualified Matrigel (Thermo Scientific) using mTeSR-1 medium (Stem Cell Technologies). HiPSCs were passaged using Versene (Life Technologies) and cultured in mTeSR-1 medium supplemented with 5 μM ROCK inhibitor (Y-27632, Stem Cell Technologies) for 24 h.

6.2.2 3D developing human engineered cardiac tissue (3D-dhECT) formation process

All chemicals were purchased from Sigma-Aldrich unless reported otherwise. PEG-fibrinogen was synthesized as previously described (Dikovsky et al. 2006, Kerscher et al. 2015b). In short, tris (2-carboxyethyl) phosphine (TCEP, Acros Organics) was mixed with 7 mg/ml fibrinogen with 8 M urea. Next, PEGDA was reacted with fibrinogen for 3 h, precipitated in acetone and dissolved in PBS with 8 M urea. The reacted PEG-fibrinogen was dialyzed in PBS for 48 h. The fibrinogen content was measured to be 12.5 mg/ml using Pierce BCA assay (Thermo Scientific).

HiPSCs were collected using Versene and combined with liquid PEG-fibrinogen precursor solution (10 mg/ml fibrinogen) containing 1.5v/v% triethanolamine (TEOA), 3.96 µl/ml N-vinyl pyrrolidone (NVP), and 10 mM eosin Y (Fisher Scientific) photoinitiator at a cell density of $(55 \pm 8.5) \times 10^6$ hiPSCs/ml of PEG-fibrinogen. 8 µl of this mixture was transferred into a circular PDMS mold on acrylated glass (Kerscher et al. 2015b) and photocrosslinked using visible light (203 mW/cm^2) for 20 s. Following photocrosslinking, the PDMS mold was removed and cell-laden hydrogels on acrylated glass were cultured in mTeSR-1 medium supplemented with 5 µM ROCK inhibitor for 24 h. On day -2 and day -1, mTeSR-1 medium was changed daily.

6.2.3 Thalidomide treatment

To determine thalidomide's effect on cardiac differentiation, the drug vehicle (highest solvent concentration), 10 µM, and 70 µM thalidomide were added to the differentiation medium from day 1 to day 40 of differentiation (**Fig. 6.1 A**).

6.2.4 Cell viability and immunofluorescence staining

HiPSC viability and proliferation 24 h after thalidomide addition were assessed using a LIVE/DEAD viability kit (Molecular Probes) and immunofluorescence staining with proliferating cell nuclear antigen (PCNA, Millipore) and 4',6-diamidino-2-phenylindole (DAPI, Molecular Probes) (n = 3 per condition). The percentages of viable and proliferating cells were calculated as the number of viable and PCNA positive cells divided by total cell number.

6.2.5 Early growth progression of thalidomide-treated tissues

Low magnification images of whole tissues were acquired using a phase contrast microscope (Ti Eclipse, Nikon) and Andor Luca S camera from day -2 to day 5. The lateral surface area of designated edges of control, 10 μM, and 70 μM thalidomide treated 3D-dhECTs were analyzed using ImageJ with standard analysis plugins (n = 3 tissues). The area of all day 1 tissues was normalized and the subsequent increase in tissue area was calculated based on a tissue-by-tissue comparison.

6.2.6 Frequency of contraction

24 h after medium exchange including thalidomide treatment groups, videos of spontaneously contracting tissues were acquired using a phase contrast microscope (Ti Eclipse, Nikon) equipped with an Andor Luca S camera. Frequency of contraction on days 11, 14, and 17 were analyzed using NIS Elements (Nikon) and ImageJ software.

6.2.7 Enzymatic cardiac tissue dissociation

Tissues were incubated at 37 ºC for 2 h with collagenase Type 2 (1 mg/ml, Worthington) in 120 mM NaCl, 5.4 mM KCl, 5 mM $MgSO_4$, 5 mM Na-pyruvate, 20 mM glucose, 20 mM taurine, and 10 mM HEPES (pH 6.9) supplemented with 30 µM $CaCl_2$ and 5 µM ROCK inhibitor. Cells were further dissociated with 0.25% trypsin (EDTA) at 37ºC for 5 min. All cells were resuspended in RPMI20 medium (RPMI 1640 medium with 20% FBS) supplemented with 5 µM ROCK inhibitor and plated onto fibronectin coated PDMS glass coverslips.

6.2.8 Immunocytochemistry of control and thalidomide-treated developing 3D-dhECTs

HiPSCs and dissociated tissues were fixed using 4% paraformaldehyde (Electron Microscopy Sciences), permeabilized using PBS-T (PBS with 1% bovine serum albumin (BSA) and 0.2% Triton X-100) and blocked in 3% fetal bovine serum (FBS, Atlanta Biologicals) in PBS. Primary antibody α-sarcomeric actinin (αSA) and secondary antibody Alexa Fluor 488 (Invitrogen) were then added consecutively. All samples were counterstained with 4',6-diamidino-2-phenylindole (DAPI, Molecular Probes) and visualized using a A1si confocal microscope (Nikon).

6.2.9 Quantification of total cell number in control and thalidomide-treated 3D-dhECTs

On day 15 of differentiation, control and 70 µM 3D-dhECTs were dissociated into single cells as described before. Singularized cells were transferred to RPMI20 media (RPMI +

20% FBS) and centrifuged at 200 g for 5 min. Cells were prepared for cell counting using flow cytometry, similar as described before (Kerscher et al. 2015b).

6.2.10 Sarcomere spacing

On day 38 of differentiation, 3D-dhECT CMs stained with αSA were analyzed with fast Fourier transform (FFT). Images were acquired using a Nikon A1si confocal microscope. All images were imported to Image J, where FFT and intensity profiles of drawn paths along well-defined, in-plane sarcomeres were collected. Data from intensity profiles were used to perform FFT. A minimum of ten sarcomeres per treatment group were selected based on continuity of sarcomeres in one field of view.

6.2.11 Mitochondria localization and analysis of thalidomide-treated hiPSCs and 3D-dhECT CMs

HiPSCs and dissociated 3D-dhECT cells of all treatment groups were stained for mitochondria (n = 3 per condition). Mitochondria were visualized using MitoTracker Red (Invitrogen) diluted to a final concentration of 1 nM in cell culture media. MitoTracker Red working solution was added to all wells and incubated at 37 °C for 30 min. Cells were rinsed with PBS, fixed, permeabilized, and blocked. 3D-dhECT cells were also stained with αSA to identify mitochondria of CMs only. All samples were counterstained with DAPI. Three images per well (areas with similar confluency) will be acquired and analyzed using MQM (Kerscher et al. 2015a), a custom developed MATLAB script, and will be used as previously described to determine number and area of mitochondria per cell.

6.2.12 Statistics

The reported results were analyzed with Minitab 17 and the mean ± SD was reported of all replicates. First, normality was checked and data with equal variance and sample size was analyzed by one-way analysis of variance (ANOVA) with Turkey's test. $P < 0.05$ was considered statistically significant.

6.3 Results

6.3.1 Thalidomide influenced the cardiac tissue formation process

Thalidomide previously showed significant changes at 10 and 70 µM during hPSC differentiation (Meganathan et al. 2012). Recent improvements in cardiac differentiation efficiency through a 2D monolayer differentiation system accompanied by the temporal addition of small molecules provides better reproducibility between experiments and allows for more accurate drug-testing due to that. To achieve high yields of CMs and reproducible results, a key aspect to success is the initial cell seeding density and cell proliferation (Lian et al. 2012, Lian et al. 2013). Ma *et. al.* investigated the effects of thalidomide with this small molecule differentiation system on a PEG substrate (Ma et al. 2015b). Although changes in chamber height, frequency of contraction and velocity were determined, significantly less constructs, which were treated with thalidomide, started to contract.

In our study, we first produced 2D monolayers on Matrigel coated 12-well plates and determined the feasibility of using this differentiation approach to study thalidomide-induced effects. The majority of monolayers formed with 70 µM thalidomide did not result in contracting monolayers and were not pursued further for this study (data not

shown). Before evaluating thalidomide's effects on differentiating hiPSCs, short term effects of the drug-carrier, DMSO, and the highest thalidomide concentration (70 μM) were tested to verify that the drug and its carrier did not cause abnormal changes in cell viability and proliferation at the selected concentrations (Gao, Sprando and Yourick 2015). HiPSC viability and proliferation 24 h after treatment-group addition did not show any changes between control and 70 μM thalidomide treated cells (**Fig. 6.1 B, C and Fig. 6.2 A, B**). We also evaluated mitochondria area and location in control and thalidomide-treated hiPSCs by using our custom developed MQM code (Kerscher et al. 2015a) which was used to obtain unbiased differences in control and thalidomide-treated cells. No significant differences in mitochondria distribution were detected between treatment groups (**Fig. 6.2 C**).

During the initial days of drug administration, changes in tissue formation progression were observed. Thalidomide treatment was administered during early stages of tissue development on days 1, 3, 5, and 7 (**Fig. 6.1 A**). A trend of increased lateral surface area was observed in control, 10 μM, and 70 μM thalidomide over time (**Fig. 6.3 A**). This change in tissue growth was accompanied by visual cell debris surrounding the 70 μM thalidomide-treated tissues. In comparison, control microislands formed tissues with more defined edges (**Fig. 6.3 B**).

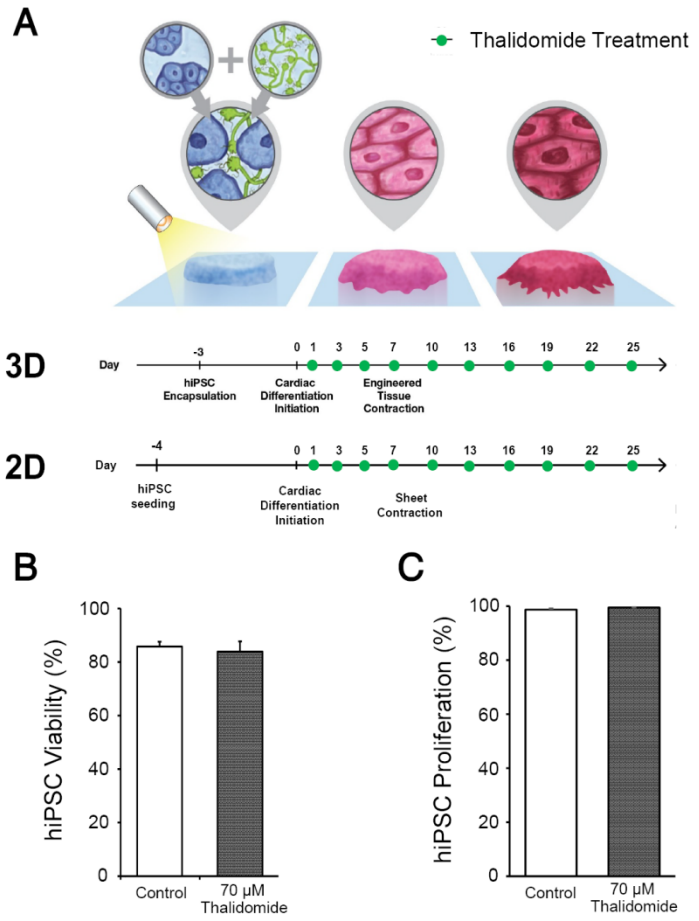

Fig. 6.1. HiPSC differentiation timeline to form 3D developing human engineered cardiac tissues (3D-dhECTs) and 2D monolayers for thalidomide drug-testing. (A) HiPSCs were combined with aqueous PEG-fibrinogen precursor solution, photocrosslinked to form 3D-dhECTs, and cultured for three days before initiating differentiation. For 2D monolayer differentiation, hiPSCs were seeded onto a Matrigel coated 12-well plate and cultured for four days, followed by initiation of cardiac differentiation on day 0. 3D and 2D differentiations obtained thalidomide treatment groups, consisting of control (drug carrier), 10 µM, and 70 µM thalidomide, on days 1, 3, 5, 7, and every three days after that. (B, C) 24 hour drug treatment group addition to hiPSCs did not influence hiPSC viability or proliferation.

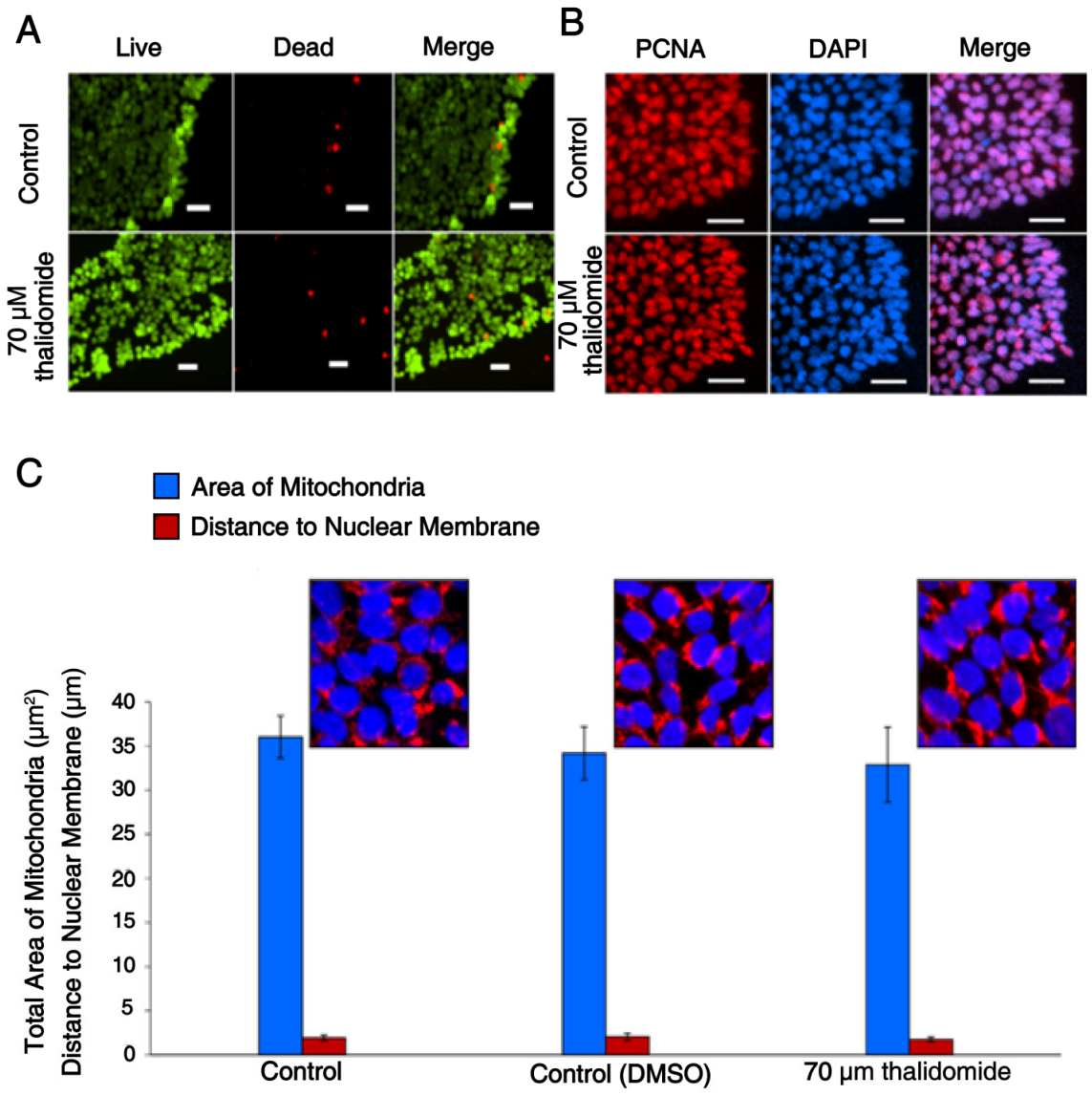

Fig. 6.2. Thalidomide exposure did not cause decreased hiPSC viability, proliferation, and mitochondria distribution. (A) Percentage of viable cells exceeded 90% for control and 70 µM thalidomide conditions. (B) Proliferating cell nuclear antigen (PCNA) staining confirmed greater than 98% cells for all tested conditions. All samples were counter stained with DAPI. Scale bar, 20 µm. (C) Total area of mitochondria and distance to nuclear membrane did not change significantly between control and 70 µM thalidomide treatments.

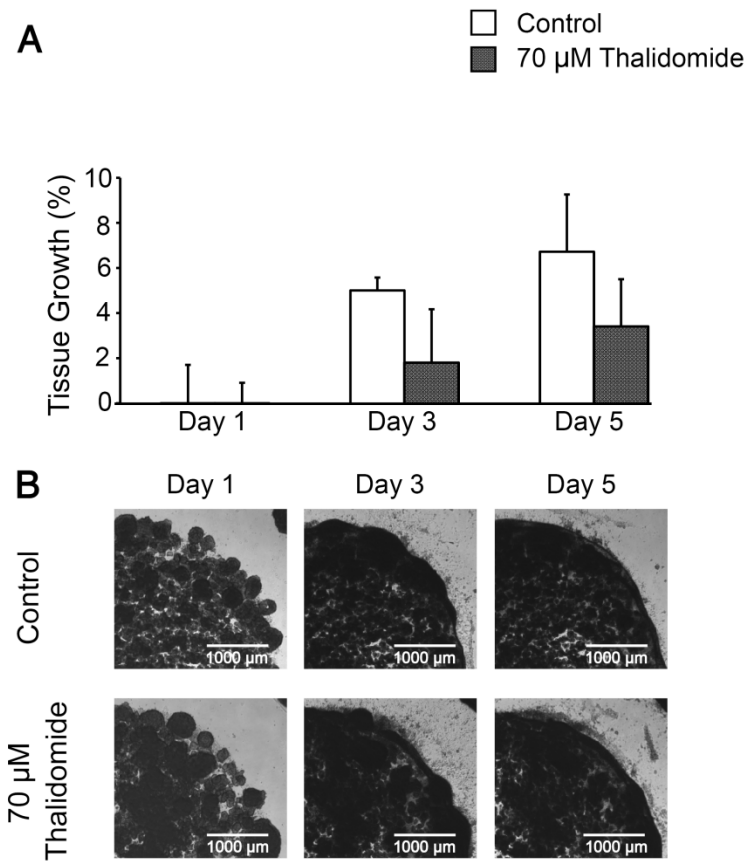

Fig. 6.3. Thalidomide influenced the early tissue formation process and growth. (A) After PEG-fibrinogen encapsulation, hiPSCs grew within the hydrogel to form a continuous tissue. Tissue growth was seen after day 1 of differentiation and continued until day 5 for all treatment groups, with a trend of less tissue growth in 70 µM thalidomide tissues when compared to controls. n = 3 tissues per group. Mean ± s.d. ANOVA $P < 0.05$, * vs. age-matched Control, # vs. Day 1 condition. (B) Edges of control and 70 µM thalidomide tissues started to differ on day 3 of differentiation, with more cell debris and less dense tissue formation in thalidomide treated tissues.

6.3.2 Thalidomide-treated 3D-dhECTs showed slower spontaneous contraction than age-matched controls

In a recent study we showed that 3D-dhECTs show first areas of contraction on day 7 of differentiation. Here, our control 3D-dhECTs also showed first areas of spontaneous contraction on day 7, while thalidomide-treated 3D-dhECTs started to contract one or two days later (day 8 or day 9). When comparing the frequency of spontaneous contraction in control, 10 μM, and 70 μM thalidomide 3D-dhECTs, significant changes were observed between days 11 and 14 of differentiation (**Fig. 6.4 A**). On day 17, 70 μM thalidomide-treated 3D-dhECTs showed significantly slower spontaneous contraction compared to age-matched controls (0.50 ± 0.03 Hz vs. 0.20 ± 0.03 Hz, respectively). Accompanied by the slower frequency of contraction was a high level of monolayer cell outgrowth surrounding the initial tissue footprint in 70 μM thalidomide-treated tissues, which contracted but failed to form a dense, 3D tissue (**Fig. 6.4 B**). Results showed that early tissue growth and tissue formation was hindered during and after the cardiac differentiation process. On day 17, we quantified the total cell number in control and thalidomide-treated 3D-dhECTs and detected significantly less cells in 70 μM thalidomide-treated tissues (**Fig. 6.4 C**).

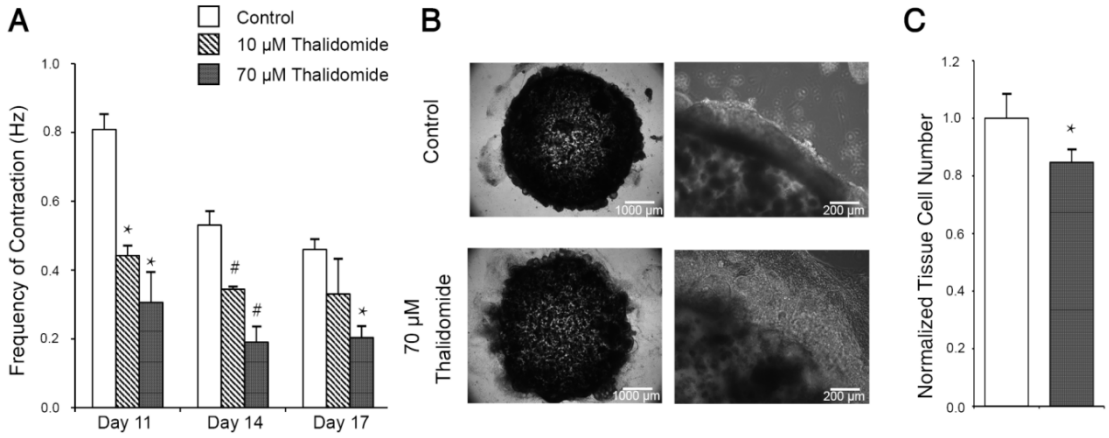

Fig. 6.4. Thalidomide-induced differences in tissue architecture influenced spontaneous frequency of contraction. (A) Significant differences in frequency of spontaneous contraction between control and thalidomide-treated tissues were observed on days 11, 14, and 17, with most differences seen on day 14. *n* = 3 tissues per condition. Mean ± s.d. ANOVA P < 0.05, * vs. same day Control, # vs. same day other conditions. (B) Control 3D-dhECTs developed a dense and clean tissue edge compared to thalidomide-treated 3D-dhECTs (images taken on day 17 of differentiation). (C) On day 17, quantification of total cell number per tissue showed a significantly lower number of cells in thalidomide-treated tissues. *n* = 3 tissues per condition. Mean ± s.d. ANOVA P < 0.05, * vs. Control.

6.3.3 CM number and sarcomere structure were influenced by thalidomide

When investigating the functionality and maturity of SC-CMs *in vitro*, certain parameters like cell size and sarcomere definition and spacing are used as indicators. On day 38 of differentiation, 3D-dhECTs of all treatment groups were dissociated into single cells and re-plated to observe CM size, sarcomere distance, and percent CMs. CMs from 3D-

dhECTs treated with 10 μm thalidomide were significantly smaller in size compared to control 3D-dhECT CMs (**Fig. 6.5 A**). 70 μM thalidomide-treated CMs only showed a trend of smaller cell size compared to age-matched controls. Similarly, sarcomere spacing in 70 μM thalidomide-treated 3D-dhECT CMs was significantly less (1.88 ± 0.19 μm) compared to control CMs (2.03 ± 0.16 μm) (**Fig. 6.5 B**). After the dissociation process, significantly more CMs were detected in control 3D-dhECTs than thalidomide-treated 3D-dhECTs (**Fig. 6.5 C, D**). A high number of cell nuclei were not counterstained with αSA, indicative of a non-CM cell type. In addition to significantly shorter sarcomere spacing and smaller CM size when compared to controls, sarcomeres of control 3D-dhECT CMs appeared to be more defined than thalidomide treated CMs (**Fig. 6.5 E**).

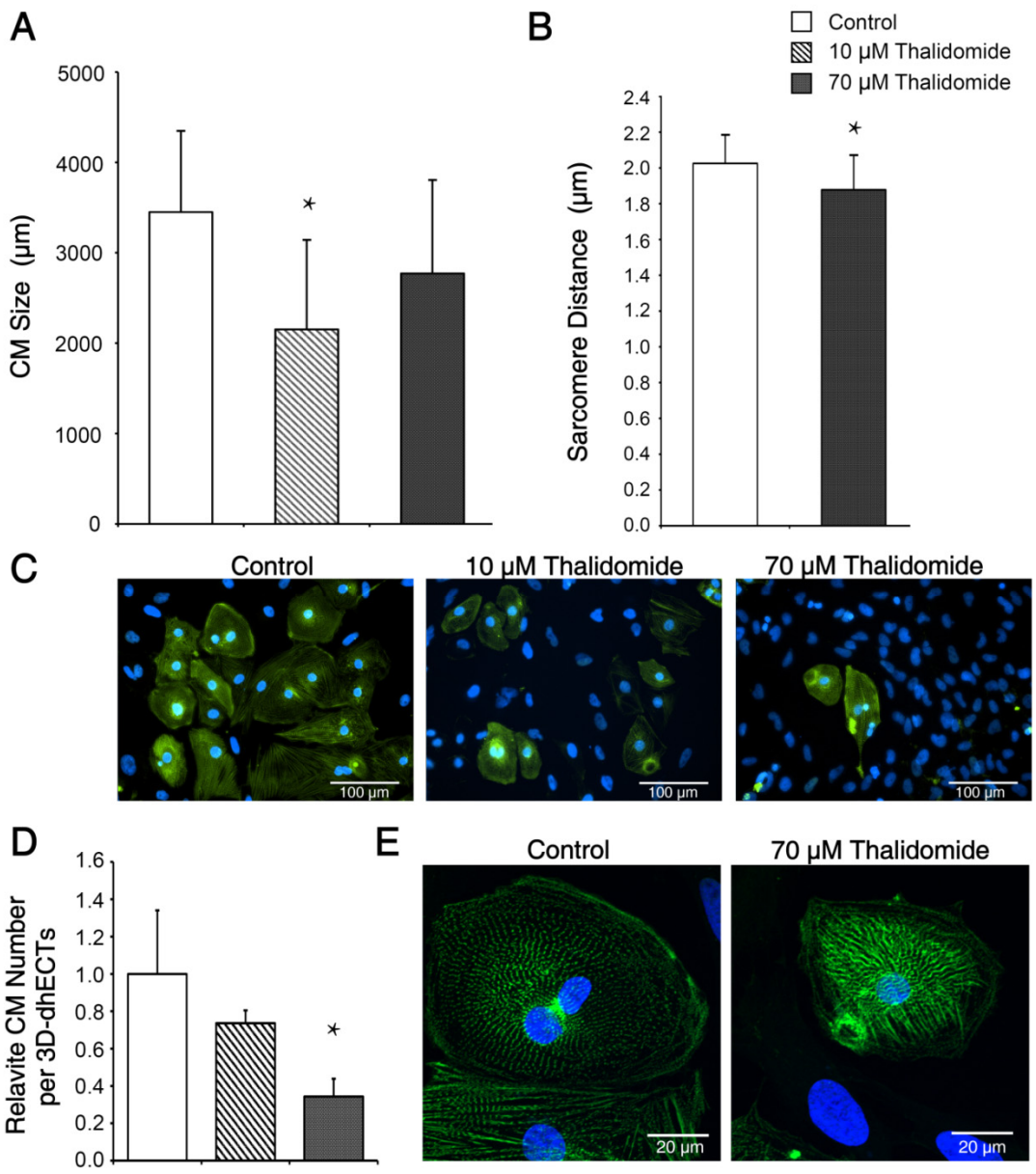

Fig. 6.5. Sarcomere distance and total number of CMs were influenced by thalidomide. (A) Day 38 dissociated 3D-dhECT CMs treated with 10 µM thalidomide were significantly smaller compared to control CMs, and 70 µM thalidomide-treated CMs showed also a trend of smaller cell size. (B) Sarcomere spacing was significantly less in 70 µM thalidomide treated tissues compared to age-matched controls. (C, D) Less αSA positive (green) cells were detected after cardiac tissue dissociation in thalidomide

groups compared to control, suggesting less efficient CM differentiation when thalidomide was administered. (E) Sarcomeres were more defined and organized in control CMs when compared to thalidomide-treated CMs.

6.3.4 Mitochondria in thalidomide-treated CMs were clustered

Mitochondria are the primary organelle responsible for energy production within the cell. Mitochondria are an important component influencing normal heart development and contractile function. During early stages of CM development, mitochondria are only a small portion within a cell's cytoplasm and are structurally visible in a reticular arrangement (Yang et al. 2014), while in the adult CM, mitochondria occupy approximately 20-40% of the total CM volume due to high energy requirements needed for contraction; at this stage mitochondria exhibit a regular distribution with a "crystal-like lattice pattern" (Schaper, Meiser and Stammler 1985). We stained control and 70 μM thalidomide-treated 3D-dhECT CMs with MitoRed to visualize mitochondria. In immature cells, a large quantity of mitochondria is normally located close to the nucleus, which was also the case in both treatment-group cells. In control CMs, mitochondria were evenly distributed throughout the entire cell, also covering areas close to well-defined sarcomeres (**Fig. 6.6 A**). But, mitochondria structure, morphology, and location in the cytoplasm were visually very different in thalidomide-treated cells, showing a clustered pattern (**Fig. 6.6 B**).

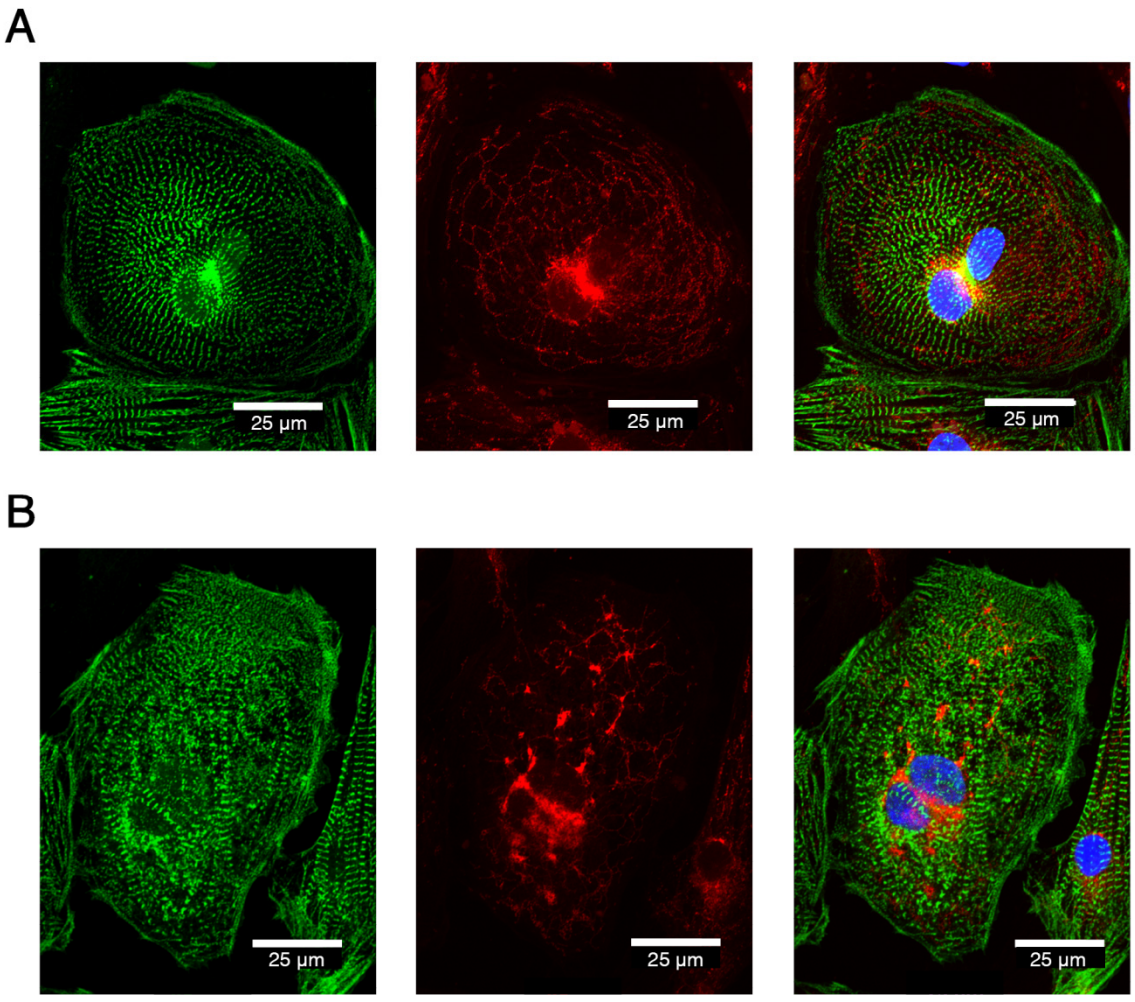

Fig. 6.6. Thalidomide treatment caused changes in mitochondria development. (A) Control and (B) 70 µM thalidomide CMs show differences in mitochondria on day 38 of differentiation. Mitochondria in control CMs were evenly distributed in the cytoplasm while thalidomide treated CMs showed a trend of clustered mitochondria. CMs were stained with αSA (green), MitoRed (red), and DAPI (blue).

6.4 Discussion

To understand the formation of human CHDs, animal models (Ho et al. 1991), culture of explanted developing myocardium (Rivera-Feliciano and Tabin 2006), and 2D cell culture models comparing control versus diseased cell lines has been used historically. Although *in vitro* models will always be an imperfect representation of the *in vivo* reality, by reducing the number of variables in the system, insights that would otherwise be clouded by complexity become apparent. Furthermore, animal models are not conducive to the development of high-throughput screening assays (Giacomotto and Segalat 2010) and in cases like thalidomide, cannot detect human-specific developmental defects. On the other hand, development is a 3D process; cell behavior in 2D culture systems varies greatly from that in 3D. Research groups that focus on detecting changes caused by thalidomide have started to use human pluripotent stem cells as model systems, but still rely on platforms that are only based on cells (Mayshar, Yanuka and Benvenisty 2011, Xing et al. 2015, Ma et al. 2015b). By creating a reproducible and straight-forward 3D developing human engineering cardiac tissue (3D-dhECT) platform for developmental pharmacology, we want to open up the opportunity to be able to detect changes that will influence the developing 3D tissue, but cannot be detected in 2D.

When looking into hPSC differentiation into all three germ layers, the number of up- and down regulated genes significantly increased with thalidomide treatment, with more genes being downregulated (Meganathan et al. 2012), including genes important for cell differentiation and organ development (Mayshar et al. 2011). Gene expression influences the function of developing cells and can play an important role in the contractile function, cell-cell coupling, and ECM production. The known cardiac mutagen, thalidomide, has

been investigated for improving the inflammatory response after heart failure; in these studies thalidomide was found to decrease the collagen content (Yndestad et al. 2006). In addition, type I collagen production was significantly inhibited in cultured human lung fibroblasts exposed to thalidomide (Tseng et al. 2013). Although the effects of thalidomide on ECM production during heart development are still unknown, we believe that our 3D-dhECT platform can be used to identify important differences that can further explain our findings, including thalidomide-induced differences in tissue formation, contractile function, and mitochondrial development.

Thalidomide, which was tested in high concentrations on mice and rats, did not show any teratogenicity; years later researchers discovered that thalidomide's teratogenic effects are species specific. This species specificity underlines the importance of human based *in vitro* studies (Parman, Wiley and Wells 1999). Additionally, thalidomide was shown to induce oxidative stress due to free radical production; in rabbits, thalidomide generates reactive oxygen species (ROS) that carry out DNA oxidation and inhibits fibroblast growth factor expression. Knobloch *et al.* showed that thalidomide induced oxidative stress enhances Bmp signaling (e.g. up-regulation of Bmp) and inhibition of Wnt/β-catenin signaling pathways (Knobloch, Shaughnessy and Ruther 2007). Both Bmp and Wnt signaling pathways are important in cardiac development and are of upmost importance in stem cell differentiation (Lian et al. 2013, Lian et al. 2012). The perturbation of important developmental signaling pathways could therefore lead to thalidomide-induced CHDs, and might have been the reason for fewer CMs in 3D-dhECTs treated with thalidomide. Furthermore, upregulation of Bmp downregulates Akt

signaling; the Akt1 gene is essential for angiogenesis in the heart (Shiojima and Walsh 2006).

Mitochondria are complex organelles that are important in ATP production and cell signaling (Dorn, Vega and Kelly 2015). Our 3D-dhECTs contained CMs with clustered mitochondria, which were not distributed in the cytoplasm of cells. In comparison, control CMs contained mitochondria close to cell nuclei, throughout the cytoplasm, and close to and between sarcomeres, which is common in healthy muscle cells (Hom and Sheu 2009). Differences in mitochondria morphology and volume are often associated with increased reactive oxygen species (ROS) production and apoptosis (Parra et al. 2008), but more experiments to understand the clustering of mitochondria in thalidomide-treated CMs have to be performed.

This study revealed that our 3D-dhECT platform is a robust drug-testing platform to detect thalidomide-induced changes during cardiac development. We detected changes in tissue formation during early stages of development as well as changes in total cell and CM number. Because the successful production of contracting 3D-dhECTs is not closely dependent on the initial seeding density and cell proliferation, all our thalidomide-treated 3D-dhECTs showed some degree of spontaneous contraction, which might have not resulted in any contracting CMs in other cell-based studies.

7. SCALABLE CARDIAC MICROSPHERE PRODUCTION USING HUMAN PLURIPOTENT STEM CELL ENCAPSULATION AND DIFFERENTIATION

7.1 Introduction

Heart disease is the leading cause of death due to the inability for damaged myocardium to efficiently regenerate (Mercola, Ruiz-Lozano and Schneider 2011, Zhang, Mignone and MacLellan 2015). Human cardiomyocytes (CMs) for myocardial repair are difficult to obtain in large quantities, to deliver efficiently through transplantation, and to achieve the necessary integration with the host myocardium (Hartman, Dai and Laflamme 2016). Current differentiation systems of human pluripotent stem cells (hPSCs) are obtained through 2D monolayers which require large surface areas during *in vitro* culture and an additional cell-handling step post-differentiation to achieve CM maturation and advanced functionality (Jenkins and Farid 2015). Tissues can be formed by combining dissociated CMs with different biomaterials that enhance cell-cell and cell-material interactions; other approaches include the self-assembly of 3D cell aggregates generated by centrifugation (Burridge et al. 2011, Burridge et al. 2007) or the stacking of multiple cell monolayers to create a 3D architecture (Shimizu et al. 2003, Nagase, Kobayashi and Okano 2009). Using these tissue fabrication approaches for cell therapy applications brings problematic translational difficulties due to the multiple cell-handling steps and technical difficulties required to form 3D cardiac tissues.

Cell therapies based on human induced pluripotent stem cells (hiPSCs) can facilitate an enhanced and autologous approach to personalized medicine (Zhao et al. 2015) compared to other available treatment options, including syngeneic and allogenic

therapies (Garbern and Lee 2013). HiPSCs can be cultured and expanded *in vitro* for an extended period of time and differentiated into cell types of all three germ layers, including cells like CMs that are normally difficult to obtain and cannot be cultured long term. These stem cell-derived cardiomyocytes (SC-CMs) can then be used for drug-testing and regenerative medicine applications to overcome interspecies and donor variations. Once large quantities of CMs are produced for cell therapy, the successful delivery of cells to the infarcted myocardium presents another hurdle in the field. It is believed that the "ideal" cell type for the repair of a chronically damaged myocardium is a cell phenotypically similar to the host tissue (Li et al. 2012, Oskouei et al. 2012, Citro et al. 2014). Cardiosphere-derived cells (CDCs), which are composed of cardiac stem cells, are commonly used in myocardial repair (Sousonis, Nanas and Terrovitis 2014). Clinical studies in animals (Cheng et al. 2014, Suzuki et al. 2014) and humans (Makkar et al. 2012, Welt et al. 2013, Tarui et al. 2015) showed that injected CDCs improved cardiac function and reduced scar tissue. HPSCs have also successfully been used alone (Chong et al. 2014), in combination with fibrin (Menasche et al. 2015) or collagen (Joanne et al. 2016), to produce SC-CMs for non-human primates, cardiac progenitors for human clinical trials, or SC-CMs in small animal models, respectively. Current clinical trials that infused or transplanted cells showed the positive effect of cell therapy. Although the mechanism of improvement is unclear, it is thought to involve endogenous repair mechanisms (Tarui et al. 2015). The reason for this theory involves the poor survival and integration of implanted cells into the host (Tarui et al. 2015, Malliaras et al. 2012).

Biomaterials are not only used to provide a 3D supporting microenvironment, they have also been shown effective for protecting encapsulated cells from shear (Li et al.

2011). Uniform and precise 3D cell-material constructs can now be produced by emerging technologies like bioprinting (Du et al. 2015, Kang et al. 2016, Ouyang et al. 2015, Ma et al. 2015a) and microfluidic systems (Chan, Zhang and Leong 2016, Zhao et al. 2016). The production of spherical cardiac tissue structures has been studied for years, starting with self-aggregated embryoid bodies (EBs) (Kehat et al. 2001), the initial stem cell differentiation approach to form spontaneously contracting CMs.

Here we describe a fast, uniform one-step hiPSC microsphere encapsulation approach to produce developing cardiac microspheres in a single unit operation. Our custom build microfluidic system can produce at least 60 hiPSC-encapsulated microspheres per minute with an approximate diameter of 917 μm and great control over circularity (0.96). Encapsulated hiPSCs remained viable in PEG-fibrinogen microspheres and grew to form larger and dense microspheres. Mechanical compression testing showed low elastic moduli on day 5 of cardiac differentiation, which we believe contributed to cell survival and high-efficiency cardiac differentiation. Microspheres consistently showed initial areas of contraction on day 8 of differentiation, with high differentiation efficiency by day 20. Microspheres that were sheared through 18 and 23 gauge needles, at a shear rate of 287 and 4,310 s^{-1}, respectively, on day 6 started to spontaneously contract by day 9 of differentiation. Produced cardiac microspheres showed appropriate functional responses to drugs including isoproterenol and propranolol. Furthermore, microsphere CMs responded to outside pacing frequencies up to 6.0 Hz. Microspheres were maintained in culture long term and developed tight cell-cell junctions and displayed aligned myofibrils. Finally, we showed that our microsphere production approach can be applied to the widely used biomaterial, gelatin methacryloyl (GelMA). These results demonstrate

our ability to produce reproducible hiPSC-laden microspheres in a high-throughput manner with high CM yield and functionality, necessary for future applications including to cell-therapy.

7.2 Materials and Methods

7.2.1 HiPSC expansion and maintenance

HiPSC lines IMR-90 Clone 1 and 19-9-11(WiCell) were cultured on hESC qualified Matrigel (Corning) using mTeSR-1 medium (Stem Cell Technologies). HiPSCs were passaged using Versene (Invitrogen) and culture in mTeSR-1 medium supplemented with 5 μM ROCK inhibitor (RI, Y-27632, Stem Cell Technologies) for 24 h.

7.2.2 HiPSC microspheres production and cardiac differentiation

Liquid PEG-fibrinogen precursor solution was prepared by combining PEG-fibrinogen with 1.5 v/v% triethanolamine (TEOA), 3.96 μl/ml N-vinyl pyrrolidone (NVP), and 10 mM eosin Y (Fisher Scientific) photoinitiator (in PBS). Cells were resuspended in PEG-fibrinogen precursor solution at 25 million cells/ml. The PEG-fibrinogen-cell mixture was added to one inlet of a custom built microfluidic system. In parallel, mineral oil (BioXtra) was added to the other inlet of the microfluidic system which, when combined with the PEG-fibrinogen-cell mixture, causes the formation of spherical structures due to immiscibility of PEG-fibrinogen and mineral oil (**Fig. 7.1 A**). Flowrates for the PEG-fibrinogen-cell mixture and mineral oil were set at 1 ml/h and 10 ml/h, respectively. A light source (Prior) was used to photocrosslink the liquid PEG-fibrinogen-cell mixture to form cell-laden microspheres. Microspheres were collected, washed with mTeSR-1 medium, and cultured in mTeSR-1 medium + 5 μM RI for 24 h (day -3).

Microspheres were then cultured for an additional 48 h in mTeSR-1 medium with daily media changes (days -2 and -1).

Three days after microsphere production (day 0), cardiac differentiation (Lian et al. 2013) was initiated by changing medium from mTeSR-1 to 4 ml RPMI/B27 w/o insulin (RPMI/B27-I, Thermo Fisher) supplemented with 12 μM CHIR (Stem Cell Technologies) per well. On day 1 (24 h after CHIR addition), medium was changed to 4 ml RPMI/B27-I. 48 h after that (day 3), 2 ml old media was combined with 2 ml fresh RPMI/B27-I supplemented with 5 μM IWP2 (Stem Cell Technologies). On day 5, media was replaced with 4 ml RPMI/B27-I and on day 7, RPMI/B27-I was changed to RPMI/B27 medium (Thermo Fisher). RPMI/B27 medium was replaced every three days after that.

7.2.3 Microsphere diameter, circularity, and early growth quantification

Daily phase contrast images of microspheres were taken from the time of encapsulation (day -3) until initiation of cardiac differentiation (day 0). After that, phase contrast images were acquired every other day.

Microsphere diameter and size of three individual batches were determined 24 h after encapsulation. Autofluorescence of the photoinitiator eosin Y in PF microspheres was captured on a fluorescence microscope at low magnification. Images were analyzed using ImageJ with standard plugins.

Microsphere growth prior to the initiation of spontaneous contraction was determined by analyzing phase contrast images on days -3, 0, 3, and 7 of differentiation by manual outlining of microspheres using ImageJ (n = 10).

7.2.4 Parallel plate mechanical testing

Day 5 microspheres formed using IMR90 and 19-9-11 hiPSCs were tested for their compressive mechanical properties using a micron-scale mechanical testing system (Microsquisher, CellScale). Force was calculated via cantilever beam deflection in response to user-defined displacement (17% displacement) with compression rate of 4 μm/s. All samples were tested in PBS at 34 ºC. The cantilever beam was composed of Tungsten (modulus = 411 GPa) with a diameter of 304.8 μm. Stress-strain characteristics of acellular and cellular tissues were obtained and the elastic modulus was directly obtained within the 5% strain range.

7.2.5 XTT assay and shear study

To verify hiPSC proliferation within PEG-fibrinogen hydrogels after encapsulation, cell activity on days -2 and -1 were determined using XTT assay (ATCC). One microsphere was placed in each well of a 96-well plate. The assay was performed by following the company's instructions.

On day 6 of differentiation, microspheres were submerged in fetal bovine serum (FBS), and sheared through a 18 gauge (inside diameter = 0.84 mm) or 23 gauge (inside diameter = 0.34 mm) syringe needle at 1 ml/min, resulting in a shear rate of 287 and 4,310 s^{-1}, respectively. Sheared microspheres were compared to age-matched, unsheared controls. Results for XTT assay were collected 24 hr after the experiment.

7.2.6 Cardiac microsphere dissociation

Microspheres were washed with PBS followed by the incubation in dissociation solution containing collagenase type 2 (1 mg/ml, Worthington) at 37°C for 2 h. The dissociation solution contained 120 mM NaCl, 5.4 mM KCl, 5 mM $MgSO_4$, 5 mM Na-pyruvate, 20 mM glucose, 20 mM taurine, and 10 mM HEPES (pH 6.9) supplemented with 30 µM $CaCl_2$ and 5 µM ROCK inhibitor. Microspheres were centrifuged, resuspended in trypsin (EDTA) and incubated at 37°C for 5 min. Trypsin was neutralized using RPMI20 (20% FBS in RPMI1640 medium); cells were resuspended in RPMI20 with 5 µM ROCK inhibitor. Dissociated cells were plated on fibronectin coated (25µg/ml, Thermo Fisher) PDMS coverslips and incubated for three days.

7.2.7 Multielectrode array

Day 20 and day 50 cardiac microspheres were dissociated for 2 hrs in collagenase solution (as previously described), resuspended in RPMI20 medium supplemented with 5 µM ROCK inhibitor, and cultured on a S2 type MEA200/30-Ti-gr (Multichannel Systems) for at least 24 hrs. Spontaneously contracting CMs were perfused with Tyrode's solution at 37 ºC using a MEA system with Multichannel Systems 1060-Inv-BC amplifier. When stabilized, baseline field potential recordings were acquired at a sampling frequency of 10 kHz. CMs were exogenously paced from 1.0 to 6.0 Hz. To assess drug response, 1 µM isoproterenol was added with a subsequent addition of 1 µM propranolol (Molecular Devices). Drugs were washed out to recover the baseline field potential profiles. Finally, 5 µM sotalol (Molecular Devices) was added and field potential recordings were analyzed.

7.2.8 Scanning electron microscopy

Microspheres were collected for SEM. First, microspheres were rinsed with PBS and fixed in 4% paraformaldehyde and 2% glutaraldehyde in PBS for 15 min. Then the microspheres were rinsed with PBS and 2% osmium tetraoxide was added for 1.5 h. After further PBS rinses, the microspheres were subjected to quick freeze with liquid nitrogen and then lyophilized (Labconco). Dried microspheres were mounted on aluminum stubs, sputter-coated with gold (Pelco SC-6 sputter coater) and imaged using JEOL JSM-7000F scanning electron microscope.

7.2.9 Statistics

To analyze the reported results, Minitab 17 was used and the mean ± SD was reported of all replicates. After checking for normal distribution, one-way analysis of variance (ANOVA) with Turkey's test was used for all studies with equal variance and equal sample size. If equal variance did not apply, the Games-Howell test was used. $P < 0.05$ was considered statistically significant.

7.3 Results

7.3.1 Fast, one-step microfluidic encapsulation device produced uniform and circular hiPSC microspheres

Within the microfluidic device, the combination of liquid PEG-fibrinogen precursor solution and hiPSCs was joined with an oil phase to form spherical structures that were photocrosslinked to form microspheres (**Fig. 7.1 A**). The aqueous PEG-fibrinogen-hiPSC mixture was traveling with a constant flow rate through the microfluidic device while

achieving sufficient crosslinking in less than 1 s to form a crosslinked microsphere. Encapsulated hiPSCs displayed a round morphology with some cells being exposed beyond the PEG-fibrinogen hydrogel boundary (**Fig. 7.1 B**). The device can produce about 60 hiPSC-encapsulated microspheres per minute with control over size and circularity (**Fig. 7.1 C-E**). Autofluorescence of the photoinitiator, eosin Y, was used as a fluorescence indicator to measure cell-laden microsphere diameter and circularity (**Fig. 7.1 C**). On the same day of encapsulation (day -3), the initial microsphere diameter was 917.2 ± 68.9 μm (**Fig. 7.1 D**) and circularity was 0.96 ± 0.03 (**Fig. 7.1 E**, n = 524 microspheres, 3 independent batches). HiPSC-encapsulated micrsosphere hydrogels displayed well-defined boundaries with cells being distributed within the PEG-fibrinogen hydrogel. HiPSCs were cultured in their pluripotent state for three days before cardiac differentiation was initiated on day 0. Previously (Kerscher et al. 2015b), three days was shown to be sufficient for hiPSCs to adjust to their new, 3D hydrogel microenvironment and to initiate cell growth within the hydrogel to form a more continuous tissue over time. Microspheres also projected the same trend in tissue growth compared to 3D-dhECTs, with cells initially growing within the borders of the PEG-fibrinogen hydrogel, occupying the majority of the spherical volume (**Fig. 7.1 F**).

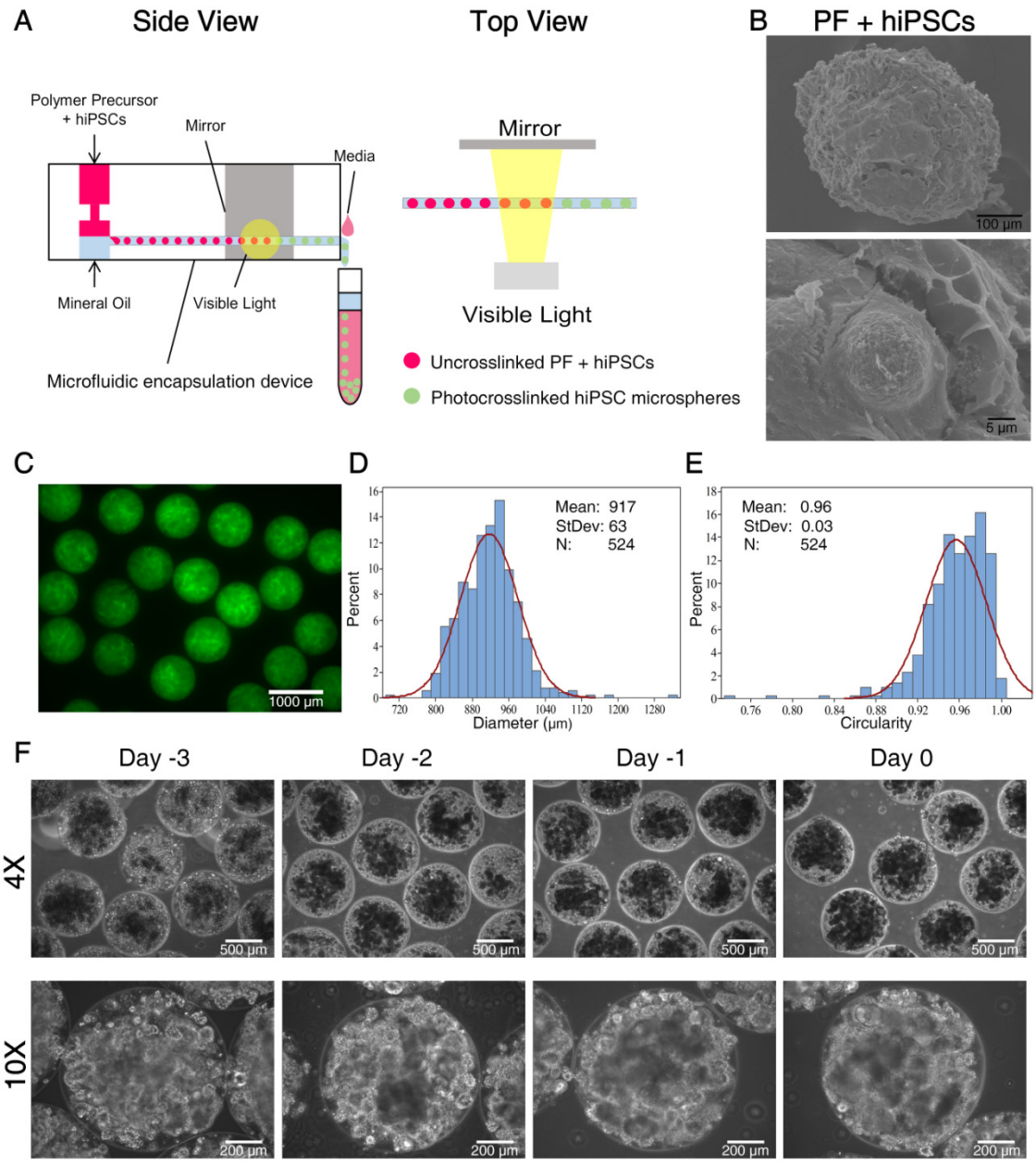

Fig. 7.1. HiPSC encapsulated microspheres can be formed with a custom-built microfluidic device. (A) HiPSCs suspended in hydrogel aqueous-precursor solution were combined with an oil phase to produce uniform cell-laden microspheres. The cell-polymer solution was infused through the tubing at 1 ml/hr and each microsphere was photocrosslinked for less than 1 s. (B) Microspheres were maintained in their pluripotent

state for three days before initiating cardiac differentiation on day 0. During this time, hiPSCs adapted to their new 3D microenvironment and were exposed beyond the PEG-fibrinogen boundary. (C) Microsphere diameter and circularity were determined by quantifying eosin Y's autofluorescence 24 h after photocrosslinking. (D) Microspheres were 917 μm in size and were highly circular (n = 3 batches, 524 spheres analyzed, 3 independent batches).

7.3.2 HiPSC-laden microspheres possessed soft mechanical characteristics which contributed to microsphere growth

Before culture medium was switched to initiate cardiac differentiation on day 0, hiPSCs grew within the initial microsphere boundaries (**Fig.7.1**). After day 0, differentiating cells continued to grow within and beyond the initial microsphere boundaries to produce denser and larger tissues with decreasing circularity (**Fig. 7.2 A**). At an initial cell encapsulation density of ~25 x 10^6 hiPSCs per ml, cells initially grew within the original hydrogel boundaries, maintaining their original diameter. To verify cell proliferation prior to initiation of differentiation on day 0, XTT assay 24 (day -2) and 48 (day -1) hrs after encapsulation was run for each tested hiPSC line (IMR90 and 19-9-11). This confirmed that cells from both hiPSC lines were more active on day -1 than 24 hr prior (**Fig. 7.2 C**). By day 3, microsphere diameter increased 1.3 times when compared to day 0, and further increased to 1.7 times by day 7 of differentiation (**Fig. 7.2 B**). Furthermore, both hiPSC lines were also used to study the mechanical properties before the onset of spontaneous contraction. On day 5 of differentiation, the elastic modulus of IMR90 and 19-9-11 encapsulated hiPSCs was 37 ± 4 Pa and 38 ± 7 Pa, respectively (**Fig. 7.2 D**).

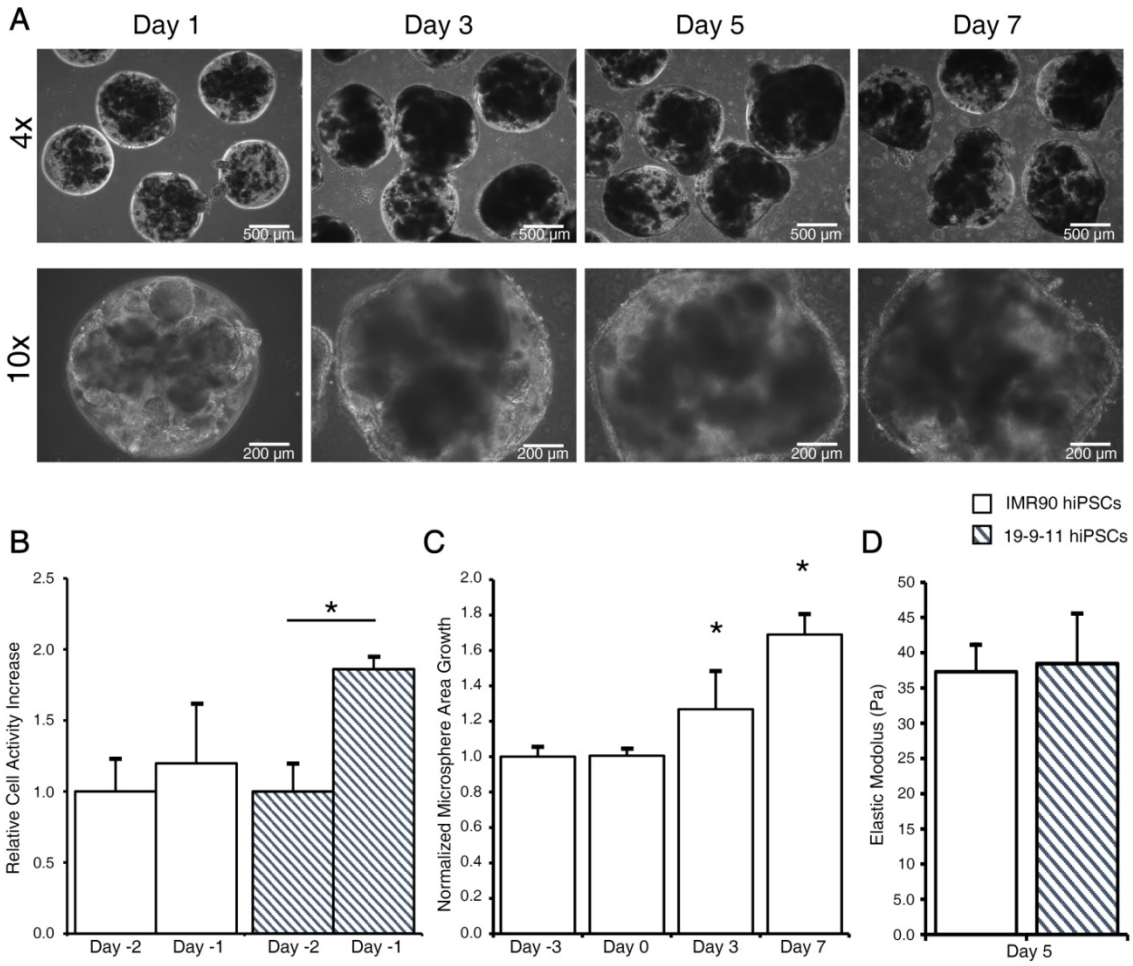

Fig. 7.2. Soft hiPSC microspheres grew to form dense tissues. (A) Phase contrast images throughout the time course of cardiac differentiation visually showed the progression of differentiating cells in PEG-fibrinogen microspheres. (B) Before cardiac differentiation, cell proliferation for two hiPSC lines was verified by XTT assay, which showed an increase in cell activity between day -2 and day -1 (n = 5 microspheres per condition). (C) From the onset of cardiac differentiation (day 0), microsphere size increased significantly by day 3, and continued to grow until day 7. (D) The elastic modulus of day 5 microspheres for both hiPSC lines was less than 40 Pa.

7.3.3 3D hiPSC-laden hydrogels become cardiac microspheres

Our microfluidic device was successfully used to produce hiPSC encapsulated microspheres in a high-throughput manner that resulted in spontaneously contracting cardiac microspheres over time. Microspheres were cultured in suspension and under stagnant conditions; due to the spherical architecture, internal cell alignment and uniform cell growth was difficult to achieve with increasing culture time, which we saw when studying the shape and cell arrangement of cardiac microspheres. Dense microspheres (**Fig. 7.3 A**) repeatedly started to spontaneously contract on day 8 of differentiation, with about 78% microspheres contracting by day 10 (n = 90 microspheres, **Supplementary Movie 7.1**). Differentiation efficiency was consistently high between batches, with 71.6 ± 8.4 % total CMs (cTnT+), 7.1 ± 1.7 % proliferating CMs (cTnT+/Ki67+), and 8.41 ± 6.5% fibroblasts (P4HB+) (n = 3 individual batches, **Fig. 7.3 B**). During the cardiac microsphere development, organoid-like structures formed with high nuclear density and αSA expression (**Fig. 7.3 C**). When sectioned, we detected areas with high cell density, holes, and pockets of epithelial-like cell arrangements (**Fig. 7.3 D**).

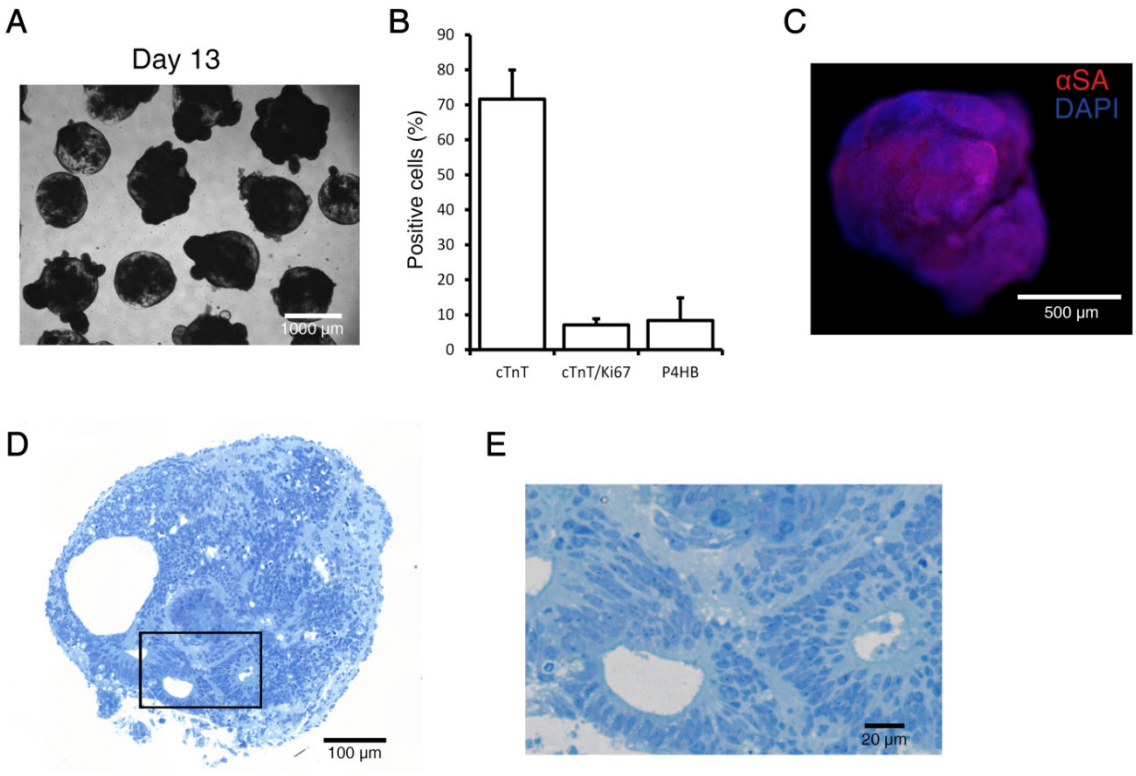

Fig. 7.3. 3D cardiac differentiation enabled high CM yield in microspheres. (A) Uncontrolled cell growth formed less uniform, but spontaneously contracting microspheres. (B) Day 20 microspheres were composed of 71.6 ± 8.4 % CMs (cTnT+), with 7.1 ± 1.7 % proliferating CMs (cTnT+/Ki67+). Microspheres were also contained of 8.41 ± 6.5% fibroblasts (P4HB+, n = 3 individual batches). (C) Whole tissue staining with cardiac marker αSA (red) and DAPI (blue) revealed an organoid-like structure with areas of high nuclear density. (D) Microsphere section showed areas of high cell density and regions similar to epithelial-like cells.

7.3.4 Microspheres survived shear and started to contract spontaneously with maintenance of their structure

The spherical tissue architecture has been shown beneficial for approaches including cell delivery through injection (Feyen et al. 2016). Here we investigated if microspheres, before the onset of spontaneous contraction, will survive shear stress and spontaneously contract afterwards. Two needle sizes, 18 gauge and 23 gauge, were used for this experiment and microspheres were sheared at a rate of 287 and 4,310, respectively and compared to unsheared, age-matched controls. The spherical structure after shear was maintained (**Fig. 7.4 A**) and microspheres from all groups attached to TCPS. One day after shearing, cell activity was highest in unsheared controls and decreased with increasing needle gauge (**Fig. 7.4 B**). The outer structural architecture appeared to be different in unsheared versus sheared microspheres. SEM images showed a smooth surface in the control (**Fig. 7.4 C**), while 18 gauge sheared microsphere exposed their internal ultrastructure (**Fig. 7.4 D**). As mentioned earlier, unsheared control microspheres spontaneously contracted on day 8; sheared spheres showed isolated areas of contraction on day 9 of differentiation (three days after shearing, **Supplementary Movie 7.2**).

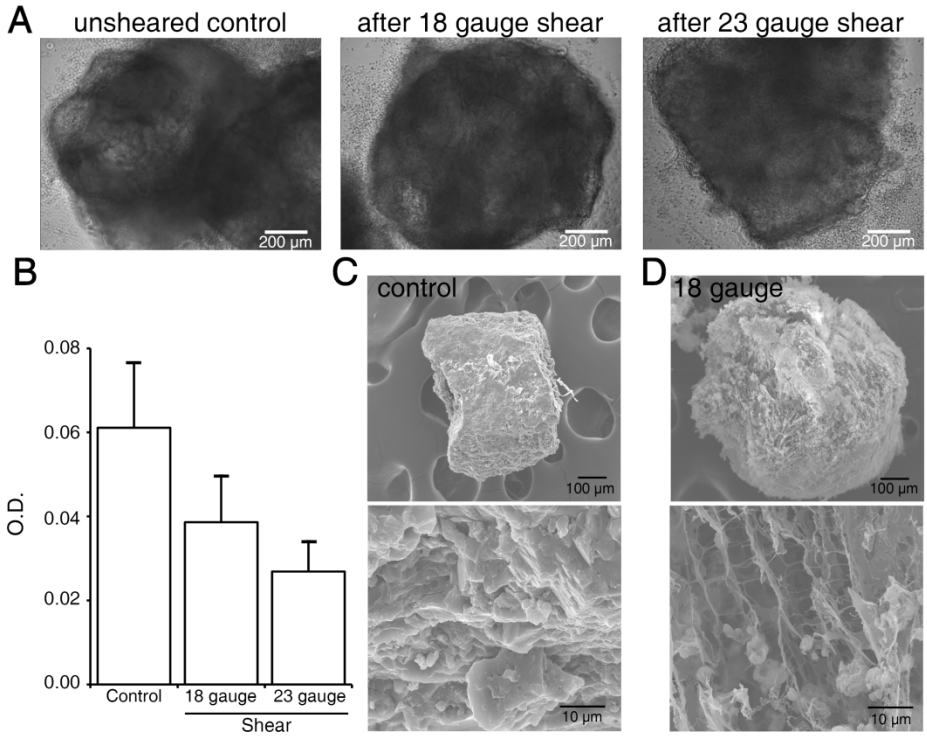

Fig. 7.4. Needle shear did not hinder microspheres from spontaneously contracting and maintaining their structure. On day 6 of differentiation, microspheres were sheared through a 18 or 23 gauge needle and compared to unsheared control microspheres. (A) After shearing, microspheres adhered to well-plates and started to spontaneously contract on day 9 (one day later than control microspheres, see **Supplementary Movie 7.2**). (B) Cell activity of sheared microspheres decreased with increase in needle gauge (n = 5 microspheres). (C) Unsheared day 6 microspheres showed a smooth outer surface with cells being exposed, while (D) architecture of sheared microspheres was shown on the tissue surface, but structural integrity was maintained.

7.3.5 Microsphere CMs responded to drug treatment and electrical stimuli

For the successful translation of engineered cardiac tissues towards regenerative medicine and drug-screening, the response to pharmacological and electrical stimuli is important to study. Using MEA analysis (**Fig. 7.5 A, Supplementary Movie 7.3**), we evaluated the response of our 20 day old cardiac microspheres to drugs including the β-adrenergic agonist, isoproterenol, β-adrenergic antagonist, propranolol, and the β-adrenergic receptor blocker, sotalol. Isoproterenol increases the frequency of contraction, while the subsequent addition of propranolol slowed down the rate of contraction (**Fig. 7.5 B**). Additionally, we studied the contraction pattern after sotalol administration. Sotalol, when compared to baseline field potentials, showed a change in contraction pattern (**Fig. 7.5 C**), associated with the blockage of potassium channels. In addition to drug-testing, we also investigated the response of microspheres to electrical pacing. Day 50 microspheres on MEA were paced up to 6.0 Hz. Microsphere CMs responded to this outside pacing up to 6.0 Hz (**Fig. 7.5 D**), which is much higher than what we previously achieved with 3D-dhECT microislands (Kerscher et al. 2015b).

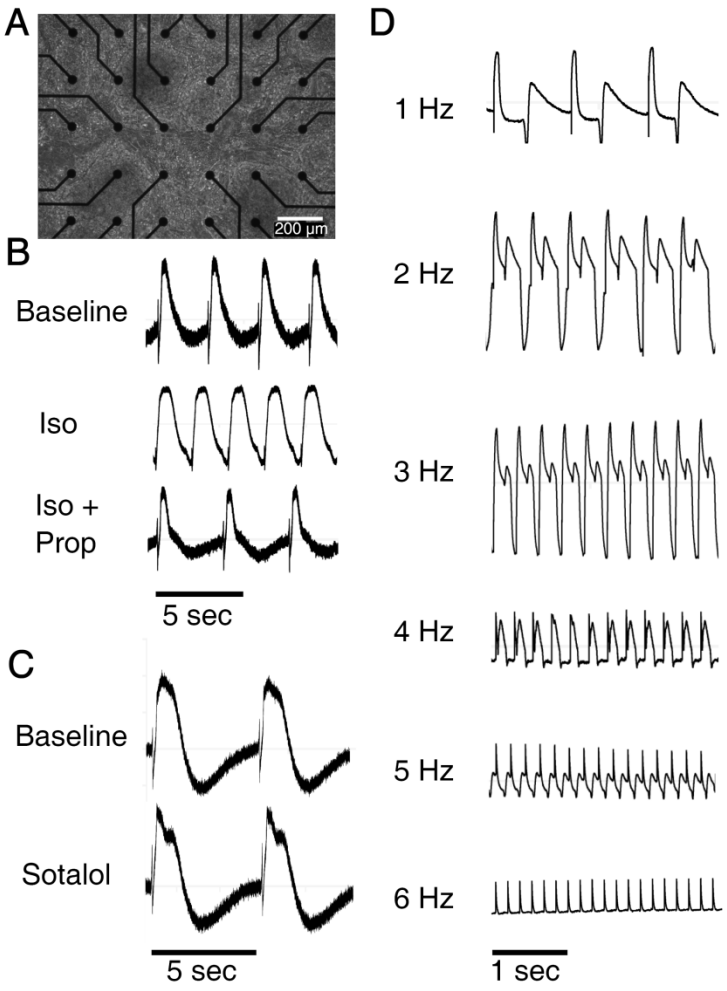

Fig. 7.5. Microsphere CMs responded to pharmacological and electrical stimuli. (A) Microspheres were dissociated and plated onto the MEA chip (**Supplementary Movie 7.3**). (B) Day 20 CMs responded to the β-adrenergic agonist, isoproterenol (Iso), increasing the contraction rate. The subsequent addition of propranolol (Prop), a β-adrenergic antagonist, reversed the initial increase in contraction rate caused by isoproterenol. (C) The addition of the non-selective β blocker, sotalol, altered the field potential pattern when compared to baseline field potentials. (D) In addition to appropriate response to drug treatment, day 50 microsphere CMs showed 1:1 correspondence to outside pacing frequencies up to 6.0 Hz.

7.3.6 Cardiac microspheres showed dynamic remodeling of their PEG-fibrinogen microenvironment

With progressing culture time, encapsulated cells remodeled their PEG-fibrinogen microenvironment by producing ECM proteins and differentiating into contracting cardiac tissues. Phase contrast microscopy and SEM of microspheres showed a smooth cell-based surface (**Fig. 7.6 A, B**). At higher magnification, a combination of tightly-connected cells and ECM deposition was revealed to be present on the microsphere surface (**Fig. 7.6 C**). Day 60 microspheres cells showed some aligning cells (**Fig. 7.7 A**), with neighboring cells forming junctions cell-cell junctions (**Fig. 7.7 B**). Understanding CM functionality on a tissue and single-cell level is often desired. We have successfully dissociated cardiac microspheres into single CMs, with CMs spontaneously contracting after dissociation (**Supplementary Movie 7.4**). CMs attached to unpatterned PDMS surfaces with elongated cell morphology (**Fig. 7.7 C**), which is normal for maturing CMs (Kerscher et al. 2015b). Dissociated cells were also immunofluorescently stained with the cardiac marker αSA to visualize and quantify developed sarcomeres. CMs displayed defined sarcomere structures with internal alignment and uniform spacing of 1.85 μm (**Fig. 7.7 D**). Organized sarcomere arrangement influences the mechanical contractile output and is indicative of maturation. Additionally, day 60 microspheres contained aligned myofibril arrangement, similar to SEM images of native human heart tissue (Saunders and Amoroso 2010).

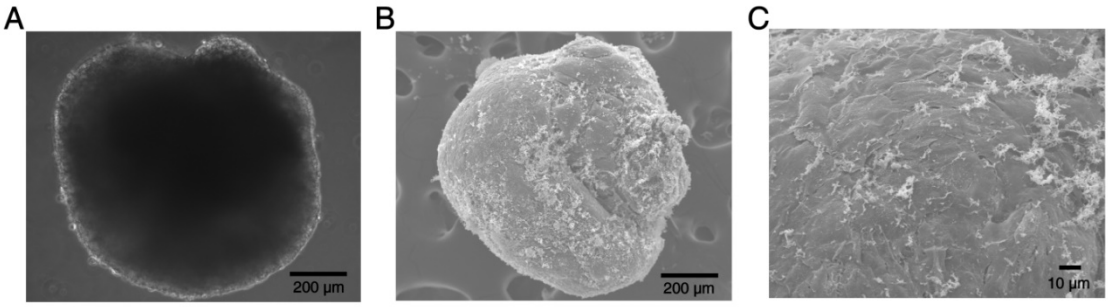

Fig. 7.6. Cells remodel their PEG-fibrinogen microenvironment to form dense cardiac microspheres. (A) Phase contract image of a cardiac microsphere showed a uniform surface (**Supplementary Movie 7.5**). SEM supported the observation from phase contrast microscopy, revealing (B) a smooth microsphere surface (C) with ECM deposition.

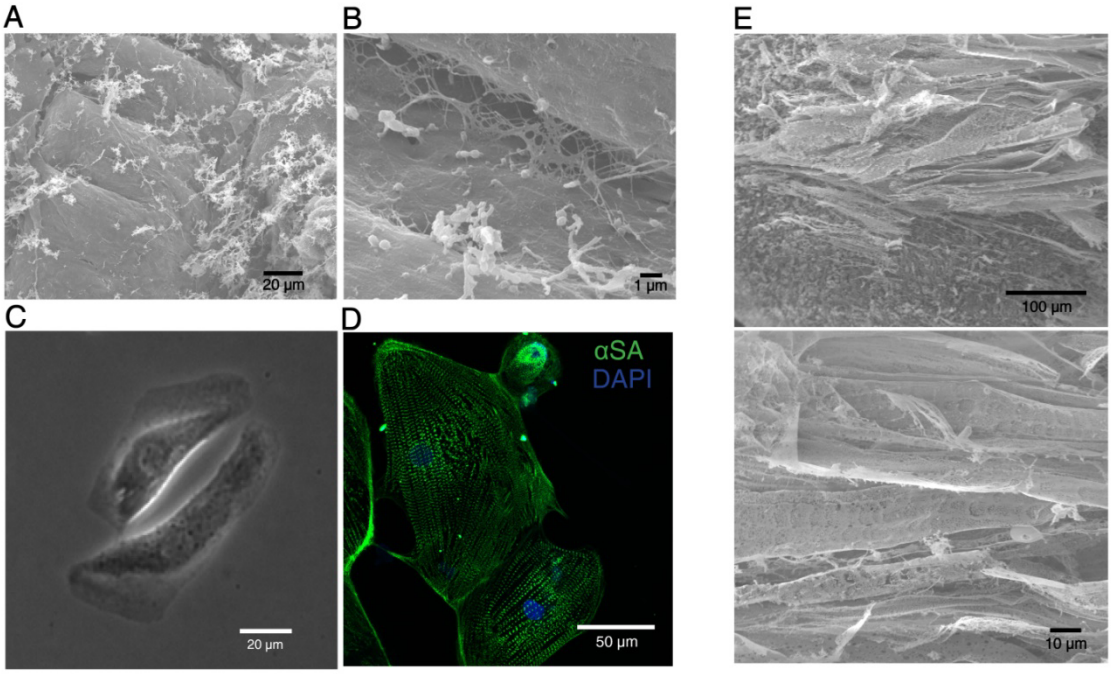

Fig. 7.7. Encapsulated CMs displayed features of maturing cells. (A) Aligned cells were visual on the surface with ECM deposition. (B) Higher magnification SEM image showed junctions between two adjoining cells. (C) Once dissociated, individual CMs showed an elongated morphology and spontaneous contraction (**Supplementary Movie 7.4**). (D) CMs stained positive for the cardiac marker αSA (green) and displayed well defined sarcomeres. Samples were counterstained with DAPI (blue). (E) Aligned myofibril structure was detected in day 60 microspheres, similar to human cardiac tissue samples.

7.3.7 One-step microfluidic microsphere production can be expanded to gelatin methacryloyl

Biomaterials that are photocrosslinkable and possess advantageous mechanical and biological properties for stem cell encapsulation and cardiac differentiation are hard to find. PEG-fibrinogen has been used for a variety of applications (Fuoco et al. 2012,

Appelman et al. 2009), including the use in cardiac tissue engineering (Plotkin et al. 2014, Shapira-Schweitzer et al. 2009). Our group has shown that PEG-fibrinogen is not only suitable for CM encapsulation, but also for direct hiPSC differentiation to produce larger 3D-dhECTs (Kerscher et al. 2015b) that were not injectable. The limited applicability led to this high-throughput microsphere production approach. Our lab has also experience with another biomaterial, gelatin methacryloyl (GelMA), which is widely used for tissue engineering and bioprinting applications. In a recent study we showed that our single-cell handling approach to encapsulate and differentiate hiPSCs within a biomimetic material is applicable to soft (22% methacryloyl substitution degree) GelMA hydrogels. Initial proof-of-concept studies showed that our custom microfluidic device can produce acellular GelMA (**Fig. 7.8**) microspheres with ultrastructural features commonly seen in GelMA hydrogels (Xiao et al. 2011). Future studies will include in-depth cellular comparison studies between the two biomaterials.

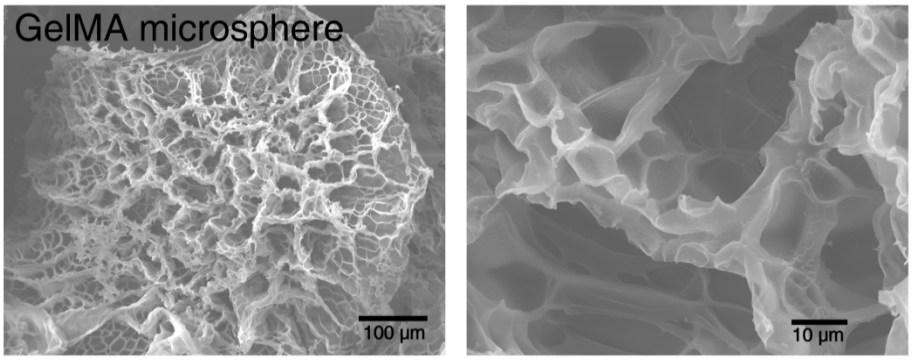

Fig. 7.8. Acellular GelMA hydrogel microspheres can be produced in our microfluidic device. GelMA hydrogels showed large pores indicative of GelMA hydrogels

7.4 Discussion

The high-throughput production of 3D cardiac tissues with only a single-cell handling step opens up the field of cardiac tissue engineering and its applications towards drug-testing and regenerative medicine. Here we show the successful implementation of our custom microfluidic device to produce about 60 hiPSC encapsulated microspheres per minute with high uniformity and circularity. HiPSCs were evenly distributed within PEG-fibrinogen hydrogels and grew within hours after encapsulation. Cell proliferation within the original microsphere boundary and beyond was observed throughout the time course of cardiac differentiation. Although cardiac microspheres became less circular over time, spontaneous contraction consistently started on day 8 of differentiation and was over 70% efficient. Microspheres survived applied shear, maintained their structure, and spontaneously contracted only one day after age-matched unsheared controls. In addition to spontaneous contraction, microsphere CMs responded appropriately to isoproterenol, propranolol, and sotalol. Furthermore, engineered microspheres responded to outside pacing frequencies up to 6.0 Hz, all of which makes these microspheres a suitable and functional tissue platform for cell-therapy. Over the time course of culture, proliferating and differentiating cells remodeled their provided PEG-fibrinogen microenvironment while depositing their own ECM proteins. We also showed that in addition to PEG-fibrinogen, we can also produce GelMA microspheres which are similar in ultrastructural architecture and seem to be a promising biomimetic material to expand our existing study.

In the field of tissue engineering, hydrogel-based microsphere size typically ranges between 100-200 μm (Chan et al. 2016, Zhao et al. 2016); microspheres with larger

diameter are more difficult to produce with high uniformity and circularity. Our recently published work showed successful hiPSC encapsulation and differentiation within PEG-fibrinogen hydrogels to produce 3D-dhECT microislands (Kerscher et al. 2015b). These microislands displayed uneven growth patterns due to the multiple millimeter-size tissue diameter. When studying the 3D-dhECT microisland growth pattern, we detected a dense tissue ring of about 1 mm in size formed on the surrounding 3D-dhECT microisland edge. Based on this observation, the desired initial microsphere diameter was chosen to be less than 1 mm.

The use of biomaterials in tissue engineering is sought to improve multiple parameters, including cell-cell and cell-materials interactions as well as recapitulating mechanical and biological cues present in the *in vivo* system of interest (Shao, Sang and Fu 2015, Guyette et al. 2016). The use of biomaterials for 2D cell culture is common, but less is known about the same material and how it will influence encapsulated cells in 3D. The heart has a known stiffness of 10 kPa and multiple studies have proven that 2D substrates with similar stiffness than the heart is beneficial to CM function and maturation (Young and Engler 2011). Cardiac differentiation was historically done on TCPS or by forming cell-based embryoid bodies (EBs). Studies showed that ridged TCPS does not represent the physiological stiffness of the heart, but that a softer substrate is beneficial for 2D cardiac differentiation (Hazeltine et al. 2014). EB formation drives on the nature of EB size and cellular interactions formed between cells; if these conditions were not met, insufficient CM differentiation and poor reproducibility were the outcome. Our high-throughput microsphere production process allows for a soft, reproducible 3D microenvironment while providing an EB-like production approach.

A bioreactor setup or similar dynamic culture conditions can provide a more uniform environment for cell and tissue growth compared to stagnant culture (Kempf et al. 2014). Fluid flow and dynamic stirring can improve nutrient and waste transport in and out of 3D tissues, providing optimal growth conditions for developing cardiac tissues (Kempf et al. 2015). Even though these facts are well-known, numerous parameters have to be optimized for ideal tissue production in a bioreactor setup. In this study we wanted to show the possibility to produce uniform hiPSC encapsulated microspheres that subsequently were differentiated to form cardiac microspheres. Although our final cardiac microspheres were not fully consistent in size and circularity, a high percentage of microspheres showed similar growth patterns and differentiation efficiencies. We believe that a more even cellular growth pattern can be achieved in a bioreactor setting.

8. DIRECT PRODUCTION OF HUMAN CARDIAC TISSUES BY PLURIPOTENT STEM CELL ENCAPSULATION IN GELATIN METHACRYLOYL

8.1 Introduction

Given that the demand for human cardiac tissue greatly exceeds the supply (Noseda, Abreu-Paiva and Schneider 2015), straight-forward, automatable *in vitro* generation of functional cardiac tissues is critical for driving advances in applications ranging from drug testing and clinical cardiac regeneration to mechanistic investigation of heart development and disease (Kempf et al. 2015, Jeziorowska et al. 2015). With the advancement of patient-specific human induced pluripotent stem cell (hiPSC) line derivation, improvements in cellular engineering and genomic editing (Hotta and Yamanaka 2015), and establishment of highly efficient differentiation protocols, autologous cell- and tissue-therapies possess great future medical potential, including for cardiac tissue regeneration. When engineering these developing cardiac tissues with differentiating hiPSCs, it is beneficial to mimic the physiological conditions in the native heart and enable positive interactions between cells and their surrounding extracellular matrix (ECM). Providing a suitable microenvironment to encapsulated cells can promote and support tissue formation by sustaining initial cell viability, facilitating subsequent proliferation, directing differentiation, and promoting cellular function (Hodge et al. 2014, Trosper et al. 2014, Burdick and Vunjak-Novakovic 2009). Hydrogel matrices can provide the necessary biomimetic microenvironment while simultaneously facilitating scalable tissue production.

Standard protocols for three-dimensional (3D) cardiac tissue production have been limited to the use of cardiomyocytes (CMs) obtained through pre-differentiation of stem cells (Lian et al. 2012, Nguyen et al. 2014, Turnbull et al. 2014, Schaaf et al. 2011) or direct isolation from the heart (Bian et al. 2014, Shapira-Schweitzer and Seliktar 2007). To form engineered cardiac tissues, the CMs are then dissociated and encapsulated within a biomaterial that provides a connective tissue-like 3D microenvironment (Masumoto et al. 2014, Zhu and Marchant 2011). This tissue production process involves multiple cell-handling steps, negatively impacting CM viability and disrupting essential cell-cell junctions and ongoing developmental processes. If, however, pluripotent stem cells are directly differentiated within a 3D hydrogel, it is possible to generate developing and functional cardiac tissues with a high CM yield and only one cell-handling step (Kerscher et al. 2015b). This ability to directly produce 3D cardiac tissues from hPSCs in an ontomimetic manner has been successfully demonstrated using the biosynthetic material poly(ethylene glycol)-fibrinogen (PEG-fibrinogen) (Kerscher et al. 2015b) as the support matrix for hPSC encapsulation and differentiation, which we called 3D developing human engineered cardiac tissues (3D-dhECTs). Understanding the potential of additional hydrogel materials to enable direct, ontomimetic cardiac tissue production is important in leveraging this approach for a range of future applications (Hodge et al. 2014).

Collagen is an abundant ECM protein in the adult human heart (Stoppel, Kaplan and Black 2015, Caulfield and Borg 1979) and, therefore, may possess potentially beneficial properties as a matrix material for supporting temporal differentiation of hPSCs into contracting CMs. However, collagen alone cannot form mechanically tunable and

photocrosslinkable hydrogels and is associated with significant batch-to-batch variability (Kumar et al. 2014). Therefore, to mimic properties of the native heart ECM while improving control over material properties, we selected gelatin methacryloyl (GelMA) for this study and tested whether it could support the growth, differentiation, and function of stem cell-derived cardiomyocytes (SC-CMs). GelMA is a degradable hydrogel composed of gelatin (denatured collagens) that has been tunably substituted with methacryloyl groups; different degrees of methacryloyl group substitution can be achieved to obtain a range of different structural and functional characteristics of the hydrogel, including cell-responsiveness from gelatin and polymerization capabilities from methacryloyl groups (Nichol et al. 2010). In particular, GelMA can be photocrosslinked to form a relatively soft hydrogel, which we have found to be advantageous for hiPSC survival and maintenance (Lutolf, Gilbert and Blau 2009, Banerjee et al. 2009).

Here we report for the first time the successful production of GelMA human engineered cardiac tissues (GEhECTs) by direct hiPSC encapsulation and differentiation within soft GelMA hydrogels. GelMA was first synthesized GelMA with a methacryloyl group substitution degree of 22% and then produced acellular GelMA hydrogels by visible-light photocrosslinking to study the enzymatic hydrogel degradation. Cellular GelMA hydrogels were formed by incorporating hiPSCs within the liquid GelMA precursor solution followed by photocrosslinking for less than one minute. HiPSC viability after encapsulation was maintained and cardiac differentiation efficiency was validated by flow cytometry. First isolated areas of spontaneous contraction were consistently observed on day 8 of differentiation, with uniformly contracting tissues

forming by day 14. Cells remodeled their 3D microenvironment and became more elongated, with larger and more elongated cell nuclei, over time. The proliferating and differentiating cells formed a connected tissue, allowing for a temporal increase in frequency and velocity of contraction. GEhECT CMs were evaluated by α-sarcomeric actinin staining with subsequent sarcomere spacing and alignment quantification. CM functionality was verified by appropriate response to drug treatments and outside pacing. These results showed that hiPSCs can be directly differentiated in GelMA hydrogels using a straight-forward, single cell-handling approach to produce GEhECTs.

8.2 Materials and Methods

8.2.1 HiPSC culture and maintenance

IMR-90 Clone 1 and 19-9-11 human induced pluripotent stem cells (hiPSCs) were purchased from WiCell and cultured on hESC qualified Matrigel (BD Biosciences) in mTeSR-1 medium (Stem Cell Technologies). HiPSCs were passaged using Versene (Life Technologies) and mTESR-1 medium supplemented with 5 μM ROCK inhibitor (RI, Y-27632, Stem Cell Technologies).

8.2.2 PDMS mold preparation

All chemicals, unless otherwise noted, were purchased from Sigma-Aldrich. A precursor solution for the polydimethylsiloxane (PDMS) molds was created as previously described (Kerscher et al. 2015b). Shortly, SLYGARD 184 silicone elastomer curing agent and SLYGARD 184 elastomer base (1:10 ratio, Dow Corning Corporation) were mixed, poured onto a glass slide, and cured at 70 °C. PDMS was peeled off and a cork borer was

used to create circular holes (4 mm in diameter). PDMS molds were soaked in 70% ethanol and exposed to UV-light. The mold was transferred to the bottom of a well of a 6-well plate prior to the encapsulation process.

8.2.3 Gelatin methacryloyl (GelMA) synthesis and precursor preparation

Gelatin methacryloyl (GelMA) was synthesized following previous protocols (Nichol et al. 2010, Van Den Bulcke et al. 2000) with modifications. Briefly, gelatin (Type B, bovine) was mixed at 5% (w/v) into phosphate buffered saline (PBS, Gibco) at 60 °C with constant stirring until fully dissolved. Methacrylic anhydride (MA) was slowly added until the target concentration was reached (15% w/v) and reacted at 60 °C for 2 h. The reaction was stopped with PBS; gelatin methacryloyl was dialyzed for seven days and lyophilized for five days. Lyophilized GelMA was dissolved in deuterium oxide (Fisher Scientific) for NMR analysis. ^{1}HNMR spectra were collected using a Bruker NMR spectrometer. Before integration, phase and baseline corrections were applied to ensure accurate methacryloyl group addition calculations.

To prepare the precursor solution, lyophilized GelMA was re-dissolved into PBS at 80 °C at a concentration of 15mg/ml and combined with 1.5v/v% triethanolamine (TEOA), 3.96 µl/ml N-vinyl pyrrolidone (NVP) and 10 mM eosin Y (Fisher Scientific) photoinitiator (Franco et al. 2011). For degradation studies, acellular GelMA hydrogels (20 µl) were crosslinked for 60 s and incubated in PBS or 5 U/ml collagenase Type 2 (Worthington) at 37 °C. Hydrogel weights were recorded at 0, 3, and 6 h (n = 3 hydrogels).

8.2.4 Fabrication of GelMA human engineered cardiac tissues (GEhECTs)

To form GelMA tissues, hiPSCs were dissociated using Versene, centrifuged, and re-suspended at 26 ± 4.1 x 10^6 hiPSCs/ml GelMA. The GelMA cell suspension precursor solution was pipetted into a circular PDMS mold and photocrosslinked using visible light (203 mW/cm^2) for 40 s (**Fig. 8.1 A**). After crosslinking, the PDMS mold was removed and newly formed tissues were suspended in mTeSR-1 medium with 5 μM RI and cultured for 24 h (day -3, three tissues per well). For the next two days, (days -2 and -1) mTeSR-1 medium was changed daily. Cardiac differentiation was initiated on the third day after encapsulation (day 0).

Three days after hiPSC encapsulation (day 0), cardiac differentiation was initiated using a well-established protocol (Lian et al. 2013, Kerscher et al. 2015b). MTeSR-1 medium was replaced with 4 ml per well of RPMI/B27 without insulin (RPMI/B27-Ins, Invitrogen) supplemented with 12 μM CHIR99021 (Stem Cell Technologies); 24 h later (day 1), the medium was replaced with 4 ml RPMI/B27-Ins. After 48 h (day 3), half of the old media was combined with an equal amount of fresh RPMI/B27-Ins supplemented with 5 μM IWP2 (Stem Cell Technologies). On day 5, the media was exchanged for 4 ml of RPMI/B27-Ins, followed by a change with 4 ml RPMI/B27 (Invitrogen) on day 7. RPMI/B27 medium was replaced every three days thereafter.

8.2.5 Parallel plate mechanical compression testing

Acellular and cellular (IMR90-1 and 19-9-11 hiPSCs) GelMA hydrogels were tested for their compressive mechanical properties 48 h after tissue formation (day -1) using a micron-scale mechanical testing system (Microsquisher, CellScale) (Kinney et al. 2014).

The force was calculated via cantilever beam deflection in response to user-defined displacement. All samples were tested in PBS at room temperature. The cantilever beam was composed of Tungsten (modulus = 411 GPa) with a diameter of 304.8 μm. Stress-strain characteristics of acellular and cellular tissues were obtained and the elastic modulus was directly obtained within the linear 10-20% strain regime (n = 3 samples).

8.2.6 Scanning electron microscopy (SEM)

Day -1 tissues (19-9-11 hiPSCs) were prepared for SEM. Tissues were rinsed with PBS, fixed with 3% glutaraldehyde (Electron Microscopy Science) for 2 hrs at room temperature, rinsed again with PBS and further fixed with 2% osmium tetroxide (Electron Microscopy Science) for 2 hrs at room temperature. After fixation tissues were dehydrated with a serial ethanol dilutions followed by hexamethyldisilazane overnight. All tissues were then sputter-coated with gold and imaged.

8.2.7 Tissue dissociation and re-plating

For assays requiring dissociated cells, tissues were incubated in a dissociation solution containing collagenase type 2 (1 mg/mL, Worthington) at 37 °C for 2 h. The dissociation solution also contained 120 mM NaCl, 5.4 mM KCl, 5 mM $MgSO_4$, 5 mM Na-pyruvate, 20 mM glucose, 20 mM taurine, and 10 mM HEPES (pH 6.9) supplemented with 30 μM $CaCl_2$. After incubation, the tissues were centrifuged and re-suspended in 0.25% trypsin (EDTA, Mediatech) and incubated at 37 °C for 5 min. Finally, the cells were singularized, centrifuged, resuspended in RPMI20 medium (RPMI 1640 medium with

20% FBS, Atlanta Biologicals) with 5 μM RI and plated on fibronectin (25μg/ml) coated PDMS glass coverslips.

8.2.8 Viability and immunofluorescence of 3D cultured cells

A LIVE/DEAD ® viability kit (Molecular Probes) was used to assess hiPSC viability one day after encapsulation (day -2). Staining was performing following manufacturer's instructions; fluorescent Z-stacks were taken randomly within each tissue (n = 3 tissues).

Protein expression within GelMA tissues was characterized through immunofluorescence staining. Whole tissues on day 0 and day 22 were stained with Phalloidin (actin filaments, Invitrogen) and dissociated tissues were stained with the cardiac marker α-sarcomeric actinin (αSA). The cells were fixed using 4% paraformaldehyde (Electron Microscopy Sciences), permeabilized with PBS-T (PBS with 1% bovine serum albumin (BSA) and 0.2% Triton X-100), and blocked with 3% FBS in PBS. The samples were then successively incubated in primary and secondary (Alexa Fluor 488) antibodies for 24 h at 4 °C. All samples were counterstained with 4' 6-diamidino-2-phenylindole (DAPI, Molecular Probes). Fluorescently labeled samples were visualized with a Nikon A1si confocal microscope.

GEhECT cells' nuclear circularities and cross-sectional areas were analyzed on day 0 and day 22 using ImageJ by manually outlining DAPI-stained nuclei (n = 30 nuclei per time-point). Sarcomere spacing and alignment from dissociated GEhECT samples were analyzed using standard ImageJ plugins. Sarcomere spacing was determined by drawing a perpendicular line through visible sarcomeres and obtaining its intensity profile to observe the intersecting sarcomere location (n = 20 CMs) (Kerscher et al.

2015b). Sarcomere alignment was determined by first drawing a perpendicular line through multiple sarcomeres within each cell. Then, a second line was created overlaying one sarcomere at a time. The angle between the perpendicular line and the sarcomere line was recorded for at least five sarcomeres per cell (n = 36 CMs).

8.2.9 Early GEhECT growth

In order to track early tissue growth, phase contrast images of whole tissues were acquired daily from day -2 to day 7 of differentiation (Ti Eclipse, Nikon equipped with an Andor Luca S camera). Tissue edges were manually tracked and the lateral surface area of whole tissues was quantified using standard plugins in ImageJ (n = 3 tissues).

8.2.10 Contraction analysis of GEhECTs

Contractions of whole GEhECTs were characterized using motion tracking software (Huebsch et al. 2015). Videos of spontaneously contracting GEhECTs were recorded on days 14, 17, and 40 (n = 3 tissues per time point). Every video frame was converted into a separate image and the motion between images was calculated. The DataEvaluation interface was used to generate a plot of average maximum contraction and relaxation velocities and to determine the frequency of contraction.

8.2.11 Flow cytometry

On day 27, cardiac tissues were dissociated as described above. Instead of re-plating, the cells were resuspended in 4 % paraformaldehyde and incubated at 25 °C for 20 min. The cells were then centrifuged, 90% cold methanol was added and cells were incubated at

4 ℃ for 15 min. Fixed cells were blocked with 5% BSA in PBS for 5 min, washed, and labeled by incubation with 100 µl of primary antibody (cTnT, Thermo Scientific; Ki67, Abcam; CD90, Abcam) diluted in 0.5% BSA and 0.1% Triton X-100 PBS. After washing, 100 µl of secondary antibody (Alexa Fluor 488/647, Invitrogen) diluted in 0.5% BSA and 0.1% Triton X-100 in PBS was added. The cells were again washed and analyzed on a BD Accuri C6 (BD Biosciences).

8.2.12 Multielectrode array and drug-response

Day 30, GEhECTs were dissociated with collagenase (as described above) and plated on a S2 type MEA200/30-Ti-gr (Multichannel Systems) in RPMI20 + RI. After 24 h, MEA was perfused with Tyrode's solution (1.8 mM $CaCl_2$, 5 mM glucose, 5 mM HEPES, 1 mM $MgCl_2$, 5.4 mM KCl, 135 mM NaCl, and 0.33 mM NaH_2PO_4, pH 7.4) at 37 °C. The MEA setup contained a Multichannel Systems 1060-Inv-BC amplifier and field potential recordings were acquired at a sampling frequency of 10 kHz. GEhECT CMs were exogenously paced from 0.5 – 3.0 Hz.

The β-adrenergic agonist isoproterenol (Molecular Devices) and antagonist propranolol (Molecular Devices) were introduced to spontaneously contracting GEhECTs and their drug-response was analyzed using video analysis. Isoproterenol (1 µM) was first added to GEhECTs with a subsequent addition of 1 µM propranolol. After that, drugs were washed out and baseline contraction frequencies were achieved. GEhECT CMs from both IMR90-1 and 19-9-11 hiPSCs were analyzed.

8.2.13 Statistics

Minitab 17 was used to analyze the reported results and the mean ± SD was reported of all replicates. After checking for normal distribution, one-way analysis of variance (ANOVA) with Turkey's test was used for all studies with equal variance and equal sample size. If equal variance did not apply, the Games-Howell test was used. $P < 0.05$ was considered statistically significant.

8.3 Results

8.3.1 GelMA forms photocrosslinked hydrogels that enzymatically degrade

GelMA hydrogels have been successfully used to encapsulate and culture multiple cell types to form engineered tissues (Benton et al. 2009, Xiao et al. 2011, Paul et al. 2014, Aubin et al. 2010). In the present study we show that GelMA can be used to encapsulate hiPSCs and support 3D differentiation to form uniformly contracting cardiac tissues. Previous work has shown that low crosslinking density GelMA (~20% methacrylation) forms soft hydrogels, while high crosslinking density GelMA (~80% methacrylation) forms stiff hydrogels (Nichol et al. 2010). Based on our previous experience with PEG-fibrinogen, GelMA with a low methacryloyl substitution degree was chosen for this study to produce soft hydrogels and successfully used to create GelMA human engineered cardiac tissues (GEhECTs). Synthesized GelMA was lyophilized to form a sponge-like solid. Using NMR, a substitution percentage of 22% was calculated (**Fig. 8.2 B**) by dividing methacryloyl group peaks (located at 5.3 ppm and 5.5 ppm) and gelatin's free amine group peak.

Initial studies confirmed that GelMA hydrogels could be successfully formed by visible light photocrosslinking using the photoinitiator eosin Y. Hydrogel stability and

temporal enzymatic degradation was validated; chemically modified gelatin can be enzymatically degraded by cells, enabling cell migration and proliferation within the provided matrix to form physiologically relevant tissues. To demonstrate that our GelMA was enzymatically degradable, acellular hydrogels were incubated in either PBS or collagenase solution at 37 °C and temporal changes in mass were quantified. Whereas hydrogels in PBS alone maintained their mass after the expected initial increase as a result of swelling, hydrogels in collagenase decreased in mass over the first 6 h, suggesting successful, temporal GelMA degradation (**Fig. 1C**). Within 24 h, hydrogels in collagenase solution degraded completely, illustrating the feasibility of cell-mediated enzymatic degradation of the GelMA, a critical feature for enabling encapsulated cells to remodel their microenvironment to form a continuous tissue in subsequent experiments.

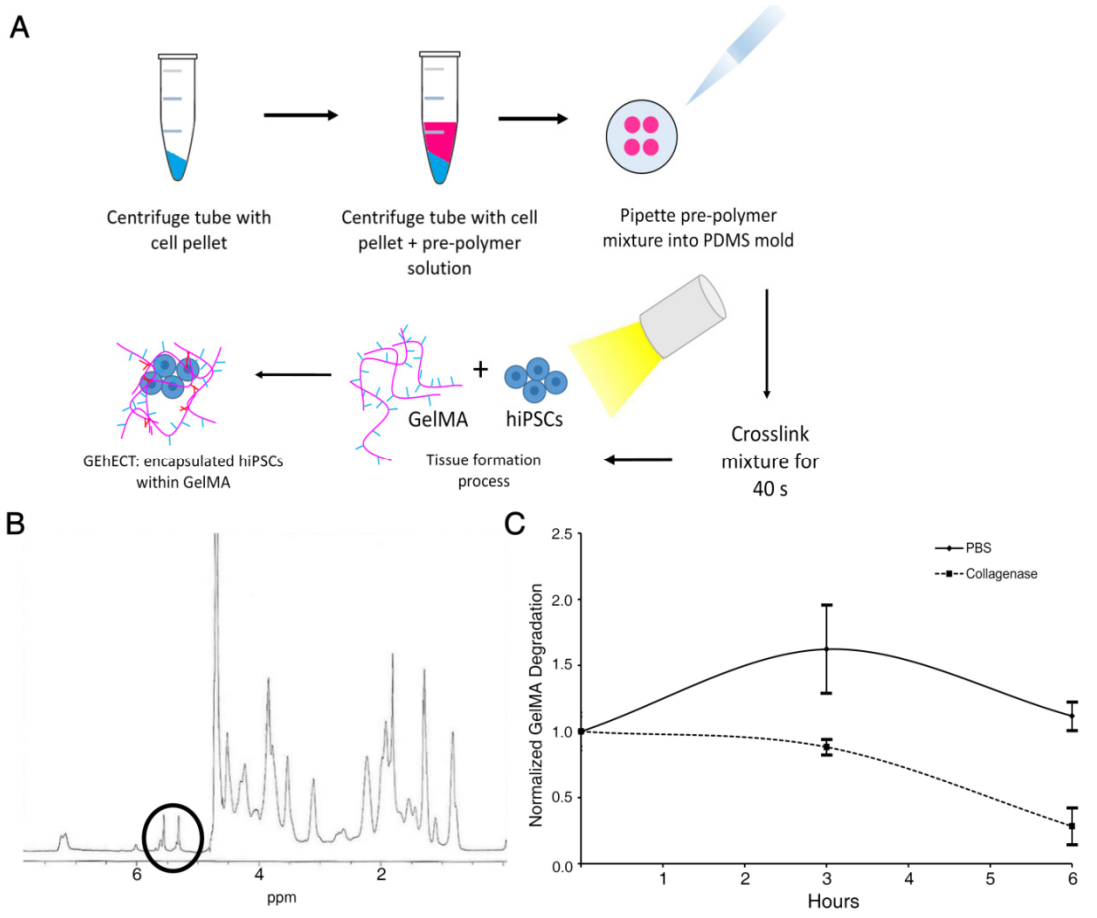

Fig. 8.1. GelMA hydrogels were successfully used to produce GEhECTs. (A) HiPSCs were collected and combined with a liquid GelMA precursor solution; this mixture was then added into a circular PDMS mold and photocrosslinked for 40 s using visible light. (B) NMR spectrum showed synthesized GelMA with a methacrylation degree of 22% (signals of methacrylate double bonds at 5.3 and 5.5 ppm). (C) Photocrosslinked GelMA hydrogels initially swelled in the presence of PBS and degraded when incubated in collagenase, with over 50% mass loss by 6 h (n = 3 tissues).

8.3.2 GelMA hydrogels support hiPSC survival, growth, and cardiac differentiation

In the present study, we produced hiPSC encapsulated GelMA hydrogels using visible light photocrosslinking for less than one minute to reproducibly form cell-laden GelMA hydrogels. Mechanical testing of acellular and cellular hydrogels verified that our low crosslinking density GelMA hydrogels with and without cells formed soft constructs; GelMA stiffness has been shown to play an important role in successful cell encapsulation and function (Engler et al. 2006, Engler et al. 2007, Nichol et al. 2010). The stiffness of cellular hydrogels on day -1 (two days after encapsulation) for both hiPSC lines were similar, with elastic moduli of 360 ± 40 Pa (IMR90, n = 3 tissues) and 470 ± 7.0 Pa (19-9-11, n = 3 tissues). Cellular hydrogels were softer than acellular GelMA hydrogels, which had an elastic moduli of 830 ± 220 Pa (**Fig. 8.2 A**, n = 4 hydrogels).

Following encapsulation, hiPSCs were uniformly distributed (**Fig. 8.2 B, C**) and remained viable within GelMA hydrogels (>75% survival, **Fig. 8.2 D**). Three days post-encapsulation (day 0, **Fig. 8.2 E**), hiPSCs had begun to grow beyond the original GelMA hydrogel boundaries, resulting in an increase in lateral surface area. Even with this enlargement in tissue size, hiPSCs maintained a round cell morphology, visualized by Phalloidin staining (F-actin, **Fig. 8.2 F**), through initiation of differentiation (day 0).

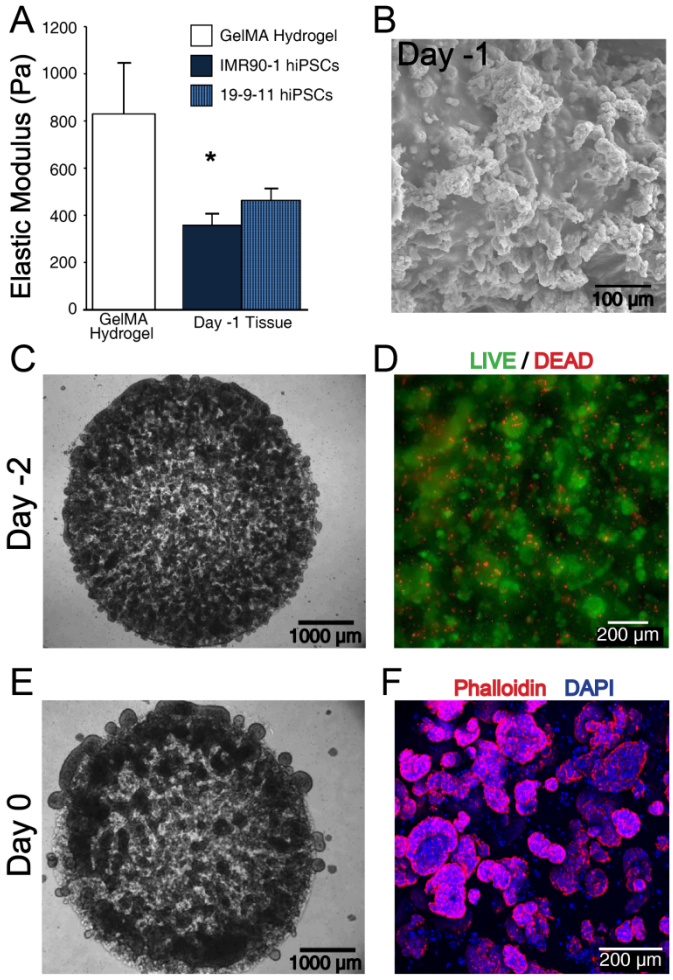

Fig. 8.2. GelMA encapsulated hiPSCs formed soft cell-laden hydrogels with hiPSCs surviving the encapsulation process to produce GEhECTs. (A) Acellular GelMA hydrogels exhibited an elastic modus of 830 ± 220 Pa (n = 4 hydrogels); in comparison, cellular GelMA tissues formed with IMR90-1 and 19-9-11 hiPSCs two days after encapsulation (day -1) were softer, with elastic moduli of 360 ± 40 Pa and 470 ± 7.0 Pa, respectively. n = 3 tissues per group. Mean ± s.d. ANOVA $P < 0.05$, * vs. GelMA hydrogel. (B) SEM image of cell-laden tissue 24 h after encapsulation (day -1) showed small cells in colonies growing in GelMA hydrogels. (C) Phase contrast image showed circular 3D cell-laden hydrogel 24 h after encapsulation (day -2) with (D) the majority of hiPSCs surviving the encapsulation process (green = viable, red = dead). (E) Three days

after encapsulation (day 0), hiPSCs formed growing clusters, (F) displaying a round cell morphology (F-actin filaments visualized by Phalloidin, red) with cells expanding beyond the original footprint of the hydrogel.

Cell proliferation and growth both prior to and during cardiac differentiation was most pronounced at the GEhECT edges (**Fig. 8.2**, **Fig. 8.3 A**), resulting in a darkening of phase contract images as a result of higher cell density and an increase in tissue surface area. From day -2 to day 5 of differentiation, the tissue surface area increased by 13.1 ± 1.7%, followed by a decrease of 2.8% between day 5 and 7 (**Fig. 8.3 B**, $n = 3$ tissues). This observed decrease in tissue area was then followed by initiation of GEhECT spontaneous contraction; first spontaneous contraction within GEhECTs was consistently detected by day 8 of differentiation. Flow cytometry on day 27 of differentiation verified successful cardiac differentiation of 3D encapsulated hiPSCs. GEhECTs contained 70.4 ± 1.6% CMs (cTnT+), of which were 10.6 ± 2.6% proliferating CMs (cTnT+, Ki67+), and 8.4 ± 0.3% fibroblasts (CD90+, **Fig. 8.3 C**, $n = 3$ tissues).

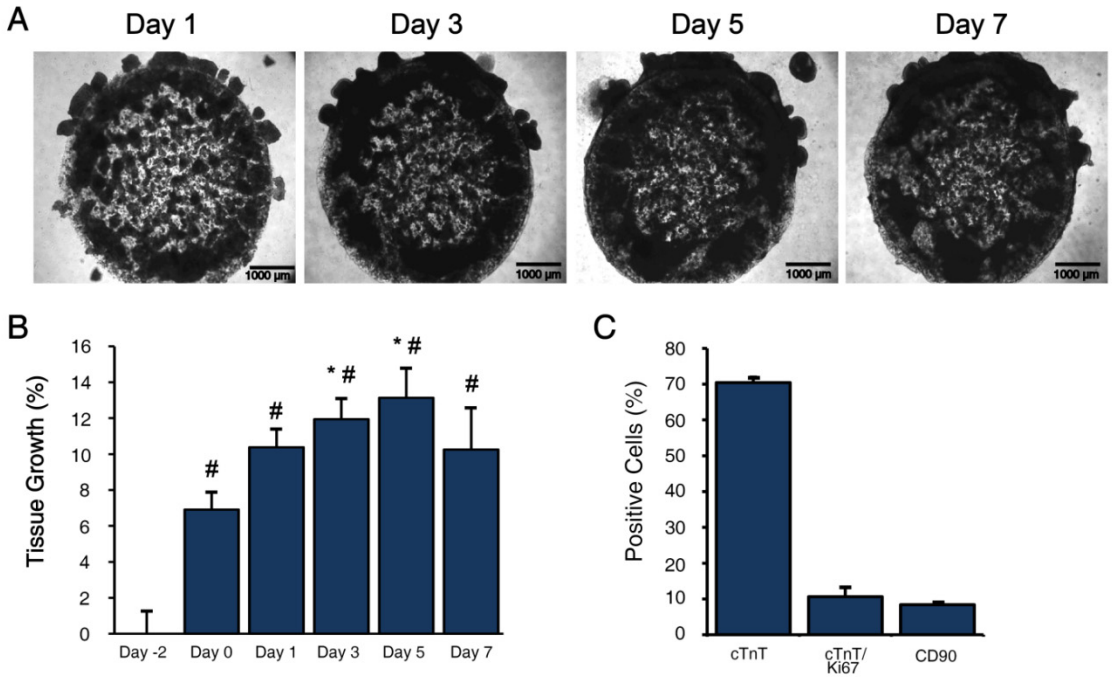

Fig. 8.3. Encapsulated hiPSCs grew and differentiated to form a continuous tissue over time. (A) After the onset of cardiac differentiation (day 0), cells continued to grow within the original GelMA construct, forming a more connected tissue over time. (B) Circular surface area of tissues increased by 13.1 ± 1.7% by day 5 and decreased somewhat thereafter to form a dense tissue by day 7 (n = 3 tissues). First initial contractions were observed consistently on day 8. n = 3 tissues. Mean ± s.d. ANOVA P < 0.05, # vs. Day -2, * vs. Day 0. (C) On day 17, differentiated cardiac tissues contained approximately 70% CMs (cTnT+), of which 11% were proliferating (cTnT+, Ki67+), and 8% fibroblasts (CD90+) (n = 3 tissues).

8.3.3 Uniformly contracting GEhECTs showed increased frequency and velocity of contraction over time

GelMA hydrogels were successfully used to facilitate direct hiPSC encapsulation and cardiac differentiation to form GEhECTs. Cardiac tissues showed first spontaneously

contracting areas by day 8 of differentiation, with more areas initiating contraction over time, resulting into uniformly contracting tissues by day 14 (**Supplementary Movie 8.1**).

Once individual areas joined and contracted uniformly, the frequency and average maximum contraction and relaxation velocity increased over time, with tissues visually deforming between contracted and relaxed states (**Supplementary Movie 8.2**). The frequency of spontaneous contraction increased significantly between day 14 (0.2 Hz) and day 40 (0.8 Hz, **Fig. 8.4 A**). The maximum contraction velocity increased from 75 ± 45 μm/s (day 14) to 360 ± 17 μm/s (day 40, **Fig. 8.4 B**). Similarly, the maximum relaxation velocity increased from 74 ± 55 μm/s (day 14) to 400 ± 28 μm/s (day 40, **Fig. 8.4 C**), all of which resulted into strong contracting tissues over time.

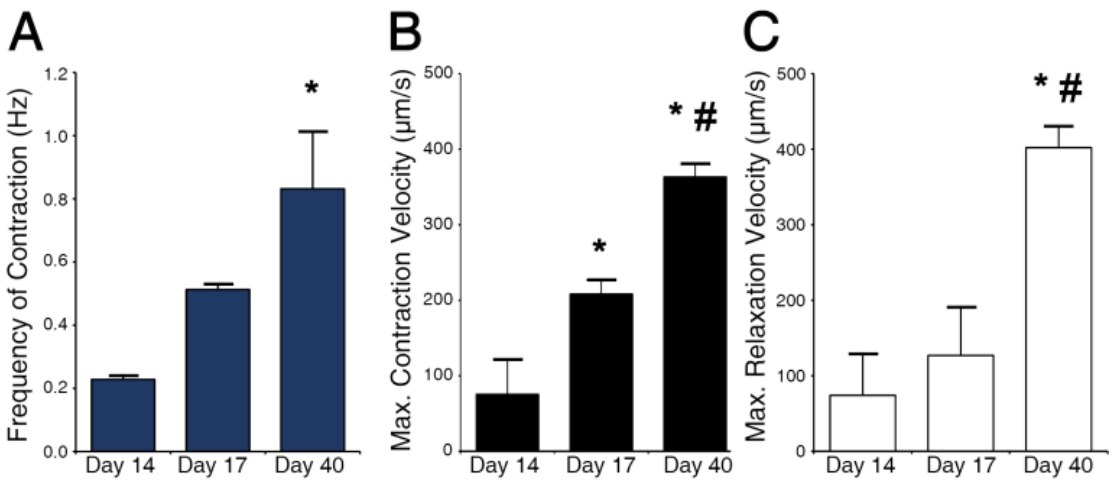

Fig. 8.4. Frequency of spontaneous contraction and contractile velocity increased with GEhECT culture time. (A) GEhECTs formed uniformly contracting tissues by day 14, with frequencies of spontaneous contraction increased significantly between days 14 and 40. (B, C) In addition to the increase in contraction frequency, average maximum contraction and relaxation velocities also increased from day 14 to day 40 of differentiation. This increase in contraction and relaxation velocity corresponded with visual observations of stronger contracting tissues. n = 2-3 tissues. Mean ± s.d. ANOVA $P < 0.05$, * vs. Day 14, # vs. Day 17.

8.3.4 Cellular remodeling and development of CMs in GEhECTs

It is expected that cells remodel the surrounding microenvironment and actively change their size and morphology during development (Auman et al. 2007). Observed changes in actin filament morphology as well as nuclei morphology and size between day 0 and day 22 of differentiation confirmed intracellular as well as microenvironmental remodeling, thereby contributing to the formation of a connective and uniformly contracting tissue. Confocal images of fluorescently stained cell-laden tissues on day 0 of differentiation

(**Fig. 8.2 F**) showed encapsulated cells with round (0.8 ± 0.1 circularity) and small (91.2 ± 30.5 μm^2) cell nuclei. After 22 days, GEhECT cells displayed elongated actin filaments (**Fig. 8.5 A**) with more elongated (0.7 ± 0.1 circularity) and larger (149 ± 52.4 μm^2) nuclei of 3D cultured cells (**Fig. 8.5 B, C**, $n = 30$), an expected trend during stem cell differentiation (Dambrot et al. 2011).

In addition to flow cytometry and video microscopy of visually contracting GEhECTs, immunofluorescence verified successful cardiac differentiation within GelMA hydrogels, showing defined and aligned sarcomeres. Contracting GEhECTs were successfully dissociated, re-adhered, and continued to synchronously contract (day 22, **Supplementary Movie 8.3**). While maintained in 2D culture, GEhECT CMs displayed well-defined (**Fig. 8.5 D**) and aligned (**Fig. 8.5 E**, $n = 36$) sarcomeres, spaced at 1.85 ± 0.1 μm ($n = 20$ cells).

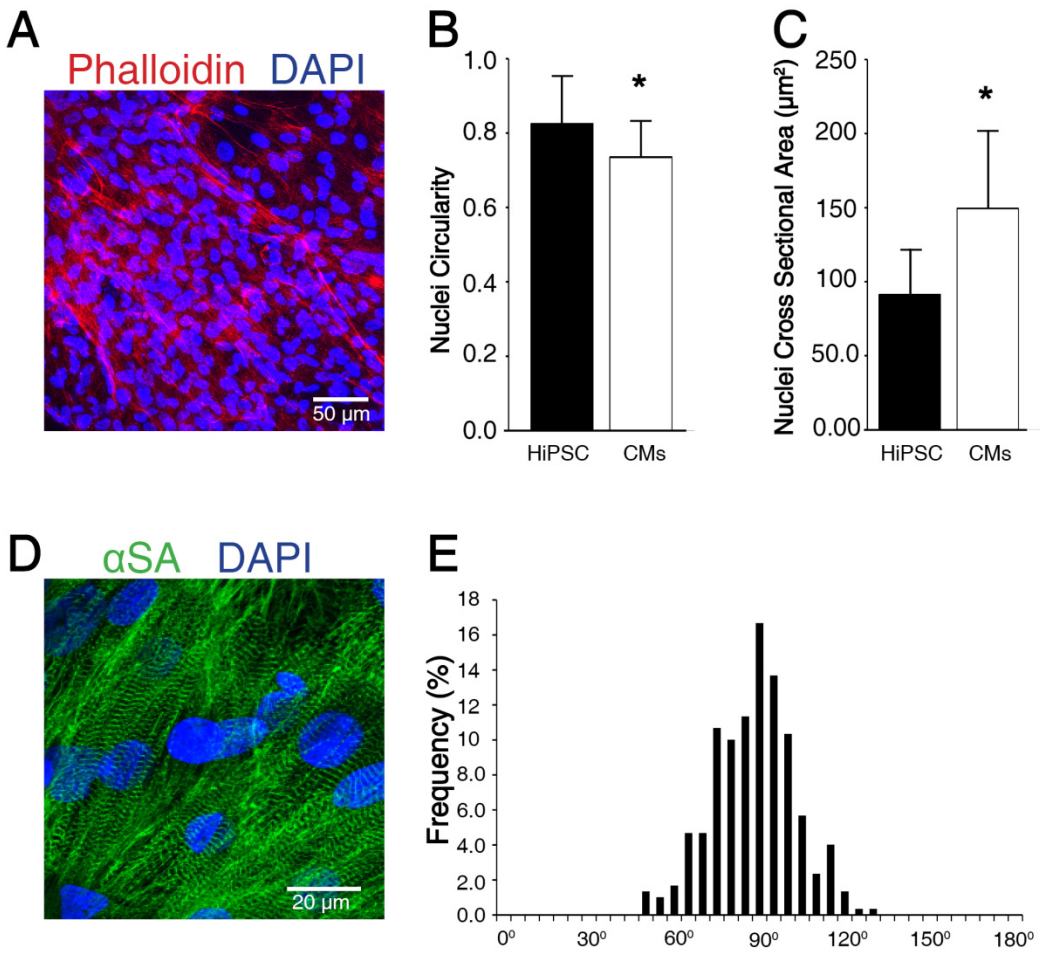

Fig. 8.5. GEhECT CMs remodeled their microenvironment and showed morphological differences expected from differentiating cells. (A) Day 22 tissues contained areas of high cell density primarily on the edges of GEhECTs where cells showed elongated F-actin filaments (Phalloidin, red). (B, C) Day 0 (hiPSCs) encapsulated cells displayed more circular and smaller nuclei compared to day 22 (CMs) cells. n = 30 nuclei per condition. Mean ± s.d. ANOVA $P < 0.05$, * vs. HiPSC. (D) Following tissue dissociation, GEhECT CMs continued to spontaneously contract (**Supplementary Movie 8.2**) and locally self-aligned with each other, displaying defined sarcomeres (αSA, green) with (E) high intracellular alignment (n = 36).

8.3.5 GEhECT CMs responded to extrinsic stimuli

To evaluate the potential of these GEhECT-derived SC-CMs to be used for future clinical applications or drug testing, the functionality of CMs was evaluated by pharmacological and electrical stimulation. Spontaneously contracting GEhECTs were exposed to the β-adrenergic agonist isoproterenol (1 μM), which caused an expected increase in frequency of contraction by ~0.2 Hz. Subsequently, propranolol (1 μM), a β-adrenergic antagonist, was added to GEhECTs which caused the frequency of contraction to slow down by ~0.36 Hz (*n* = 3 tissues, **Fig. 8.6 A**). Although GEhECTs initial frequency of contraction varied between tissues, changes caused by the administered drugs were consistent, even with different hiPSC lines. GEhECTs were also successfully dissociated and plated onto a MEA chip (**Fig. 8.6 B**). Spontaneously contracting GEhECT CMs were electrically paced from 0.5 Hz to 3.0 Hz; field potential recordings showed 1:1 correspondence to outside pacing up to 3.0 Hz.

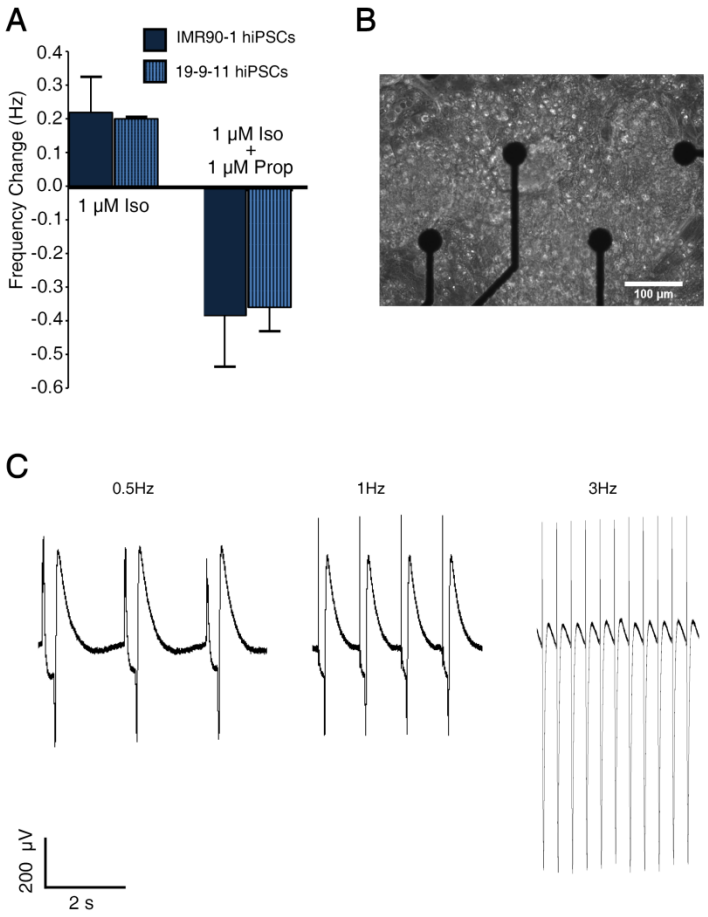

Fig. 8.6. Cardiac tissues responded to drug treatment and outside pacing. Cardiac tissues responded to drug treatment and outside pacing. (A) GEhECTs produced with IMR90-1 and 19-9-11 hiPSC lines responded to the β-adrenergic agonist isoproterenol (Iso) and β-adrenergic antagonist propranolol (Prop); 1 μM Iso increased the frequency of spontaneous contraction, the subsequent addition of 1 μM Prop slowed down the contraction. (B) Day 30 dissociated tissues (from IMR90-1 hiPSCs) were cultured on MEA (**Supplementary Movie 8.4**) and (C) extrinsically paced. GEhECT CMs responded to outside pacing frequencies up to 3.0 Hz.

8.4 Discussion

In this study we show that GelMA is a suitable biomaterial for hiPSC encapsulation, culture, and cardiac differentiation to form uniformly contracting GelMA human engineered cardiac tissues (GEhECTs). GelMA is an ECM-based biomaterial that enables cell-responsive hydrogel degradation and subsequent remodeling of the cellular microenvironment. Soft GelMA hydrogels surrounding encapsulated hiPSCs were produced using GelMA with a methacryloyl substitution degree of 22%, which results in the formation of gels with a low crosslinking density. The elastic modulus of GelMA hydrogels can be altered by changing the methacryloyl substitution degree during synthesis and the exposure time and light intensity during photocrosslinking, in addition to being influenced by temperature (Kolesky et al. 2014). During compression testing, acellular GelMA hydrogels showed a higher elastic modulus than GelMA hydrogels containing encapsulated hiPSCs, suggesting that acellular hydrogels are stiffer than their cellular counterparts, but still remain softer than 1 kPa. GelMA having a high degree of methacryloyl substitution, which would have resulted in gels with increased elastic modulus, was not chosen for this project based on its slower degradation rate and reported inhibition of cell spreading (Frisman, Seliktar and Bianco-Peled 2011). Although lineage specification is influenced by matrix stiffness (Engler et al. 2006), microenvironmental cues exerted on cells by biomaterials exploited in 2D or 3D culture (Nichol et al. 2010) have to be carefully distinguished and evaluated separately.

Identifying suitable biomaterials to produce developing human cardiac tissues using only a single cell-handling step is challenging; success depends on a variety of parameters, including but not limited to mechanical properties, rate and mode of material

degradation, crosslinking density, initial cell-seeding density, and potential to support cell maintenance and differentiation processes. Biomimetic material design to facilitate cardiac tissue production and cardiac regeneration is the subject of significant research efforts (Hodge et al. 2014) and incorporation of additional biomimetic cues may further enhance GEhECT function and maturation (Shin et al. 2013, Kerscher et al. 2015b). In the past, natural materials such as Matrigel, collagen, or fibrin have been used to create cardiac tissues (Nunes et al. 2013, Radisic et al. 2004b, Yuan Ye, Sullivan and Black 2011, Stoehr et al. 2014), recapitulating aspects of the native ECM composition. In order to better control and tune the properties of hydrogels, purely synthetic materials have also been used for 3D cell culture (Loessner et al. 2010). However, these systems frequently require the addition of bioactive sites necessary for the survival, adhesion, and growth of cells, as well as for the cell-responsive and temporal degradation of the material, and have generally not been amendable to formation of robust engineered cardiac tissues.

Based on the drawbacks of purely synthetic or natural biomaterials alone, hybrid and functionally modified natural biomaterials that possess suitable mechanical, biological, and physical characteristics necessary for cell survival, attachment, and growth have unique advantages and are becoming more widely used in tissue engineering, bioprinting, and microfluidic applications (Mironi-Harpaz et al. 2012, Wang et al. 2015). Hybrid and functionally modified natural biomaterials, including PEG-fibrinogen and GelMA, are therefore advantageous for the direct production of developing human cardiac tissues, as reported here. We recently showed that PEG-fibrinogen is a favorable biomaterial for hiPSC encapsulation and ontomimetic cardiac differentiation (Kerscher et al. 2015b). PEG-fibrinogen has previously been tested for use in a range of biomedical applications,

including cardiac regeneration (Bearzi et al. 2014, Plotkin et al. 2014) and in clinical trials for cartilage repair (Trattnig et al. 2015). However, although PEG-fibrinogen has high potential, it has not yet been assessed in bioprinting applications, which would facilitate the transition from bench top research to biomanufacturing and advancements in cell-therapy. GelMA has also been used alone and in combination with other materials (Du et al. 2015, Kolesky et al. 2014) to successfully produce tissues for a range of applications. In addition, methacryloyl-containing biomaterials, including GelMA, have been used for bioprinting 3D tissues (Kolesky et al. 2014, Ma et al. 2015a), a technology with high potential for advancing the field of biomanufacturing (Ozbolat 2015).

Bioprinting not only allows for fast production of 3D cell-laden hydrogels, but also for increased reproducibility and production speed. Experimentation with printing of hPSCs has been challenging due to the fragile nature of this cell type. Nevertheless, pluripotent stem cells have been successfully printed with high viability and maintenance of pluripotency (Ouyang et al. 2015, Faulkner-Jones et al. 2015). Printing hPSCs in combination with a hybrid or naturally modified biomaterial followed by subsequent cardiac differentiation has not yet been investigated, but, based on our results, could have high potential for the fabrication of engineered heart tissues. To manufacture the high number of cells necessary for cell-therapy and other regenerative applications, microcarriers or hydrogel encapsulation to support cell attachment and survival can be advantageous in bioreactor setup; GelMA hydrogels containing hPSCs could be fabricated to meet this need. By employing only a single cell-handling step and direct differentiation approach, our reported GEhECT platform has advantages for use in both

bioprinting and scalable cell production to obtain functional human cardiac tissues for drug testing and regenerative medicine applications.

CM function and mechanical contraction are physical characteristics of healthy cardiac tissues that can be monitored easily throughout *in vitro* development and maturation. Without the necessity of tissue dissociation, changes in frequency, contraction and relaxation velocities of spontaneously contracting GEhECTs were monitored and showed significant increases with culture time. GEhECTs were maintained in suspension without physical constraints or applied load. Contraction and relaxation velocities at early time points (day 14) were of the same magnitude as other hPSC-CMs cultured 2D monolayers on solid substrates (Huebsch et al. 2015). Starting on day 17, as CMs within GEhECTs developed robust cell-cell connections, tissues physically contracted faster and with greater tissue-scale deformation; this continual increase in contraction and relaxation velocities progressed through at least day 40 of differentiation. Differences in frequency of contraction can be linked to the level of maturation of cultured cells and can also differ between tissues in suspension culture versus those mechanically anchored to a substrate or other outside support (Tulloch et al. 2011). Although GEhECTs increased in their frequency of spontaneous contraction with culture time, the rate of contraction was slower than other human cardiac tissues cultured *in vitro* with mechanical load applied by a stiff substrate (Kerscher et al. 2015b) or mechanical posts. Overall, tissues showed regular contraction patterns and uniform frequency of contraction, properties which have previously been correlated to uniform cell distribution in contracting tissue areas and cell alignment (Tsang et al. 2015). The *in*

vitro functional responsiveness of these developing cardiac tissues is critical for use in future drug testing and regenerative medicine applications.

9. CONCLUSIONS

This research focused on the production of a novel 3D model of the developing human heart to better understand human heart development and research factors contributing to congenital heart defects, create better *in vitro* drug-testing platforms to screen novel pharmaceuticals, and enable patient-specific drug-screening to minimize severe cardiac side effects. With our scalable cardiac microsphere production approach we have also developed a procedure for implementing our single-cell handling approach for cell-therapy applications. Finally, with this research we want to show the advantages of providing a suitable 3D microenvironment throughout hPSC differentiation by incorporating photocrosslinkable and degradable biomaterials and how it benefits tissue formation *in vitro.*

The presented results show our ability to create a suitable 3D microenvironment to support hiPSC encapsulation, culture, and differentiation. PEG-fibrinogen and GelMA, with their ability to photocrosslink using visible light to form soft cell-laden hydrogels seem to be advantageous for successful stem cell culture.

The first encapsulation technique focused on the production of 3D developing human engineered cardiac tissue (3D-dhECT) microislands on acrylated glass using cluster and single dissociated hiPSCs. 3D-dhECTs formed synchronously contracting cardiac tissues (> 70% cTnT+) with gene expression and electrophysiological properties similar to 2D monolayers. 3D-dhECTs also showed the ability for long-term culture, which resulted in cells with features of mature CMs.

2D monolayers and 3D-dhECTs were then used to investigate their applicability to detect species-specific developmental abnormalities during CM development caused

by thalidomide. Reproducible results in control and thalidomide-treated 3D-dhECTs were detected, while thalidomide-treated 2D monolayers did not always result in contracting sheets. Our improved 3D platform of the developing human heart detected thalidomide-induced changes in tissue formation and growth, CM differentiation efficiency and total cell numbers per tissues. Frequencies of contraction were significantly slower in thalidomide-treated tissues compared to age-matched controls, sarcomere development was detained, and mitochondria morphology and distribution in thalidomide-treated CMs was visually different compared to control CM mitochondria. Overall, our 3D-dhECT platform proved applicable to detect difficult to study drug-induced congenital heart defects.

In addition to drug-testing applications, stem cell-derived cardiomyocytes are sought to be used in cell-therapy for myocardial repair. Immobilized 3D-dhECT microislands, although advantageous for their applicability in drug-testing, cannot be used for injectable cell therapy. We therefore translated our single-cell handling approach to produce cardiac microspheres. About 60 hiPSC-laden microspheres per minute were produced in our custom-built microfluidic device and efficiently differentiated to form cardiac microspheres. Appropriate responses to drug-treatment and outside pacing confirmed CM functionality and SEM images revealed the remodeling of the PEG-fibrinogen hydrogel to form dense spheres with cells producing their own ECM proteins. The cell and structural survival after shear also proved the applicability of our cardiac microspheres for cell-therapy applications.

Finally, we wanted to expand our studies with PEG-fibrinogen and find another favorable biomaterial for stem cell encapsulation, survival, and cardiac differentiation.

Gelatin methacryloyl (GelMA) with a low methacryloyl substitution degree (22%) was successfully synthesized and formed acellular and cellular hydrogels by photocrosslinking with the photoinitiator eosin Y and visible light for less than 1 min. Our approach allowed for high hiPSC survival and cardiac differentiation to produce GelMA developing human engineered cardiac tissues (GEhECTs).

Taken together, these studies showed the first successful hiPSC differentiation within biomimetic materials to form functional cardiac tissues with mature features. Our tissues were successfully used to detect thalidomide-induced congenital heart defect and produced in high-throughput for potential uses in regenerative medicine.

REFERENCES

Adler, S., C. Pellizzer, L. Hareng, T. Hartung & S. Bremer (2008) First steps in establishing a developmental toxicity test method based on human embryonic stem cells. *Toxicol In Vitro,* 22**,** 200-11.

Almany, L. & D. Seliktar (2005) Biosynthetic hydrogel scaffolds made from fibrinogen and polyethylene glycol for 3D cell cultures. *Biomaterials,* 26**,** 2467-77.

Amit, M., I. Laevsky, Y. Miropolsky, K. Shariki, M. Peri & J. Itskovitz-Eldor (2011) Dynamic suspension culture for scalable expansion of undifferentiated human pluripotent stem cells. *Nat Protoc,* 6**,** 572-9.

Appelman, T. P., J. Mizrahi, J. H. Elisseeff & D. Seliktar (2009) The differential effect of scaffold composition and architecture on chondrocyte response to mechanical stimulation. *Biomaterials,* 30**,** 518-25.

Arduini, D. (1995) Fetal Cardiac Function. 43-49.

Aubin, H., J. W. Nichol, C. B. Hutson, H. Bae, A. L. Sieminski, D. M. Cropek, P. Akhyari & A. Khademhosseini (2010) Directed 3D cell alignment and elongation in microengineered hydrogels. *Biomaterials,* 31**,** 6941-6951.

Auman, H. J., H. Coleman, H. E. Riley, F. Olale, H. J. Tsai & D. Yelon (2007) Functional modulation of cardiac form through regionally confined cell shape changes. *PLoS Biol,* 5**,** e53.

Baharvand, H., M. Azarnia, K. Parivar & S. K. Ashtiani (2005) The effect of extracellular matrix on embryonic stem cell-derived cardiomyocytes. *J Mol Cell Cardiol,* 38**,** 495-503.

Ban, K., H. J. Park, S. Kim, A. Andukuri, K. W. Cho, J. W. Hwang, H. J. Cha, S. Y. Kim, W. S. Kim, H. W. Jun & Y. S. Yoon (2014) Cell therapy with embryonic stem cell-derived cardiomyocytes encapsulated in injectable nanomatrix gel enhances cell engraftment and promotes cardiac repair. *ACS Nano,* 8**,** 10815-25.

Banerjee, A., M. Arha, S. Choudhary, R. S. Ashton, S. R. Bhatia, D. V. Schaffer & R. S. Kane (2009) The influence of hydrogel modulus on the proliferation and differentiation of encapsulated neural stem cells. *Biomaterials,* 30**,** 4695-9.

Bauwens, C., T. Yin, S. Dang, R. Peerani & P. W. Zandstra (2005) Development of a perfusion fed bioreactor for embryonic stem cell-derived cardiomyocyte generation: oxygen-mediated enhancement of cardiomyocyte output. *Biotechnol Bioeng,* 90**,** 452-61.

Bearzi, C., C. Gargioli, D. Baci, O. Fortunato, K. Shapira-Schweitzer, O. Kossover, M. V. Latronico, D. Seliktar, G. Condorelli & R. Rizzi (2014) PlGF-MMP9-engineered iPS cells supported on a PEG-fibrinogen hydrogel scaffold possess an enhanced capacity to repair damaged myocardium. *Cell Death Dis,* 5**,** e1053.

Beers, J., D. R. Gulbranson, N. George, L. I. Siniscalchi, J. Jones, J. A. Thomson & G. Chen (2012) Passaging and colony expansion of human pluripotent stem cells by enzyme-free dissociation in chemically defined culture conditions. *Nat Protoc,* 7**,** 2029-40.

Bensley, J. G., V. K. Stacy, R. De Matteo, R. Harding & M. J. Black (2010) Cardiac remodelling as a result of pre-term birth: implications for future cardiovascular disease. *Eur Heart J,* 31**,** 2058-66.

Benson, D. W., G. M. Silberbach, A. Kavanaugh-McHugh, C. Cottrill, Y. Zhang, S. Riggs, O. Smalls, M. C. Johnson, M. S. Watson, J. G. Seidman, C. E. Seidman, J. Plowden & J. D. Kugler (1999) Mutations in the cardiac transcription factor NKX2.5 affect diverse cardiac developmental pathways. *J Clin Invest,* 104**,** 1567-73.

Benton, J. A., C. A. DeForest, V. Vivekanandan & K. S. Anseth (2009) Photocrosslinking of gelatin macromers to synthesize porous hydrogels that promote valvular interstitial cell function. *Tissue Eng Part A,* 15**,** 3221-30.

Bertassoni, L. E., J. C. Cardoso, V. Manoharan, A. L. Cristino, N. S. Bhise, W. A. Araujo, P. Zorlutuna, N. E. Vrana, A. M. Ghaemmaghami, M. R. Dokmeci & A. Khademhosseini (2014) Direct-write bioprinting of cell-laden methacrylated gelatin hydrogels. *Biofabrication,* 6**,** 024105.

Bian, W., N. Badie, H. D. t. Himel & N. Bursac (2014) Robust T-tubulation and maturation of cardiomyocytes using tissue-engineered epicardial mimetics. *Biomaterials,* 35**,** 3819-28.

Bird, S. D., P. A. Doevendans, M. A. van Rooijen, A. Brutel de la Riviere, R. J. Hassink, R. Passier & C. L. Mummery (2003) The human adult cardiomyocyte phenotype. *Cardiovasc Res,* 58**,** 423-34.

Bowers, S. L., I. Banerjee & T. A. Baudino (2010) The extracellular matrix: at the center of it all. *J Mol Cell Cardiol,* 48**,** 474-82.

Bray, M. A., S. P. Sheehy & K. K. Parker (2008) Sarcomere alignment is regulated by myocyte shape. *Cell Motil Cytoskeleton,* 65**,** 641-51.

Brown, L. (2005) Cardiac extracellular matrix: a dynamic entity. *Am J Physiol Heart Circ Physiol,* 289**,** H973-4.

Bui, A. L., T. B. Horwich & G. C. Fonarow (2011) Epidemiology and risk profile of heart failure. *Nat Rev Cardiol,* 8**,** 30-41.

Burdick, J. A., C. Chung, X. Jia, M. A. Randolph & R. Langer (2005) Controlled degradation and mechanical behavior of photopolymerized hyaluronic acid networks. *Biomacromolecules,* 6**,** 386-91.

Burdick, J. A. & G. Vunjak-Novakovic (2009) Engineered microenvironments for controlled stem cell differentiation. *Tissue Eng Part A,* 15**,** 205-19.

Burridge, P. W., D. Anderson, H. Priddle, M. D. Barbadillo Munoz, S. Chamberlain, C. Allegrucci, L. E. Young & C. Denning (2007) Improved human embryonic stem cell embryoid body homogeneity and cardiomyocyte differentiation from a novel V-96 plate aggregation system highlights interline variability. *Stem Cells,* 25**,** 929-38.

Burridge, P. W., G. Keller, J. D. Gold & J. C. Wu (2012) Production of de novo cardiomyocytes: human pluripotent stem cell differentiation and direct reprogramming. *Cell Stem Cell,* 10**,** 16-28.

Burridge, P. W., E. Matsa, P. Shukla, Z. C. Lin, J. M. Churko, A. D. Ebert, F. Lan, S. Diecke, B. Huber, N. M. Mordwinkin, J. R. Plews, O. J. Abilez, B. Cui, J. D. Gold & J. C. Wu (2014) Chemically defined generation of human cardiomyocytes. *Nat Methods,* 11**,** 855-60.

Burridge, P. W., S. Thompson, M. A. Millrod, S. Weinberg, X. Yuan, A. Peters, V. Mahairaki, V. E. Koliatsos, L. Tung & E. T. Zambidis (2011) A universal system

for highly efficient cardiac differentiation of human induced pluripotent stem cells that eliminates interline variability. *PLoS One,* 6**,** e18293.

Bursac, N., Y. Loo, K. Leong & L. Tung (2007) Novel anisotropic engineered cardiac tissues: studies of electrical propagation. *Biochem Biophys Res Commun,* 361**,** 847-53.

Caspi, O., I. Itzhaki, I. Kehat, A. Gepstein, G. Arbel, I. Huber, J. Satin & L. Gepstein (2009) In vitro electrophysiological drug testing using human embryonic stem cell derived cardiomyocytes. *Stem Cells Dev,* 18**,** 161-72.

Caulfield, J. B. & T. K. Borg (1979) The collagen network of the heart. *Lab Invest,* 40**,** 364-72.

Chan, C. K., M. W. Rolle, S. Potter-Perigo, K. R. Braun, B. P. Van Biber, M. A. Laflamme, C. E. Murry & T. N. Wight (2010) Differentiation of cardiomyocytes from human embryonic stem cells is accompanied by changes in the extracellular matrix production of versican and hyaluronan. *J Cell Biochem,* 111**,** 585-96.

Chan, H. F., Y. Zhang & K. W. Leong (2016) Efficient One-Step Production of Microencapsulated Hepatocyte Spheroids with Enhanced Functions. *Small*.

Chen, A., E. Lee, R. Tu, K. Santiago, A. Grosberg, C. Fowlkes & M. Khine (2014) Integrated platform for functional monitoring of biomimetic heart sheets derived from human pluripotent stem cells. *Biomaterials,* 35**,** 675-83.

Cheng, K., K. Malliaras, R. R. Smith, D. Shen, B. Sun, A. Blusztajn, Y. Xie, A. Ibrahim, M. A. Aminzadeh, W. Liu, T. S. Li, M. A. De Robertis, L. Marban, L. S. Czer, A. Trento & E. Marban (2014) Human cardiosphere-derived cells from advanced

heart failure patients exhibit augmented functional potency in myocardial repair. *JACC Heart Fail,* 2**,** 49-61.

Chong, J. J., X. Yang, C. W. Don, E. Minami, Y. W. Liu, J. J. Weyers, W. M. Mahoney, B. Van Biber, S. M. Cook, N. J. Palpant, J. A. Gantz, J. A. Fugate, V. Muskheli, G. M. Gough, K. W. Vogel, C. A. Astley, C. E. Hotchkiss, A. Baldessari, L. Pabon, H. Reinecke, E. A. Gill, V. Nelson, H. P. Kiem, M. A. Laflamme & C. E. Murry (2014) Human embryonic-stem-cell-derived cardiomyocytes regenerate non-human primate hearts. *Nature,* 510**,** 273-7.

Chopra, A., V. Lin, A. McCollough, S. Atzet, G. D. Prestwich, A. S. Wechsler, M. E. Murray, S. A. Oake, J. Y. Kresh & P. A. Janmey (2012) Reprogramming cardiomyocyte mechanosensing by crosstalk between integrins and hyaluronic acid receptors. *J Biomech,* 45**,** 824-31.

Chung, B. G., K. H. Lee, A. Khademhosseini & S. H. Lee (2012a) Microfluidic fabrication of microengineered hydrogels and their application in tissue engineering. *Lab Chip,* 12**,** 45-59.

Chung, C., E. Anderson, R. R. Pera, B. L. Pruitt & S. C. Heilshorn (2012b) Hydrogel crosslinking density regulates temporal contractility of human embryonic stem cell-derived cardiomyocytes in 3D cultures. *Soft Matter,* 8**,** 10141-10148.

Chung, F., J. Lu, B. D. Palmer, P. Kestell, P. Browett, B. C. Baguley, M. Tingle & L. M. Ching (2004) Thalidomide pharmacokinetics and metabolite formation in mice, rabbits, and multiple myeloma patients. *Clin Cancer Res,* 10**,** 5949-56.

Citro, L., S. Naidu, F. Hassan, M. L. Kuppusamy, P. Kuppusamy, M. G. Angelos & M. Khan (2014) Comparison of human induced pluripotent stem-cell derived

cardiomyocytes with human mesenchymal stem cells following acute myocardial infarction. *PLoS One,* 9**,** e116281.

Claycomb, W. C., N. A. Lanson, Jr., B. S. Stallworth, D. B. Egeland, J. B. Delcarpio, A. Bahinski & N. J. Izzo, Jr. (1998) HL-1 cells: a cardiac muscle cell line that contracts and retains phenotypic characteristics of the adult cardiomyocyte. *Proc Natl Acad Sci U S A,* 95**,** 2979-84.

Daley, W. P., S. B. Peters & M. Larsen (2008) Extracellular matrix dynamics in development and regenerative medicine. *J Cell Sci,* 121**,** 255-64.

Dambrot, C., R. Passier, D. Atsma & C. L. Mummery (2011) Cardiomyocyte differentiation of pluripotent stem cells and their use as cardiac disease models. *Biochem J,* 434**,** 25-35.

de Lazaro, I., A. Yilmazer & K. Kostarelos (2014) Induced pluripotent stem (iPS) cells: a new source for cell-based therapeutics? *J Control Release,* 185**,** 37-44.

Dean, E. W., B. Udelsman & C. K. Breuer (2012) Current advances in the translation of vascular tissue engineering to the treatment of pediatric congenital heart disease. *Yale J Biol Med,* 85**,** 229-38.

Dikovsky, D., H. Bianco-Peled & D. Seliktar (2006) The effect of structural alterations of PEG-fibrinogen hydrogel scaffolds on 3-D cellular morphology and cellular migration. *Biomaterials,* 27**,** 1496-506.

Dobner, S., D. Bezuidenhout, P. Govender, P. Zilla & N. Davies (2009) A synthetic non-degradable polyethylene glycol hydrogel retards adverse post-infarct left ventricular remodeling. *J Card Fail,* 15**,** 629-36.

Dorn, G. W., 2nd, R. B. Vega & D. P. Kelly (2015) Mitochondrial biogenesis and dynamics in the developing and diseased heart. *Genes Dev,* 29**,** 1981-91.

Doyle, M. J., J. L. Lohr, C. S. Chapman, N. Koyano-Nakagawa, M. G. Garry & D. J. Garry (2015) Human Induced Pluripotent Stem Cell-Derived Cardiomyocytes as a Model for Heart Development and Congenital Heart Disease. *Stem Cell Rev,* 11**,** 710-27.

Du, M., B. Chen, Q. Meng, S. Liu, X. Zheng, C. Zhang, H. Wang, H. Li, N. Wang & J. Dai (2015) 3D bioprinting of BMSC-laden methacrylamide gelatin scaffolds with CBD-BMP2-collagen microfibers. *Biofabrication,* 7**,** 044104.

Duan, Y., Z. Liu, J. O'Neill, L. Q. Wan, D. O. Freytes & G. Vunjak-Novakovic (2011) Hybrid gel composed of native heart matrix and collagen induces cardiac differentiation of human embryonic stem cells without supplemental growth factors. *J Cardiovasc Transl Res,* 4**,** 605-15.

Dunn, D. A., A. J. Hodge & E. A. Lipke (2014) Biomimetic materials design for cardiac tissue regeneration. *Wiley Interdiscip Rev Nanomed Nanobiotechnol,* 6**,** 15-39.

Ebben, J. D., M. Zorniak, P. A. Clark & J. S. Kuo (2011) Introduction to induced pluripotent stem cells: advancing the potential for personalized medicine. *World Neurosurg,* 76**,** 270-5.

Elliott, D. A., S. R. Braam, K. Koutsis, E. S. Ng, R. Jenny, E. L. Lagerqvist, C. Biben, T. Hatzistavrou, C. E. Hirst, Q. C. Yu, R. J. Skelton, D. Ward-van Oostwaard, S. M. Lim, O. Khammy, X. Li, S. M. Hawes, R. P. Davis, A. L. Goulburn, R. Passier, O. W. Prall, J. M. Haynes, C. W. Pouton, D. M. Kaye, C. L. Mummery, A. G.

Elefanty & E. G. Stanley (2011) NKX2-5(eGFP/w) hESCs for isolation of human cardiac progenitors and cardiomyocytes. *Nat Methods,* 8**,** 1037-40.

Engler, A. J., S. Sen, H. L. Sweeney & D. E. Discher (2006) Matrix elasticity directs stem cell lineage specification. *Cell,* 126**,** 677-89.

Engler, A. J., H. L. Sweeney, D. E. Discher & J. E. Schwarzbauer (2007) Extracellular matrix elasticity directs stem cell differentiation. *J Musculoskelet Neuronal Interact,* 7**,** 335.

Faulkner-Jones, A., C. Fyfe, D. J. Cornelissen, J. Gardner, J. King, A. Courtney & W. Shu (2015) Bioprinting of human pluripotent stem cells and their directed differentiation into hepatocyte-like cells for the generation of mini-livers in 3D. *Biofabrication,* 7**,** 044102.

Feyen, D. A., R. Gaetani, J. Deddens, D. van Keulen, C. van Opbergen, M. Poldervaart, J. Alblas, S. Chamuleau, L. W. van Laake, P. A. Doevendans & J. P. Sluijter (2016) Gelatin Microspheres as Vehicle for Cardiac Progenitor Cells Delivery to the Myocardium. *Adv Healthc Mater*.

Fink, C., S. Ergun, D. Kralisch, U. Remmers, J. Weil & T. Eschenhagen (2000) Chronic stretch of engineered heart tissue induces hypertrophy and functional improvement. *FASEB J,* 14**,** 669-79.

Franco, C. L., J. Price & J. L. West (2011) Development and optimization of a dual-photoinitiator, emulsion-based technique for rapid generation of cell-laden hydrogel microspheres. *Acta Biomater,* 7**,** 3267-76.

Frank, C., D. U. Himmelstein, S. Woolhandler, D. H. Bor, S. M. Wolfe, O. Heymann, L. Zallman & K. E. Lasser (2014) Era of faster FDA drug approval has also seen

increased black-box warnings and market withdrawals. *Health Aff (Millwood),* 33**,** 1453-9.

Frey, N. & E. N. Olson (2003) Cardiac hypertrophy: the good, the bad, and the ugly. *Annu Rev Physiol,* 65**,** 45-79.

Frisman, I., D. Seliktar & H. Bianco-Peled (2011) Nanostructuring PEG-fibrinogen hydrogels to control cellular morphogenesis. *Biomaterials,* 32**,** 7839-46.

Fuoco, C., M. L. Salvatori, A. Biondo, K. Shapira-Schweitzer, S. Santoleri, S. Antonini, S. Bernardini, F. S. Tedesco, S. Cannata, D. Seliktar, G. Cossu & C. Gargioli (2012) Injectable polyethylene glycol-fibrinogen hydrogel adjuvant improves survival and differentiation of transplanted mesoangioblasts in acute and chronic skeletal-muscle degeneration. *Skelet Muscle,* 2**,** 24.

Galis, Z. S. & J. J. Khatri (2002) Matrix metalloproteinases in vascular remodeling and atherogenesis: the good, the bad, and the ugly. *Circ Res,* 90**,** 251-62.

Gao, X., R. L. Sprando & J. J. Yourick (2015) Thalidomide induced early gene expression perturbations indicative of human embryopathy in mouse embryonic stem cells. *Toxicol Appl Pharmacol,* 287**,** 43-51.

Garbern, J. C. & R. T. Lee (2013) Cardiac stem cell therapy and the promise of heart regeneration. *Cell Stem Cell,* 12**,** 689-98.

Garg, V., I. S. Kathiriya, R. Barnes, M. K. Schluterman, I. N. King, C. A. Butler, C. R. Rothrock, R. S. Eapen, K. Hirayama-Yamada, K. Joo, R. Matsuoka, J. C. Cohen & D. Srivastava (2003) GATA4 mutations cause human congenital heart defects and reveal an interaction with TBX5. *Nature,* 424**,** 443-7.

Georges, P. C. & P. A. Janmey (2005) Cell type-specific response to growth on soft materials. *J Appl Physiol (1985),* 98**,** 1547-53.

Gerdes, A. M., S. E. Kellerman, J. A. Moore, K. E. Muffly, L. C. Clark, P. Y. Reaves, K. B. Malec, P. P. McKeown & D. D. Schocken (1992) Structural remodeling of cardiac myocytes in patients with ischemic cardiomyopathy. *Circulation,* 86**,** 426-30.

Gerecht, S., J. A. Burdick, L. S. Ferreira, S. A. Townsend, R. Langer & G. Vunjak-Novakovic (2007) Hyaluronic acid hydrogel for controlled self-renewal and differentiation of human embryonic stem cells. *Proc Natl Acad Sci U S A,* 104**,** 11298-303.

Geuss, L. R., A. C. Allen, D. Ramamoorthy & L. J. Suggs (2015) Maintenance of HL-1 cardiomyocyte functional activity in PEGylated fibrin gels. *Biotechnol Bioeng,* 112**,** 1446-56.

Gherghiceanu, M., L. Barad, A. Novak, I. Reiter, J. Itskovitz-Eldor, O. Binah & L. M. Popescu (2011) Cardiomyocytes derived from human embryonic and induced pluripotent stem cells: comparative ultrastructure. *J Cell Mol Med,* 15**,** 2539-51.

Giacomotto, J. & L. Segalat (2010) High-throughput screening and small animal models, where are we? *Br J Pharmacol,* 160**,** 204-16.

Glesby, M. J. & R. E. Pyeritz (1989) Association of mitral valve prolapse and systemic abnormalities of connective tissue. A phenotypic continuum. *JAMA,* 262**,** 523-8.

Gonen-Wadmany, M., L. Gepstein & D. Seliktar (2004) Controlling the cellular organization of tissue-engineered cardiac constructs. *Ann N Y Acad Sci,* 1015**,** 299-311.

Gosselin, L. E., C. Adams, T. A. Cotter, R. J. McCormick & D. P. Thomas (1998) Effect of exercise training on passive stiffness in locomotor skeletal muscle: role of extracellular matrix. *J Appl Physiol (1985),* 85**,** 1011-6.

Guyette, J. P., J. M. Charest, R. W. Mills, B. J. Jank, P. T. Moser, S. E. Gilpin, J. R. Gershlak, T. Okamoto, G. Gonzalez, D. J. Milan, G. R. Gaudette & H. C. Ott (2016) Bioengineering Human Myocardium on Native Extracellular Matrix. *Circ Res,* 118**,** 56-72.

Han, L., Y. Li, J. Tchao, A. D. Kaplan, B. Lin, Y. Li, J. Mich-Basso, A. Lis, N. Hassan, B. London, G. C. Bett, K. Tobita, R. L. Rasmusson & L. Yang (2014) Study Familial Hypertrophic Cardiomyopathy Using Patient Specific Induced Pluripotent Stem Cells. *Cardiovasc Res*.

Hansen, A., A. Eder, M. Bonstrup, M. Flato, M. Mewe, S. Schaaf, B. Aksehirlioglu, A. P. Schwoerer, J. Uebeler & T. Eschenhagen (2010) Development of a drug screening platform based on engineered heart tissue. *Circ Res,* 107**,** 35-44.

Hartman, M. E., D. F. Dai & M. A. Laflamme (2016) Human pluripotent stem cells: Prospects and challenges as a source of cardiomyocytes for in vitro modeling and cell-based cardiac repair. *Adv Drug Deliv Rev,* 96**,** 3-17.

Hatcher, C. J. & C. T. Basson (2001) Getting the T-box dose right. *Nat Med,* 7**,** 1185-6.

Hawkins, N. M., M. C. Petrie, M. R. MacDonald, K. J. Hogg & J. J. McMurray (2006) Selecting patients for cardiac resynchronization therapy: electrical or mechanical dyssynchrony? *Eur Heart J,* 27**,** 1270-81.

Hazeltine, L. B., M. G. Badur, X. Lian, A. Das, W. Han & S. P. Palecek (2014) Temporal impact of substrate mechanics on differentiation of human embryonic stem cells to cardiomyocytes. *Acta Biomater,* 10**,** 604-12.

Hazeltine, L. B., C. S. Simmons, M. R. Salick, X. Lian, M. G. Badur, W. Han, S. M. Delgado, T. Wakatsuki, W. C. Crone, B. L. Pruitt & S. P. Palecek (2012) Effects of substrate mechanics on contractility of cardiomyocytes generated from human pluripotent stem cells. *Int J Cell Biol,* 2012**,** 508294.

Henderson, D. J. & A. J. Copp (1998) Versican expression is associated with chamber specification, septation, and valvulogenesis in the developing mouse heart. *Circ Res,* 83**,** 523-32.

Hirt, M. N., J. Boeddinghaus, A. Mitchell, S. Schaaf, C. Bornchen, C. Muller, H. Schulz, N. Hubner, J. Stenzig, A. Stoehr, C. Neuber, A. Eder, P. K. Luther, A. Hansen & T. Eschenhagen (2014) Functional improvement and maturation of rat and human engineered heart tissue by chronic electrical stimulation. *J Mol Cell Cardiol,* 74**,** 151-61.

Ho, S. Y., R. P. Thompson, S. R. Gibbs, M. M. Swindle & R. H. Anderson (1991) Ventricular septal defects in a family of Yucatan miniature pigs. *Int J Cardiol,* 33**,** 419-25.

Hodge, A. J., P. Kerscher, D. A. Dunn & E. A. Lipke. 2014. BIOMIMETIC MATERIALS FOR CARDIAC REGENERATION. In *Handbook of Biomimetics and Bioinspiration: 3 Tissue Models*, 1037-1067.

Hom, J. & S. S. Sheu (2009) Morphological dynamics of mitochondria--a special emphasis on cardiac muscle cells. *J Mol Cell Cardiol,* 46**,** 811-20.

Hotta, A. & S. Yamanaka (2015) From Genomics to Gene Therapy: Induced Pluripotent Stem Cells Meet Genome Editing. *Annu Rev Genet,* 49**,** 47-70.

Huebsch, N., P. Loskill, M. A. Mandegar, N. C. Marks, A. S. Sheehan, Z. Ma, A. Mathur, T. N. Nguyen, J. C. Yoo, L. M. Judge, C. I. Spencer, A. C. Chukka, C. R. Russell, P. L. So, B. R. Conklin & K. E. Healy (2015) Automated Video-Based Analysis of Contractility and Calcium Flux in Human-Induced Pluripotent Stem Cell-Derived Cardiomyocytes Cultured over Different Spatial Scales. *Tissue Eng Part C Methods,* 21**,** 467-79.

Hughes, C. S., L. M. Postovit & G. A. Lajoie (2010) Matrigel: a complex protein mixture required for optimal growth of cell culture. *Proteomics,* 10**,** 1886-90.

Ito, T., H. Ando & H. Handa (2011) Teratogenic effects of thalidomide: molecular mechanisms. *Cell Mol Life Sci,* 68**,** 1569-79.

Itzhaki, I., S. Rapoport, I. Huber, I. Mizrahi, L. Zwi-Dantsis, G. Arbel, J. Schiller & L. Gepstein (2011) Calcium handling in human induced pluripotent stem cell derived cardiomyocytes. *PLoS One,* 6**,** e18037.

Jacot, J. G., J. C. Martin & D. L. Hunt (2010) Mechanobiology of cardiomyocyte development. *J Biomech,* 43**,** 93-8.

Jenkins, K. J., A. Correa, J. A. Feinstein, L. Botto, A. E. Britt, S. R. Daniels, M. Elixson, C. A. Warnes, C. L. Webb & Y. American Heart Association Council on Cardiovascular Disease in the (2007) Noninherited risk factors and congenital cardiovascular defects: current knowledge: a scientific statement from the American Heart Association Council on Cardiovascular Disease in the Young: endorsed by the American Academy of Pediatrics. *Circulation,* 115**,** 2995-3014.

Jenkins, M. J. & S. S. Farid (2015) Human pluripotent stem cell-derived products: advances towards robust, scalable and cost-effective manufacturing strategies. *Biotechnol J,* 10**,** 83-95.

Jeziorowska, D., A. Korniat, J. E. Salem, K. Fish & J. S. Hulot (2015) Generating patient-specific induced pluripotent stem cells-derived cardiomyocytes for the treatment of cardiac diseases. *Expert Opin Biol Ther***,** 1-11.

Joanne, P., M. Kitsara, S. E. Boitard, H. Naemetalla, V. Vanneaux, M. Pernot, J. Larghero, P. Forest, Y. Chen, P. Menasche & O. Agbulut (2016) Nanofibrous clinical-grade collagen scaffolds seeded with human cardiomyocytes induces cardiac remodeling in dilated cardiomyopathy. *Biomaterials,* 80**,** 157-68.

Kang, H. W., S. J. Lee, I. K. Ko, C. Kengla, J. J. Yoo & A. Atala (2016) A 3D bioprinting system to produce human-scale tissue constructs with structural integrity. *Nat Biotechnol,* 34**,** 312-9.

Kattman, S. J., A. D. Witty, M. Gagliardi, N. C. Dubois, M. Niapour, A. Hotta, J. Ellis & G. Keller (2011) Stage-specific optimization of activin/nodal and BMP signaling promotes cardiac differentiation of mouse and human pluripotent stem cell lines. *Cell Stem Cell,* 8**,** 228-40.

Kehat, I., D. Kenyagin-Karsenti, M. Snir, H. Segev, M. Amit, A. Gepstein, E. Livne, O. Binah, J. Itskovitz-Eldor & L. Gepstein (2001) Human embryonic stem cells can differentiate into myocytes with structural and functional properties of cardiomyocytes. *J Clin Invest,* 108**,** 407-14.

Kehat, I., L. Khimovich, O. Caspi, A. Gepstein, R. Shofti, G. Arbel, I. Huber, J. Satin, J. Itskovitz-Eldor & L. Gepstein (2004) Electromechanical integration of

cardiomyocytes derived from human embryonic stem cells. *Nat Biotechnol,* 22**,** 1282-9.

Kempf, H., C. Kropp, R. Olmer, U. Martin & R. Zweigerdt (2015) Cardiac differentiation of human pluripotent stem cells in scalable suspension culture. *Nat Protoc,* 10**,** 1345-61.

Kempf, H., R. Olmer, C. Kropp, M. Ruckert, M. Jara-Avaca, D. Robles-Diaz, A. Franke, D. A. Elliott, D. Wojciechowski, M. Fischer, A. Roa Lara, G. Kensah, I. Gruh, A. Haverich, U. Martin & R. Zweigerdt (2014) Controlling expansion and cardiomyogenic differentiation of human pluripotent stem cells in scalable suspension culture. *Stem Cell Reports,* 3**,** 1132-46.

Kern, C. B., R. A. Norris, R. P. Thompson, W. S. Argraves, S. E. Fairey, L. Reyes, S. Hoffman, R. R. Markwald & C. H. Mjaatvedt (2007) Versican proteolysis mediates myocardial regression during outflow tract development. *Dev Dyn,* 236**,** 671-83.

Kern, C. B., W. O. Twal, C. H. Mjaatvedt, S. E. Fairey, B. P. Toole, M. L. Iruela-Arispe & W. S. Argraves (2006) Proteolytic cleavage of versican during cardiac cushion morphogenesis. *Dev Dyn,* 235**,** 2238-47.

Kerscher, P., B. S. Bussie, K. M. DeSimone, D. A. Dunn & E. A. Lipke (2015a) Characterization of mitochondrial populations during stem cell differentiation. *Methods Mol Biol,* 1264**,** 453-63.

Kerscher, P., I. C. Turnbull, A. J. Hodge, J. Kim, D. Seliktar, C. J. Easley, K. D. Costa & E. A. Lipke (2015b) Direct hydrogel encapsulation of pluripotent stem cells

enables ontomimetic differentiation and growth of engineered human heart tissues. *Biomaterials,* 83**,** 383-395.

Kim, D. H., E. A. Lipke, P. Kim, R. Cheong, S. Thompson, M. Delannoy, K. Y. Suh, L. Tung & A. Levchenko (2010) Nanoscale cues regulate the structure and function of macroscopic cardiac tissue constructs. *Proc Natl Acad Sci U S A,* 107**,** 565-70.

Kinney, M. A., T. A. Hookway, Y. Wang & T. C. McDevitt (2014) Engineering three-dimensional stem cell morphogenesis for the development of tissue models and scalable regenerative therapeutics. *Ann Biomed Eng,* 42**,** 352-67.

Knobloch, J., J. D. Shaughnessy, Jr. & U. Ruther (2007) Thalidomide induces limb deformities by perturbing the Bmp/Dkk1/Wnt signaling pathway. *FASEB J,* 21**,** 1410-21.

Knollmann, B. C. (2013) Induced pluripotent stem cell-derived cardiomyocytes: boutique science or valuable arrhythmia model? *Circ Res,* 112**,** 969-76; discussion 976.

Kodama, T., M. Abe, S. Iida, S. Ozaki, A. Sakai, M. Sawamura, C. Shimazaki, A. Miyata, T. Wakayama & H. Murakami (2009) A pharmacokinetic study evaluating the relationship between treatment efficacy and incidence of adverse events with thalidomide plasma concentrations in patients with refractory multiple myeloma. *Clin Lymphoma Myeloma,* 9**,** 154-9.

Kolesky, D. B., R. L. Truby, A. S. Gladman, T. A. Busbee, K. A. Homan & J. A. Lewis (2014) 3D bioprinting of vascularized, heterogeneous cell-laden tissue constructs. *Adv Mater,* 26**,** 3124-30.

Kruithof, B. P., S. A. Krawitz & V. Gaussin (2007) Atrioventricular valve development during late embryonic and postnatal stages involves condensation and extracellular matrix remodeling. *Dev Biol,* 302**,** 208-17.

Kumar, N., U. Sharma, C. Singh & B. Singh (2012) Thalidomide: chemistry, therapeutic potential and oxidative stress induced teratogenicity. *Curr Top Med Chem,* 12**,** 1436-55.

Kumar, V. A., N. L. Taylor, A. A. Jalan, L. K. Hwang, B. K. Wang & J. D. Hartgerink (2014) A nanostructured synthetic collagen mimic for hemostasis. *Biomacromolecules,* 15**,** 1484-90.

Kutschka, I., I. Y. Chen, T. Kofidis, T. Arai, G. von Degenfeld, A. Y. Sheikh, S. L. Hendry, J. Pearl, G. Hoyt, R. Sista, P. C. Yang, H. M. Blau, S. S. Gambhir & R. C. Robbins (2006) Collagen matrices enhance survival of transplanted cardiomyoblasts and contribute to functional improvement of ischemic rat hearts. *Circulation,* 114**,** I167-73.

Laflamme, M. A., K. Y. Chen, A. V. Naumova, V. Muskheli, J. A. Fugate, S. K. Dupras, H. Reinecke, C. Xu, M. Hassanipour, S. Police, C. O'Sullivan, L. Collins, Y. Chen, E. Minami, E. A. Gill, S. Ueno, C. Yuan, J. Gold & C. E. Murry (2007) Cardiomyocytes derived from human embryonic stem cells in pro-survival factors enhance function of infarcted rat hearts. *Nat Biotechnol,* 25**,** 1015-24.

Laflamme, M. A. & C. E. Murry (2011) Heart regeneration. *Nature,* 473**,** 326-35.

Lasser, K. E., P. D. Allen, S. J. Woolhandler, D. U. Himmelstein, S. M. Wolfe & D. H. Bor (2002) Timing of new black box warnings and withdrawals for prescription medications. *JAMA,* 287**,** 2215-20.

Lei, Y. & D. V. Schaffer (2013) A fully defined and scalable 3D culture system for human pluripotent stem cell expansion and differentiation. *Proc Natl Acad Sci U S A,* 110**,** E5039-48.

Lev, S., I. Kehat & L. Gepstein (2005) Differentiation pathways in human embryonic stem cell-derived cardiomyocytes. *Ann N Y Acad Sci,* 1047**,** 50-65.

Li, F., X. Wang, J. M. Capasso & A. M. Gerdes (1996) Rapid transition of cardiac myocytes from hyperplasia to hypertrophy during postnatal development. *J Mol Cell Cardiol,* 28**,** 1737-46.

Li, Q. Y., R. A. Newbury-Ecob, J. A. Terrett, D. I. Wilson, A. R. Curtis, C. H. Yi, T. Gebuhr, P. J. Bullen, S. C. Robson, T. Strachan, D. Bonnet, S. Lyonnet, I. D. Young, J. A. Raeburn, A. J. Buckler, D. J. Law & J. D. Brook (1997) Holt-Oram syndrome is caused by mutations in TBX5, a member of the Brachyury (T) gene family. *Nat Genet,* 15**,** 21-9.

Li, R. K., Z. Q. Jia, R. D. Weisel, D. A. Mickle, A. Choi & T. M. Yau (1999) Survival and function of bioengineered cardiac grafts. *Circulation,* 100**,** II63-9.

Li, T. S., K. Cheng, K. Malliaras, R. R. Smith, Y. Zhang, B. Sun, N. Matsushita, A. Blusztajn, J. Terrovitis, H. Kusuoka, L. Marban & E. Marban (2012) Direct comparison of different stem cell types and subpopulations reveals superior paracrine potency and myocardial repair efficacy with cardiosphere-derived cells. *J Am Coll Cardiol,* 59**,** 942-53.

Li, Z., X. Guo, S. Matsushita & J. Guan (2011) Differentiation of cardiosphere-derived cells into a mature cardiac lineage using biodegradable poly(N-isopropylacrylamide) hydrogels. *Biomaterials,* 32**,** 3220-32.

Lian, X., C. Hsiao, G. Wilson, K. Zhu, L. B. Hazeltine, S. M. Azarin, K. K. Raval, J. Zhang, T. J. Kamp & S. P. Palecek (2012) Robust cardiomyocyte differentiation from human pluripotent stem cells via temporal modulation of canonical Wnt signaling. *Proc Natl Acad Sci U S A,* 109**,** E1848-57.

Lian, X., J. Zhang, S. M. Azarin, K. Zhu, L. B. Hazeltine, X. Bao, C. Hsiao, T. J. Kamp & S. P. Palecek (2013) Directed cardiomyocyte differentiation from human pluripotent stem cells by modulating Wnt/beta-catenin signaling under fully defined conditions. *Nat Protoc,* 8**,** 162-75.

Liang, P., F. Lan, A. S. Lee, T. Gong, V. Sanchez-Freire, Y. Wang, S. Diecke, K. Sallam, J. W. Knowles, P. J. Wang, P. K. Nguyen, D. M. Bers, R. C. Robbins & J. C. Wu (2013) Drug screening using a library of human induced pluripotent stem cell-derived cardiomyocytes reveals disease-specific patterns of cardiotoxicity. *Circulation,* 127**,** 1677-91.

Liberatore, C. M., R. D. Searcy-Schrick, E. B. Vincent & K. E. Yutzey (2002) Nkx-2.5 gene induction in mice is mediated by a Smad consensus regulatory region. *Dev Biol,* 244**,** 243-56.

Liberatore, C. M., R. D. Searcy-Schrick & K. E. Yutzey (2000) Ventricular expression of tbx5 inhibits normal heart chamber development. *Dev Biol,* 223**,** 169-80.

Lien, C. L., J. McAnally, J. A. Richardson & E. N. Olson (2002) Cardiac-specific activity of an Nkx2-5 enhancer requires an evolutionarily conserved Smad binding site. *Dev Biol,* 244**,** 257-66.

Lien, C. L., C. Wu, B. Mercer, R. Webb, J. A. Richardson & E. N. Olson (1999) Control of early cardiac-specific transcription of Nkx2-5 by a GATA-dependent enhancer. *Development,* 126**,** 75-84.

Lieu, D. K., J. Liu, C. W. Siu, G. P. McNerney, H. F. Tse, A. Abu-Khalil, T. Huser & R. A. Li (2009) Absence of transverse tubules contributes to non-uniform Ca(2+) wavefronts in mouse and human embryonic stem cell-derived cardiomyocytes. *Stem Cells Dev,* 18**,** 1493-500.

Limperopoulos, C., A. Majnemer, M. I. Shevell, B. Rosenblatt, C. Rohlicek & C. Tchervenkov (1999) Neurologic status of newborns with congenital heart defects before open heart surgery. *Pediatrics,* 103**,** 402-8.

Liu, H., S. F. Collins & L. J. Suggs (2006) Three-dimensional culture for expansion and differentiation of mouse embryonic stem cells. *Biomaterials,* 27**,** 6004-14.

Liu, H. & K. Roy (2005) Biomimetic three-dimensional cultures significantly increase hematopoietic differentiation efficacy of embryonic stem cells. *Tissue Eng,* 11**,** 319-30.

Liu, X., H. Wu, M. Byrne, S. Krane & R. Jaenisch (1997) Type III collagen is crucial for collagen I fibrillogenesis and for normal cardiovascular development. *Proc Natl Acad Sci U S A,* 94**,** 1852-6.

Loessner, D., K. S. Stok, M. P. Lutolf, D. W. Hutmacher, J. A. Clements & S. C. Rizzi (2010) Bioengineered 3D platform to explore cell-ECM interactions and drug resistance of epithelial ovarian cancer cells. *Biomaterials,* 31**,** 8494-506.

Lou, Q., V. V. Fedorov, A. V. Glukhov, N. Moazami, V. G. Fast & I. R. Efimov (2011) Transmural heterogeneity and remodeling of ventricular excitation-contraction coupling in human heart failure. *Circulation,* 123**,** 1881-90.

Louch, W. E., K. A. Sheehan & B. M. Wolska (2011) Methods in cardiomyocyte isolation, culture, and gene transfer. *J Mol Cell Cardiol,* 51**,** 288-98.

Lowes, B. D., W. Minobe, W. T. Abraham, M. N. Rizeq, T. J. Bohlmeyer, R. A. Quaife, R. L. Roden, D. L. Dutcher, A. D. Robertson, N. F. Voelkel, D. B. Badesch, B. M. Groves, E. M. Gilbert & M. R. Bristow (1997) Changes in gene expression in the intact human heart. Downregulation of alpha-myosin heavy chain in hypertrophied, failing ventricular myocardium. *J Clin Invest,* 100**,** 2315-24.

Lowry, W. E., L. Richter, R. Yachechko, A. D. Pyle, J. Tchieu, R. Sridharan, A. T. Clark & K. Plath (2008) Generation of human induced pluripotent stem cells from dermal fibroblasts. *Proc Natl Acad Sci U S A,* 105**,** 2883-8.

Lu, H. R., E. Vlaminckx, A. N. Hermans, J. Rohrbacher, K. Van Ammel, R. Towart, M. Pugsley & D. J. Gallacher (2008) Predicting drug-induced changes in QT interval and arrhythmias: QT-shortening drugs point to gaps in the ICHS7B Guidelines. *Br J Pharmacol,* 154**,** 1427-38.

Lundy, S. D., W. Z. Zhu, M. Regnier & M. A. Laflamme (2013) Structural and functional maturation of cardiomyocytes derived from human pluripotent stem cells. *Stem Cells Dev,* 22**,** 1991-2002.

Lutolf, M. P., P. M. Gilbert & H. M. Blau (2009) Designing materials to direct stem-cell fate. *Nature,* 462**,** 433-41.

Ma, Y., Y. Ji, G. Huang, K. Ling, X. Zhang & F. Xu (2015a) Bioprinting 3D cell-laden hydrogel microarray for screening human periodontal ligament stem cell response to extracellular matrix. *Biofabrication,* 7**,** 044105.

Ma, Z., J. Wang, P. Loskill, N. Huebsch, S. Koo, F. L. Svedlund, N. C. Marks, E. W. Hua, C. P. Grigoropoulos, B. R. Conklin & K. E. Healy (2015b) Self-organizing human cardiac microchambers mediated by geometric confinement. *Nat Commun,* 6**,** 7413.

Makkar, R. R., R. R. Smith, K. Cheng, K. Malliaras, L. E. Thomson, D. Berman, L. S. Czer, L. Marban, A. Mendizabal, P. V. Johnston, S. D. Russell, K. H. Schuleri, A. C. Lardo, G. Gerstenblith & E. Marban (2012) Intracoronary cardiosphere-derived cells for heart regeneration after myocardial infarction (CADUCEUS): a prospective, randomised phase 1 trial. *Lancet,* 379**,** 895-904.

Malliaras, K., T. S. Li, D. Luthringer, J. Terrovitis, K. Cheng, T. Chakravarty, G. Galang, Y. Zhang, F. Schoenhoff, J. Van Eyk, L. Marban & E. Marban (2012) Safety and efficacy of allogeneic cell therapy in infarcted rats transplanted with mismatched cardiosphere-derived cells. *Circulation,* 125**,** 100-12.

Mann, B. K. & J. L. West (2002) Cell adhesion peptides alter smooth muscle cell adhesion, proliferation, migration, and matrix protein synthesis on modified surfaces and in polymer scaffolds. *J Biomed Mater Res,* 60**,** 86-93.

Mansour, H., P. P. de Tombe, A. M. Samarel & B. Russell (2004) Restoration of resting sarcomere length after uniaxial static strain is regulated by protein kinase Cepsilon and focal adhesion kinase. *Circ Res,* 94**,** 642-9.

Masumoto, H., T. Ikuno, M. Takeda, H. Fukushima, A. Marui, S. Katayama, T. Shimizu, T. Ikeda, T. Okano, R. Sakata & J. K. Yamashita (2014) Human iPS cell-engineered cardiac tissue sheets with cardiomyocytes and vascular cells for cardiac regeneration. *Sci Rep,* 4**,** 6716.

Matsa, E., P. W. Burridge & J. C. Wu (2014) Human stem cells for modeling heart disease and for drug discovery. *Sci Transl Med,* 6**,** 239ps6.

Matsuura, K., T. Nagai, N. Nishigaki, T. Oyama, J. Nishi, H. Wada, M. Sano, H. Toko, H. Akazawa, T. Sato, H. Nakaya, H. Kasanuki & I. Komuro (2004) Adult cardiac Sca-1-positive cells differentiate into beating cardiomyocytes. *J Biol Chem,* 279**,** 11384-91.

Mayshar, Y., O. Yanuka & N. Benvenisty (2011) Teratogen screening using transcriptome profiling of differentiating human embryonic stem cells. *J Cell Mol Med,* 15**,** 1393-401.

McCulley, D. J. & B. L. Black (2012) Transcription factor pathways and congenital heart disease. *Curr Top Dev Biol,* 100**,** 253-77.

McDevitt, T. C., J. C. Angello, M. L. Whitney, H. Reinecke, S. D. Hauschka, C. E. Murry & P. S. Stayton (2002) In vitro generation of differentiated cardiac myofibers on micropatterned laminin surfaces. *J Biomed Mater Res,* 60**,** 472-9.

Meganathan, K., S. Jagtap, V. Wagh, J. Winkler, J. A. Gaspar, D. Hildebrand, M. Trusch, K. Lehmann, J. Hescheler, H. Schluter & A. Sachinidis (2012) Identification of thalidomide-specific transcriptomics and proteomics signatures during differentiation of human embryonic stem cells. *PLoS One,* 7**,** e44228.

Menasche, P., V. Vanneaux, A. Hagege, A. Bel, B. Cholley, I. Cacciapuoti, A. Parouchev, N. Benhamouda, G. Tachdjian, L. Tosca, J. H. Trouvin, J. R. Fabreguettes, V. Bellamy, R. Guillemain, C. Suberbielle Boissel, E. Tartour, M. Desnos & J. Larghero (2015) Human embryonic stem cell-derived cardiac progenitors for severe heart failure treatment: first clinical case report. *Eur Heart J,* 36**,** 2011-7.

Mercola, M., P. Ruiz-Lozano & M. D. Schneider (2011) Cardiac muscle regeneration: lessons from development. *Genes Dev,* 25**,** 299-309.

Mihic, A., J. Li, Y. Miyagi, M. Gagliardi, S. H. Li, J. Zu, R. D. Weisel, G. Keller & R. K. Li (2014) The effect of cyclic stretch on maturation and 3D tissue formation of human embryonic stem cell-derived cardiomyocytes. *Biomaterials,* 35**,** 2798-808.

Mironi-Harpaz, I., D. Y. Wang, S. Venkatraman & D. Seliktar (2012) Photopolymerization of cell-encapsulating hydrogels: crosslinking efficiency versus cytotoxicity. *Acta Biomater,* 8**,** 1838-48.

Mollova, M., K. Bersell, S. Walsh, J. Savla, L. T. Das, S. Y. Park, L. E. Silberstein, C. G. Dos Remedios, D. Graham, S. Colan & B. Kuhn (2013) Cardiomyocyte proliferation contributes to heart growth in young humans. *Proc Natl Acad Sci U S A,* 110**,** 1446-51.

Morgan, K. Y. & L. D. Black, 3rd (2014) Creation of a bioreactor for the application of variable amplitude mechanical stimulation of fibrin gel-based engineered cardiac tissue. *Methods Mol Biol,* 1181**,** 177-87.

Munshi, N. V., J. McAnally, S. Bezprozvannaya, J. M. Berry, J. A. Richardson, J. A. Hill & E. N. Olson (2009) Cx30.2 enhancer analysis identifies Gata4 as a novel regulator of atrioventricular delay. *Development,* 136**,** 2665-74.

Murphy, S. V. & A. Atala (2014) 3D bioprinting of tissues and organs. *Nat Biotechnol,* 32**,** 773-85.

Murry, C. E., H. Reinecke & L. M. Pabon (2006) Regeneration gaps: observations on stem cells and cardiac repair. *J Am Coll Cardiol,* 47**,** 1777-85.

Musah, S., S. A. Morin, P. J. Wrighton, D. B. Zwick, S. Jin & L. L. Kiessling (2012) Glycosaminoglycan-binding hydrogels enable mechanical control of human pluripotent stem cell self-renewal. *ACS Nano,* 6**,** 10168-77.

Nagase, K., J. Kobayashi & T. Okano (2009) Temperature-responsive intelligent interfaces for biomolecular separation and cell sheet engineering. *J R Soc Interface,* 6 Suppl 3**,** S293-309.

Naito, A. T., I. Shiojima, H. Akazawa, K. Hidaka, T. Morisaki, A. Kikuchi & I. Komuro (2006) Developmental stage-specific biphasic roles of Wnt/beta-catenin signaling in cardiomyogenesis and hematopoiesis. *Proc Natl Acad Sci U S A,* 103**,** 19812-7.

Nelson, D. M., Z. Ma, K. L. Fujimoto, R. Hashizume & W. R. Wagner (2011) Intra-myocardial biomaterial injection therapy in the treatment of heart failure: Materials, outcomes and challenges. *Acta Biomater,* 7**,** 1-15.

Nguyen, D. C., T. A. Hookway, Q. Wu, R. Jha, M. K. Preininger, X. Chen, C. A. Easley, P. Spearman, S. R. Deshpande, K. Maher, M. B. Wagner, T. C. McDevitt & C. Xu (2014) Microscale generation of cardiospheres promotes robust enrichment of

cardiomyocytes derived from human pluripotent stem cells. *Stem Cell Reports,* 3**,** 260-8.

Nichol, J. W., S. T. Koshy, H. Bae, C. M. Hwang, S. Yamanlar & A. Khademhosseini (2010) Cell-laden microengineered gelatin methacrylate hydrogels. *Biomaterials,* 31**,** 5536-44.

Nie, Y., P. Walsh, D. L. Clarke, J. A. Rowley & T. Fellner (2014) Scalable passaging of adherent human pluripotent stem cells. *PLoS One,* 9**,** e88012.

Norton, G. R., J. Tsotetsi, B. Trifunovic, C. Hartford, G. P. Candy & A. J. Woodiwiss (1997) Myocardial stiffness is attributed to alterations in cross-linked collagen rather than total collagen or phenotypes in spontaneously hypertensive rats. *Circulation,* 96**,** 1991-8.

Noseda, M., M. Abreu-Paiva & M. D. Schneider (2015) The Quest for the Adult Cardiac Stem Cell. *Circ J,* 79**,** 1422-30.

Nunes, S. S., J. W. Miklas, J. Liu, R. Aschar-Sobbi, Y. Xiao, B. Zhang, J. Jiang, S. Masse, M. Gagliardi, A. Hsieh, N. Thavandiran, M. A. Laflamme, K. Nanthakumar, G. J. Gross, P. H. Backx, G. Keller & M. Radisic (2013) Biowire: a platform for maturation of human pluripotent stem cell-derived cardiomyocytes. *Nat Methods,* 10**,** 781-7.

Ong, S. G., B. C. Huber, W. H. Lee, K. Kodo, A. D. Ebert, Y. Ma, P. K. Nguyen, S. Diecke, W. Y. Chen & J. C. Wu (2015) Microfluidic Single-Cell Analysis of Transplanted Human Induced Pluripotent Stem Cell-Derived Cardiomyocytes After Acute Myocardial Infarction. *Circulation,* 132**,** 762-71.

Oskouei, B. N., G. Lamirault, C. Joseph, A. V. Treuer, S. Landa, J. Da Silva, K. Hatzistergos, M. Dauer, W. Balkan, I. McNiece & J. M. Hare (2012) Increased potency of cardiac stem cells compared with bone marrow mesenchymal stem cells in cardiac repair. *Stem Cells Transl Med,* 1**,** 116-24.

Ouyang, L., R. Yao, S. Mao, X. Chen, J. Na & W. Sun (2015) Three-dimensional bioprinting of embryonic stem cells directs highly uniform embryoid body formation. *Biofabrication,* 7**,** 044101.

Ozbolat, I. T. (2015) Bioprinting scale-up tissue and organ constructs for transplantation. *Trends Biotechnol,* 33**,** 395-400.

Paige, S. L., S. Thomas, C. L. Stoick-Cooper, H. Wang, L. Maves, R. Sandstrom, L. Pabon, H. Reinecke, G. Pratt, G. Keller, R. T. Moon, J. Stamatoyannopoulos & C. E. Murry (2012) A temporal chromatin signature in human embryonic stem cells identifies regulators of cardiac development. *Cell,* 151**,** 221-32.

Parman, T., M. J. Wiley & P. G. Wells (1999) Free radical-mediated oxidative DNA damage in the mechanism of thalidomide teratogenicity. *Nat Med,* 5**,** 582-5.

Parra, V., V. Eisner, M. Chiong, A. Criollo, F. Moraga, A. Garcia, S. Hartel, E. Jaimovich, A. Zorzano, C. Hidalgo & S. Lavandero (2008) Changes in mitochondrial dynamics during ceramide-induced cardiomyocyte early apoptosis. *Cardiovasc Res,* 77**,** 387-97.

Paul, A., A. Hasan, H. A. Kindi, A. K. Gaharwar, V. T. Rao, M. Nikkhah, S. R. Shin, D. Krafft, M. R. Dokmeci, D. Shum-Tim & A. Khademhosseini (2014) Injectable graphene oxide/hydrogel-based angiogenic gene delivery system for vasculogenesis and cardiac repair. *ACS Nano,* 8**,** 8050-62.

Peacock, J. D., Y. Lu, M. Koch, K. E. Kadler & J. Lincoln (2008) Temporal and spatial expression of collagens during murine atrioventricular heart valve development and maintenance. *Dev Dyn,* 237**,** 3051-8.

Pecha, S., T. Eschenhagen & H. Reichenspurner (2016) Myocardial tissue engineering for cardiac repair. *J Heart Lung Transplant,* 35**,** 294-8.

Pediatric Cardiac Genomics, C., B. Gelb, M. Brueckner, W. Chung, E. Goldmuntz, J. Kaltman, J. P. Kaski, R. Kim, J. Kline, L. Mercer-Rosa, G. Porter, A. Roberts, E. Rosenberg, H. Seiden, C. Seidman, L. Sleeper, S. Tennstedt, J. Kaltman, C. Schramm, K. Burns, G. Pearson & E. Rosenberg (2013) The Congenital Heart Disease Genetic Network Study: rationale, design, and early results. *Circ Res,* 112**,** 698-706.

Peled, E., J. Boss, J. Bejar, C. Zinman & D. Seliktar (2007) A novel poly(ethylene glycol)-fibrinogen hydrogel for tibial segmental defect repair in a rat model. *J Biomed Mater Res A,* 80**,** 874-84.

Phinney, D. G. & D. J. Prockop (2007) Concise review: mesenchymal stem/multipotent stromal cells: the state of transdifferentiation and modes of tissue repair--current views. *Stem Cells,* 25**,** 2896-902.

Plageman, T. F., Jr. & K. E. Yutzey (2005) T-box genes and heart development: putting the "T" in heart. *Dev Dyn,* 232**,** 11-20.

Planat-Benard, V., C. Menard, M. Andre, M. Puceat, A. Perez, J. M. Garcia-Verdugo, L. Penicaud & L. Casteilla (2004) Spontaneous cardiomyocyte differentiation from adipose tissue stroma cells. *Circ Res,* 94**,** 223-9.

Plotkin, M., S. R. Vaibavi, A. J. Rufaihah, V. Nithya, J. Wang, Y. Shachaf, T. Kofidis & D. Seliktar (2014) The effect of matrix stiffness of injectable hydrogels on the preservation of cardiac function after a heart attack. *Biomaterials,* 35**,** 1429-38.

Posch, M. G., L. H. Boldt, M. Polotzki, S. Richter, S. Rolf, A. Perrot, R. Dietz, C. Ozcelik & W. Haverkamp (2010) Mutations in the cardiac transcription factor GATA4 in patients with lone atrial fibrillation. *Eur J Med Genet,* 53**,** 201-3.

Pouzet, B., J. T. Vilquin, A. A. Hagege, M. Scorsin, E. Messas, M. Fiszman, K. Schwartz & P. Menasche (2001) Factors affecting functional outcome after autologous skeletal myoblast transplantation. *Ann Thorac Surg,* 71**,** 844-50; discussion 850-1.

Prakash, Y. S., M. J. Cody, P. R. Housmans, J. D. Hannon & G. C. Sieck (1999) Comparison of cross-bridge cycling kinetics in neonatal vs. adult rat ventricular muscle. *J Muscle Res Cell Motil,* 20**,** 717-23.

Priori, S. G., C. Napolitano, E. Di Pasquale & G. Condorelli (2013) Induced pluripotent stem cell-derived cardiomyocytes in studies of inherited arrhythmias. *J Clin Invest,* 123**,** 84-91.

Qu, X., H. Jia, D. M. Garrity, K. Tompkins, L. Batts, B. Appel, T. P. Zhong & H. S. Baldwin (2008) Ndrg4 is required for normal myocyte proliferation during early cardiac development in zebrafish. *Dev Biol,* 317**,** 486-96.

Radisic, M., H. Park, H. Shing, T. Consi, F. J. Schoen, R. Langer, L. E. Freed & G. Vunjak-Novakovic (2004a) Functional assembly of engineered myocardium by electrical stimulation of cardiac myocytes cultured on scaffolds. *Proc Natl Acad Sci U S A,* 101**,** 18129-34.

Radisic, M., L. Yang, J. Boublik, R. J. Cohen, R. Langer, L. E. Freed & G. Vunjak-Novakovic (2004b) Medium perfusion enables engineering of compact and contractile cardiac tissue. *Am J Physiol Heart Circ Physiol,* 286**,** H507-16.

Rahmani, M., J. M. Carthy & B. M. McManus (2012) Mapping of the Wnt/beta-catenin/TCF response elements in the human versican promoter. *Methods Mol Biol,* 836**,** 35-52.

Rivera-Feliciano, J. & C. J. Tabin (2006) Bmp2 instructs cardiac progenitors to form the heart-valve-inducing field. *Dev Biol,* 295**,** 580-8.

Rizzi, R., E. Di Pasquale, P. Portararo, R. Papait, P. Cattaneo, M. V. Latronico, C. Altomare, L. Sala, A. Zaza, E. Hirsch, L. Naldini, G. Condorelli & C. Bearzi (2012) Post-natal cardiomyocytes can generate iPS cells with an enhanced capacity toward cardiomyogenic re-differentation. *Cell Death Differ,* 19**,** 1162-74.

Robertson, C., D. D. Tran & S. C. George (2013) Concise review: maturation phases of human pluripotent stem cell-derived cardiomyocytes. *Stem Cells,* 31**,** 829-37.

Rojas, A., S. W. Kong, P. Agarwal, B. Gilliss, W. T. Pu & B. L. Black (2008) GATA4 is a direct transcriptional activator of cyclin D2 and Cdk4 and is required for cardiomyocyte proliferation in anterior heart field-derived myocardium. *Mol Cell Biol,* 28**,** 5420-31.

Ruan, J. L., N. L. Tulloch, M. Saiget, S. L. Paige, M. V. Razumova, M. Regnier, K. C. Tung, G. Keller, L. Pabon, H. Reinecke & C. E. Murry (2015) Mechanical Stress Promotes Maturation of Human Myocardium From Pluripotent Stem Cell-Derived Progenitors. *Stem Cells,* 33**,** 2148-57.

Russell, B., D. Motlagh & W. W. Ashley (2000) Form follows function: how muscle shape is regulated by work. *J Appl Physiol (1985),* 88**,** 1127-32.

Ryan, C., B. T. Nguyen & S. J. Sullivan (1995) Rapid assay for mycobacterial growth and antibiotic susceptibility using gel microdrop encapsulation. *J Clin Microbiol,* 33**,** 1720-6.

Saunders, R. & M. Amoroso (2010) SEM investigation of heart tissue samples. *J. Phys.: Conf. Ser. ,* 241

Schaaf, S., A. Eder, I. Vollert, A. Stohr, A. Hansen & T. Eschenhagen (2014) Generation of strip-format fibrin-based engineered heart tissue (EHT). *Methods Mol Biol,* 1181**,** 121-9.

Schaaf, S., A. Shibamiya, M. Mewe, A. Eder, A. Stohr, M. N. Hirt, T. Rau, W. H. Zimmermann, L. Conradi, T. Eschenhagen & A. Hansen (2011) Human engineered heart tissue as a versatile tool in basic research and preclinical toxicology. *PLoS One,* 6**,** e26397.

Schaper, J., E. Meiser & G. Stammler (1985) Ultrastructural morphometric analysis of myocardium from dogs, rats, hamsters, mice, and from human hearts. *Circ Res,* 56**,** 377-91.

Schott, J. J., D. W. Benson, C. T. Basson, W. Pease, G. M. Silberbach, J. P. Moak, B. J. Maron, C. E. Seidman & J. G. Seidman (1998) Congenital heart disease caused by mutations in the transcription factor NKX2-5. *Science,* 281**,** 108-11.

Serpooshan, V., M. Zhao, S. A. Metzler, K. Wei, P. B. Shah, A. Wang, M. Mahmoudi, A. V. Malkovskiy, J. Rajadas, M. J. Butte, D. Bernstein & P. Ruiz-Lozano (2013)

The effect of bioengineered acellular collagen patch on cardiac remodeling and ventricular function post myocardial infarction. *Biomaterials,* 34**,** 9048-55.

Shao, Y., J. Sang & J. Fu (2015) On human pluripotent stem cell control: The rise of 3D bioengineering and mechanobiology. *Biomaterials,* 52**,** 26-43.

Shapira-Schweitzer, K., M. Habib, L. Gepstein & D. Seliktar (2009) A photopolymerizable hydrogel for 3-D culture of human embryonic stem cell-derived cardiomyocytes and rat neonatal cardiac cells. *J Mol Cell Cardiol,* 46**,** 213-24.

Shapira-Schweitzer, K. & D. Seliktar (2007) Matrix stiffness affects spontaneous contraction of cardiomyocytes cultured within a PEGylated fibrinogen biomaterial. *Acta Biomater,* 3**,** 33-41.

Shimizu, T., M. Yamato, T. Akutsu, T. Shibata, Y. Isoi, A. Kikuchi, M. Umezu & T. Okano (2002a) Electrically communicating three-dimensional cardiac tissue mimic fabricated by layered cultured cardiomyocyte sheets. *J Biomed Mater Res,* 60**,** 110-7.

Shimizu, T., M. Yamato, Y. Isoi, T. Akutsu, T. Setomaru, K. Abe, A. Kikuchi, M. Umezu & T. Okano (2002b) Fabrication of pulsatile cardiac tissue grafts using a novel 3-dimensional cell sheet manipulation technique and temperature-responsive cell culture surfaces. *Circ Res,* 90**,** e40.

Shimizu, T., M. Yamato, A. Kikuchi & T. Okano (2003) Cell sheet engineering for myocardial tissue reconstruction. *Biomaterials,* 24**,** 2309-16.

Shin, S. R., S. M. Jung, M. Zalabany, K. Kim, P. Zorlutuna, S. B. Kim, M. Nikkhah, M. Khabiry, M. Azize, J. Kong, K. T. Wan, T. Palacios, M. R. Dokmeci, H. Bae, X.

S. Tang & A. Khademhosseini (2013) Carbon-nanotube-embedded hydrogel sheets for engineering cardiac constructs and bioactuators. *ACS Nano,* 7**,** 2369-80.

Shiojima, I. & K. Walsh (2006) Regulation of cardiac growth and coronary angiogenesis by the Akt/PKB signaling pathway. *Genes Dev,* 20**,** 3347-65.

Shu, X. Z., Y. Liu, Y. Luo, M. C. Roberts & G. D. Prestwich (2002) Disulfide cross-linked hyaluronan hydrogels. *Biomacromolecules,* 3**,** 1304-11.

Smithells, R. W. & C. G. Newman (1992) Recognition of thalidomide defects. *J Med Genet,* 29**,** 716-23.

Snir, M., I. Kehat, A. Gepstein, R. Coleman, J. Itskovitz-Eldor, E. Livne & L. Gepstein (2003) Assessment of the ultrastructural and proliferative properties of human embryonic stem cell-derived cardiomyocytes. *Am J Physiol Heart Circ Physiol,* 285**,** H2355-63.

Sousonis, V., J. Nanas & J. Terrovitis (2014) Cardiosphere-derived progenitor cells for myocardial repair following myocardial infarction. *Curr Pharm Des,* 20**,** 2003-11.

Spach, M. S., J. F. Heidlage, R. C. Barr & P. C. Dolber (2004) Cell size and communication: role in structural and electrical development and remodeling of the heart. *Heart Rhythm,* 1**,** 500-15.

Stanton, M. M., J. Samitier & S. Sanchez (2015) Bioprinting of 3D hydrogels. *Lab Chip,* 15**,** 3111-5.

Stevens, K. R., L. Pabon, V. Muskheli & C. E. Murry (2009) Scaffold-free human cardiac tissue patch created from embryonic stem cells. *Tissue Eng Part A,* 15**,** 1211-22.

Stoehr, A., C. Neuber, C. Baldauf, I. Vollert, F. W. Friedrich, F. Flenner, L. Carrier, A. Eder, S. Schaaf, M. N. Hirt, B. Aksehirlioglu, C. W. Tong, A. Moretti, T. Eschenhagen & A. Hansen (2014) Automated analysis of contractile force and Ca2+ transients in engineered heart tissue. *Am J Physiol Heart Circ Physiol,* 306**,** H1353-63.

Stoppel, W. L., D. L. Kaplan & L. D. Black, 3rd (2015) Electrical and mechanical stimulation of cardiac cells and tissue constructs. *Adv Drug Deliv Rev*.

Sun, Y., L. G. Villa-Diaz, R. H. Lam, W. Chen, P. H. Krebsbach & J. Fu (2012) Mechanics regulates fate decisions of human embryonic stem cells. *PLoS One,* 7**,** e37178.

Suzuki, G., B. R. Weil, M. M. Leiker, A. E. Ribbeck, R. F. Young, T. R. Cimato & J. M. Canty, Jr. (2014) Global intracoronary infusion of allogeneic cardiosphere-derived cells improves ventricular function and stimulates endogenous myocyte regeneration throughout the heart in swine with hibernating myocardium. *PLoS One,* 9**,** e113009.

Suzuki, T., J. Takeuchi, K. Koshiba-Takeuchi & T. Ogura (2004) Tbx Genes Specify Posterior Digit Identity through Shh and BMP Signaling. *Dev Cell,* 6**,** 43-53.

Takahashi, K., K. Tanabe, M. Ohnuki, M. Narita, T. Ichisaka, K. Tomoda & S. Yamanaka (2007) Induction of pluripotent stem cells from adult human fibroblasts by defined factors. *Cell,* 131**,** 861-72.

Takahashi, K. & S. Yamanaka (2006) Induction of pluripotent stem cells from mouse embryonic and adult fibroblast cultures by defined factors. *Cell,* 126**,** 663-76.

Tambara, K., Y. Sakakibara, G. Sakaguchi, F. Lu, G. U. Premaratne, X. Lin, K. Nishimura & M. Komeda (2003) Transplanted skeletal myoblasts can fully replace the infarcted myocardium when they survive in the host in large numbers. *Circulation,* 108 Suppl 1**,** II259-63.

Tao, Z. W., M. Mohamed, M. Hogan, L. Gutierrez & R. K. Birla (2014) Optimizing a spontaneously contracting heart tissue patch with rat neonatal cardiac cells on fibrin gel. *J Tissue Eng Regen Med*.

Tarui, S., S. Ishigami, D. Ousaka, S. Kasahara, S. Ohtsuki, S. Sano & H. Oh (2015) Transcoronary infusion of cardiac progenitor cells in hypoplastic left heart syndrome: Three-year follow-up of the Transcoronary Infusion of Cardiac Progenitor Cells in Patients With Single-Ventricle Physiology (TICAP) trial. *J Thorac Cardiovasc Surg,* 150**,** 1198-1207, 1208 e1-2.

Therapontos, C., L. Erskine, E. R. Gardner, W. D. Figg & N. Vargesson (2009) Thalidomide induces limb defects by preventing angiogenic outgrowth during early limb formation. *Proc Natl Acad Sci U S A,* 106**,** 8573-8.

Thomson, J. A., J. Itskovitz-Eldor, S. S. Shapiro, M. A. Waknitz, J. J. Swiergiel, V. S. Marshall & J. M. Jones (1998) Embryonic stem cell lines derived from human blastocysts. *Science,* 282**,** 1145-7.

Tiburcy, M., M. Didie, O. Boy, P. Christalla, S. Doker, H. Naito, B. C. Karikkineth, A. El-Armouche, M. Grimm, M. Nose, T. Eschenhagen, A. Zieseniss, D. M. Katschinksi, N. Hamdani, W. A. Linke, X. Yin, M. Mayr & W. H. Zimmermann (2011) Terminal differentiation, advanced organotypic maturation, and modeling of hypertrophic growth in engineered heart tissue. *Circ Res,* 109**,** 1105-14.

Trattnig, S., K. Ohel, V. Mlynarik, V. Juras, S. Zbyn & A. Korner (2015) Morphological and compositional monitoring of a new cell-free cartilage repair hydrogel technology - GelrinC by MR using semi-quantitative MOCART scoring and quantitative T2 index and new zonal T2 index calculation. *Osteoarthritis Cartilage,* 23**,** 2224-32.

Trosper, N., P. Kerscher, J. Macadangdang, D. Carson, E. Lipke & D.-H. Kim. 2014. Micro-and Nanofabrication Approaches to Cardiac Tissue Engineering. In *Tissue and Organ Regeneration: Advances in Micro-and Nanotechnology*, 725-754. Pan Stanford Publishing.

Tsang, K. M., N. Annabi, F. Ercole, K. Zhou, D. Karst, F. Li, J. M. Haynes, R. A. Evans, H. Thissen, A. Khademhosseini & J. S. Forsythe (2015) Facile One-step Micropatterning Using Photodegradable Methacrylated Gelatin Hydrogels for Improved Cardiomyocyte Organization and Alignment. *Adv Funct Mater,* 25**,** 977-986.

Tseng, C. M., Y. H. Hsiao, V. Y. Su, K. C. Su, Y. C. Wu, K. T. Chang & D. W. Perng (2013) The suppression effects of thalidomide on human lung fibroblasts: cell proliferation, vascular endothelial growth factor release, and collagen production. *Lung,* 191**,** 361-8.

Tulloch, N. L., V. Muskheli, M. V. Razumova, F. S. Korte, M. Regnier, K. D. Hauch, L. Pabon, H. Reinecke & C. E. Murry (2011) Growth of engineered human myocardium with mechanical loading and vascular coculture. *Circ Res,* 109**,** 47-59.

Turnbull, I. C., I. Karakikes, G. W. Serrao, P. Backeris, J. J. Lee, C. Xie, G. Senyei, R. E. Gordon, R. A. Li, F. G. Akar, R. J. Hajjar, J. S. Hulot & K. D. Costa (2014) Advancing functional engineered cardiac tissues toward a preclinical model of human myocardium. *FASEB J,* 28**,** 644-54.

Ueno, S., G. Weidinger, T. Osugi, A. D. Kohn, J. L. Golob, L. Pabon, H. Reinecke, R. T. Moon & C. E. Murry (2007) Biphasic role for Wnt/beta-catenin signaling in cardiac specification in zebrafish and embryonic stem cells. *Proc Natl Acad Sci U S A,* 104**,** 9685-90.

Van Den Bulcke, A. I., B. Bogdanov, N. De Rooze, E. H. Schacht, M. Cornelissen & H. Berghmans (2000) Structural and rheological properties of methacrylamide modified gelatin hydrogels. *Biomacromolecules,* 1**,** 31-8.

van den Heuvel, N. H., T. A. van Veen, B. Lim & M. K. Jonsson (2014) Lessons from the heart: mirroring electrophysiological characteristics during cardiac development to in vitro differentiation of stem cell derived cardiomyocytes. *J Mol Cell Cardiol,* 67**,** 12-25.

Van den Steen, P. E., B. Dubois, I. Nelissen, P. M. Rudd, R. A. Dwek & G. Opdenakker (2002) Biochemistry and molecular biology of gelatinase B or matrix metalloproteinase-9 (MMP-9). *Crit Rev Biochem Mol Biol,* 37**,** 375-536.

van der Linde, D., E. E. Konings, M. A. Slager, M. Witsenburg, W. A. Helbing, J. J. Takkenberg & J. W. Roos-Hesselink (2011) Birth prevalence of congenital heart disease worldwide: a systematic review and meta-analysis. *J Am Coll Cardiol,* 58**,** 2241-7.

Wang, G., M. L. McCain, L. Yang, A. He, F. S. Pasqualini, A. Agarwal, H. Yuan, D. Jiang, D. Zhang, L. Zangi, J. Geva, A. E. Roberts, Q. Ma, J. Ding, J. Chen, D. Z. Wang, K. Li, J. Wang, R. J. Wanders, W. Kulik, F. M. Vaz, M. A. Laflamme, C. E. Murry, K. R. Chien, R. I. Kelley, G. M. Church, K. K. Parker & W. T. Pu (2014a) Modeling the mitochondrial cardiomyopathy of Barth syndrome with induced pluripotent stem cell and heart-on-chip technologies. *Nat Med,* 20**,** 616-23.

Wang, L., G. Huang, B. Sha, S. Wang, Y. L. Han, J. Wu, Y. Li, Y. Du, T. J. Lu & F. Xu (2014b) Engineering three-dimensional cardiac microtissues for potential drug screening applications. *Curr Med Chem,* 21**,** 2497-509.

Wang, Z., R. Abdulla, B. Parker, R. Samanipour, S. Ghosh & K. Kim (2015) A simple and high-resolution stereolithography-based 3D bioprinting system using visible light crosslinkable bioinks. *Biofabrication,* 7**,** 045009.

Wei, S., A. Guo, B. Chen, W. Kutschke, Y. P. Xie, K. Zimmerman, R. M. Weiss, M. E. Anderson, H. Cheng & L. S. Song (2010) T-tubule remodeling during transition from hypertrophy to heart failure. *Circ Res,* 107**,** 520-31.

Welt, F. G., R. Gallegos, J. Connell, J. Kajstura, D. D'Amario, R. Y. Kwong, O. Coelho-Filho, R. Shah, R. Mitchell, A. Leri, L. Foley, P. Anversa & M. A. Pfeffer (2013) Effect of cardiac stem cells on left-ventricular remodeling in a canine model of chronic myocardial infarction. *Circ Heart Fail,* 6**,** 99-106.

Wendel, J. S., L. Ye, R. Tao, J. Zhang, J. Zhang, T. J. Kamp & R. T. Tranquillo (2015) Functional Effects of a Tissue-Engineered Cardiac Patch From Human Induced

Pluripotent Stem Cell-Derived Cardiomyocytes in a Rat Infarct Model. *Stem Cells Transl Med,* 4**,** 1324-32.

Weng, Z., C. W. Kong, L. Ren, I. Karakikes, L. Geng, J. He, M. Z. Chow, C. F. Mok, W. Keung, H. Chow, A. Y. Leung, R. J. Hajjar, R. A. Li & C. W. Chan (2014) A simple, cost-effective but highly efficient system for deriving ventricular cardiomyocytes from human pluripotent stem cells. *Stem Cells Dev,* 23**,** 1704-16.

Workman, V. L., S. B. Dunnett, P. Kille & D. D. Palmer (2007) Microfluidic chip-based synthesis of alginate microspheres for encapsulation of immortalized human cells. *Biomicrofluidics,* 1**,** 14105.

Xiao, W., J. He, J. W. Nichol, L. Wang, C. B. Hutson, B. Wang, Y. Du, H. Fan & A. Khademhosseini (2011) Synthesis and characterization of photocrosslinkable gelatin and silk fibroin interpenetrating polymer network hydrogels. *Acta Biomater,* 7**,** 2384-93.

Xing, J., Y. C. Toh, S. Xu & H. Yu (2015) A method for human teratogen detection by geometrically confined cell differentiation and migration. *Sci Rep,* 5**,** 10038.

Yamamura, H., M. Zhang, R. R. Markwald & C. H. Mjaatvedt (1997) A heart segmental defect in the anterior-posterior axis of a transgenic mutant mouse. *Dev Biol,* 186**,** 58-72.

Yang, L., M. H. Soonpaa, E. D. Adler, T. K. Roepke, S. J. Kattman, M. Kennedy, E. Henckaerts, K. Bonham, G. W. Abbott, R. M. Linden, L. J. Field & G. M. Keller (2008) Human cardiovascular progenitor cells develop from a KDR+ embryonic-stem-cell-derived population. *Nature,* 453**,** 524-8.

Yang, X., L. Pabon & C. E. Murry (2014) Engineering adolescence: maturation of human pluripotent stem cell-derived cardiomyocytes. *Circ Res,* 114**,** 511-23.

Yazawa, M. & R. E. Dolmetsch (2013) Modeling Timothy syndrome with iPS cells. *J Cardiovasc Transl Res,* 6**,** 1-9.

Yazawa, M., B. Hsueh, X. Jia, A. M. Pasca, J. A. Bernstein, J. Hallmayer & R. E. Dolmetsch (2011) Using induced pluripotent stem cells to investigate cardiac phenotypes in Timothy syndrome. *Nature,* 471**,** 230-4.

Yndestad, A., L. E. Vinge, R. Bjornerheim, T. Ueland, J. E. Wang, S. S. Froland, H. Attramadal, P. Aukrust & E. Oie (2006) Thalidomide attenuates the development of fibrosis during post-infarction myocardial remodelling in rats. *Eur J Heart Fail,* 8**,** 790-6.

Young, J. L. & A. J. Engler (2011) Hydrogels with time-dependent material properties enhance cardiomyocyte differentiation in vitro. *Biomaterials,* 32**,** 1002-9.

Yuan Ye, K., K. E. Sullivan & L. D. Black (2011) Encapsulation of cardiomyocytes in a fibrin hydrogel for cardiac tissue engineering. *J Vis Exp*.

Zandstra, P. W., C. Bauwens, T. Yin, Q. Liu, H. Schiller, R. Zweigerdt, K. B. Pasumarthi & L. J. Field (2003) Scalable production of embryonic stem cell-derived cardiomyocytes. *Tissue Eng,* 9**,** 767-78.

Zhang, D., I. Y. Shadrin, J. Lam, H. Q. Xian, H. R. Snodgrass & N. Bursac (2013) Tissue-engineered cardiac patch for advanced functional maturation of human ESC-derived cardiomyocytes. *Biomaterials,* 34**,** 5813-20.

Zhang, J., M. Klos, G. F. Wilson, A. M. Herman, X. Lian, K. K. Raval, M. R. Barron, L. Hou, A. G. Soerens, J. Yu, S. P. Palecek, G. E. Lyons, J. A. Thomson, T. J.

Herron, J. Jalife & T. J. Kamp (2012) Extracellular matrix promotes highly efficient cardiac differentiation of human pluripotent stem cells: the matrix sandwich method. *Circ Res,* 111**,** 1125-36.

Zhang, J., G. F. Wilson, A. G. Soerens, C. H. Koonce, J. Yu, S. P. Palecek, J. A. Thomson & T. J. Kamp (2009) Functional cardiomyocytes derived from human induced pluripotent stem cells. *Circ Res,* 104**,** e30-41.

Zhang, Y., J. Mignone & W. R. MacLellan (2015) Cardiac Regeneration and Stem Cells. *Physiol Rev,* 95**,** 1189-204.

Zhao, S., P. Agarwal, W. Rao, H. Huang, R. Zhang, Z. Liu, J. Yu, N. Weisleder, W. Zhang & X. He (2014) Coaxial electrospray of liquid core-hydrogel shell microcapsules for encapsulation and miniaturized 3D culture of pluripotent stem cells. *Integr Biol (Camb),* 6**,** 874-84.

Zhao, T., Z. N. Zhang, P. D. Westenskow, D. Todorova, Z. Hu, T. Lin, Z. Rong, J. Kim, J. He, M. Wang, D. O. Clegg, Y. G. Yang, K. Zhang, M. Friedlander & Y. Xu (2015) Humanized Mice Reveal Differential Immunogenicity of Cells Derived from Autologous Induced Pluripotent Stem Cells. *Cell Stem Cell,* 17**,** 353-9.

Zhao, X., S. Liu, L. Yildirimer, H. Zhao, R. Ding, H. Wang, W. Cui & D. Weitz (2016) Injectable Stem Cell-Laden Photocrosslinkable Microspheres Fabricated Using Microfluidics for Rapid Generation of Osteogenic Tissue Constructs. *Advanced Functional Materials***,** n/a-n/a.

Zhu, J. & R. E. Marchant (2011) Design properties of hydrogel tissue-engineering scaffolds. *Expert Rev Med Devices,* 8**,** 607-26.

Ziman, A. P., C. W. Ward, G. G. Rodney, W. J. Lederer & R. J. Bloch (2010) Quantitative measurement of Ca(2)(+) in the sarcoplasmic reticulum lumen of mammalian skeletal muscle. *Biophys J,* 99**,** 2705-14.

Zimmermann, W. H., K. Schneiderbanger, P. Schubert, M. Didie, F. Munzel, J. F. Heubach, S. Kostin, W. L. Neuhuber & T. Eschenhagen (2002) Tissue engineering of a differentiated cardiac muscle construct. *Circ Res,* 90**,** 223-30.

Zweigerdt, R., R. Olmer, H. Singh, A. Haverich & U. Martin (2011) Scalable expansion of human pluripotent stem cells in suspension culture. *Nat Protoc,* 6**,** 689-700.

Zwi-Dantsis, L., I. Huber, M. Habib, A. Winterstern, A. Gepstein, G. Arbel & L. Gepstein (2013) Derivation and cardiomyocyte differentiation of induced pluripotent stem cells from heart failure patients. *Eur Heart J,* 34**,** 1575-86.

Zwi, L., O. Caspi, G. Arbel, I. Huber, A. Gepstein, I. H. Park & L. Gepstein (2009) Cardiomyocyte differentiation of human induced pluripotent stem cells. *Circulation,* 120**,** 1513-23.

APPENDIX A

Materials

Store all reagents at 4 ºC and pre-warm to room temperature before use (unless indicated otherwise). Perform all cell culture and staining procedures under sterile conditions using a laminar flow hood.

1.1 hiPSC culture and maintenance

1.1.1 6-well plates (tissue culture polystyrene treated) (Corning).

1.1.2 CO_2 incubator: 37 ºC, 5% CO_2, and 85% relative humidity.

1.1.3 Human induced pluripotent stem cells (*e.g.* IMR-90 Clone 1, WiCell).

1.1.4 Human embryonic stem cell (hESC) qualified Matrigel (BD Bioscience) (*see* **Note 1**).

1.1.5 DMEM-F12 (Thermo Scientific).

1.1.6 mTeSR-1 media (Stem Cell Technologies).

1.1.7 ROCK inhibitor (Y-27632, R&D Systems): Combine 6.24 mL PBS with 10 mg ROCK inhibitor. Aliquot and store at -20 ºC (*see* **Note 2**).

1.1.8 Versene (Gibco).

1.2 Differentiation of hiPSCs to CMs

1.2.1 12-well or 6-well plate (Corning).

1.2.2 CO_2 incubator: 37 ºC, 5% CO_2, and 85% relative humidity.

1.2.3 Human embryonic stem cell (hESC) qualified Matrigel (BD Bioscience) (*see* **Note 1**).

1.2.4 DMEM-F12 (Thermo Scientific).

1.2.5 Accutase (Innovative Cell Technologies).

1.2.6 0.25% Trypsin (EDTA, Mediatech).

1.2.7 mTeSR-1 media (Stem Cell Technologies).

1.2.8 ROCK inhibitor (Y-27632, R&D Systems) Combine 6.24 mL PBS with 10 mg ROCK inhibitor. Aliquot and store at -20 ºC (*see* **Note 2**).

1.2.9 RPMI 1640 media (Gibco).

1.2.10 B-27 supplement without insulin (Gibco) (*see* **Note 3**).

1.2.11 B-27 supplement (Gibco) (*see* **Note 4**).

1.2.12 CHIR99021 (Selleckchem): Add 1.49 mL DMSO to 25 mg CHIR99021. Aliquot and store at -20 ºC.

1.2.13 IWP-2 (Tocris): Add 4.28 mL DMSO to 10 mg IWP2. Incubate at 37 ºC for 10 minutes or until IWP2 is in solution. Aliquot and store at -20 ºC.

1.2.14 Fetal Bovine Serum (FBS, Atlanta Biologicals) (*see* **Note 5**).

1.3 Preparation of glass coverslips for cell seeding

1.3.1 Glass coverslips (21 mm, #1, Fisher Scientific).

1.3.2 Polydimethylsiloxane (PDMS) precursor: Mix SLYGARD 184 silicone elastomer curing agent and SLYGARD 184 elastomer base (Dow Corning Corporation) at a ratio of 1:10. Add PDMS precursor onto glass coverslips and evenly coat glass by spin coating using a WS-400-6NPP spin coater (Laurell Technologies

Corporation) at 3,000 RPM for 10 seconds. PDMS coated glass coverslips are dried at 60 ºC for several hours (*see* **Note 6**) and sterilized using 70% ethanol and UV light.

1.3.3 Fibronectin (40X, Thermo Scientific): Add 25 µL fibronectin to 975 µL ice cold, sterile ultrapure water.

1.4 Fluorescent labeling of mitochondria

1.4.1 MitoTracker Red working solution (1 µM, Molecular Probes): Dilute 1 µL MitoTracker Red stock solution (1 mM) in 1 mL mTeSR-1 (hiPSCs) or RPMI/B27 (CMs).

1.4.2 Phosphate buffered saline without calcium and magnesium (PBS, 10X, Lonza): Add 10 mL 10X PBS into 990 mL ultrapure water. Filter sterilize.

1.4.3 Filter for sterilization: polyethersulfone filter, pore size 0.22 µm (VWR International).

1.4.4 Blocking buffer: Combine 3 mL FBS with 97 mL 1X PBS. Filter before use.

1.4.5 Paraformaldehyde (16%, Electron Microscopy Sciences): Add 10 mL 16% paraformaldehyde to 30 mL 1X PBS.

1.4.6 PBS-T: Add 25 mL 10X PBS, 225 mL ultrapure water, 2,500 mg bovine serum albumin (BSA, Fisher Scientific), and 0.5 mL Triton X-100 (Fisher Scientific). Filter sterilize.

1.4.7 4’,6-diamidino-2-phenylindole (DAPI, Molecular Probes) (1:36000 of primary stock in 1X PBS).

1.4.8 50% ethanol: Combine 25 mL DI water with 25 mL ethanol.

1.4.9 70% ethanol: Combine 15 mL DI water with 35 mL ethanol.

1.4.10 95% ethanol: Combine 2.5 mL DI with 47.5 mL ethanol.

1.4.11 ProLong Gold antifade reagent (Life Technologies).

1.4.12 Rectangular glass coverslide: e.g. 25x75 mm, 1 mm thick (VWR International).

1.4.13 Clear nail polish (*e.g.* Electron Microscopy Science).

1.5 Image Acquisition

1.5.1 Confocal microscope (Nikon A1): 40X-100X oil objective, TRITC (Ex/Em: 561/595 nm) and DAPI (Ex/Em: 405/450 nm) filter sets.

1.5.2 Imaging acquisition software (e.g. NIS Elements).

1.6 Image Analysis using MQM

1.6.1 Windows 7 or higher, or equivalent operating system.

1.6.2 MATLAB 12 or higher with Statistics Toolbox (Mathworks, Inc.).

1.6.3 MQM script: function files *MitoMAT* and *Measurements* are available for download from MATLAB Central, the Lipke Lab website or by request from the corresponding author.

1.6.4 Microsoft Excel 2007 or higher.

Methods

Current state of the art stem cell culture and differentiation change rapidly and in depth training is available through WiCell and many major research institutions. Based on selected hiPSC cell lines, differentiation parameters might have to be adjusted ***(Lian et***

al. 2013). Parameters influencing current state-of-the-art SC-CM differentiation have been covered in detail by Lian, X. *et al.* ***(Lian et al. 2013)***.

1.7 hiPSC Maintenance and Expansion

1.7.1 Culture hiPSCs as colonies on Matrigel coated 6-well plates in mTeSR-1 with daily media exchange until passage.

1.7.2 Passage cells of a confluent well using Versene. Aspirate off old mTeSR-1, rinse and incubate cells in Versene at 37 ºC for 4 minutes. Aspirate off Versene and resuspend cells in 1 mL mTeSR-1 + RI. Passage cells (e.g. 1:10 ratio) into a new Matrigel coated well containing 2 mL mTeSR-1 + RI.

1.8 hiPSC dissociation for mitochondria labeling

1.8.1 Rinse hiPSCs of a confluent well with 1X PBS and incubated in 1 mL Accutase at 37 ºC for 8 minutes.

1.8.2 Combine cells with mTeSR-1 and centrifuge cells at 200 g for 5 minutes.

1.8.3 Aspirate off supernatant and resuspend cells in 1 mL mTeSR-1 + RI and plated onto a Matrigel coated PDMS glass coverslip (*see* **Note 7**).

1.8.4 Culture hiPSCs for two days in mTeSR-1 before fluorescently labeling cells.

1.9 CM differentiation of hiPSCs

1.9.1 Rinse confluent well of hiPSCs using 1X PBS.

1.9.2 Incubate hiPSCs in Accutase at 37 ºC for 8 minutes.

1.9.3 Combine cells with mTeSR-1, centrifuge at 200 g for 5 minutes.

1.9.4 Resuspend cells in 3 mL mTeSR-1 + RI (1 x 10^6 cells/mL) and add 1 mL into each well of a Matrigel coated 12-well plate.

1.9.5 After 24 hours, replace media with 2 mL mTeSR-1. Repeat this step twice.

1.9.6 Replace media with 2 mL RPMI/B27 without insulin + 0.67 µL CHIR99021.

1.9.7 After 24 hours, replace media with 2 mL RPMI/B27 without insulin.

1.9.8 After 48 hours, apply combined media (1 mL old RPMI/B27 without insulin and 1 mL new RPMI/B27 without insulin + 2 µL IWP2).

1.9.9 After 48 hours, replace media with 2 mL RPMI/B27 without insulin.

1.9.10 After 48 hours, change media to 2 mL RPMI/B27. Replace RPMI/B27 every three days until use.

1.10 CM dissociation for mitochondria labeling

1.10.1 Rinse and incubate spontaneously contracting CMs in 0.25% Trypsin (EDTA) at 37 ºC for 5 minutes.

1.10.2 Singularize cells using a P1000 pipette tip, combine with RPMI20, and centrifuge cells at 200 g for 5 minutes.

1.10.3 Aspirate off supernatant and resuspend cells in 1 mL RPMI20 + RI (*see* **Note 8**) and plate cells onto fibronectin coated PDMS coverslips (*see* **Note 7**).

1.10.4 Culture cells for three days post dissociation to allow cells to adhere and re-establish their phenotypic cell morphology and function before fluorescently labeling the cells (*see* **Note 9**).

1.11 ***Fluorescence labeling of cells*** (*see* **Notes 10 - 12**)

1.11.1 Rinse cells with 1X PBS.

1.11.2 Add sufficient MitoTracker Red working solution into each well and incubate at 37 ºC for 30 minutes.

1.11.3 Rinse three times with 1X PBS.

1.11.4 Add 4% paraformaldehyde, incubate cells at room temperature for 10 minutes.

1.11.5 Rinse with 1X PBS.

1.11.6 Incubate cells in PBS-T at room temperature for 10 minutes. Repeat this step twice.

1.11.7 Block cells in blocking buffer at 4 ºC over night.

1.11.8 Remove blocking buffer and add DAPI to all wells. Incubate at room temperature for 30 minutes.

1.11.9 Rinse off DAPI with 1X PBS. Repeat this step twice.

1.11.10 Dehydrate all samples using 50%, 70%, 95%, and 100% ethanol for 5 minutes each.

1.11.11 Air dry all samples until completely dry.

1.11.12 Apply small drop of ProLong Gold to each sample, invert sample onto a rectangular glass coverslide (*see* **Note 13**).

1.11.13 All samples should be dried over night, sealed using nail polish, and stored at 4 ºC.

1.12 Image Acquisition

1.12.1 Follow appropriate procedure to turn on and start up confocal microscope.

1.12.2 While using the scanning feature, adjust the scanning time and size of the image to be captured to at least 1/8 frame/sec and 1024 pixels, respectively (*see* **Note 14**). Also adjust the confocal laser settings and pinhole to ensure clear, bright, and crisp images of the mitochondria and nuclei (*see* **Note 15**).

1.12.3 Capture and save the image as both .nd2 and separate .png, .jpg, or .tiff files in a location to be retrieved for later image analysis (*see* **Note 16**).

1.13 Image analysis using MQM

1.13.1 Start MATLAB by clicking on the MATAB icon on the start menu or by opening the MQM files, *MitoMAT* and *Measurements.*

1.13.2 Copy and import all image files to be analyzed to the same folder containing the MQM files.

1.13.3 Prepare for analysis by running the *Measurements* function file by clicking the green play button at the top of the home screen in

MATLAB. Switch between files by clicking on the different function file tabs within MATLAB.

1.13.4 Press the green play button at the top of the home screen when the *MitoMAT* file is on the editor screen to begin the analysis (**Fig. 6.16**).

1.13.5 When prompted, enter information about the images to be analyzed, i.e. image name, image magnification (in μm/pixel), and cell type for a label, if desired.

1.13.6 In the user-interface, select the types of results to be collected and specify a name for the Excel results file. After verifying this information, press continue (*see* **Note 17**).

1.13.7 An image of the fluorescently labeled mitochondria will appear. Click around the edges of the cell to be analyzed (*see* **Note 18 - 21**).

1.13.8 Data can be analyzed in Excel (or similar software, *e.g.* Minitab, Origin) (**Fig. 1**).

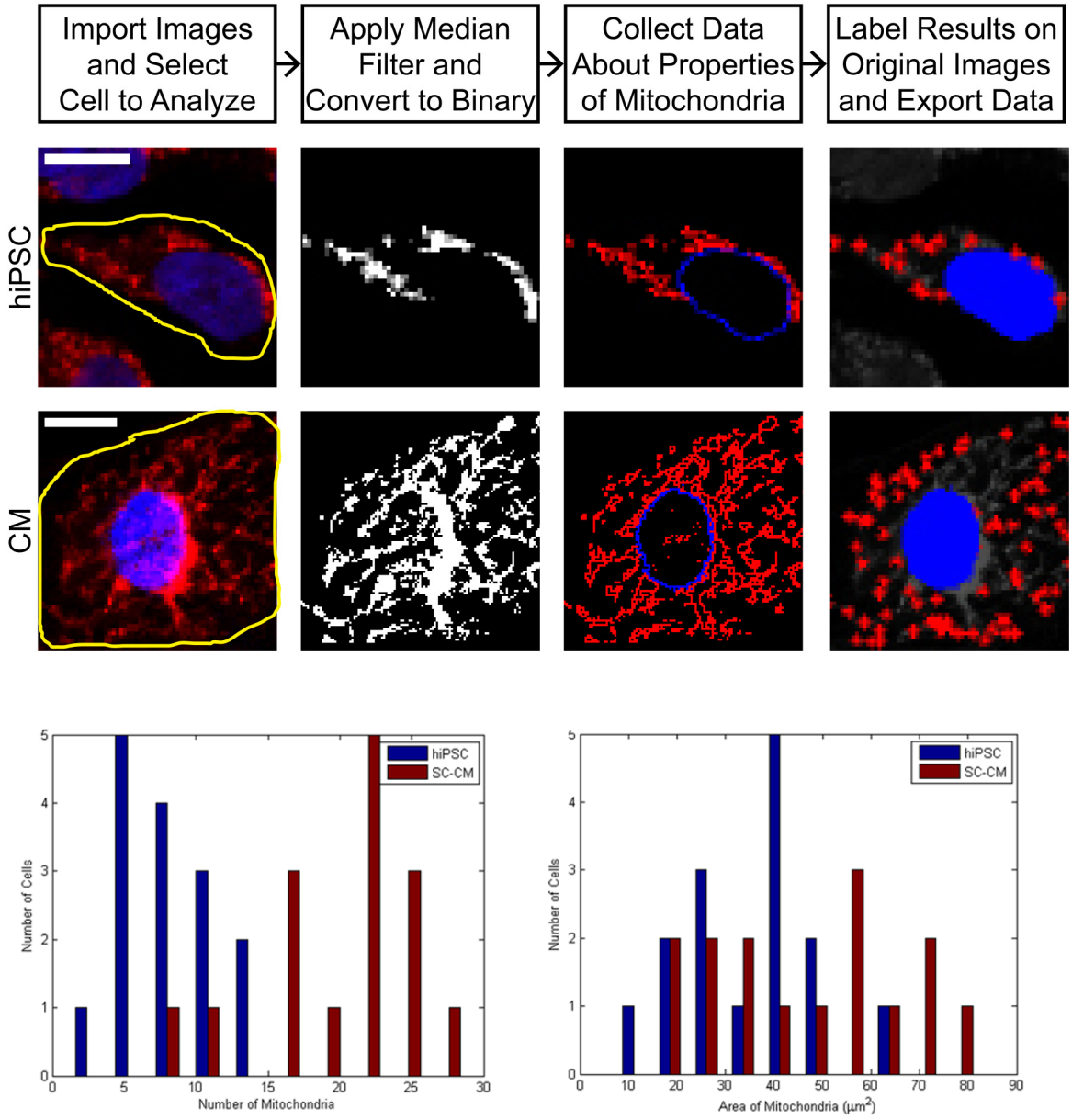

Fig. 1. Number and total area of mitochondria per cell increases during hiPSC differentiation. Mitochondria play an essential role in actively contracting CMs and need to be analyzed at different stages of development. Mitochondria (red) of hiPSCs and SC-CMs are processed and analyzed using a custom MATLAB script to detect number of mitochondria and area of mitochondria per cell. Few mitochondria were present in

hiPSCs with locations close to the cell nucleus. On the other hand, SC-CMs showed increased number of mitochondria which was spread out throughout the cell.

Notes

1. Matrigel coated 6-well and 12-well plates: Remove Matrigel aliquot from -80 ºC freezer and transfer into a sterile tissue culture hood. Resuspend Matrigel aliquot in 1 mL cold DMEM-F12 and transfer to a 15 mL centrifuge tube. Add additional 11 mL cold DMEM-F12, mix, and add 1 mL Matrigel solution into each well of a 6-well plate (0.5 mL into each well of a 12-well plate). Incubate Matrigel solution for 30 minutes at room temperature. Add an additional 1 mL DMEM-F12 to each well and store at 37 ºC.
2. mTeSR-1 + RI: Add 50 µL 5 mM ROCK inhibitor to 50 mL mTeSR-1 media, mix well.
3. RPMI/B27 without insulin: Combine 500 mL RPMI1640 media with 10 mL B-27 supplement without insulin, mix well and store at 4 ºC.
4. RPMI/B27: Combine 500 mL RPMI1640 media with 10 mL B-27 supplement, mix well.
5. RPMI20: Combine 40 mL RPMI1640 media with 10 mL FBS. Filter sterilize.

6. PDMS-coated coverslips can also be dried at room temperature overnight, or until dry.
7. Seeding density of cells used for imaging experiments must be uniform across all groups to eliminate cell density effects as a source of variation in mitochondrial dynamics.
8. RPMI20 + RI: Add 50 µL 5 mM ROCK inhibitor to 50 mL RPMI20, mix well.
9. CMs can be multinucleated; for the MQM module needed to analyze cells with more than one nucleus, email the corresponding author.
10. If necessary, adjust immunostaining protocol to ensure bright, clear, images with no unspecific antibody binding or background fluorescence – it impossible to analyze the mitochondria if the staining is not clear.
11. After MitoTracker Red working solution is applied, cells have to be handled in the dark to avoid photobleaching.
12. All staining procedures should be done under sterile conditions.
13. Any glass coverslide that fits onto an available confocal microscope stage holder can be chosen.
14. Images can be acquired at slower scan speed (e.g. 1/16 frame/sec) and higher resolutions (e.g. 2048 pixels), if desired.
15. Making meaningful comparisons between samples requires that all images must be acquired at the same magnification and using

identical image capture methods. Data from confocal images will not be comparable to those from non-confocal fluorescence images due to unequal contributions from nonfocal planes. Similarly images from different magnifications will have unequal amounts of pixel bleeding from adjacent areas of the sample.

16. In order to be able to access the image files of interest, files must be stored in the same folder as the MQM files.
17. MATLAB is unable to write to an Excel document while it is open. Therefore it is important to make sure that all Excel result files are closed during analysis.
18. Currently, MQM can only analyze one cell at a time.
19. Analysis time is between 2-4 minutes per cell, with time decreasing with use.
20. If the experimenter decides to reject the data from a particular cell, if there was inconsistency with labeling or a general error in use, the user must delete the data written in the Excel file associated with that run.
21. Label cell membrane to make it easier to identify which mitochondria belongs to which cell.

APPENDIX B

Motivation

We anticipate that the exposure of known mutagens, in particular thalidomide, will cause identifiable changes in gene expression, ECM production, and electrophysiological characteristics of differentiating hiPSCs. The selected experiments for this project will answer fundamental questions about hiPSCs' ability to detect thalidomide-induced changes in electrophysiological function of these developing heart cells when exposed to the known cardiac teratogen thalidomide. HiPSCs have successfully been used to determine drug-induced changes, but this specific 2D monolayer differentiation procedure with small molecule addition has yet to be explored in more details. Although thalidomide is a widely studied pharmaceutical, less is known about its interactions with differentiating hiPSCs. The overall outcomes of this project will be the determination of mutations known to cause CHDs, especially changes in ECM composition secreted by hiPSCs during cardiac differentiation. Additionally, gene and protein expression, mitochondria organization and number, as well as electrophysiological changes during cardiac differentiation will be assessed. This 2D monolayer cardiac differentiation protocol is used as a simplified model system, but will provide great insights into physiological changes. Once these changes are successfully determined, a more relevant 3D engineered developing heart model will be applied for in-depth studies on ECM production and mechanical changes during thalidomide treatment.

This simplified developing human heart model will enhance our understanding of CHD formation and explore hiPSC's efficacy for detecting anticipated mutations caused by thalidomide, opening up more in-depth studies for the future.

Materials and Methods

HiPSC culture and maintenance

IMR-90 Clone 1 hiPSCs were purchased from WiCell and maintained at 37 ºC, 5% CO_2, and 85% relative humidity. HiPSCs were cultured as colonies on hESC qualified Matrigel (BD Biosciences) using mTeSR-1 media (Stem Cell Technologies). HiPSCs were passaged using Versene (Life Technologies) and 5 μM ROCK inhibitor (Y-27632, R&D Systems) was added to the mTeSR-1 media for 24 h post-seeding.

Thalidomide preparation, storage, and stability

Thalidomide (MP Biomedicals), was dissolved (stock solution 55 mg/ml) in DMSO, and stored at 4 ºC in the dark until use. Due to adverse effects on cell viability, total volume percent DMSO is kept as low as possible, while maintaining thalidomide's stability when exposed to cell culture media. Thalidomide's stability in cell culture media was tested by measuring absorbance using a UV-vis spectrophotometer (Genesys 10S). Tested groups included: DMSO, 1 μM, 70 μM, and 250 μM thalidomide in RPMI/B27 without insulin, which is the primary media component used throughout cardiac differentiation. Total DMSO percentage was held constant at 0.2% or 0.5%.

2D monolayer differentiation for highly reproducible and efficient cardiac differentiation

For 2D monolayer differentiation of hiPSCs, the composition of the media and timeline of differentiation was similar to that in a previously published protocol(Lian et al. 2013). Briefly, hiPSCs were dissociated using Accutase, resuspended in mTeSR-1 media,

counted, and centrifuged. HiPSCs were seeded at 0.5×10^6 hiPSCs/well of a Matrigel coated 12-well plate in 2 ml mTeSR-1 media + 5 μM ROCK inhibitor for 24 h (day -4). From day -3 until day 0, mTeSR-1 media was replaced daily. On day 0 of differentiation, media was changed to 2 ml RPMI/B27 without insulin + 12 μM CHIR99021 (Selleckchem) for 24 h. Media was changed to 2 ml RPMI/B27 without insulin for an additional 48 h. On day 3, 1 ml RPMI/B27 without insulin and 5 μM IWP2 (Tocris) were combined with 1 ml old RPMI/B27 without insulin ("combined media") and cells were cultured until day 5, when media was changed back to RPMI/B27 without insulin. On day 7 and successively every three days, media was replaced with RPMI/B27.

Substrate selection for 2D sheet differentiation

For accuracy, our goal is to minimize cell handling and cell dissociation steps. Before starting any drug-testing experiments, an alternative culture platform base for cardiac differentiation has to be found. 2D cardiac monolayers are historically produced in 12-well plates, which significantly limit our ability to image fluorescently labeled samples or to detect calcium traces at high resolutions due to a thick plastic bottom; this method thereafter requires a cell dissociation step to transfer SC-CMs onto a thin coverslip. This process significantly influences cell-cell interactions and CM viability post-dissociation. Therefore, PDMS coated glass (circular glass coverslips, 21 mm, No. 1, Fisher Scientific) and plastic coverslips which can easily be added to and extracted from a standard 12-well plate, will be UV/ozone treated (PSD Benchtop UV/Ozone System, Novascan Technologies) followed by additional sterilization under UV-light. Matrigel coating, cell seeding, and differentiation on PDMS glass and plastic coverslips will not change

compared to previously optimized conditions (see "2D monolayer differentiation for highly reproducible and efficient cardiac differentiation"). Every 24 h, images will be taken to observe differences in cell attachment and ability to differentiate and contract.

2D cardiac sheet differentiation of hiPSCs and thalidomide treatment

With the knowledge that thalidomode's mean steady state concentration ranges between 1-10 μM(Kodama et al. 2009, Chung et al. 2004) and that significant gene expression changes occurred at 1 and 70 μM during hPSC differentiation(Meganathan et al. 2012), 1 and 70 μM thalidomide concentrations will be investigated in future studies. In summary, control, control (carrier), 1 μM, and 70 μM thalidomide treatment groups will be used for all experiments throughout this project. Treatments will be added to differentiating hiPSCs of 3 wells per condition every 48 hours, from day 1 to day 15 (in addition to differentiation media). Equal volumes of the drug carrier (final volume percent: 0.2% DMSO) will be used in control (carrier), 1 μM, and 70 μM thalidomide treatment groups.

Mitochondria localization and analysis of thalidomide-treated SC-CMs

Mitochondria are the primary organelle responsible for energy production within the cell. This is the reason why it is important to understand how a drug influences mitochondria quantity, organization, and localization throughout the developmental process, from a stem cell until a functional CM. Mitochondria are an important component influencing normal heart development and contractile function. During early stages of CM development, mitochondria are only a small portion within a cell's cytoplasm and are structurally visible in a reticular arrangement(Yang et al. 2014), while in the adult CM,

mitochondria occupy approximately 20-40% of the total CM volume due to high energy requirements needed for contraction; at this stage mitochondria exhibit a regular distribution with a “crystal-like lattice pattern”(Schaper et al. 1985).

Cells of all treatment groups will be stained for mitochondria on days 0, 15, and 30 of differentiation (n=3 per condition). Mitochondria will be visualized using MitoTracker Red (Invitrogen) diluted to a final concentration of 1 nM in cell culture media. MitoTracker Red working solution will be added to all wells and incubated at 37 °C for 30 min. Cells will be rinsed with PBS, fixed, permeabilized, and blocked. Cells will be counterstained with 4’,6-diamidino-2-phenylindole (DAPI, Molecular Probes). Three images per well (areas with similar confluency) will be acquired and analyzed using MQM, a custom developed MATLAB script, and will be used as previously described (**Appendix A**) to determine number and area of mitochondria per cell in an effective, unbiased, and reproducible manner.

Immunofluorescent staining of thalidomide treated SC-CMs

To assess changes in protein expression and localization of age-matched thalidomide treated and untreated SC-CMs, cardiac markers αSA, cTnT, and Nkx2.5, proliferation marker Ki67, as well as versican, collagen Type I, and elastin will be visualized using confocal microscopy. In addition to age-matched comparisons, internal protein development will be compared over time, specifically on days 10, 20, and 30 of differentiation.

Wavefront propagation and calcium transient velocity of control and thalidomide treated SC-CMs

Day 17 2D cardiac monolayers were incubated in the calcium sensitive dye Rhod-2 (Invitrogen) for 30 min followed by thorough rinsing with PBS before experimentation. To study calcium transient durations, 2D monolayers were optically mapped; recordings were taken using an Andor iXon+ 860 EMCCD camera and results were analyzed in MATLAB. recordings will be taken using an Andor iXon+ 860 EMCCD camera. Optical mapping data will be processed using custom written MATLAB scripts to measure velocities of wavefront propagation and durations of calcium transients and APs.

Results

Thalidomide remains stable in cell culture medium

When testing thalidomide's stability in cell culture media (RPMI/B27 without insulin), absorbance spectra revealed that both 0.2% and 0.5% total volume of DMSO stabilizes thalidomide (1-250 μM, **Fig. 2**). For this reason, 0.2% total volume percent will be used to stabilize thalidomide.

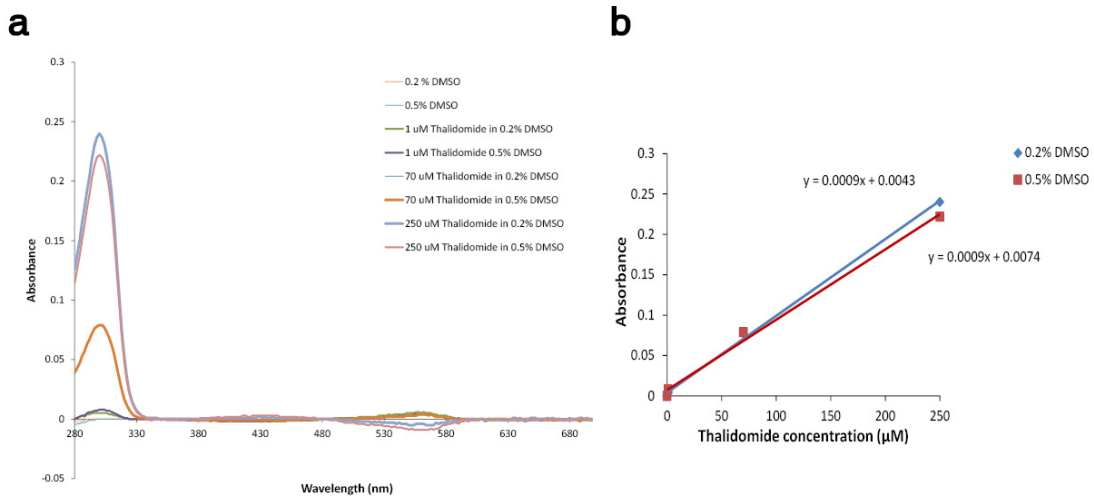

Fig. 2. Thalidomide at 1 - 250 µM remains stable in cell culture media with 0.2% and 0.5% total volume percent DMSO. Thalidomide has an absorption peak at 300 nm. UV-vis absorbance of thalidomide stabilized with 0.2% and 0.5% total DMSO did not show a peak shift or a significant decrease in absorbance value (a). Absorbance vs. concentration did not show a difference in slope when comparing 0.2% and 0.5% total DMSO for thalidomide stabilization up to 250 µM (b). Note: minor changes in absorbance peak height is most likely due to pipetting errors.

Thalidomide significantly decreased EB diameter during cardiac differentiation.

During initial stages of this project, a different cardiac differentiation protocol was used to produce SC-CMs (Zwi et al. 2009). Preliminary results of thalidomide's effects on hiPSC differentiation were investigated using the formation of EBs (**Fig. 3**). Control, control (0.5% DMSO), 1 µM, and 70 µM thalidomide treatments were added on days 0 and 3 of differentiation after cells have been dissociated and transferred to a non-coated 60 mm culture dish where cells are allowed to self-aggregate to form EBs within 10 days. EB diameters were recorded and measured on day 3 and day 5 of differentiation for all

treatment groups. The carrier (0.5% DMSO) did not significantly influence EB diameter compared to the control (as expected), whereas 1 and 70 µM thalidomide showed significant decrease in EB diameter on both days (**Fig. 4, 5**).

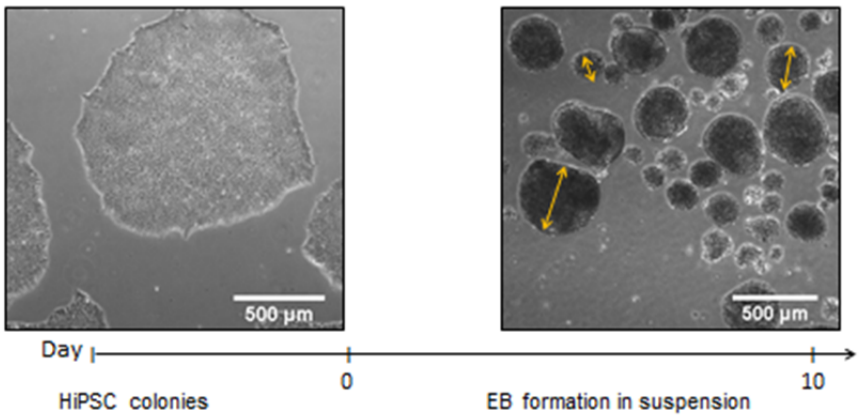

Fig. 3. Initial hiPSC differentiation method using EB suspension culture produced CMs in an inefficient and unreproducible way. HiPSCs were cultured, dissociated, and transferred to a non-coated culture dish. Within 10 days of suspension culture, cells aggregate to form EBs. EBs (~5-10%) start contracting between days 10-15 of differentiation.

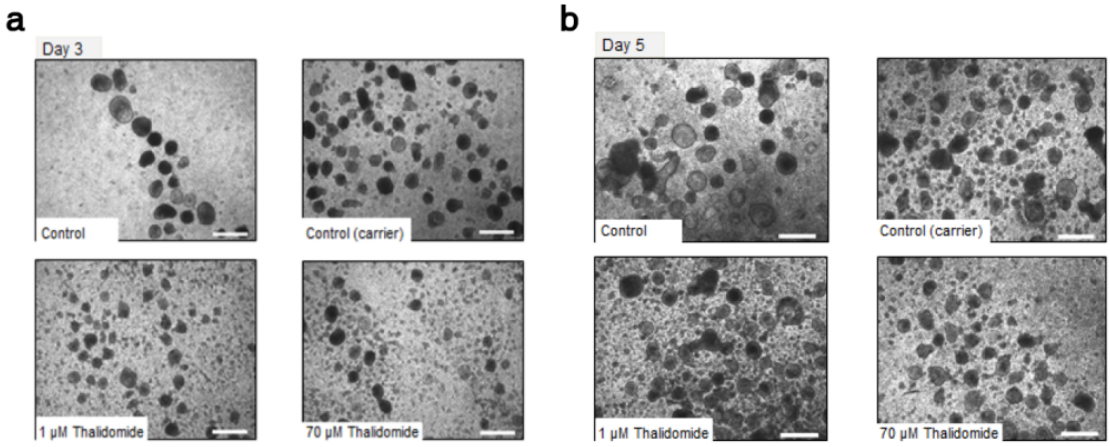

Fig. 4. Thalidomide did cause a decrease in EB diameter during cardiac differentiation. (a, b) Phase contrast images showed that the addition of thalidomide on day 0 and day 3 of differentiation caused a change in EB diameter of thalidomide treatment groups. Additionally, thalidomide treated samples showed more cell debris in culture dishes. Scale bar = 500 μm.

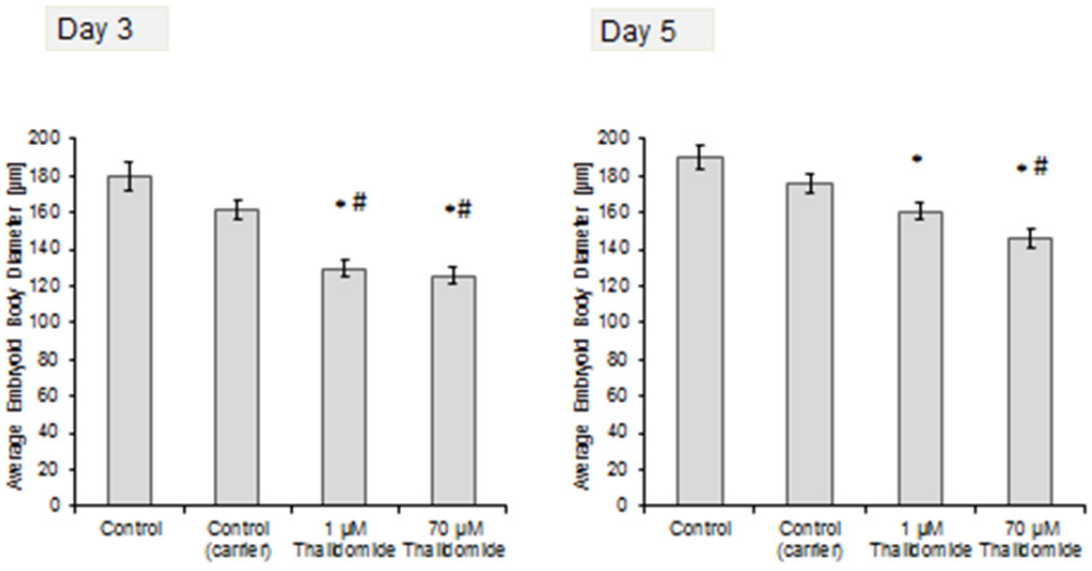

Fig. 5. Thalidomide caused a significant decrease in EB diameter on day 3 and day 5 of cardiac differentiation. On day 3, EB diameter decreased from 180±51.4 µm (control) to 129 ± 37.7 µm (1 µM thalidomide) and 126 ± 35.2 µm (70 µM thalidomide). Consequently, on day 5, EB diameter varied from 190 ± 65.1 µm (control) to 161 ± 43.2 µm (1 µM thalidomide) and 146 ± 52.6 µm (70 µM thalidomide). **P* < 0.05 when compared to control, #*P* < 0.05 when compared to control (carrier).

Due to the high batch-to-batch variability and low efficiency of cardiac differentiation, this EB formation protocol will not be used in future studies. Overall, we believe that the significant decrease in EB diameter is due to the lack of ECM proteins essential for tight cell-cell interactions, but further experiments have to be conducted to confirm this theory. As mentioned previously, due to fast and exciting developments to improve stem cell differentiation, a more efficient and reproducible differentiation protocol was adapted from Lian *et al* (Lian et al. 2013).

HiPSCs can be differentiated into contracting CMs using a 2D monolayer differentiation protocol.

During preliminary results of normal 2D monolayer differentiation (no thalidomide treatment), we have found that the stem cell line IMR90-1 can successfully be differentiated into a fully contracting 2D cardiac sheet (**Fig. 6**). Efficiency of CM production was determined to be 74.3±4.4% (**Fig. 7**). CMs expressed αSA and Nkx2.5 (**Fig. 8**) which are important cardiac proteins. Furthermore, changes in versican localization (**Fig. 9**), area of mitochondria, and mitochondria localization in hiPSCs and CMs (**Fig.10**) were investigated during hiPSC differentiation without thalidomide.

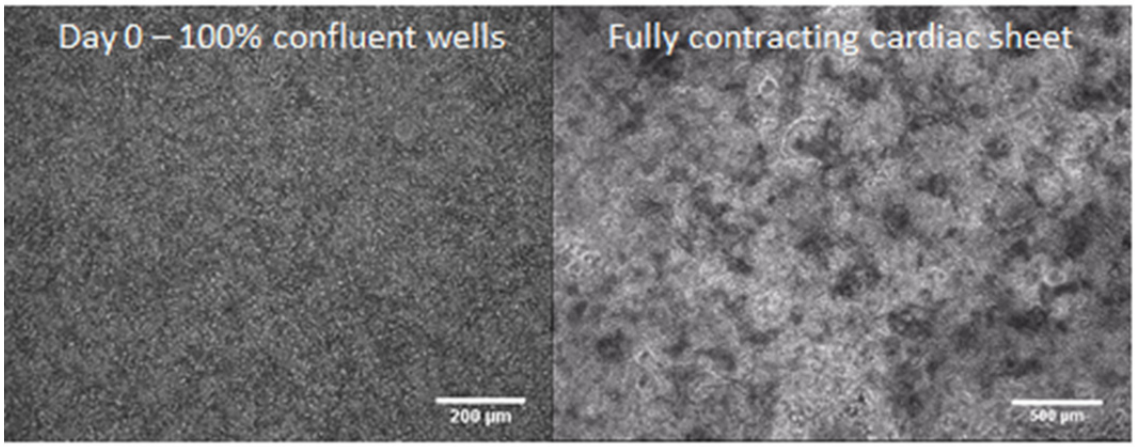

Fig. 6. 2D monolayer differentiation produces fully contracting cardiac sheets. 2D monolayer differentiation protocol is used as a simplified model of heart development and to determine initial effects of thalidomide on differentiating cells. For all differentiations, first areas of contractions are expected to occur within the first 10 days of differentiation.

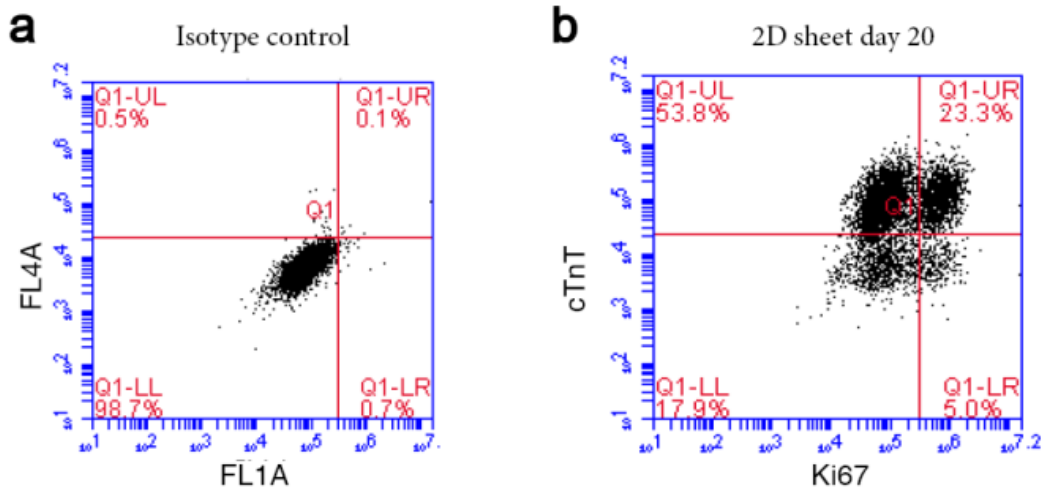

Fig. 7. Quantitative analysis of CM differentiation efficiency. Day 20 2D cardiac monolayers were used for flow cytometry and analyzed. (a) Isotype controls and (b) cTnT/Ki67 stained samples of three separate cardiac tissues were quantified. 2D monolayer differentiations produce 74.3±4.4% cTnT and 26.6±0.5% Ki67 positive cells by day 20.

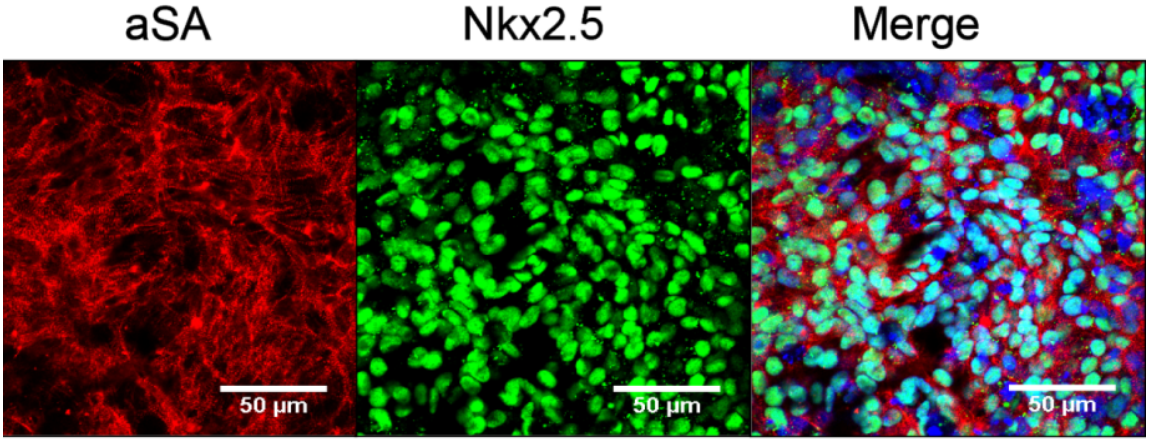

Fig. 8. 2D monolayer differentiation results in CMs that express cardiac markers. Dissociated monolayer CMs express (a) αSA and (b) Nkx2.5 located in cell nuclei. (c) Samples were counterstained using DAPI.

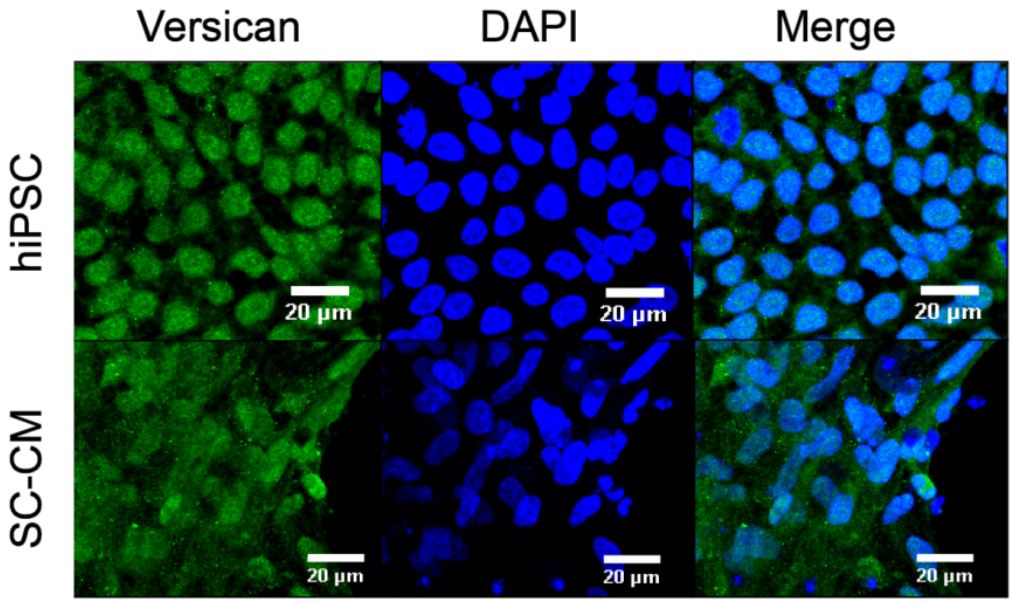

Fig. 9. Versican expression changes with hiPSC differentiation and is critical in heart development. Preliminary data shows, versican (green) in hiPSCs (top row) is primarily located within the cell nucleus, whereas versican (green) in SC-CMs (bottom row) is located in the cell nucleus and cytoplasm. Samples were counterstained with DAPI (blue).

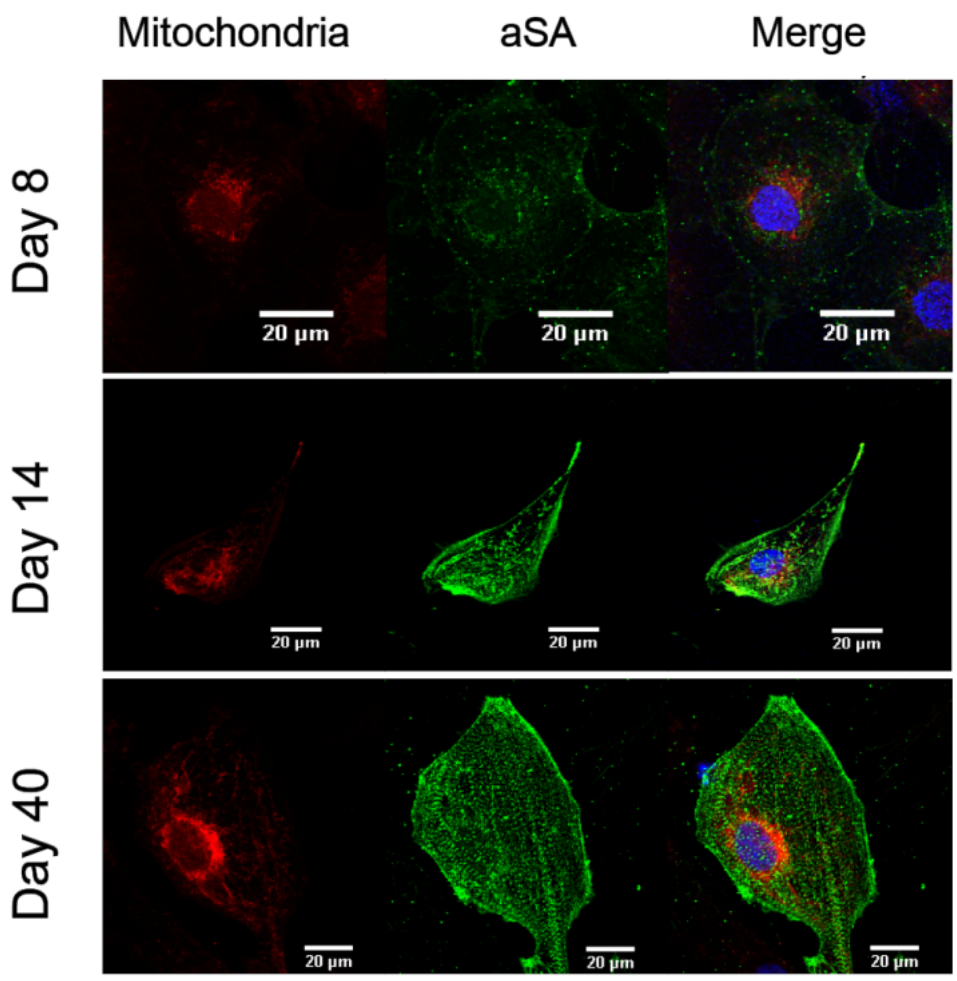

Fig. 10. Mitochondria can be tracked throughout stem cell differentiation. While SC-CMs increase in size and develop more defined sarcomeres (green), mitochondria (red) number increases and location spreads when CMs mature.

Wavefront propagation of dissociated SC-CMs can be captured and analyzed. Preliminary optical mapping results using spontaneously contracting monolayers of hiPSC derived CMs show successful capture and processing of calcium transient wavefront propagation.

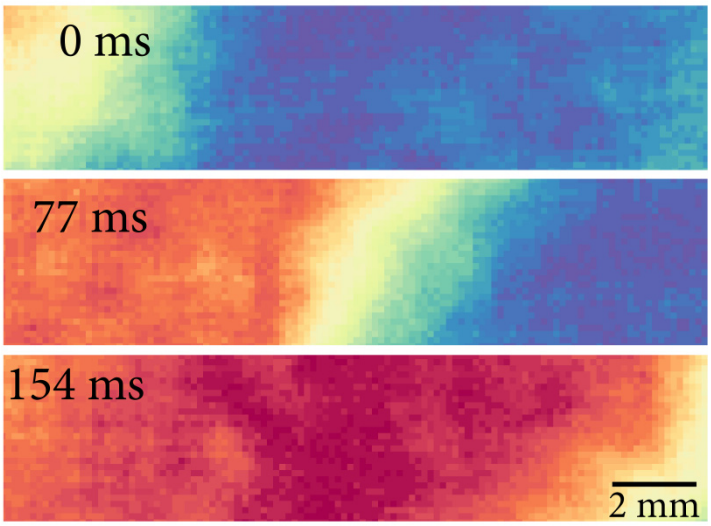

Fig. 11. Calcium handling can be captured of dissociated SC-CMs. HiPSC-CMs support uniform wavefront propagation with a calcium transient velocity of approximately 8 cm/sec (at 25ºC). Yellow indicates wavefront during upstroke.

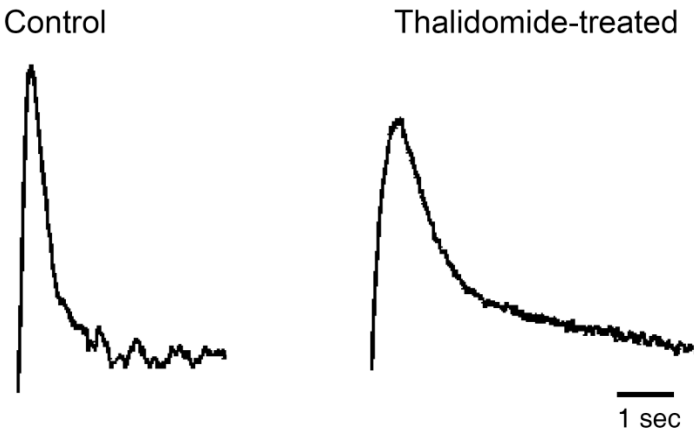

Fig. 12. Optical mapping results showed longer calcium transient traces in thalidomide-treated 2D cardiac monolayers. Calcium transients of control 2D monolayers exhibited faster time to baseline when compared to day 17 age-matched 70 μM thalidomide-treated CMs.

Conclusion

The question arises if it was safe to launch thalidomide to the market without knowing exact mechanisms on how it interferes with the developing and adult body. Understanding exact mechanisms which were involved in limb formation and internal organ defects could aid chemists design a similar medication or antagonist drug which can bind to thalidomide and minimize its interference with essential signaling pathways and protein production to minimize serious side effects. Up until now we have shown that the drug carrier (DMSO) and thalidomide did not cause any significant effects on hiPSC viability, proliferation, and mitochondria number and location. During initial stages of this project, an inefficient and highly variable cardiac differentiation protocol was used as a model platform of the developing human heart. Although insights in initial thalidomide-induced changes in EB diameter during cardiac differentiation were detected, due to high variability between batches, this differentiation protocol is not applicable for accurate drug-testing. For this reason, a highly efficient and reproducible cardiac differentiation protocol was adapted and has proven sufficient in combination with the available hiPSC line. The essential skill set of successful cardiac differentiation, determination of differentiation efficiency using flow cytometry, immunostaining with cardiac marker αSA and Nkx2.5, as well as versican and mitochondria visualization and quantification were accomplished. Future results including thalidomide-treated SC-CMs may include: a possible decrease of CM production, downregulation of versican, and changes in mitochondria compared to age-matched control groups are highly possible due to thalidomode's interference with the Wnt signaling pathway which is also involved in the cardiac differentiation process.